NASA CONTRACTOR REPORT

NASA CR - 61038

NASA CR - 61038

DESIGN TECHNIQUES FOR STRUCTURE-CRYOGENIC INSULATION INTEGRATION

Prepared under Contract No. NAS8-5268 by

THE MARTIN COMPANY
Baltimore Division
Baltimore, Maryland

For

NASA - GEORGE C. MARSHALL SPACE FLIGHT CENTER
Huntsville, Alabama

January

CR-61038

DESIGN TECHNIQUES FOR STRUCTURE-CRYOGENIC INSULATION INTEGRATION

Prepared under Contract No. NAS 8-5268 by
THE MARTIN COMPANY
Baltimore Division
Baltimore, Maryland

For

Structures Division
Propulsion and Vehicle Engineering Laboratory
George C. Marshall Space Flight Center
Huntsville, Alabama

NASA-GEORGE C. MARSHALL SPACE FLIGHT CENTER

01

FOREWORD

This report was prepared by the Space Systems Division of the Martin Marietta Corporation at Baltimore, Maryland. The work was performed under Contract NAS 8-5268 with sponsorship by National Aeronautics and Space Administration, George C. Marshall Space Flight Center, Huntsville, Alabama. The NASA Contracting Officer's Technical Representative was Mr. Clyde D. Nevins, M-P and VE-SA.

Dr. J. M. Hedgepeth was the Martin Company's Program Manager for this program and Mr. R. F. Crawford was the Technical Director. Principal investigators were Mr. R. G. Hannah and Mr. O. J. Bush with Mr. F. J. Keefe responsible for the design effort.

CONTENTS

CONTENTS (continued)

SUMMARY

The objective of this program was to develop design techniques and solutions for integrating highly efficient thermal insulations with cryogenic tankage for space vehicles. Emphasis was placed upon developing insulation systems and their attachments having high structural and thermal reliability consistent with maintaining efficient mission performance and manufacturing practicability.

A uniform basis for the development, evaluation and comparison of the design solutions was provided by prescribing a typical but idealized set of conceptual design criteria for use in developing all insulation systems. Of the existing insulation materials only National Research Corporation's "NRC-2" and Linde Division of Union Carbide's "Super Insulation" were found to be efficient enough for feasibility of the prescribed mission. Three different methods of augmenting each to satisfy insulation requirements in the atmosphere were considered: passive with subinsulation, purged and ground evacuated. Another type of insulation named Marshield was designed that consists typically of a fewer number of thicker, more widely and positively spaced radiation barriers than either NRC-2 or Linde SI. Its estimated thermal performance is lower than NRC-2 and Linde SI.

Penalties for using Marshield* are shown by optimum design and mission performance studies. These studies also showed that achievement of the last degree of high projected efficiencies of NRC-2 and Linde SI is not crucial for either the conceptual model or other vehicles and missions within the scope of this study.

Of the many investigated combinations of basic insulation materials, the ways of augmenting them and their methods of installation, six systems were selected for detailed consideration. Each is estimated to be capable of satisfactorily performing the conceptual mission. Their preliminary designs are presented in Chapter IV of this report. Adaptations of one of the systems developed for the conceptual spherical tanks are shown for an integral cylindrical tank and a toroidal tank.

The systems developed for the spherical tanks were rated relative to one another on the basis of thermal and structural reliability, efficiency, suitability for manufacturing, quality control, installation, service, maintenance and required GSE and their projected development cost. A passive NRC-2 system was rated highest.

A performance test program is recommended in the final chapter of this report. It provides a plan for experimentally screening and developing the six systems to a point where the two highest performing ones are selected for installation on a large scale tank and environmental testing.

*Proprietary name

05

I. INTRODUCTION

Multiple radiation barrier types of insulation blankets will be required for space storage of cryogens if the storage duration is to exceed a few days, since only this type of insulation is efficient enough to make such missions feasible. Linde's "Super Insulation" and National Research Corporation's NRC-2 are multiple radiation barrier insulations; they have been used successfully for such commercial applications as insulating tank cars for transporting cryogens. In those installations the insulations are contained, uncompressed, between evacuated interspaces of double wall tanks. Their potential for space storage applications has therefore been demonstrated.

However, weight is not critical in the commercial applications so that the structural weight penalty for utilizing the necessary double-wall tank is not significant. It is noted that these insulations could not function effectively in the commercial applications without the use of a double-wall tank to provide the vacuum environment along with no compression of the insulation.

Such an installation as the commercial one is readily shown to be nonfeasible for large space vehicle tankage, primarily because of excessive structural weight required to prevent buckling of the exterior tank wall under the crushing pressure of one atmosphere. The alternatives are, then, to install the insulations on the outer surface of a single wall tank, and either let the vacuum of space evacuate the insulation or else encase the insulation in a flexible vacuum bag which would be evacuated prior to launching the vehicle. The passive feature of the first alternative is attractive, but it requires either an auxiliary subinsulation or purging the space insulation with a noncondensible gas for thermal protection during ground hold and ascent heating. The second alternative has the attractive feature that both Linde SI and NRC-2 can also be quite effective as ground insulations, even when compressed by one atmosphere, if they are evacuated. The auxiliary requirements of the first alternative are thus circumvented.

Neither of these methods for insulating space vehicle cryogenic tankage for extended storage nor others have, however, been demonstrated by actually integrating them into a practicable space vehicle tankage design, fabricating it and subjecting it to the environment it would experience.

One problem area in developing a practicable insulation system of either Linde SI or NRC-2 arises from the fact that they are composed of many layers of thin (1/4- to 1/2-mil) foils of metal or metallized plastic sheets. Being very thin, they present many installation problems, both thermal and structural. In addition, many thermal pene-

trations of the blanket are required, e. g., suction, vent and fill lines and structural supports. Each penetration can be an excessive conduction path for heating if not carefully treated.

The objective of this program was, therefore, to develop practicable design solutions to these and other problems arising in integrating these insulations with typical tankage configurations for space storage of cryogens. Emphasis was placed on maintaining structural integrity and minimum heating consistent with maximizing mission performance and meeting realistic manufacturing requirements.

The approach taken in developing these design solutions was first to set design criteria to which the systems should be designed. The results of that effort are presented in Chapter II where the environment, both thermal and structural, is defined and characteristics of the insulation materials are given. Some experimental work was performed to resolve certain problem areas regarding characteristics of the insulations. Their results are summarized in Chapter II and presented in detail in the appendices.

The next step in the program was to devise proper design methods. This resulted in various theoretical analyses to determine heat transfer and optimum insulation and structural proportions for the systems. The criterion for optimum design in these analyses was to maximize efficiency of mission performance. The design analysis methods are derived in the appendices, and in Chapter III their results and recommended utilization are presented. An important result of this part of the study was that it showed the highly efficient insulations have ample margin for accepting rather large installation and heat leak penalties. Moreover, it emphasized that a point of diminishing returns may soon be reached in devising means for minimizing the heat leaks.

Chapter IV then presents designs of tankage/insulation systems that resulted from applying the design criteria, design methods and direction given in Chapters II and III. Three categories of insulation systems are given: passive, purged and evacuated. These designs show various means for installing the systems and each is discussed in the text.

In Chapter V, the systems are rated relative to one another; however, it is emphasized that the ratings should be considered preliminary since they are based on data, concepts and theoretical evaluations that are, in many instances, unproved.

Because of these current limitations on the state of the art in this particular design problem, a plan for further experimental development and performance testing is recommended in Chapter VI.

II. DESIGN CRITERIA: ENVIRONMENT, DESIGN REQUIREMENTS AND INSULATION PROPERTIES

A uniform basis was required for the development of the insulation system designs so that the resulting designs could be evaluated and screened by their relative performance; there was no other established standard. Therefore, the common environment, design requirements and basic insulation properties to which all designs were developed are presented in this chapter. These design criteria are in some cases arbitrary choices when a particular choice is of no particular significance to the study. In other cases the criteria are simplified relative to actuality when inclusion of complexities, as in the somewhat non-uniform heating in space, is not necessary to the development of design solutions. In general, the design criteria are upper limits so as to force the design solutions to cover all cases within the scope of this program.

A. ENVIRONMENT

1. Thermal

a. Ground hold

Optimization of an insulation system design should include the effects of ground hold and ascent flight performance. However, for cryogenic vehicles which must perform extended space storage missions, the insulation system should be optimized for the space part of the mission, it being dominant, as long as the resulting design is compatible with the ground hold and ascent flight phases. Accordingly, the philosophy in the conduct of this study has been to accept the ground hold performance which results from the use of optimum insulation thickness based on the space phase of the mission whenever the ground hold heat transfer rate did not exceed approximately 150 Btu/hr-ft^2 for hydrogen filled tankage. (This implies, of course, that no areas are present upon which air can liquefy.) The resulting boiloff rates are compatible with current topping capability at the present launch sites. It was further assumed that topping of the stage would be accomplished up to 2 min prior to liftoff, and thus, the ground hold performance penalty in any event is small.

The equilibrium ground hold heat leak and performance penalty was established from the design conditions specified on Table II-1.

b. Ascent flight

The heat transferred to the propellant tank during the aerodynamic heating portion of the trajectory varies considerably from one insulation system to another. However, the total heat which eventually reaches the propellant as a result of this phase of the mission is nearly constant for a given trajectory. That is, most of the heat stored in the insulation system will subsequently be absorbed by the propellant. The assumptions for the ascent portion of the mission are given in Table II-1 and in Fig. II-1.

c. Earth orbit

Typical orbit elements are shown in Fig. II-2. These were used to establish the average equilibrium skin temperature of 460° R during orbit. This assumes infinite lateral thermal conductivity around the shell which is slightly conservative in predicting heat transfer to the tank (see Ref. II-1). Table II-1 presents the other ground rules used to make comparisons of the different insulation systems.

2. Basic Structural Loads

The basic structural loadings selected for use in this study are those associated with the Gemini launch trajectory shown in Fig. II-1. This trajectory is typical of various launch vehicles and closely approximates the launch trajectory of the Saturn V shown in Fig. 3 of Ref. II-2. The trajectory data, i.e., Mach No., dynamic pressure and altitude variations with time, effectively define the structural design requirements for the vehicle. These boost requirements combined with the specific problems associated with cryogenic fuel tankage, its storage times in orbit and its mission requirements, form the basis for the design criteria applied to the tankage and insulation systems investigated.

a. Static loads

The steady state load factors consistent with the prescribed launch trajectories are: $n_x = +6, -1$, n_y (any direction) $= +1$. A factor of safety of 1.4 should be applied to these loads, and room temperature allowables should be used without benefit of material property increases at cryogenic temperatures.

b. Dynamic loads

Dynamic loads consistent with the typical booster launch conditions were given consideration in the design of the insulation systems.

TABLE II-1

Thermal Environment Design Criteria, Ground Rules and Assumptions for Screening and Comparison Purposes

Item	Ground Hold	Ascent Flight	Earth Orbit
Ambient (or) equilibrium temperautre	560° R	Variable	460° R; α_s/ϵ_{IR} = 0.65(1)
Wind velocity	0-40 kn(2)		
Propellant temperature	36° R	36° R	36° R
Tank diameter and shape	250-in. sphere	250-in. sphere	250-in. sphere
Dominant heat transfer modes	Convection(3)	Convection	Radiation and conduction
Neglected heat inputs	Ground and atmospheric radiation penetration conduction leaks	Penetration conduction leaks	Payload-to-dome and engine compartment-to-dome radiation
Source temperature for conduction heat leaks			530° R--engine suction line 460° R--all others
Mission time	2-min ground hold after topping ceases	150-sec heating period	30 days
Ascent trajectory		Typical Gemini launch vehicle trajectory(4)	
Ascent trajectory heating		64 Btu/ft^2(5)	

(1) See Fig. II-2, Propellant Tankage Equilibrium Temperature for Model Orbit.

(2) For comparison, internally supported tankage is assumed and natural convection is primary mode of heat transfer to tankage.

(3) See Fig. II-3, Heat Flux to Propellant Tankage at Launch Pad Conditions.

(4) See Fig. II-1, Typical Boost Trajectory Elements.

(5) Heat transferred to tank during boost and during "soak in" period after aero heating period.

Typical vibration spectrums demonstrate two peak periods of vibration, one at launch and the other in the Mach 1 to max "q" vicinity. These peak periods of vibration typically demonstrate vibration levels of 10 g rms over a relatively wide frequency range: frequency ranges to which the very lightweight plies of multilayer insulations do not respond.

During this program a Marshield specimen having aluminum reflectors of 0.003 thickness (twelve times thicker than the Linde reflectors or the NRC plies) was subjected to a vibration test in which a vibration level of 20 g rms over a frequency range of 1000 cps was imposed for a period of 5 min, and no sensible damage was incurred. Hence, it was considered that vibratory effects upon the multilayer insulations per se were negligible.

Although vibratory loads had no influence on the design of the insulation systems presented, it is recommended that any systems selected for further development be subjected to at least a 6.0-g level of vibration over a 20 to 150 cps range of frequencies for proof testing.

c. Acoustic environments

As shown in Fig. II-1, two peaks occur in the sound pressure level during a typical boost trajectory; one at launch and the other at approximately the max "q" condition. These peaks indicate maximum sound pressure levels of about 150 db. The magnitude of the sound pressure levels, at the insulation, will be attenuated by the interposed basic structure or shroud. However, during the study, samples of Marshield were subjected to 155 db noise level for 4 min and for 1 min at 160 db with no apparent damage being incurred.

Previous testing at the Martin Company of both Linde Super Insulation and NRC-2 insulation at equivalent sound pressure levels has indicated no effective damage to the multilayer insulations with the exception of some slight abrasion and fraying of the unsupported edges of the Linde fiber glass paper separators and some abrasion of the deposited aluminum on the NRC-2 at contact points. However, in the present designs involving Linde insulations, edge treatment of the blankets has been made in such fashion as to provide additional damping of the edges.

Because of these results, no further treatment of the acoustic response of the insulations is given in the design studies (Chapter IV) of this report. But it is recommended that any proof testing of these insulation systems include approximately 5 min acoustic excitation at the 150 db sound pressure level, combined with the previously recommended vibratory testing.

3. Meteoroid Model

The 1963 modification of the Whipple model was selected for use in this program because it agrees well with existing meteoroid data taken from satellites and because it is based upon improved methods of measuring luminous efficiency in the meteoroid experiments of Trailblazer I. The Whipple model is discussed more thoroughly in Appendix A to this report where evidence is also given that the selected meteoroid environment does not appear to influence design problems of this program. This conclusion is based upon experiments (described in Appendix A) that show multilayer insulations naturally form a very effective meteoroid barrier.

B. DESIGN REQUIREMENTS

1. Operational Requirements

The history of the insulation system from manufacturing and installation through handling, transportation, launch pad operations, tankage cooldown and fill operations, ground hold, boost and orbit operations must be considered in addition to thermal performance and weight to ensure that a practicable and reliable design results. Throughout the design phases of this study, each system should incorporate design features which reflect consideration of these factors. Factors which were used to continually check each design approach for satisfaction of operational requirements and the desirable design features sought for each, are indicated in Table II-2. The extent to which the various systems satisfy operational requirements was considered in the rating of the systems as seen in Chapter V.

2. Configuration Requirement

The general range of cryogenic tankage configurations to which the present study is applicable includes the following:

Cylindrical tanks	- 150- to 400-in. diameter
Spherical tanks	- 150- to 250-in. diameter
Toroidal tanks	- 150- to 250-in. outside diameter

The spherical and toroidal tanks are considered to be within a cylindrical, load-carrying outer structure.

Since many of the problem areas of analyzing, designing and optimizing insulation systems for integration with the tank are common to the various configurations listed, the bulk of the effort (especially in the design area) is on a 250-in. diameter spherical tank which poses

TABLE II-2

Operational Requirements

Ground Evacuated Systems	Reliable vacuum bag installation Leak detection must be possible Vacuum bag must be repairable or serviceable on site Evacuation system must be practical for on-site evacuation Means of opening the vacuum jacket to space environment may be required Vacuum bag must allow insulation to recover Evacuation techniques should consider cleanliness, conductance, and entrapped water vapor of the insulation
Purged Systems	Design must eliminate the boost inflation problem Purge system must be simple and efficient Adequate gas escape area must be provided in insulation system without incurring large thermal penalty Slightly positive purge pressure must be maintained on pad and during ascent Maintenance, repair or servicing must be as easy as practicable once installed on tank
Passive and Misc Systems	Design must alleviate the boost inflation problem Subinsulation seal integrity must be maintained Adequate gas escape area must be provided in insulation system without incurring large thermal penalty Subinsulation attachment method must be reliable and accommodate tankage shrinkage during fill Provisions should be made to prevent oxidation of the reflective insulation surfaces

TABLE II-2 (continued)

General Requirements

Insulation installation method must consider tank shrinkage upon cool down and fill	Procedure for installing insulation system should be as uncomplicated as practicable
Tank supports must be designed to accommodate tank shrinkage	Extremely complex procedures required at the launch site should be avoided
Insulation system design should reflect a solution to or attack on the hydrogen leak diffusion problem	Specialized equipment requirements should be kept to a minimum at the launch site
Insulation attachment method must be positive and reliable and must resist handling and ascent flight g-forces	Ground hold performance must be compatible with GSE equipment
Insulation system performance should be as reliably predictable as practical	Manufacture of basic insulation system should be practical, cheap and easy
Efficient thermal performance during orbit or interplanetary operations should not be dependent upon vehicle orientation	Insulated tanks must be capable of being handled and shipped without damage to the insulation system
Basic loads should be carried through that structural component which minimizes overall performance penalty including heat leak effects	Stringent quality control requirements should be avoided if possible

most of the design problems of integrating the insulation systems. Some design effort is then given to adapting the solutions to the toroidal and cylindrical tanks. The analytical methods of optimization in general treat size and shape parametrically.

3. Thermal Design Requirement

Other than such requirement as no air liquefaction during ground hold and boost, there appears to be no need for specification of limiting levels of heat transfer. Instead, the approach taken is that of optimizing heat transfer consistent with maximization of mission performance. The thermal environmental criteria on which this approach is based are those given in Section A of this chapter.

4. Structural Design Requirements

The basic structural requirements for the design of the structure-cryogenic insulation systems are those necessary for structural integrity and reliability of the installations under the environmental criteria established in Section A of this chapter. Three categories of insulation systems are considered in this study: passive, purged, and those that are pre-evacuated. Each represents a different way of achieving the necessary insulation performance on the ground and during boost in the systems, and their structural design requirements vary. These requirements and the approaches used for satisfying them are discussed in the following paragraphs:

a. Boost inflation of the blankets

The insulation blankets of the purged and passive systems (see Designs in Chapter IV) are provided with exterior netting to support the blankets during boost when they tend to inflate as ambient pressure becomes less than that of purgant or air contained therein. This problem area and some experimental work performed on it are discussed further in Appendix C. The air or purgant would not be permanently entrapped, but some resistance to evacuation to the environment will be present (as shown in Appendix C) and result in a net bursting pressure during boost. The magnitude and duration of these bursting pressures for any particular system and installation technique requires experimental determination. Therefore, the netting configurations shown in Chapter IV for the vulnerable systems are nominal.

b. Blanket restraint techniques

The evacuated systems have at least one structural advantage over the purged and passive systems inasmuch as they incur no boost inflation problems. These systems, being pre-evacuated, are compressed

A tradeoff study should be made when long cylindrical tankage is specified to determine whether large heating through supports that are primary structure or the extra weight of an exterior primary structure is more tolerable. In the later case, no additional provisions for aerodynamic-meteoroid shroud would be required; perhaps, offsetting the weight penalty of the exterior primary structure.

d. Shroud design

An integral cylindrical tank design is shown in Chapter IV wherein the shroud's chief function is that of protecting the insulation against ascent aerodynamic forces. The shroud design given consists of intermittent, longitudinal corrugated sections connecting wider monocoque shell sections. The corrugations are designed to provide, through spring tension, a crushing pressure of 3 psi on the insulation when the tank is not filled. The spring rate of the corrugation is such that a pressure of approximately 2 psi will remain when the tank (aluminum) is cooled to liquid hydrogen temperature. This secondary structure will be exposed, of course, to the aerodynamic forces of the boost trajectory and must not flutter.

The uncorrugated sections of the shroud whose surfaces fay on the insulation present no flutter problem; the damping of the insulation and the pressure produced by the corrugations preclude conditions for cyclic oscillations necessary for flutter to occur. The particular titanium corrugations used in this shroud are designed by spring rate requirements and resulted in corrugation elements 1.5 in. wide and 0.056 in. thick. Extrapolating the flutter boundary design curves of Fig. II-4 show this geometry is in a stable regime at the design condition $\left(\sqrt{M^2 - 1}/q\right)^{1/3} = 0.60$.

C. INSULATION PROPERTIES

Properties of multilayer insulations that were used throughout the program are presented in this section along with those for several other types of insulations suitable for ground and boost augmentation of the multilayer systems. Only multilayer insulations are considered for the space-storage phase of the mission since others are not efficient enough to make feasible extended space storage of cryogens.

Besides basic physical properties presented in this Section, general characteristics of the insulations, manufacturer suggestions for their installation and anticipated method of utilizing each insulation are also given.

1. Multilayer Insulations

a. Linde Company insulations

For cryogenic applications this family of insulations consists basically of a sandwich of a large number of very thin (1/4 mil), highly reflective, aluminum foils separated by glass fiber papers or fiber glass mats. The density of these insulations varies from 2 to 7.5 lb/ft^3 depending upon the number of layers per inch and the nature of the spacer material. Typical values of density and conductivity are given below along with their product which is an indication of the insulation's efficiency:

Type	Layers/in.	Density (lb/ft^3)	Apparent Thermal Conductivity (530° - 36°R) (Btu/ft-hr-°R)	$k\rho$
SI-44	35-70	4.7	2.0×10^{-5}	9.4×10^{-5}
SI-62	50-100	5.5	1.8×10^{-5}	9.9×10^{-5}
SI-91	75-150	7.5	1.0×10^{-5}	7.5×10^{-5}

The above properties are presented to illustrate that although the density increases with number of layers per inch, the thermal performance (as shown in the last column) improves also. More importantly, however, the most significant index of performance, apparent thermal conductivity times density, is lower at the higher density at least up to a certain number of layers per inch. On the basis of the above data, it may seem that SI-91 would always be the most desirable. This is not always the case when installation factors and all mission phases are considered; therefore, each application must be separately examined.

(1) Thermal conductivity of Linde SI. The thermal conductivities listed for multilayer insulations are apparent values since they are a function of both warm and cold boundary temperatures. When properly applied and used, the dominant heat transfer modes are radiation and conduction; therefore, the apparent thermal conductivity is a very weak function of the cold boundary temperature but is a strong function of the warm boundary temperature. Figure II-5 illustrates this dependency for one SI-type insulation.

(2) Effect of insulation internal pressure. Achieving the values of thermal conductivity shown in Fig. II-5 requires lowering the pressure within the insulation layers to below 10^{-4} torr where gaseous conduction is very low. Failure to reach this pressure level results in the thermal degradation as shown in Fig. II-6. This degradation is due

to increasing gas conduction with increasing pressure. The residual gas assumed here is air, but for a purged insulation (e.g., a helium purged one) the higher thermal conductivity of the purge gas can result in even poorer performance (see Fig. II-7), if a low blanket pressure is not achieved.

(3) Achieving low insulation pressures. Recognizing this fact, and anticipating the use of purged insulation systems and/or unpurged, unevacuated systems, a series of evacuation tests was conducted This test program was designed to determine how easily and under what conditions the vacuum of space could be expected to pump down the various multilayer insulations to the desired pressure levels. Details of this program and the results are fully documented in Appendix D. In general, the program results indicate that if sufficient insulation blanket edge area can be exposed to the vacuum with no impedance of edge scrolling or constrictions by an external flexible bag, the desired pressure levels can be attained in a short time with no significant thermal performance penalty for a long term orbit storage mission. Since exposure of the edges has attendant heat leak increases, and no edge conditions other than free edges were tested, extension of these tests to include more realistic edge and blanket juncture treatments is indicated before final judgments on evacuation time can be made.

Low insulation blanket pressures might be achieved by pre-evacuating the blankets prior to installation on the tank or while on the tank but some time prior to liftoff. This approach requires that the insulation be enclosed in a flight-weight flexible vacuum jacket.* To date vacuum jacket material has been almost exclusively a laminate of 1/2-mil mylar, 1-mil aluminum foil and 1/2-mil mylar, "Zero-Perm Vapor Barrier," made by Alumiseal Corp. Vacuum jackets of this composition have not been very satisfactory because of the development of pin hole leaks during evacuation when the bag and insulation are crushed under the external bearing pressure of the atmosphere. In addition, sealing of the jacket to the various surfaces required to complete the enclosure has proved to be difficult.

Vacuum bags are still under development and much more development work is necessary before this system approach can be considered reliable. There is little doubt that a lightweight, reliable bag can be developed, but the extent to which it can or should be pre-evacuated is still an open question. Certain groups studying this problem area (notably, see Ref. II-3) feel that even if this development is accomplished it will still be necessary to open the vacuum jacket, once in orbit, to permit venting of: gases which diffuse through the jacket during boost, hydrogen gas which may diffuse through the tank walls, residual gases,and other gases which result from subsequent outgassing of insulation and metallic surfaces. The magnitude of this problem has yet

*This approach is not recommended by the Linde Division of Union Carbide Corp for use with Linde SI-91 insulation.

to be established; however, should venting of the bag to space vacuum prove to be necessary, some of the advantages of this system concept would be negated.

(4) Effects of compression of insulation. Analyses of the vacuum jacketed system's performance during ground hold and boost require a knowledge of the insulation performance under the external bearing pressure of the atmosphere. For the ground hold condition, the Linde SI-type insulation is compressed to approximately one fourth of its original thickness. The variation of thermal conductivity with external bearing pressure is presented in Fig. II-8. This data is also required for evaluating certain methods proposed for installing these insulations on the tankage which involve local compression of the insulation to resist the vibration and g-forces of the ascent flight.

The extent to which these insulations recover after the bearing pressures are released is also of importance, since failure to return to the original thickness can have a significant effect on the effective thermal conductance of the insulation blanket. This is due, principally, to increased solid conduction between layers. Data on the recovery of insulation thickness vary from Linde Company's reported value of 95% with no external restraint such as a vacuum jacket, to 72% with a relatively heavy 2-mil jacket present. This is felt to be primarily the result of the jacket taking a permanent set when compressed, not permitting the insulation to fully recover. Lighter weight jackets did not appear to hinder the insulation recovery, according to Linde Company (Ref. II-4). The results of an experimental program (Ref. II-5) conducted by NASA-Lewis and Linde Company, wherein a hydrogen tank was insulated with vacuum jacketed Linde SI-62, also indicated that the residual compression of the insulation due to the vacuum jacket's permanent set prevents attainment of ideal performance--at least with the Zero-Perm Vapor Barrier type vacuum jacket, manufactured by Alumiseal Corp.

Since each application will undoubtedly exhibit a different recovery characteristic, experimental data will probably be required for each different configuration, unless a less restrictive-type vacuum bag is developed.

(5) Transient thermal analyses. Transient analyses of the cool down and ascent flight phases require data on the specific heat of the insulation materials as a function of temperature. Figure II-9 shows this data for Linde SI-62 which is typical of this type of insulation in general. Transient analyses also require a knowledge of the point thermal conductivity (i.e., absolute temperature dependence) rather than the apparent value (based on temperature difference). Reference II-4 presents an approximate equation which can be adapted for this type of analysis. This is reproduced below, and a typical plot is shown in Fig. II-10. Note in Fig. II-10 that approximately 55% of the temperature drop occurs in the last 20% of the insulation thickness. Therefore,

any liquefaction would occur first in the colder region and would lower the effectiveness of the insulation in that region.

$$\frac{x}{\delta} = \frac{0.18 \times 10^{-6} (T_1^{3/2} - T^{3/2}) + 0.07 \times 10^{-12} (T_1^4 - T^4)}{0.18 \times 10^{-6} (T_1^{3/2} - T_2^{3/2}) + 0.07 \times 10^{-12} (T_1^4 - T_2^4)}$$

where T_1 warm boundary

T_2 cold boundary

T temperature at station x

δ insulation thickness

(6) Installation and application considerations. Insulation of flight-type tankage requires that blankets be terminated, joints or seams formed, penetrations be insulated, and devices be used to attach the insulation to the tank and hold it there against the boost and handling forces. The insulation properties discussed thus far do not include these more realistic considerations.

Lateral thermal conductivity. The thermal conductivity of the Linde SI type of insulation in the plane parallel to the foils is from 10^5 to 10^6 times that in the plane perpendicular to the foils. Linde Company's estimates of lateral thermal conductivity as a function of the number of layers per inch and for several temperature ranges are presented in the table below.

Temperature Range Layers per Inch	530° to 36° R	530° to 130° R
50	1.8 Btu/hr-ft-°R	1.63
100	3.6	3.25
300	10.8	9.75

It is apparent from the anisotropy of the thermal conductivity of these insulations that the edges of the foils must be guarded from either "seeing" a warmer surface or butting up against one. Experimental and theoretical work performed under Contract NAS W-615 has resulted in some recommendations of techniques for decreasing the effects of this type of thermal short (see Ref. II-3).

Seams, joints, and junctures. Linde SI insulation could be spirally wrapped with alternate layers of foil and spacer material thus providing many overlaps but no significant seam or joint thermal problems. One could even consider filament-type winding of the tank surfaces with relatively narrow strips of foil and spacer material. This approach could be used with almost any shape tank. Another possibility is to precut individual gores of foil and spacer material and apply them one at a time, overlapping each such that no seams or joints having direct heat leak paths exist.

None of the above methods adequately handles the problem of providing a positive method for securing the insulation in place during the preflight handling and ascent flight periods. In addition, some of the methods would be extremely time-consuming in application. Local compression of the insulation by external bands, and the use of many miles of tape appear to be the only way that these systems could be held to the tank. Tapes exhibit, in general, severe outgassing characteristics incurring evacuation problems. The extent to which pressure bands are effective in securing Linde SI flight-weight tanks is yet to be established.

Recommended installation approach. An approach developed in the design stage of this program is to fabricate a limited number of insulation blanket sections or gores having packets of their layers interleaved with adjacent sections as shown in Fig. IV-5. Interleaving of each layer appears unnecessary. Therefore, the compromise recommended is to interleave groups or packets of 10 layers forming the saw-tooth joint section shown in Fig. IV-5. The blanket sections would then be attached to the tank by a system of nylon ropes and anchors. Details of each system design are discussed more fully under Chapter IV.

Seam heat leak. Estimates of the heat leak through the sawtooth- (or finger) type seam have been made for the Linde-type insulation. For a typical joint using a 3-in. finger length, the estimated heat leak per foot of seam is 0.049 Btu/hr-ft (seam). This value was used to determine the joint contribution to the overall heat leak for the Linde system shown in Table V-I "Comparison of Systems."

Attachment heat leak. The proposed method of attaching the blanket sections to the tank (see Fig. IV-5 involves considerable local compression of the insulation around the nylon ropes. The heat leak through this area of the blanket was estimated at 0.13 Btu/hr-ft length which was used to develop the performance figures given in Table V-1.

(7) Purged and unevacuated insulation performance. Some insulation system concepts using Linde SI or NRC-2 are based on achieving adequate ground hold and ascent flight performance by purging the insulation with helium gas or some other gas such as nitrogen which is noncondensible in the temperature range within the insulation. The multilayer insulations when purged exhibit a thermal conductivity approaching that of the purged gas. Figure II-1 presents the heat flux through helium purged multilayer insulations as a function of insulation thickness and warm boundary temperature for liquid hydrogen tankage. This curve is applicable to both Linde SI and NRC-2 insulations. A subinsulation would be required to maintain a temperature above that for nitrogen liquefaction at the innermost layer of the multilayer insulation if a nitrogen purge is used on a liquid hydrogen tank.

Unevacuated and unpurged insulations attached to liquid hydrogen tanks exhibit totally unacceptable ground hold performance because of air liquefaction within the insulation. However, by the use of a subinsulation, the air temperature within the insulation can be maintained above air liquefaction temperature and satisfactory ground hold and ascent flight performance achieved. Although under these conditions some water vapor condenses and frost forms in the insulation, the amount is small and is estimated to have very little effect on the ground hold performance (see Appendix D). The probable main effect will be inhibition of space evacuation of the insulation due to subsequent outgassing.

The performance of air-filled multilayer insulations, based on the results shown in Ref. II-16 that the effective conductivity of Linde SI is approximately that of air, is plotted on Fig. II-12 for three insulation thicknesses and a number of boundary temperature conditions. While no system concepts are considered here using unevacuated NRC-2 for which it may be assumed Fig. II-12 is equally applicable.

b. National Research Corporation (NRC-2) insulation

NRC-2 insulation is a multiple-ply blanket composed of a large number of layers of plastic film, one side of which is metallized by vacuum deposition. In one form, the plastic material is 1/4-mil mylar and the metallic film is aluminum (approximately 1×10^{-6} in. thick). Other plastic materials such as Saran, Tedlar, Teflon FEP, or H-film can be used with such metallizing materials as gold, tin and silver, providing a reflective surface. Each layer is individually crumpled or crinkled to minimize conduction paths between layers.

(1) Advantages of NRC-2 over Linde SI. NRC-2 insulation appears to have a number of advantages when compared to the Linde superinsulations. Briefly, there are considered to be:

(1) Lower bulk density for the same thermal performance.

(2) Single component insulation.

(3) Lower lateral thermal conductivity.

(4) Ease of application (lower man-hours per pound applied).

(5) More pliable and formable (easier to gather around doubly curved surfaces).

(6) Greater strength in tension.

The main disadvantage of NRC-2 insulation is that it does not possess any sensible resistance to crushing loads or external bearing pressure. Therefore, it cannot be used alone in a pre-evacuated system using the flexible vacuum jacket approach as can the Linde insulation. Since this deficiency affects only the ground hold and ascent flight performance, it can be circumvented somewhat by:

(1) The use of fiber glass cloth spacers (or other) between some or all of the layers.

(2) The use of a subinsulation such as sealed cork, foam or mylar honeycomb.

(3) Purging of the insulation with a noncondensible gas such as helium.

(2) Thermal performance. Attaining efficient space thermal performance with NRC-2, just as with Linde SI, requires low pressure (less than 10^{-4} torr) within the insulation. At these low pressures where the effect of gas conduction is negligible, the thermal conductivity is a function of density and boundary temperatures only. Figure II-13 presents the heat flux through NRC-2 insulation as a function of number of layers per inch, for several boundary temperatures. The solid line is based on experimental results as reported by NRC-2. The curves for the other boundary temperatures have been estimated from the NRC-2 brochure (Ref. II-6). The points called out in Fig. II-13 indicate the trend of thermal conductivity and density with varying number of layers per inch. While minimum $k\rho$ occurs at about 40 layers per in., the minimum thermal conductivity occurs at approximately 70 layers per in. In the present study, the minimum k values (i.e., 70 layers per in.) were used because it is more practical to apply the insulation at the greater than at the lighter density. Figure II-14 shows these trends more clearly and is based on experimental results reported in Ref. II-3 and II-6.

(3) Effect of insulation internal pressure. While the conductivity of NRC-2 increases with gas pressure in a manner similar to that previously

shown for Linde SI, Fig. II-6, NRC-2 appears to have some advantage over Linde SI at pressures below 10^{-4} torr due to its continuing decrease in conductivity with decreasing pressure.

(4) Achieving desired internal pressure levels. One method of achieving low pressures in the insulation blanket is to allow space to do the job once in orbit. Appendix D presents the results of evacuation tests performed at the Denver and Baltimore Divisions on NRC-2 insulation. While the results of these tests are not conclusive, since actual installation configurations were not simulated, they do give some confidence that the space vacuum environment could be used to pump down those insulations in a relatively short time if actual edge treatments permit evacuation rates approaching those achieved with the open edges used in the experiments.

The effects of failure to reach the desired pressure level in the insulation system are shown in Fig. II-15, for a typical hydrogen tank performing a 30-day orbital storage mission.

Another method of obtaining desired pressure levels in the NRC-2 is to pre-evacuate the blanket sections either prior to installation on the tank, or subsequent to installation but before loading the tank with cryogenic propellant. As mentioned earlier, this requires the use of a subinsulation or spacers between layers to prevent air liquefaction on the outer surface of the insulation. Since the spacers add considerable weight, and are not required throughout, only the inner third of the layers are assumed to be spaced. The estimated thermal performance of the NRC-2 insulation with spacers is presented in Fig. II-16 for both the space condition (uncompressed) and the ground-hold (compressed) condition. This performance is based on the experimental results presented in Ref. II-7.

(5) Effects of compression of NRC-2 insulation. Compressed performance data on NRC-2 are important because:

(1) Proposed methods of installing and holding the insulation in place require local compression of the insulation.

(2) Ascent flight g-forces tend to locally compress the insulation.

(3) Compressed and recovered performance characteristics are required for pre-evacuated systems.

Mechanical compression tests were performed under contract NAS W-615 (see Ref. II-3) on a number of different types of multilayer insulations. The NRC-2 insulation is subject to a more rapid increase in heat flux due to external pressure than the Linde SI class insulations. If spacers are used between the NRC-2 layers, however, the performances are quite similar above 3 psi (see Ref. II-3).

According to Refs. II-7 and II-8, the thermal performance of NRC-2 type insulation with or without spacers improves upon recovery after being compressed one cycle to 15 psi or so and then released. No explanation is offered in Ref. II-7 or II-8 for this phenomenon, but it may be due to an increase in overall contact thermal resistance when only one load cycle is involved. Repeated cycling of an external bearing load on the insulation causes permanent flattening of the crinkles and large decreases from the original thickness (see Ref. II-3). Reference II-3 discusses the test of 1-in. thick sample of 20 layers of crinkled polyester film which was repeatedly loaded with a resultant increase in sample density of 530% after only three cycles. Figure II-17 presents the compression characteristics of NRC-2 taken from the above references.

(6) Transient thermal analyses. While there have been no reported values of the specific heat of NRC-2 insulation, the use of mylar values should be sufficiently accurate. These data are available in Ref. II-9. Point thermal conductivity values of NRC-2 insulation are not available but perhaps could be derived from the apparent thermal conductivity data which exist.

(7) Installation and application considerations. The installation of the NRC-2 insulation on flight-type tankage appears to present fewer thermal problems than does Linde SI because it is easier to apply around penetrations, and it can be formed in joints and seams without incurring large heat leak penalties. This is primarily due to its lateral thermal conductivity being much lower than that of Linde SI.

Lateral thermal conductivity. While NRC-2 is also highly anisotropic, and its lateral thermal conductivity is approximately 10^4 times that perpendicular to the layers, this ratio is still one to two orders of magnitude lower than the corresponding Linde SI value. This is sufficient to reduce comparable joint or penetration thermal shorts from strong thermal short areas to weak ones. Design techniques for effecting blanket terminations and junctures, insulating penetrations, etc., which would normally be prohibited by high heat leaks can be considered using NRC-2 because of this property.

Seams, joints and junctures. National Research Corporation recommended methods of making blanket junctures are shown in Figs. II-18 (a), (b), (c), and (d). In addition, several other methods are shown which have been employed in this program. Estimates of the heat leak per foot of seam or juncture are given in the table below for several types of joints.

Type of Joint	Heat Leak Per Foot Length
Full Scroll (a)	0.0225 Btu/hr-ft
Half Scroll (b)	0.03 "
Full Interleave (c)	0 "
*Partial Interleave (d)	-- --
Sawtooth (e)	0.049 "
‡Extreme Overlap (f)	0.05 "

*Not estimated--probably similar to (e).
‡Extreme overlap is defined as insulation blanket edges overlapping by 10 to 12 in. or more.

From a thermal standpoint, the complete interleaving of the layers of adjacent blankets is obviously the preferred method of joining two blanket sections. This, however, increases the problem of evacuating the insulation either before launch or by space once in orbit because the pumping path length is significantly increased. In addition, this type of joint severely impedes the rapid venting of gases from the insulation during boost (see Appendix C). A recommended solution is to use the sawtooth-type joint (e) which is quite similar to the partially interleaved joint. In addition, the edges of the teeth (or fingers) are shown scalloped to provide more escape area for the air or purge gas (see dwg. No. 1).

In several designs wherein reliance is placed upon the space environment to evacuate the blanket sections, the extreme overlap is employed (mainly for dome caps) to expose maximum edge area.

The scrolled-type seam is utilized for those systems designed in this program that have individual blanket sections that are pre-evacuated either prior to or after installation on the tank. The scrolls can be utilized here because the joints are not being used as exits for the evacuation process. For those system concepts where rapid venting of the air or purge gases in the insulation during ascent is required the scrolled-type joint is not recommended since it acts as a very effective seal as shown in Appendix C.

Recommendations have been made by A. D. Little personnel, performing work under Contract NAS W-615, that consideration be given to perforating multilayer insulations to alleviate boost inflation of the insulation and to assist in subsequent evacuation of the insulation by the space vacuum environment.

The theoretical considerations presented in Ref. II-3 present arguments in favor of broadside pumping through perforated foils as opposed to edgewise pumping of the insulation. Attendant with perforations is an increase in radiative heat leak which must be traded off with reduction in gas pressure. The consequence of such a tradeoff, according to Ref. II-3, is the establishment of a minimum attainable

heat flux which depends upon the outgassing rate and the hydrogen gas leak rate from the tank. If leak-free welds cannot be manufactured, either some method of ducting the hydrogen gas overboard before it enters the insulation must be provided or a heat leak which is considerably higher than the ideal must be accepted according to Ref. II-3.

Additional conclusions resulting from the analyses presented in Ref. II-3 include the fact that the perforation configuration is of importance in determining how well the insulation can be pumped for a given perforation fraction (i.e., radiation leakage). In theory, better gas-pumping performance should be obtained with a large number of small holes whose spacing is much less than the foil separation distance.

It is obvious that, in view of the concern expressed here (and elsewhere in the literature) about this problem area, space evacuation, ensuing experimental programs should thoroughly explore this approach, and determine the validity of these theoretical considerations and the potentials of using perforations to alleviate problems of evacuation, as well as the boost inflation of the insulation should it prove to be a serious problem.

Perforations might also serve to enhance the probability of attaining the desired insulation pressure in a given length of time for a vacuum jacketed system which is permitted to cryopump upon introduction of the liquid hydrogen into the tank.

(8) Miscellaneous recommended procedures for installation and handling NRC-2 insulation. The following recommendations are based primarily upon the recommendation of NRC personnel:

(1) For areas of high compression, the number of layers per inch should be doubled or tripled.

(2) Generally, NRC-2 should not be compressed beyond 150 layers per in., and above 300 layers per in. the performance degrades rapidly.

(3) Generally, cold layers should not contact warm layers except where long lateral path lengths are provided; the cold-to-cold and warm-to-warm layer relationship should be maintained at all joints and boundaries.

(4) At joints, no optical paths should be present and at least a 4 or 5 in. overlap should be provided along the web between warm and cold boundaries.

(5) NRC-2 should be kept dry, free of dust and other contaminants. It should be handled with lint-free cotton gloves.

(6) Taping the insulation to tank supports, etc., should be done with heat sealable polyester-based tape. For temporary

supports during installation, mylar-based pressure sensitive tape can be used.

(7) For temperatures above 200° F, the maximum continuous duty temperature of mylar-based NRC-2, one of the higher temperature films (e.g., H-film) would have to be used.

(9) Martin recommended method of attaching NRC-2 insulation to cryogenic tankage. Two methods for attaching NRC-2 have been recommended for the system concepts evolved in this study. For those systems where the sealed mylar honeycomb subinsulation is used to provide adequate ground hold and ascent flight performance, the individual blanket sections are bonded to the subinsulation, the layers being connected at the boundaries of the sections. For other concepts, the nylon ropes and anchor system mentioned under the Linde SI discussion is employed. For this case, spacers are utilized locally where the ropes are attached to provide greater inherent thickness and less thermal degradation in these local areas. A more detailed discussion of each system is presented in Chapter IV.

Estimates of the thermal performance of a typical rope attachment area were made in order to assess the overall performance shown in Table V-1. The heat leak per foot estimated for this attachment concept is 0.06 Btu/hr-ft length.

c. Marshield insulations

The Marshield insulation is a class of insulations based upon the concept of using a limited number of relatively thick (3 to 5 mil) radiation barriers either self-separating or separated by low conductivity spacers. Marshield insulations differ from Linde and NRC multilayer insulations in that the foils and/or spacers are thicker, providing the shield with greater structural rigidity, and the foil spacing distance is wide compared to the present types. The low conductivity spacing may be provided by either of a number of methods as in Fig. II-19 and listed below:

(1) Radiation barrier separation methods

(1) Separate sheets as separators

a) Dimpled nonreflecting separator, e.g., impregnated fiber glass cloth

b) Corrugated nonreflecting separator

c) Reflecting-type separator, e.g., Al deposit on one side

(2) Radiation barrier self-separating

a) Dimpled barrier

b) Corrugated barrier

(3) Radiation barriers separated by discrete low conductivity spacers

a) Washers

b) Blocks

In each of these concepts, the spacers either may or may not be connected to adjacent sheets, depending on the method of attachment desired.

The primary impetus for conceiving the Marshield designs was to eliminate some of the major problems associated with the installation and use of the Linde SI and NRC-2-type insulations. The inherent advantages of the Marshield over that of the presently available multilayer insulations are considered to be as follows:

(1) A more positive structural attachment of the insulation to the tank or other members can be effected.

(2) Venting of the purge gases during ascent flight and subsequent evacuation of the Marshield to the desired pressure level by the space environment should be safe, quick and reliable.

(3) Hydrogen gases diffusing through the tank walls or welds and other material outgasses should be quickly and efficiently removed from the insulation by space evacuation.

(4) Efficient purging of the insulation should be readily accomplished.

(5) Thermal performance should be highly predictable and repeatable once basic thermal data are known.

(6) No compression or insulation recovery problems exist.

The major disadvantages appear to be poorer thermal performance and the larger insulation thicknesses required.

(2) Density and thermal performance. The density of an acceptable Marshield design will vary from 2 to 5 lb/ft^3 depending on foil thickness, spacer thickness and material, and foil separation distance. A typical Marshield insulation might include ten 3-mil aluminum foils and ten dimpled, phenolic-impregnated, 5-mil fiber glass cloth spacers. Typical foil spacing is 1/8 of an inch which is provided, for example, by the dimple height.

The ideal heat leak through Marshield has been estimated to be from 4 to 6 times higher than for the other multilayer insulations, i.e., the effective thermal conductivity is an order of magnitude higher but the useful thickness is greater. However, when the estimated penetration, installation, and joint heat leaks are included in the performance of each, the resulting overall payload penalty is reduced to a factor of two to three times greater. There appears to be a fairly wide range of missions for which this would be an acceptable penalty--particularly in view of the fact that this comparison assumes ideal performance for the other multilayer insulations (which may not be attainable).

Appendix B presents a theoretical analysis of Marshield. To date no thermal tests have been performed on Marshield--these should be performed at the earliest possible opportunity to determine if this concept warrants any further development.

(3) Optimum spacing. For some Marshield concepts, the spacing distance between foils is not too critical insofar as affecting the weight of the insulation (e.g., the dimpled spacer concept). The primary effect of varying spacing distance for this concept is to change the conductive component of the heat leak and the insulation thickness.

For the Marshield concept involving the use of discrete spacers, there is an optimum spacing distance. That optimum occurs where the weight increase due to spacer material increase no longer can be offset by the reduction in heat leak due to the longer conduction path provided by the spacer. In general, however, the optimum spacing appears too large to be practical for most installations (i.e., insulation thickness becomes too great). Therefore, each configuration must be examined to determine the maximum allowable thickness which can be utilized. The general trends associated with spacing changes are indicated below.

Optimum Spacing Increases With:	Optimum Spacing is Independent of:	Optimum Spacing Decreases With:
1. Decreasing number of foils	1. Foil thickness or density	1. Decreasing orbit time
2. Velocity increment decreases		2. Decreasing shroud temperature
3. I_{sp} increases		3. Increasing spacer density or k-value

(4) Acoustic and mechanical vibration response. Acoustic and mechanical vibration tests have been conducted on the Marshield insulation at the Baltimore Division. The results of these tests indicate that these environments present no problems.

The Marshield specimen used in these tests consisted of eight 0.003-in. thick aluminum radiation shields that were two by two feet square. They were separated by 0.004-in. thick sheets of phenolic impregnated fiber glass, dimpled alternately up and down with a 1-in. square spacing. The alternating dimples spaced the radiation shields approximately 1/4 in. The sheets were not interconnected. They were secured to a base panel by being placed loosely over 1/2-in. diameter pins through holes in their four corners.

The specimen was subjected first to an acoustic sound pressure level of 155 db for 5 min followed by 160 db for 1 min. Observation during test showed no significant response and the specimen was generally undamaged by the test.

The specimen was then subjected to random vibratory excitation perpendicular to its plane. The excitation was 25 g rms with the input spectrum flat between 100 and 1000 cps and 6 db per octave roll-off on each end. The response of the Marshield was minimal, with no resulting damage.

(5) Installation considerations. Type 1a,(see (1)a under radiation barrier separation methods) Marshield is used in the present design study where the pieces are installed on the tank by slipping precut holes in the foils and spacers over a row of nonmetallic pins around the manhole and a row around the equator. There exists a small radiation window in the area around the pins. The total additional heat leak per pin including the conduction through the pin has been estimated at 0.365 Btu/hr-pin. At the other joints in the shield, the intersecting foils and spacers are overlapped and joined with clips. No additional heat leak is estimated for these junctures.

(a) Edge effects. The very low solidity of the Marshield design makes it necessary to be extremely careful not to expose the edges to radiative heat fluxes. For the spherical tankage used for comparing the various system concepts, no edge problems exist. However, for cylindrical tankage, the edges where the shield terminate must be guarded. This could be accomplished by turning down the foil edges to minimize the optical path, or by the use of auxiliary patches of another type of insulation such as NRC-2 to cover the edges.

(b) Tank supports and line penetrations. While it is considered possible to use Marshield insulation to cover the penetrating components, it is unnecessary, inefficient, and can be better accomplished by the use of other insulation types, e.g., NRC-2.

(6) Ground hold performance. Marshield insulations may be purged with helium to provide adequate ground hold performance when used on hydrogen tanks for short periods of ground hold. This type of ground augmentation presently appears more reasonable than adding a subinsulation unless longer ground hold periods are specified.

The helium gas between many layers will not be in a stagnant condition as it will be in the Linde SI and NRC-2 insulations. Natural convection loops will occur between some layers, and the nature of the heat transfer will vary from almost pure gas conduction in the outer hotter gaps to laminar-free convection in the inner colder gaps.

The Marshield ground hold performance for the example design was computed by assuming conduction throughout and increasing this to account for the convection effect in the inner layers. The convection effect will vary with ambient conditions, but for the design criteria used in this study (see Table II-1) this was estimated to be from 10 to 15%.

2. Insulations for Augmenting Multilayer Insulations*

Multilayer insulations are highly efficient for protection against thermal radiation. But the radiation heat transfer mode becomes dominant only when gas conduction is essentially eliminated and solid conduction is minimized.

Because of this, multilayer insulations alone do not provide adequate protection while the tankage is in the atmosphere, unless the insulation in encased in a vacuum-tight jacket or the condensible gases in the insulation are purged and replaced with a non-condensible gas.

a. Purpose of subinsulations

An alternative method of using multilayer insulations without having to evacuate or purge is to employ a subinsulation adjacent to the tank wall. The purpose of using a subinsulation is to provide a sufficient temperature rise across its thickness to prevent air liquefaction within the multilayer insulation. Candidate subinsulations being considered are corkboard, foam and mylar honeycomb. These insulations likewise have air or condensible gases trapped in them which would condense or freeze upon filling the tank with liquid hydrogen.

b. Sealing of subinsulations

Use of subinsulations is predicated upon sealing its outer surface in order that it may be cryopumped to an evacuated condition. This evacuation improves the thermal conductivity of the subinsulation, and can also be useful in holding the subinsulation on the tank.

Successful sealing of these insulations has been accomplished. For example, polyurethane foam as reported in Ref. II-10 was sealed with a mylar-aluminum foil laminate. Also mylar honeycomb has been reportedly sealed with the mylar-aluminum laminate--called Zero

*The state of the art in this field of subinsulations is rapidly advancing so that some of the information presented here may be outmoded.

Perm Vapor Barrier in the Saturn program. Extensive work on cork sealing methods has been conducted by the Martin Denver Division. This effort has included sealing methods such as bonding of glass cloth to cork with polyurethane adhesive, lamination of the cork with polyurethane adhesive, the use of aluminum foil and mylar laminates, etc.

c. Properties and performance of corkboard

Corkboard can be obtained at a variety of densities from 7 lb/ft^3 to as high as 30 lb/ft^3. The properties of corkboard vary with density. The thermal conductivity of corkboard is a weak function of density, but varies significantly with temperature. For thermal and performance calculations, a cork density of 12 lb/ft^3 was assumed, and the thermal conductivity data was semiempirically represented by $k_{cork} = 8.4 \times 10^{-4} T^{0.53}$ Btu/ft-hr-°R. Figure II-20 gives the heat flux through a corkboard layer installed on liquid hydrogen tankage as a function of cork thickness and warm boundary temperature.

Other properties of corkboard of interest are:

$$C_{p_{cork}} \cong 1.5\, C_{p_{air}}$$

Thermal expansion coefficient, $\alpha \cong 10\, \alpha_{aluminum}$

Service temperature--up to 250° F before charring begins.

Martin-Denver experience with cork indicates that corkboard can be successfully bonded to liquid hydrogen tanks without cracking or splitting occurring due to thermal stresses if bonded to the tank wall under compression. The bonding materials with the best low temperature properties appear to be the polyurethane resin adhesives.

d. Properties and performance of foams

Sealed foam subinsulations are attractive because they can provide the same thermal performance as corkboard at lower weight per square foot of tank surface. There are at least eight basic types of foams having a variety of densities from 1.0 lb/ft^3 to as high as 70 lb/ft^3. The thermophysical properties of each foam are moderately different, and the choice depends upon the application. References II-11, II-12 and II-13 give properties and the results of tests performed on various foams for use in cryogenic applications.

The available thermal conductivity data on the selected foam was represented by the following equation:

$$k_{foam} = 1.72 \times 10^{-4} T^{0.7465} \text{ Btu/hr-ft-°R.}$$

Figure II-21 presents the heat flux through the foam layer as a function of foam thickness and warm boundary temperature.

Evacuation of foams, as with corkboard, either by active pumping or by cryopumping (as assumed in this study) may lower the thermal conductivity by a factor of 1.5 to 2 in some cases. This is due to the lowering of the gas conduction component of the thermal conductivity to negligible proportions.

Sealed foam can be bonded to the external surfaces of hydrogen tankage. However, since thermal stresses are likely to be high due to tank shrinkage as well as the temperature drop across the foam layer, it appears desirable not to rely wholly on the bond to keep the foam in place. If the foam seal is tight, the nearly one atmosphere of pressure across it should keep the foam positioned. In addition, a method of foam installation reported in Ref. II-10 appears to have merit. This involves using a constrictive over-wrap of fiber glass yarn to hold the sealed foam to the tank.

e. Sealed mylar honeycomb as a subinsulation

Mylar honeycomb is made by Hexcell Products, Inc., and is available at densities from 0.5 lb/ft^3 to 2.25 lb/ft^3 and cell sizes from 3/8 to 1-1/2 in. When bonded, surface sealed and cryopumped, it has been found to be an excellent ground insulation. For the purposes of this study a 3/8-in. cell mylar honeycomb having a density of 2.1 lb/ft^3 was selected and it was assumed that its thermal performance was at least as good as that of the sealed, cryopumped polyurethane foam. Recent experimental data on the thermal conductivity of cryopumped mylar honeycomb is available in Ref. II-15.

For bonding of the honeycomb to metal, Hexcell recommends one of several hot-melt adhesives (e.g., Fuller R-4145), Shell Chemical Epon 828 epoxy adhesive, or duPont 40901 polyester adhesive. The outer surface seal may be bonded to the honeycomb face with similar adhesives. The Saturn V vehicle liquid hydrogen tankage insulation experimental program has had success with a Narmco polyurethane adhesive for the above purposes, however (see Ref. II-15).

D. REFERENCES

II-1. "Analysis of Thermal Protection Systems for Propellant Storage During Space Missions," A. D. Little, Inc., Report No. 63270-04-03, Contract NAS 5-664 (ASTIA No. 270973), December 1961.

II-2. "Cryogenic Insulation Research," Martin Company Report ER 13346P, April 1964.

II-3. "Final Report on Contract No. NAS W-615," A. D. Little, Inc., Report No. 65008-00-04, October 1963.

II-4. "Linde Company Superinsulation Applied to Space Vehicles," Revised 1 December 1962, C. R. Lindquist, Linde Company, Division of Union Carbide Corporation.

II-5. "Preliminary Test Results on a Compressed Multilayer Insulation System for a Liquid-Hydrogen-Fueled Rocket," by P. J. Perkins, M. A. Colaluca and L. S. Smith, Vol. 9, Advances in Cryogenic Engineering Paper B-1, 1963 Conference.

II-6. "NRC-2 Insulation" brochure, 1962, National Research Corporatio Cambridge, Massachusetts.

II-7. "First Quarterly Progress Report for the Period 1 September 1962 to 31 December 1962," A. D. Little, Inc., Contract NAS W-615, Report No. 65008-00-01, January 1963.

II-8. "Second Quarterly Progress Report for the Period 1 January 1963 to 31 March 1963," A. D. Little, Inc., Contract NAS W-615, Report No. 65008-00-02, April 1963.

II-9. "Thermophysical Properties of Solid Materials," WADC TR-58-476 (Vol. IV), November 1960.

II-10. Perkins, P. J., Jr. and Eager, J. B., "A Lightweight Insulation System for Liquid Hydrogen Tanks of Boost Vehicles," Fifth Annual Structures and Materials Conference, April 1964.

II-11. Spieth, C. W., et al., "Rocket Vehicle Tankage Research for a Cryogenic Propellant," Beechcraft R&D, Inc., WADC TR-58-530, September 1958.

II-12. Haskins, J. F., "Thermal Conductivity of Plastic Foams from 423° to 75° F," Advances in Cryogenic Engineering, Vol. 7, Proceedings of 1961 Cryogenic Engineering Conference, Plenum Press, New York, 1962.

II-13. Coxe, E. F., et al., "An Investigation of the Use of Internal Insulation for Liquid Hydrogen Fueled Missiles," Proceedings of the 1962 Cryogenic Engineering Conference, Vol. 8, Plenum Press, New York.

II-14. Barron, R. F., "Superinsulators," Machine Design, 2 March 1961.

II-15. Middleton, R. L., et al., "Development of a Lightweight External Insulation System for Liquid Hydrogen Stages of the Saturn V Vehicle," 1964 Cryogenic Engineering Conference, Paper L-3.

II-16. Frainier, R. J., "Experimental Performance and Selection of Cryogenic Rocket Insulation Systems," Proceedings of the 1960 Cryogenic Engineering Conference, Vol. 5, 1961.

E. ILLUSTRATIONS

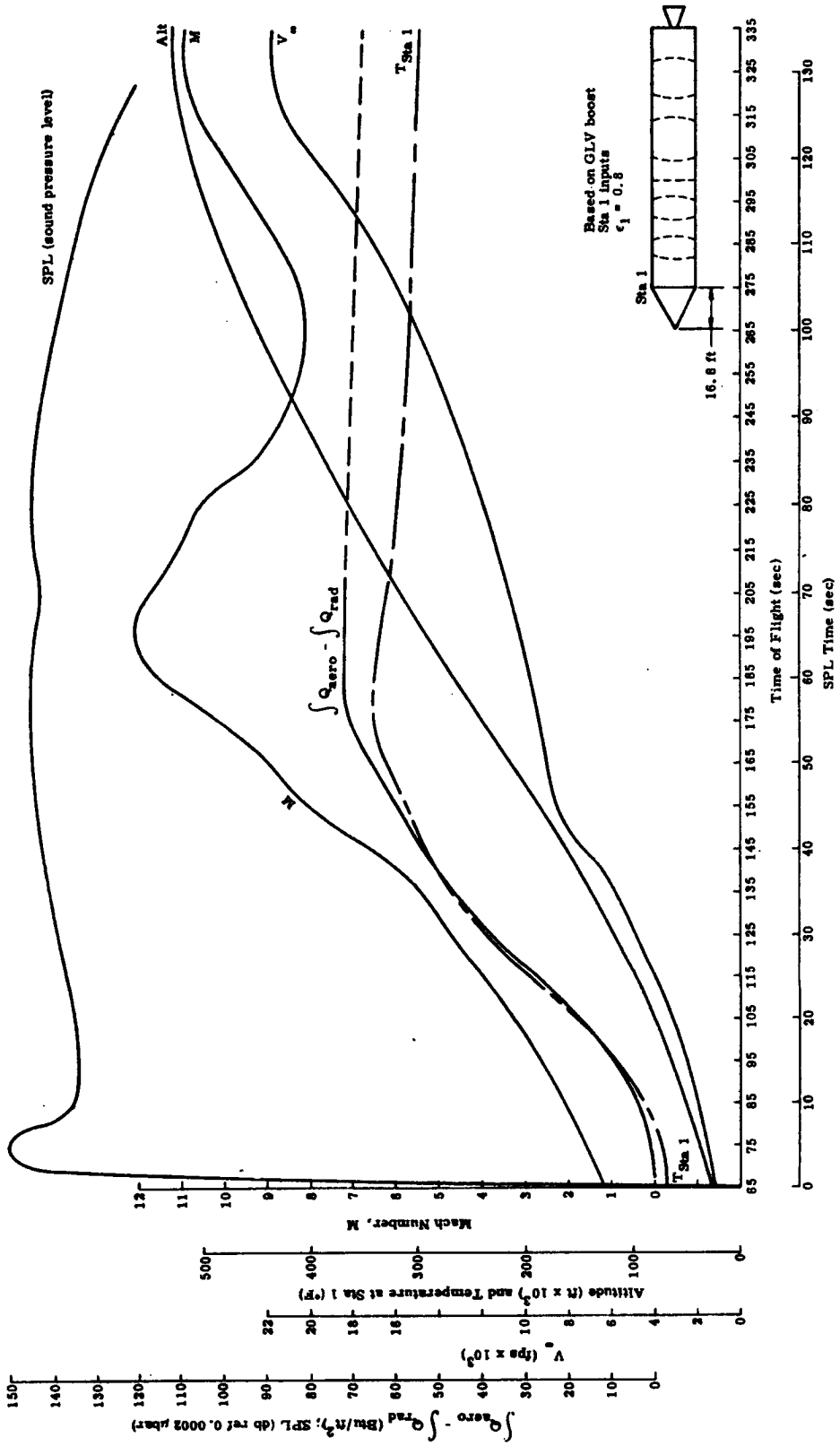

Fig. II-1. Typical Boost Trajectory Elements

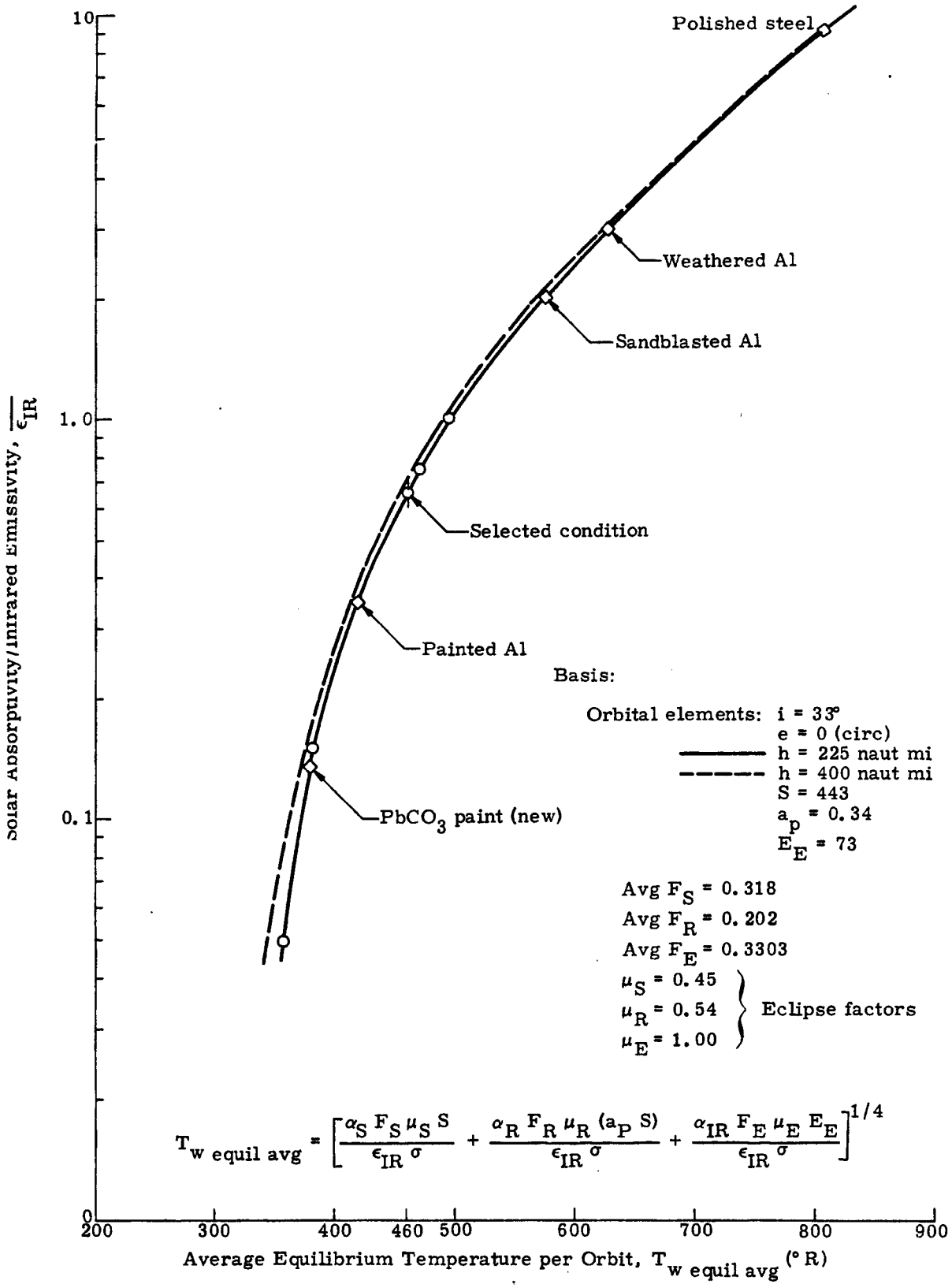

Fig. II-2. Propellant Tankage Equilibrium Temperature for Model Orbit

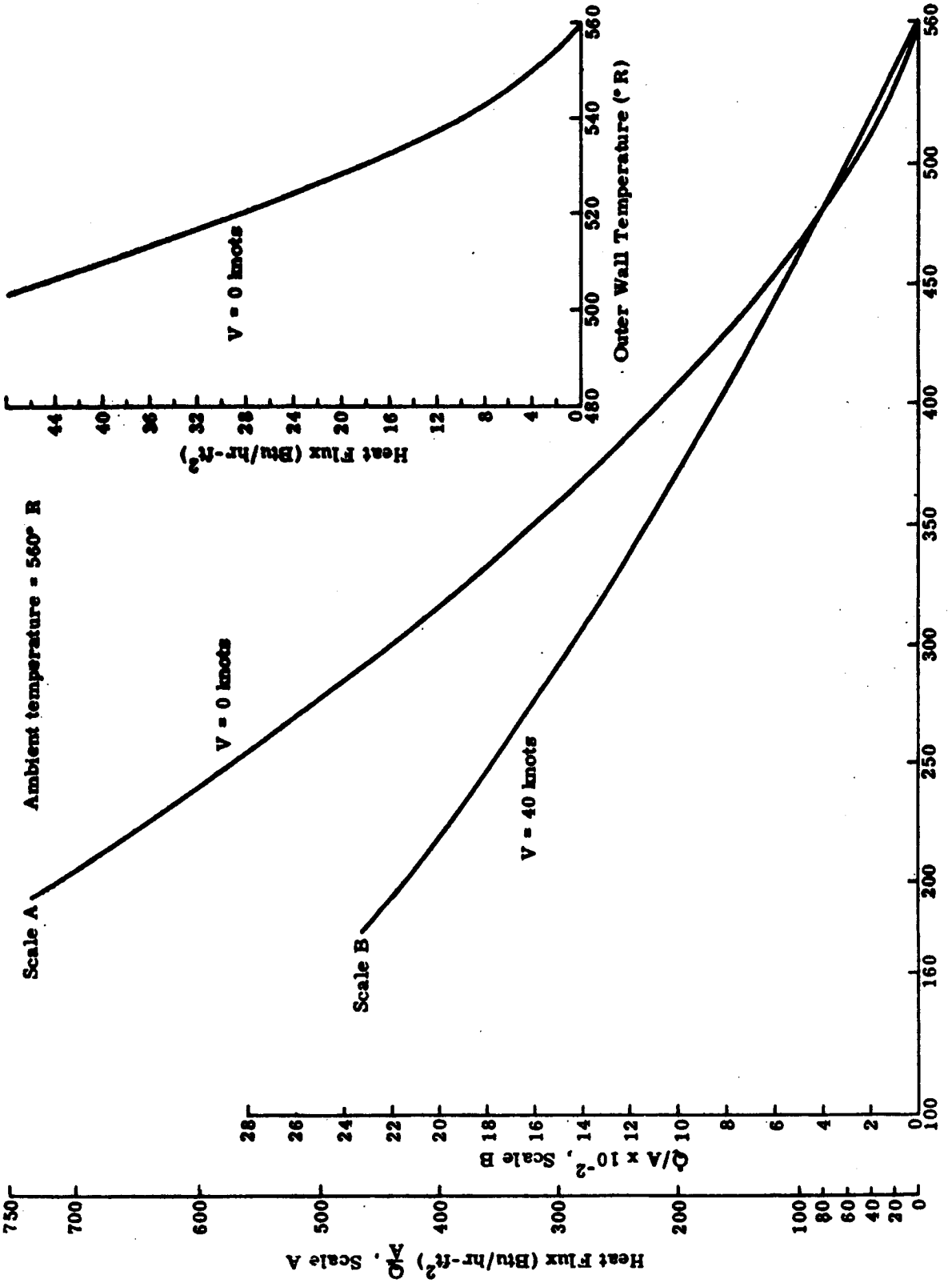

Fig. II-3. Convective Heat Flux to Cylindrical Tankage at Launch Pad Conditions

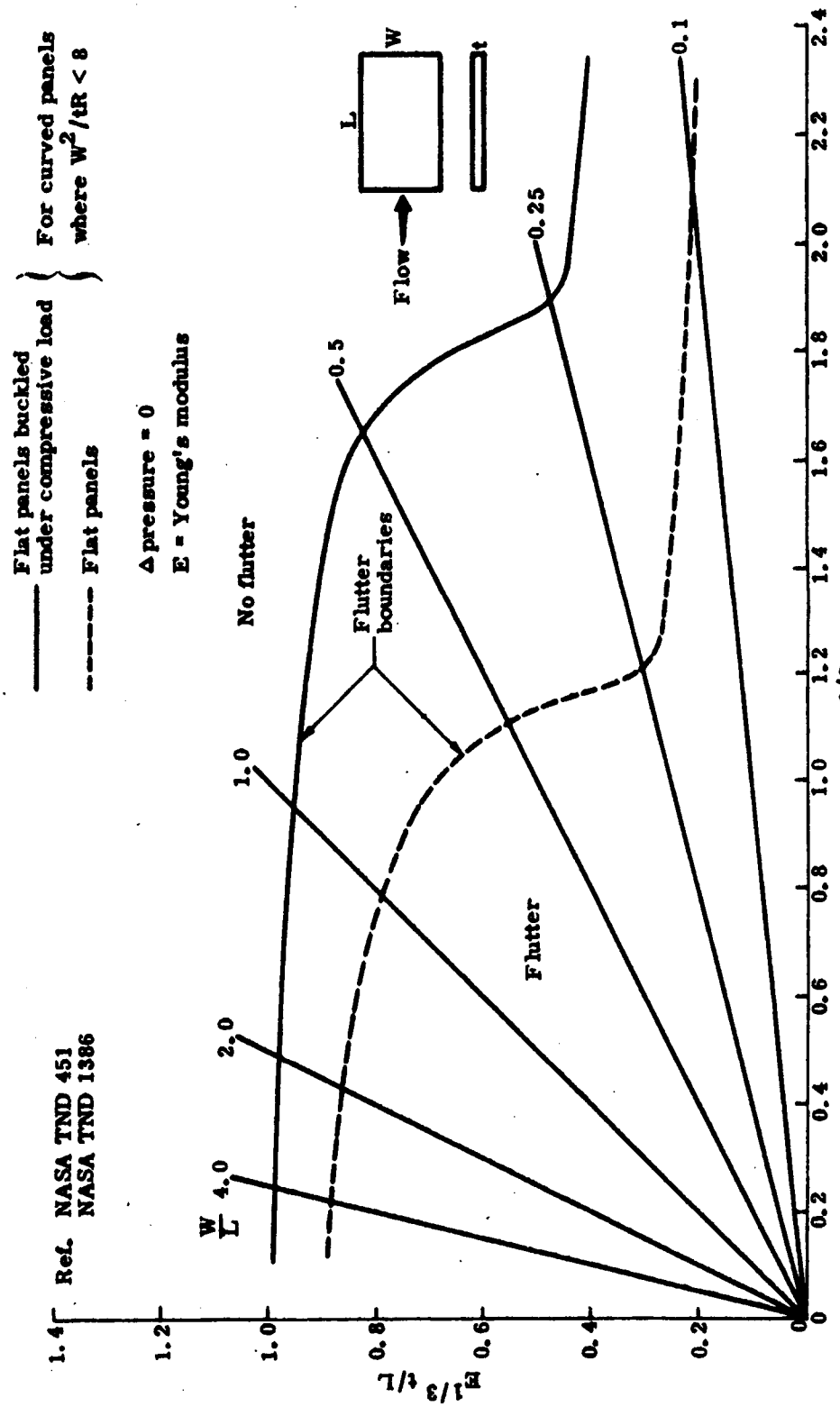

Fig. II-4. Design Flutter Boundaries for $(\sqrt{M^2-1}/q)^{1/3} = 0.60$

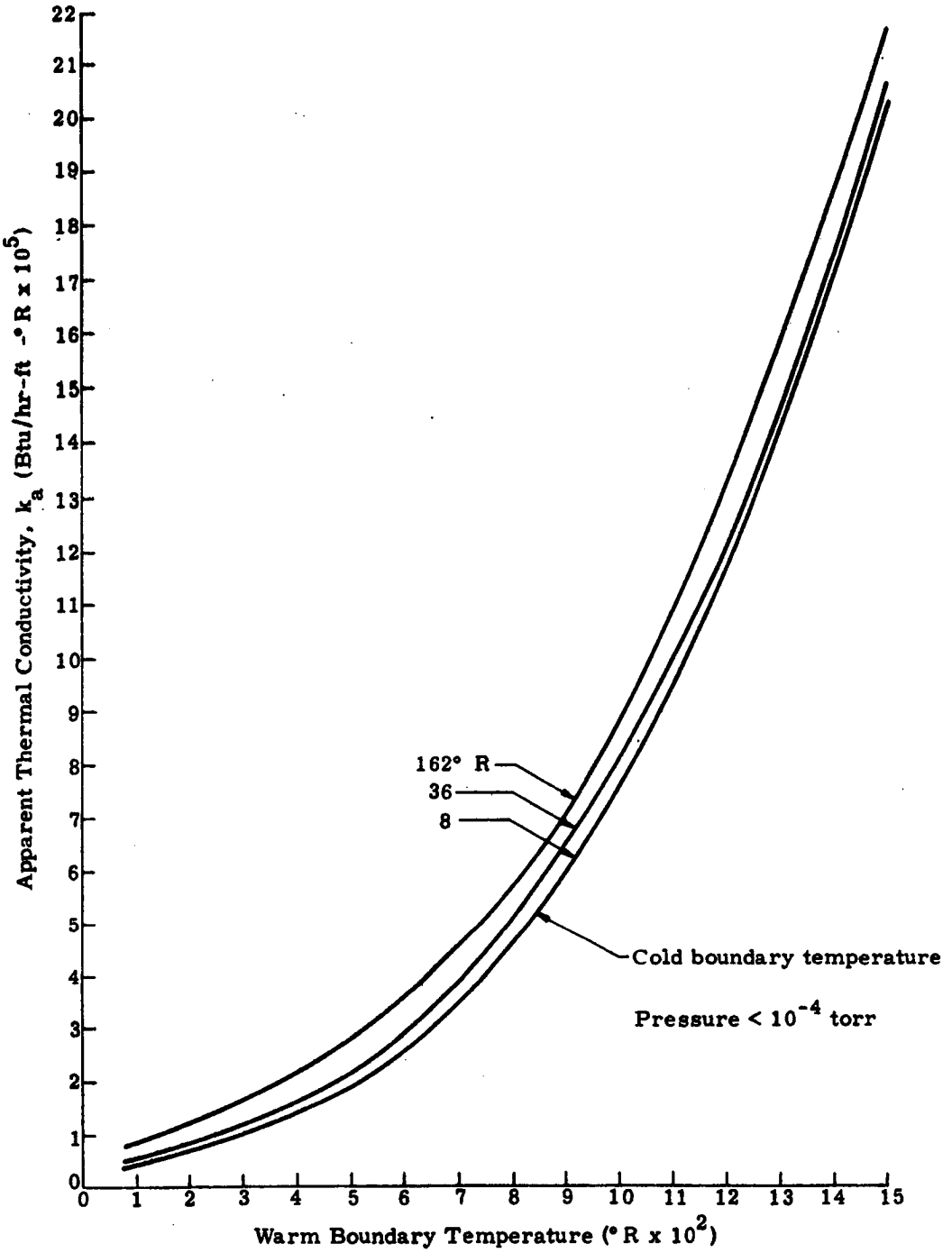

Fig. II-5. Apparent Thermal Conductivity of Linde SI-44

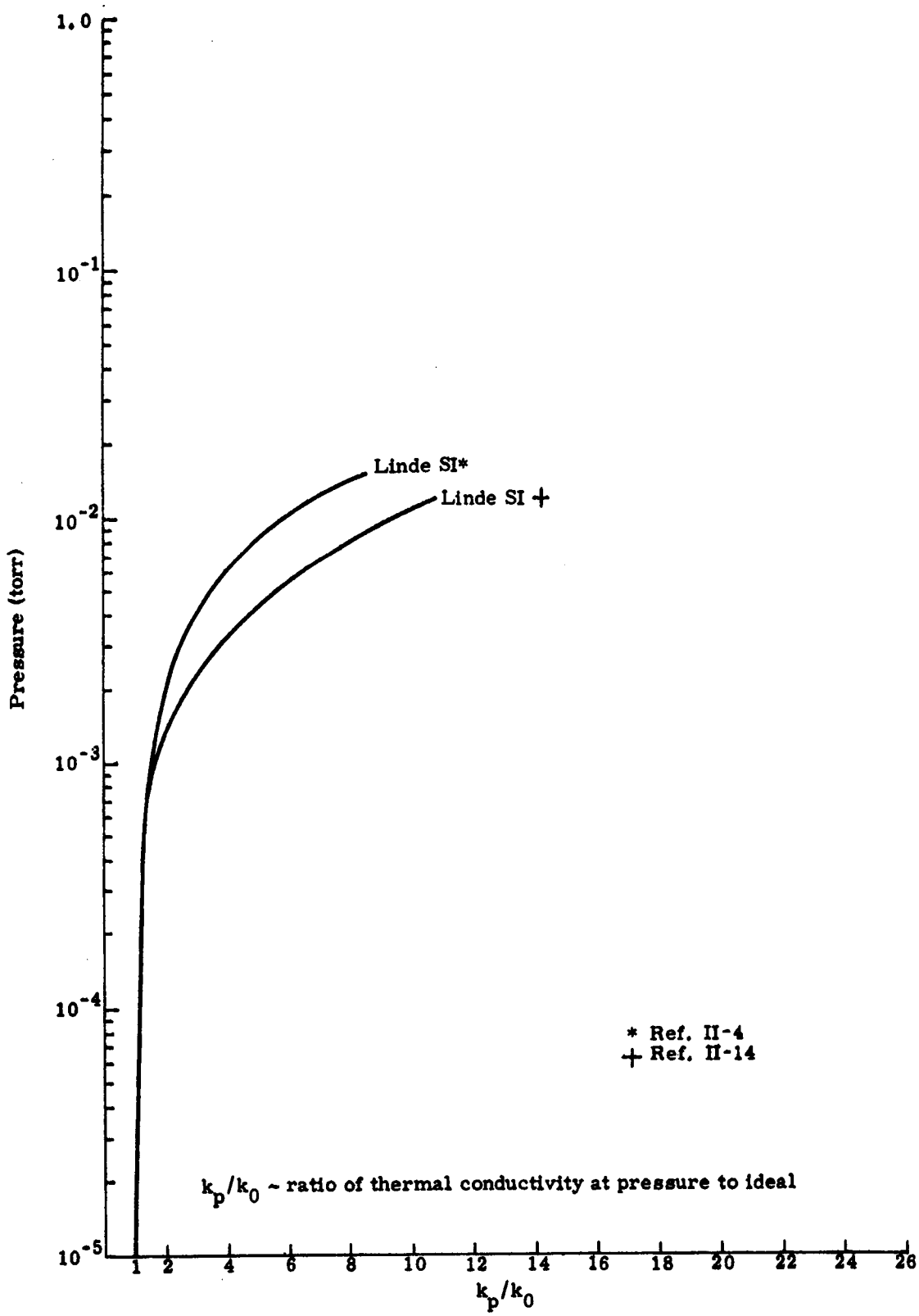

Fig. II-6. Effect of Residual Gas (air) Pressure on Thermal Performance of Multilayer Insulations

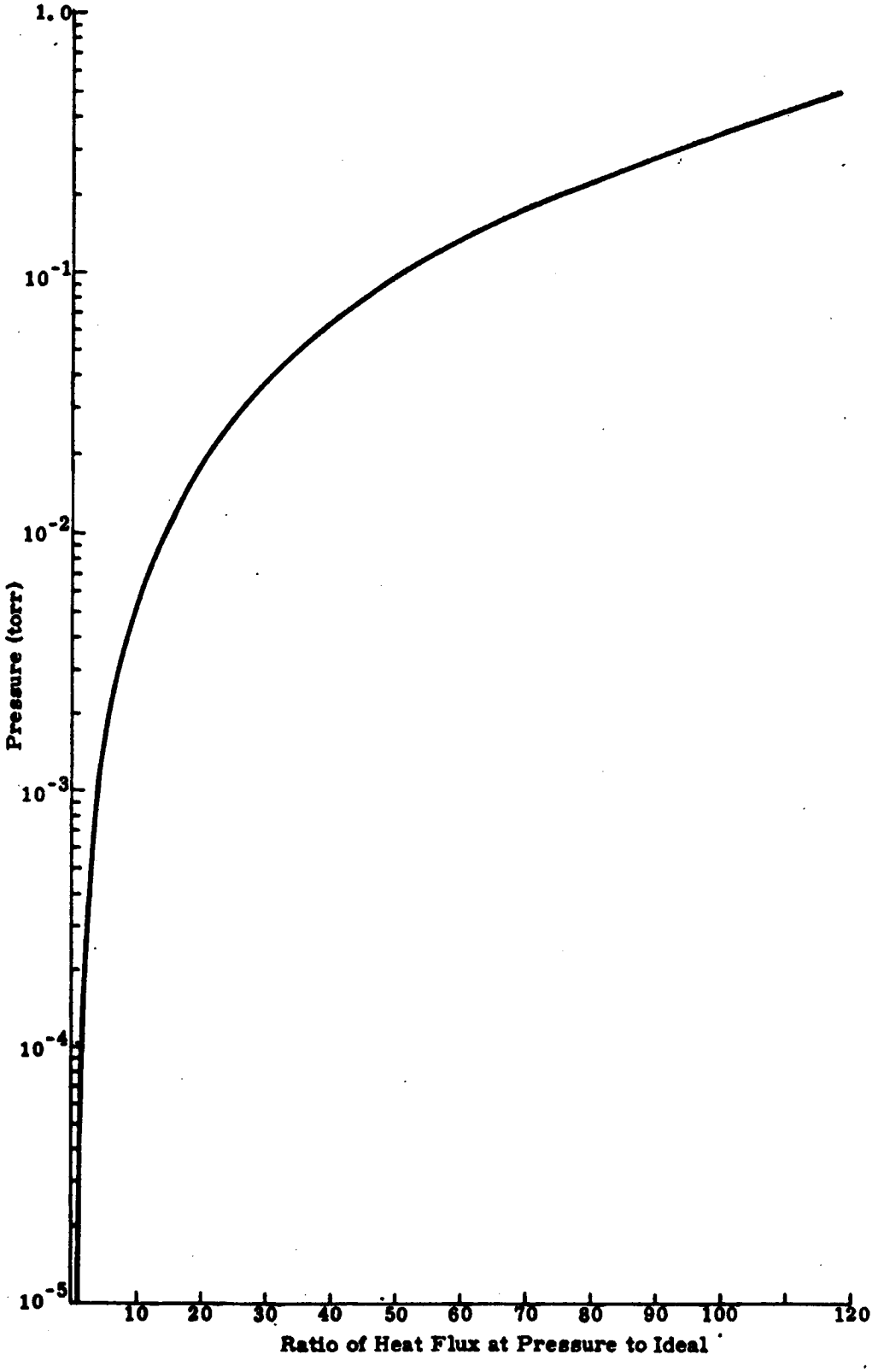

Fig. II-7. Effect of Residual Helium Purge Gas Pressure on the Performance of Linde SI

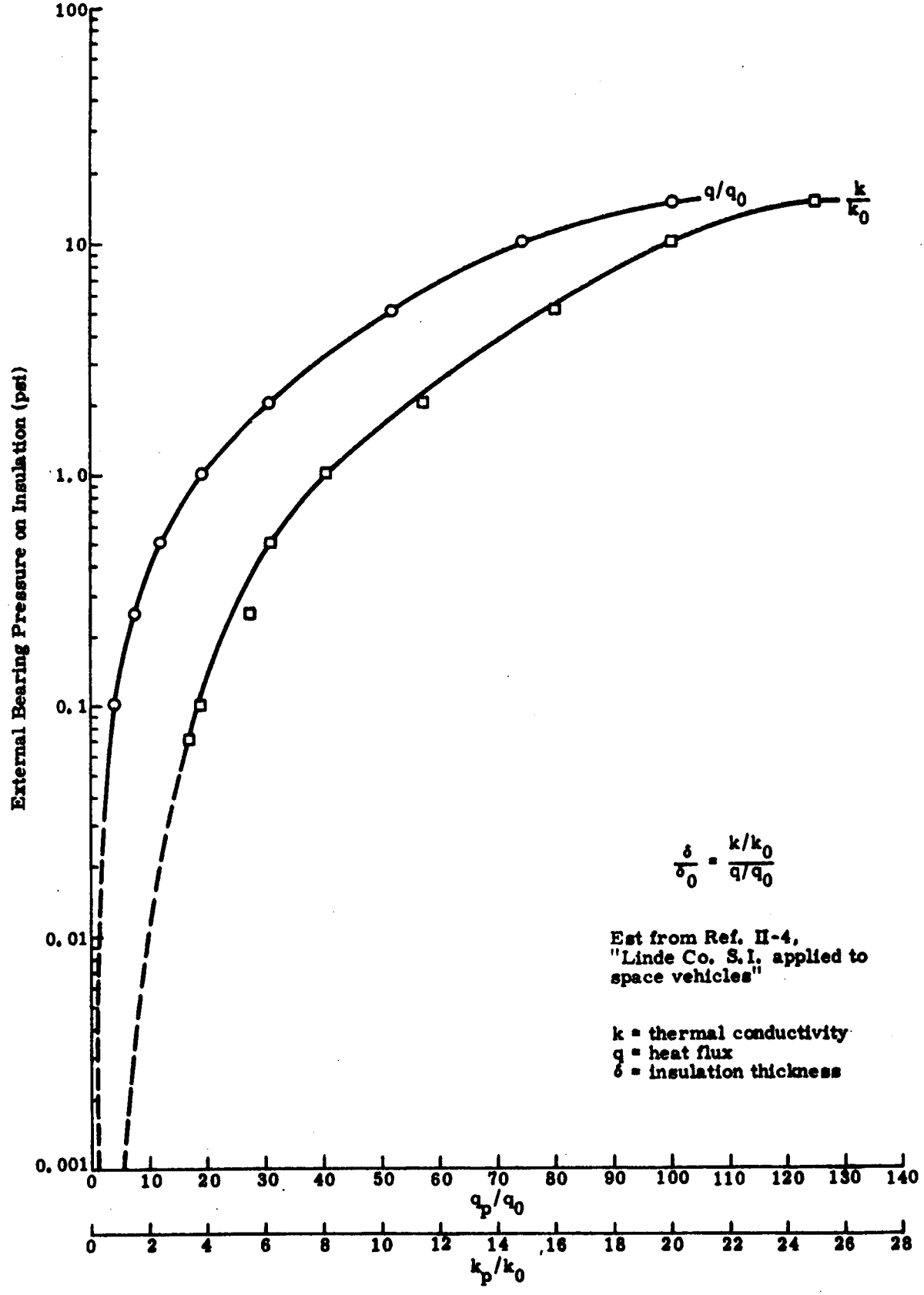

Fig. II-8. Performance of Superinsulation Under External Pressure

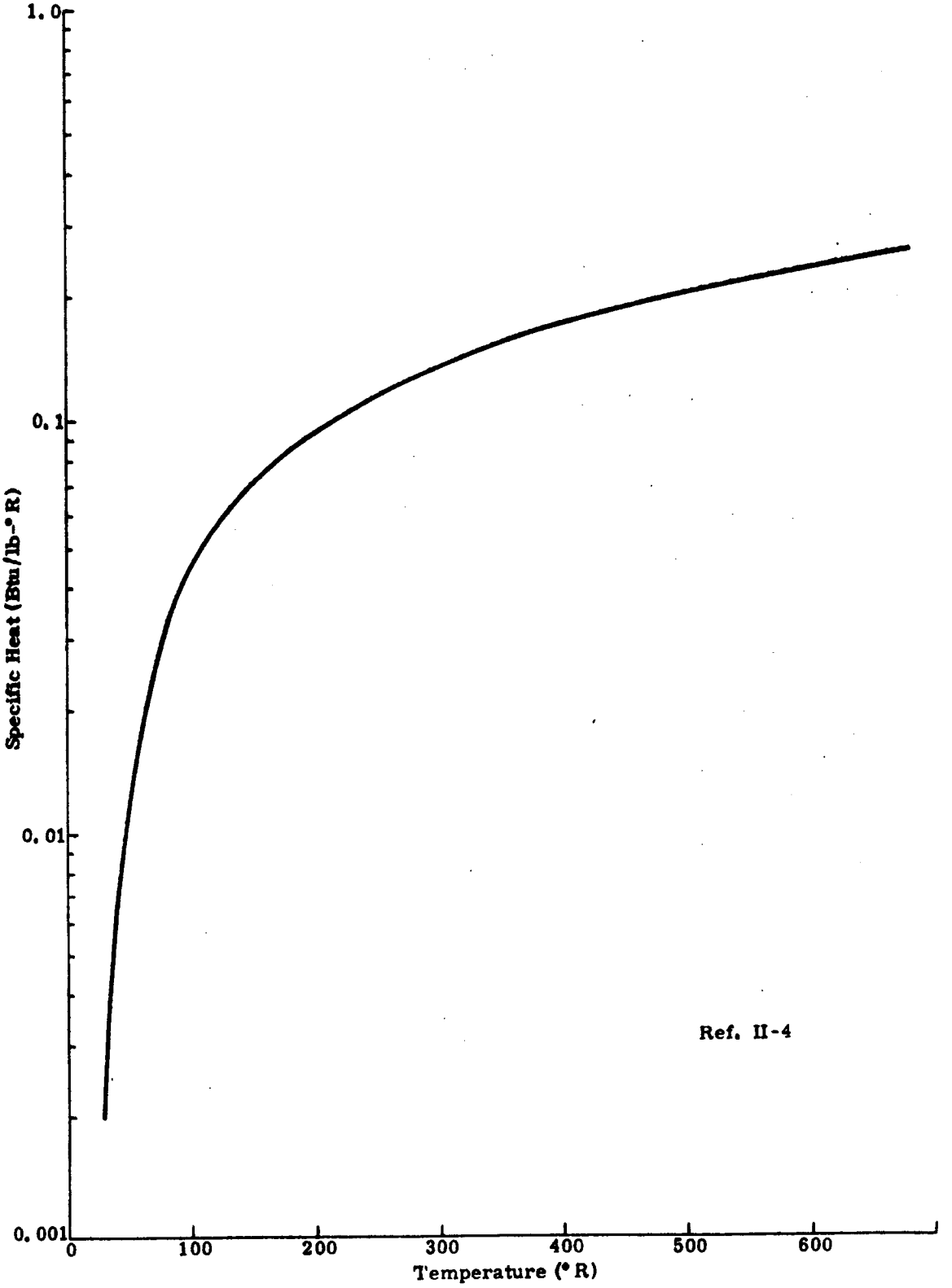

Fig. II-9. Specific Heat of Linde SI Versus Temperature

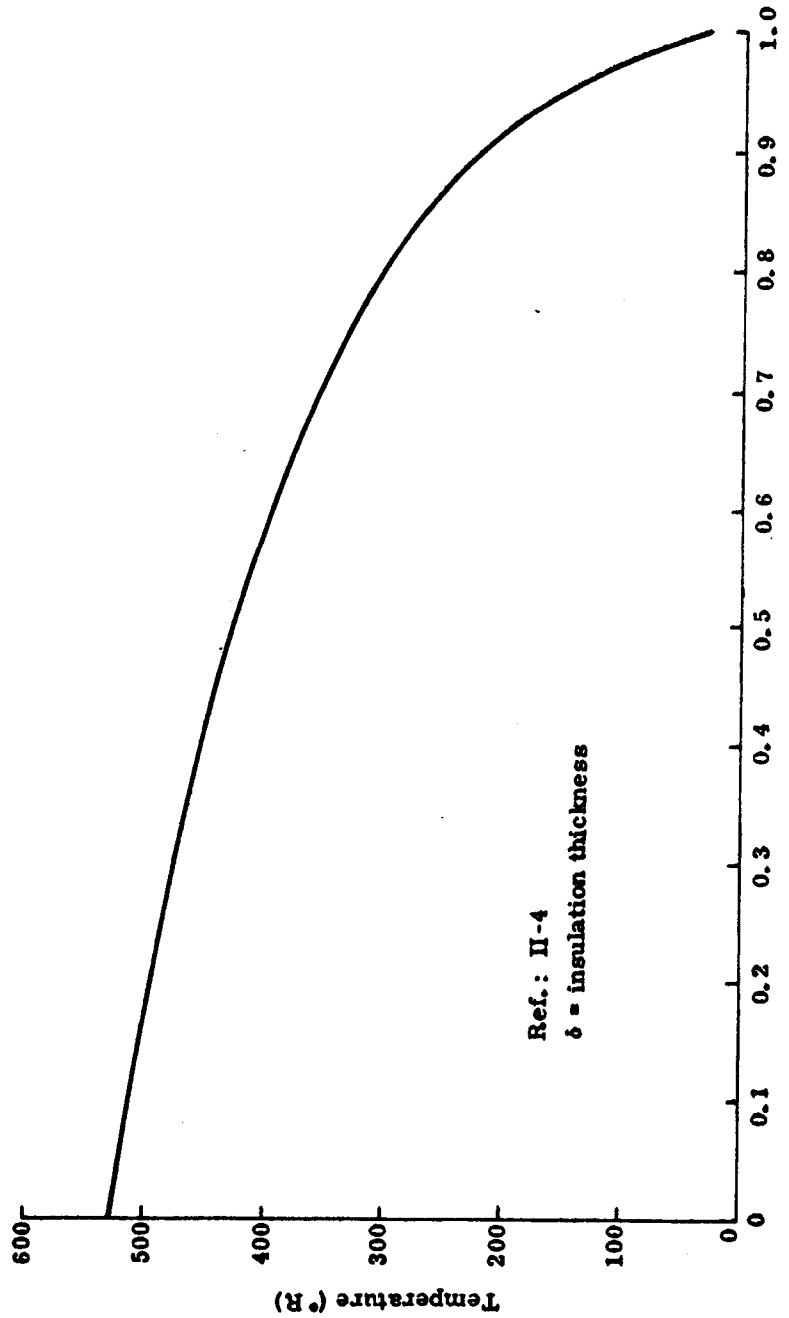

Fig. II-10. Typical Temperature Distribution Across a Linde Superinsulation

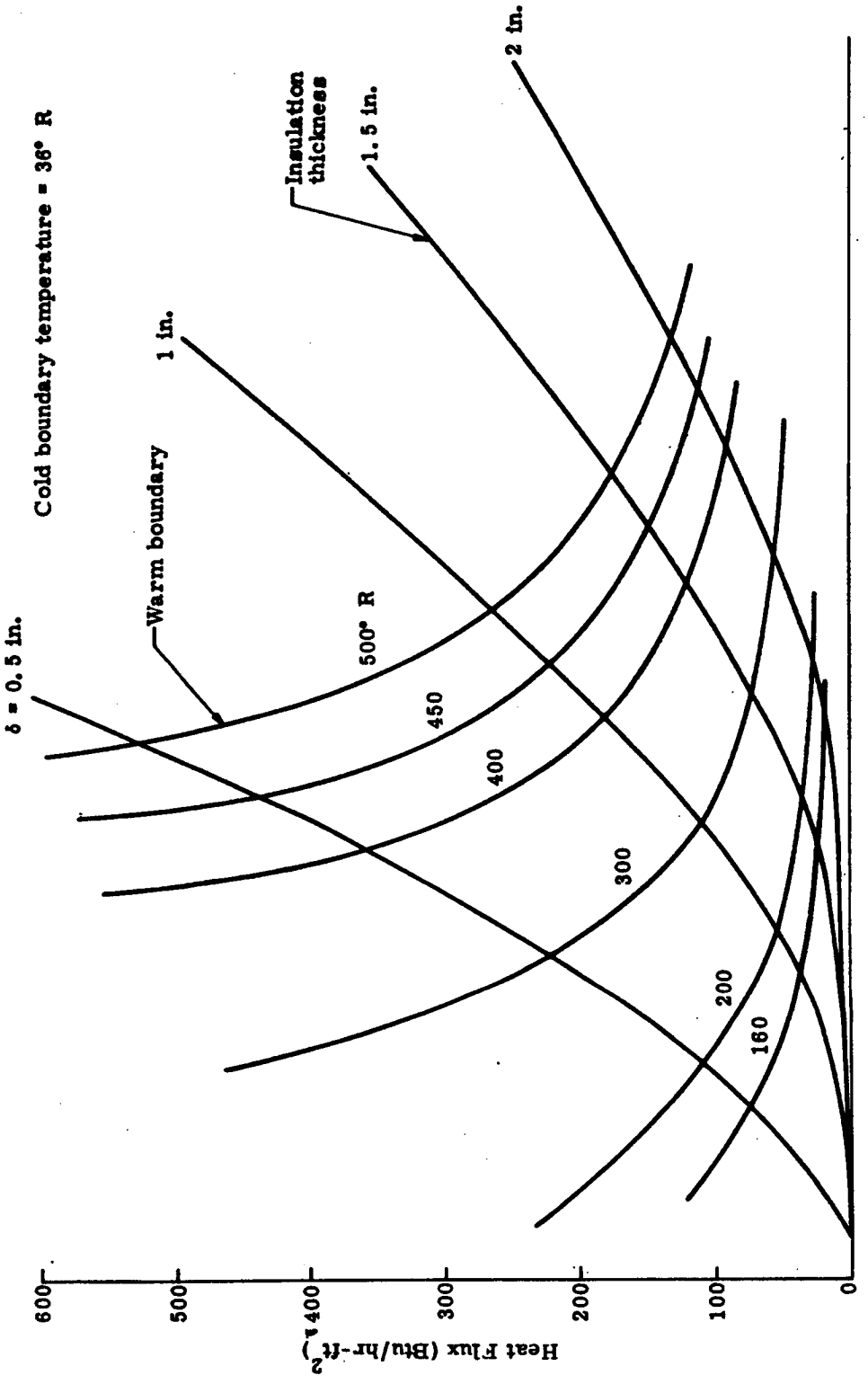

Fig. II-11. Heat Flux Across Helium Purged Multilayer Insulations

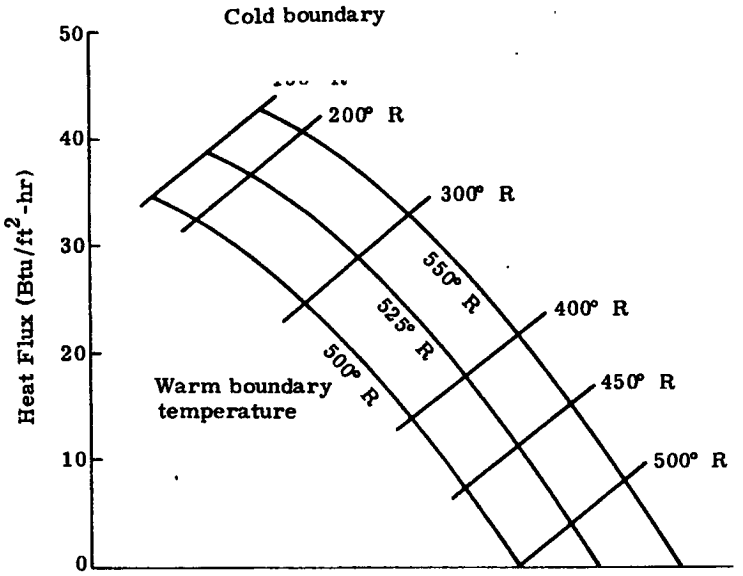

$$\dot{Q}/A = \frac{1.542 \times 10^{-4}}{\delta_i} (T_h^2 - T_c^2)$$

where

δ_i = in

T = °R

and the following empirical expression for conductivity of air in this temperature range has been used:

$$k = 2.57 \times 10^{-5} T \left(\frac{\text{Btu-ft}}{\text{ft}^2\text{-hr-°R}} \right)$$

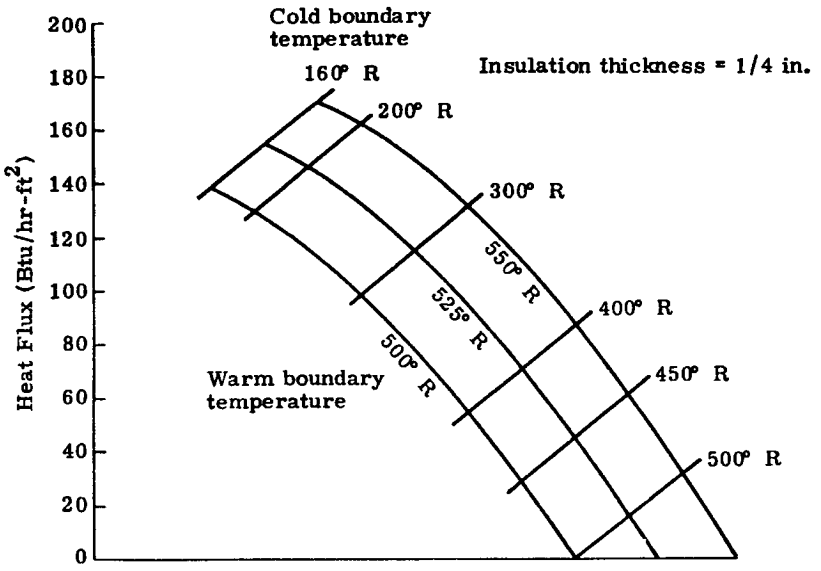

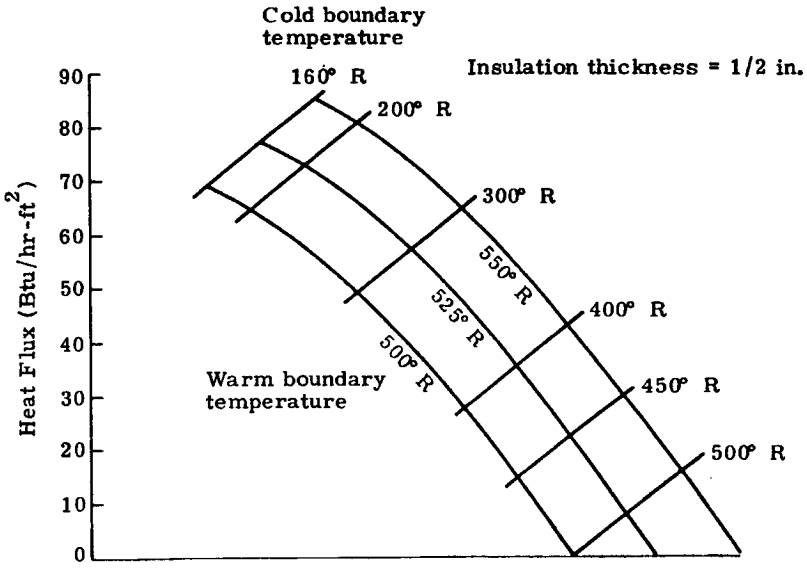

Fig. II-12. Heat Flux Across Air-Filled Multilayer Insulations at Launch Pad Conditions

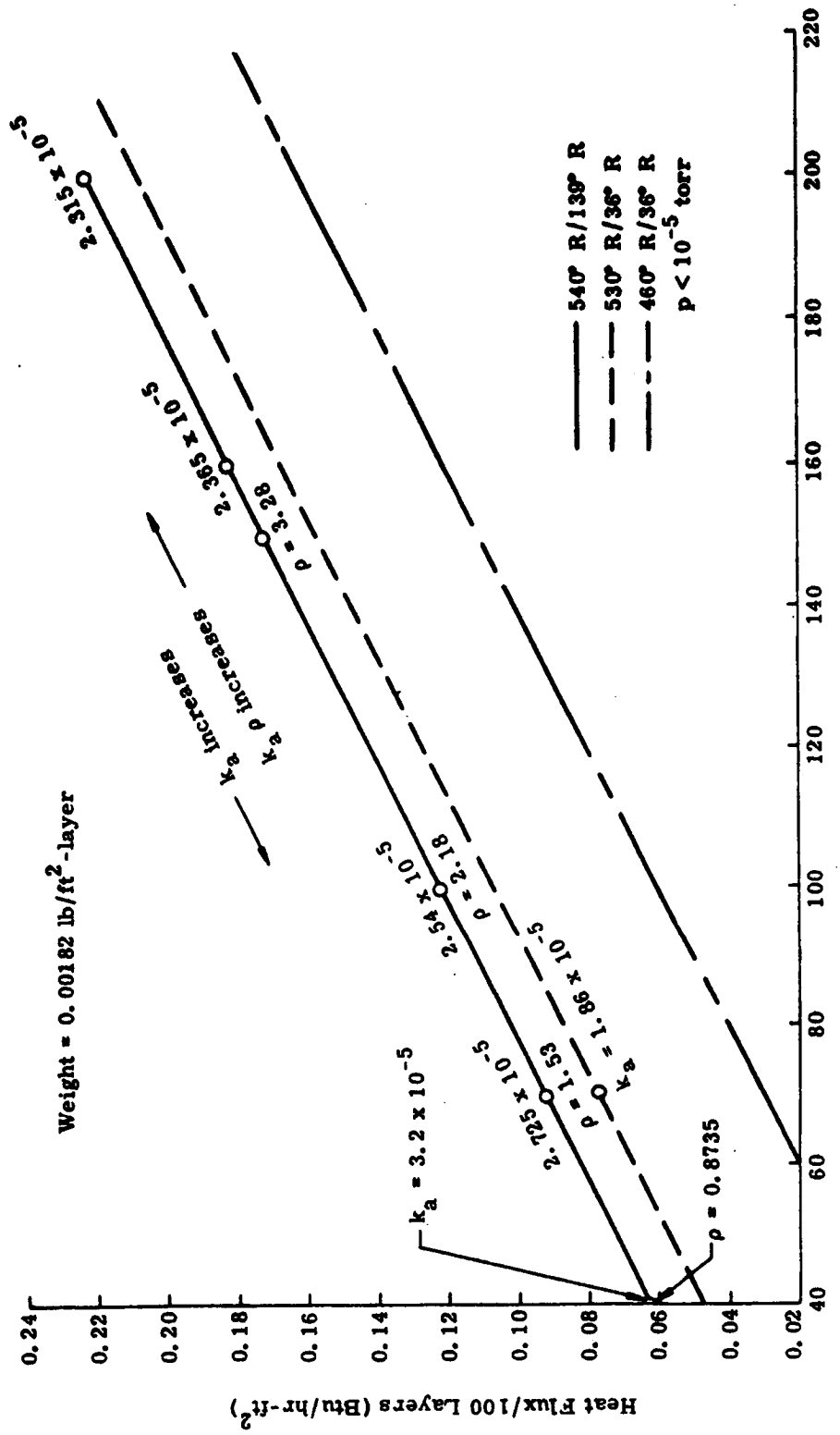

Fig. II-13. Thermal Performance of Evacuated NRC-2 Insulation

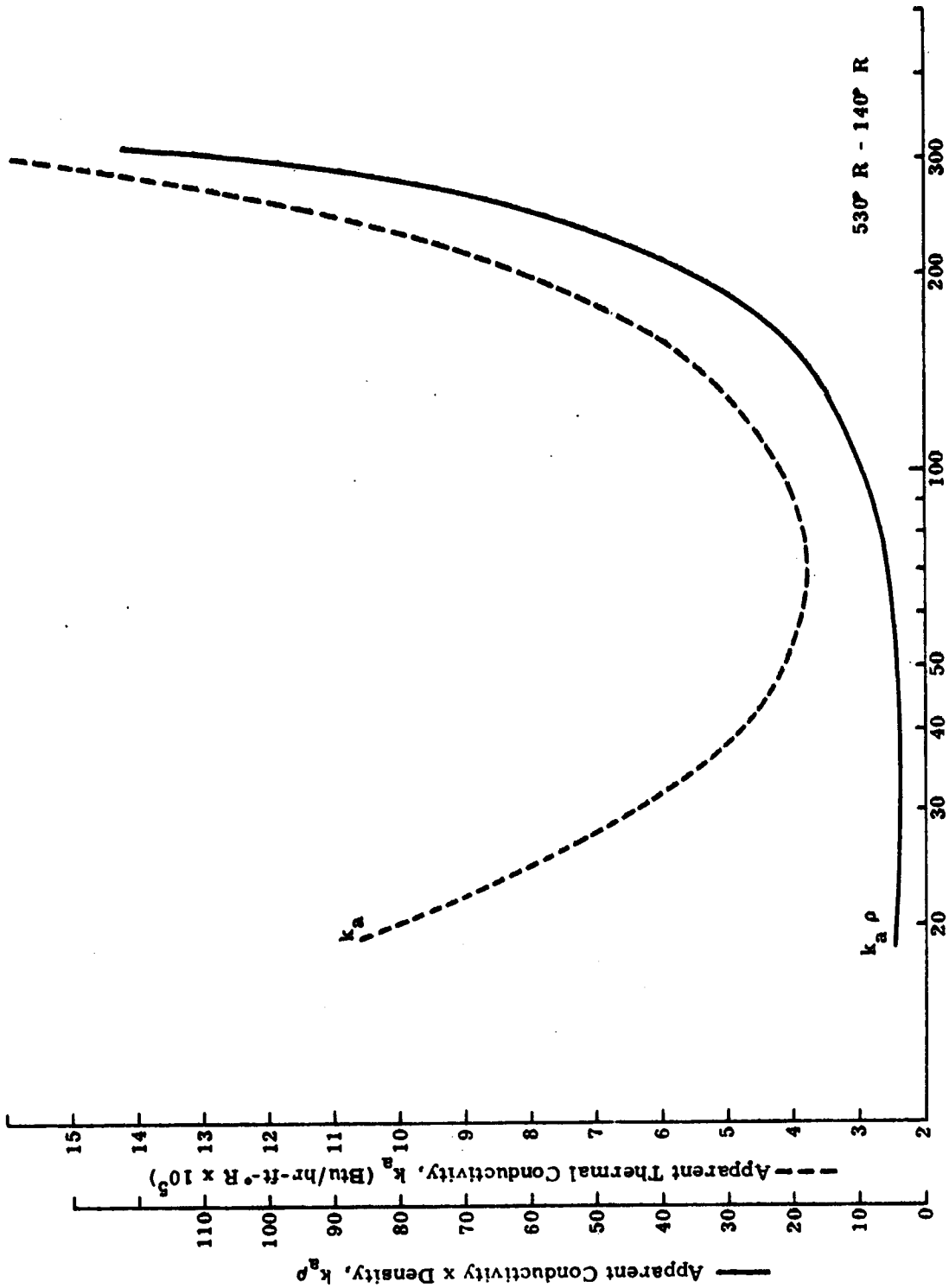

Fig. II-14. NRC-2 Thermal Conductivity and Conductivity-Density Product as a Function of Number of Layers per Inch

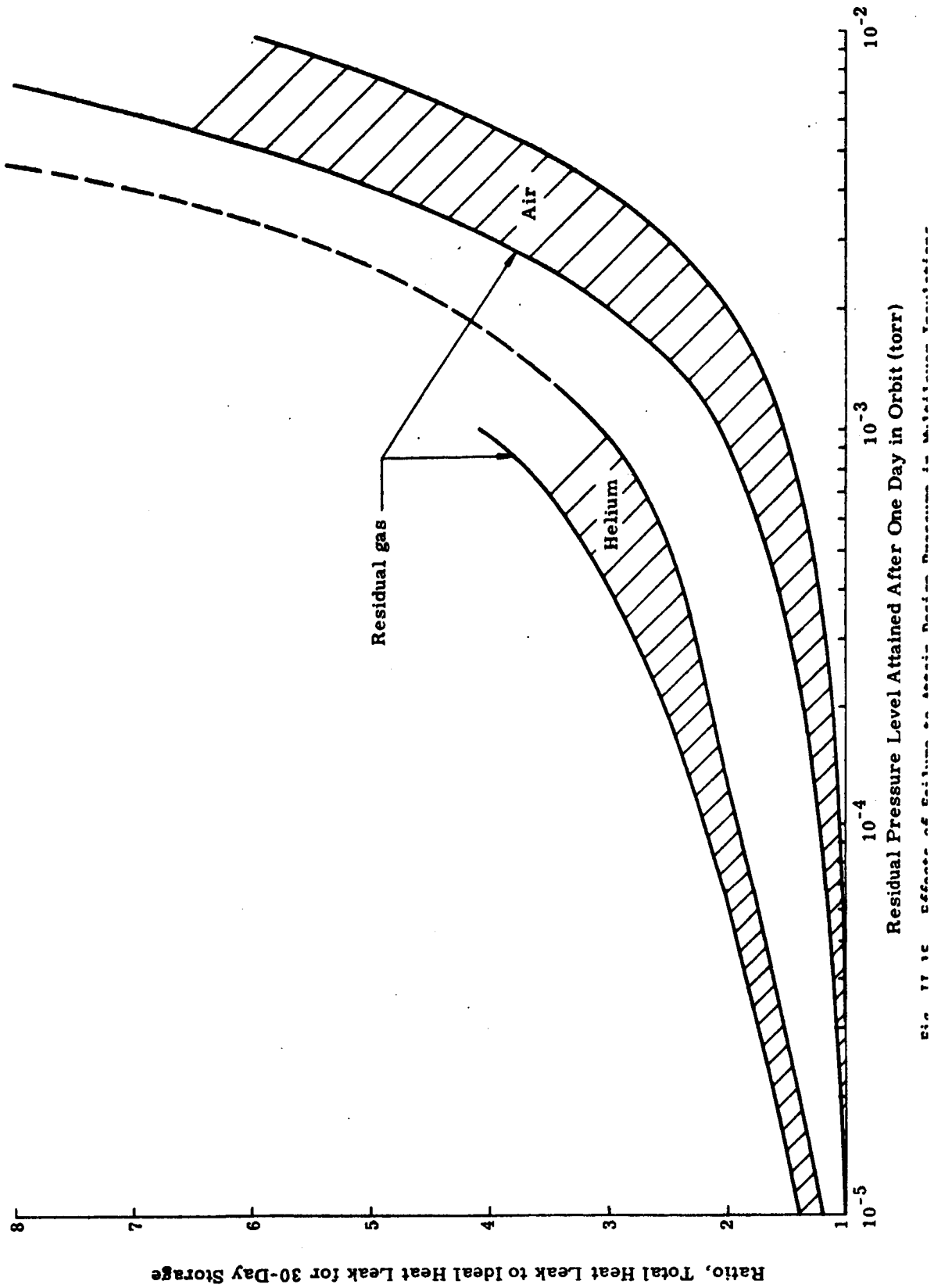

Fig. II-15 Effects of Helium or Argon Residual Pressure in Multilayer Insulation

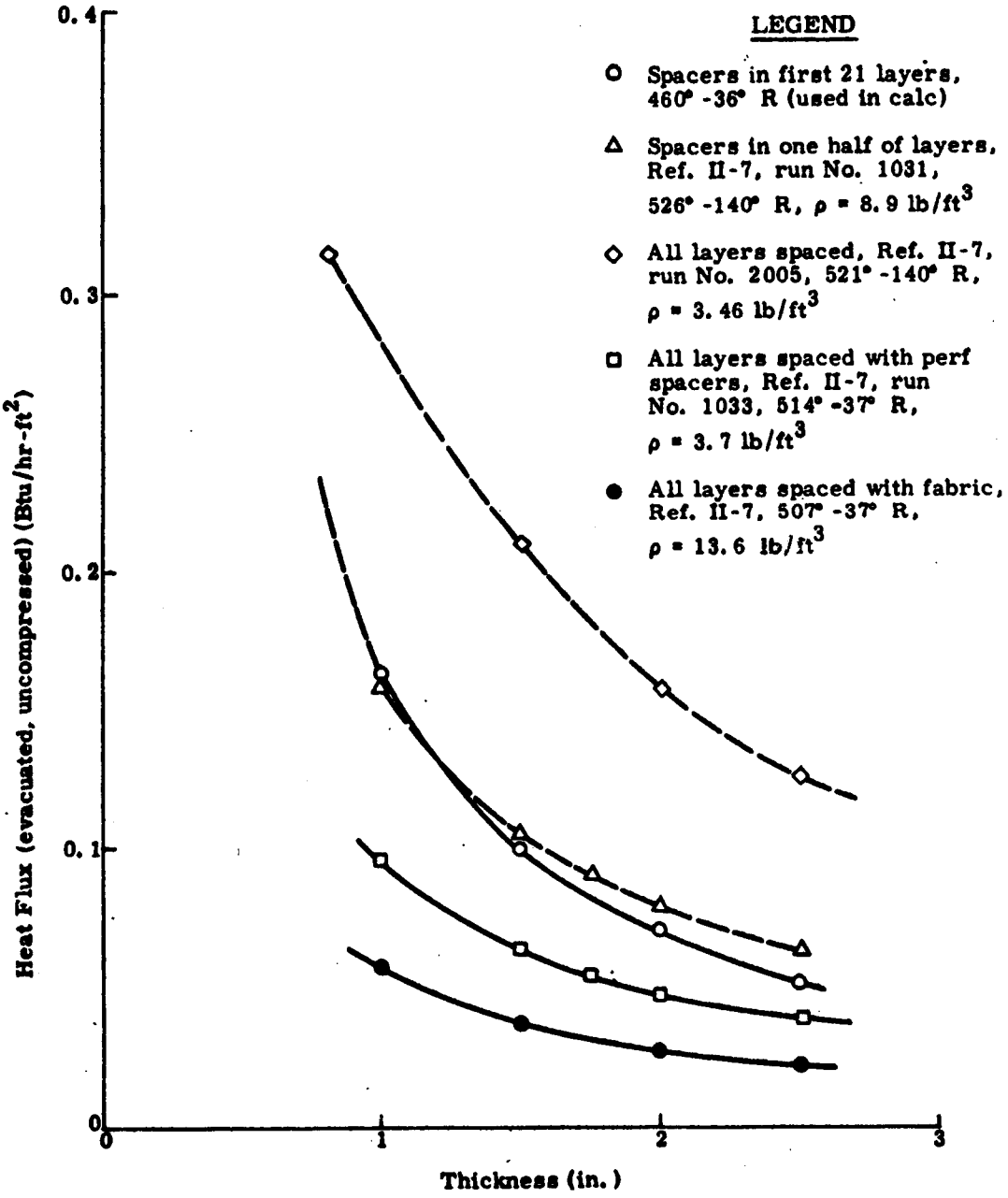

Fig. II-16a. Thermal Performance of NRC-2 Type Insulation with Various Spacer Configurations

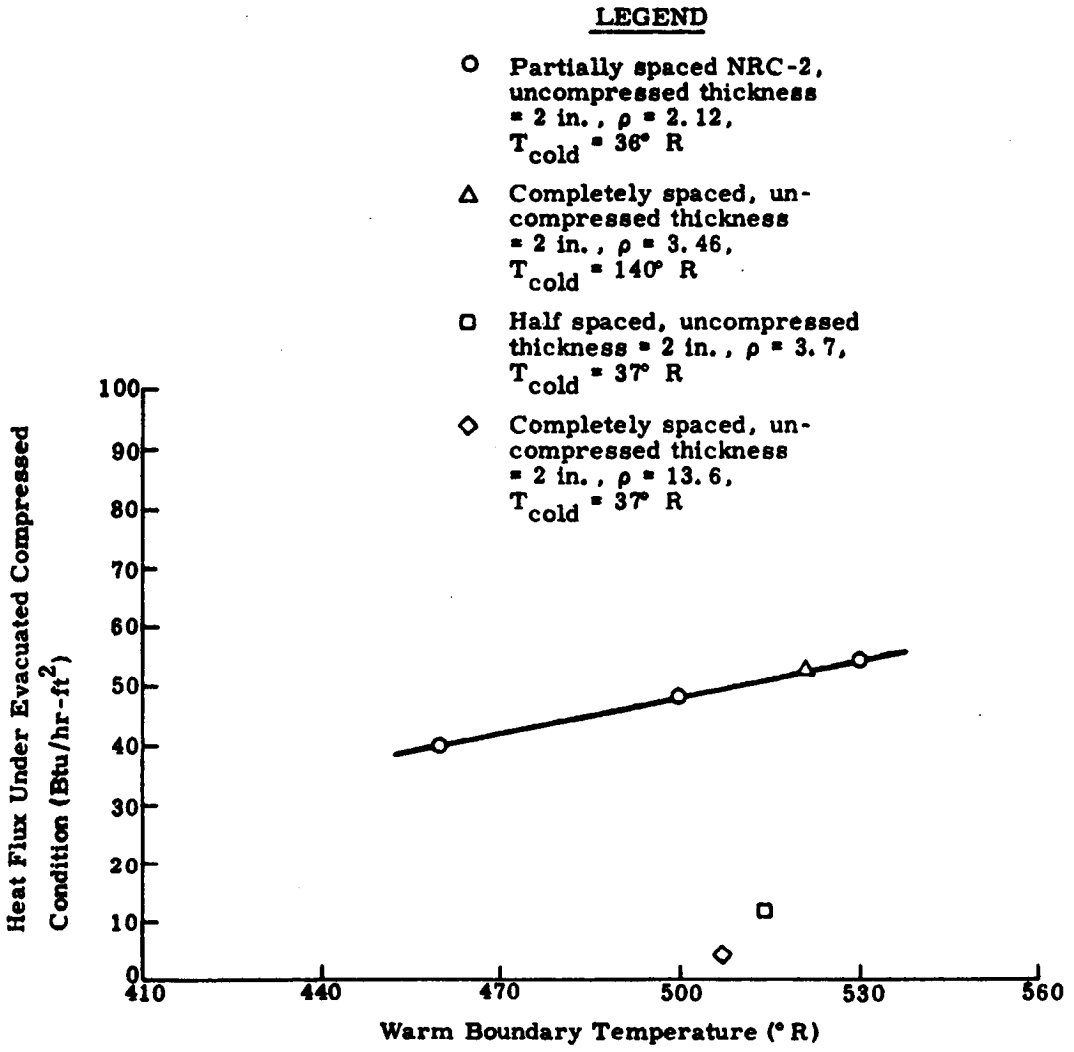

Fig. II-16b. Assumed Performance for NRC Insulation with Partial Spacers at Compressed (1 atm), Evacuated Conditions

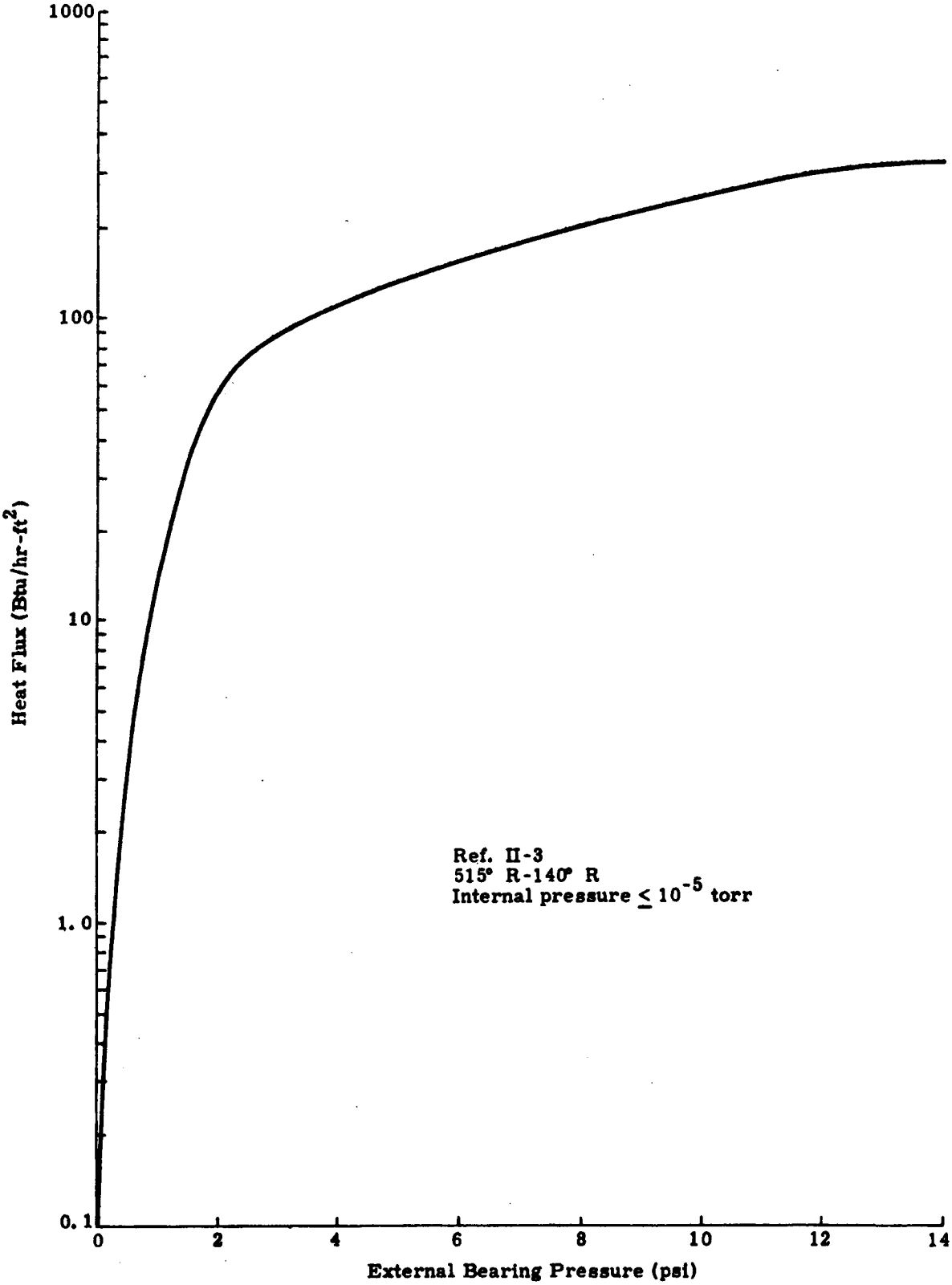

Fig. II-17. Effect of External Compression Loading on NRC-2 Thermal Performance

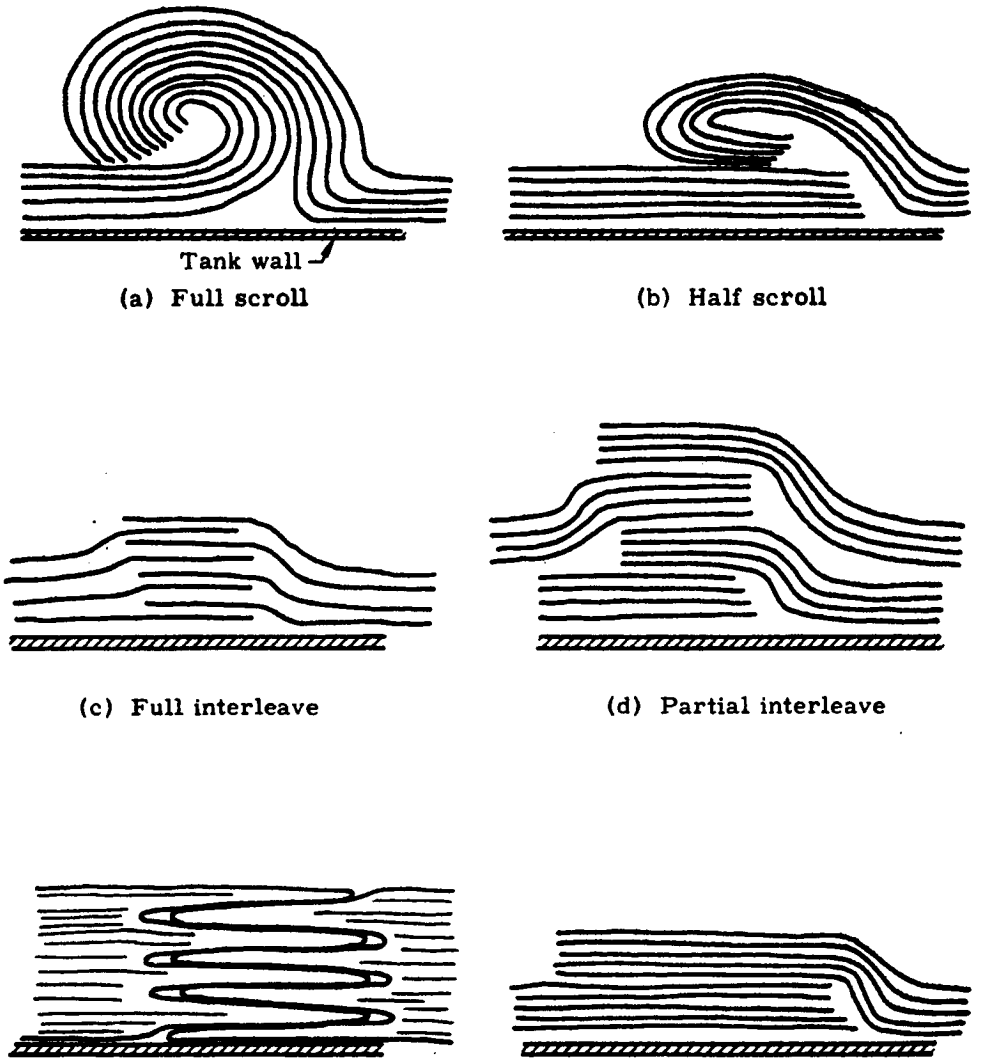

Fig. II-18. Insulation Blanket Juncture Methods

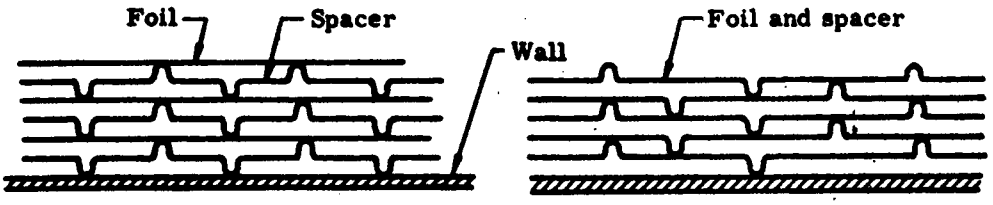

(a) Continuous spacer dimpled in both directions

(b) Foils dimpled in both directions, also act as spacers

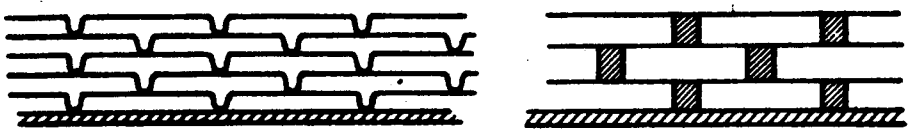

(c) Foils dimpled in one direction, also act as spacers

(d) Foils separated by discrete spacer blocks

(e) Foils, double corrugated, also act as spacers

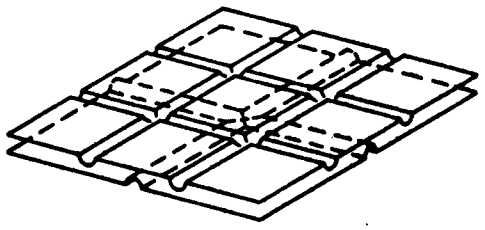

Fig. II-19. Marshield Spacing Methods

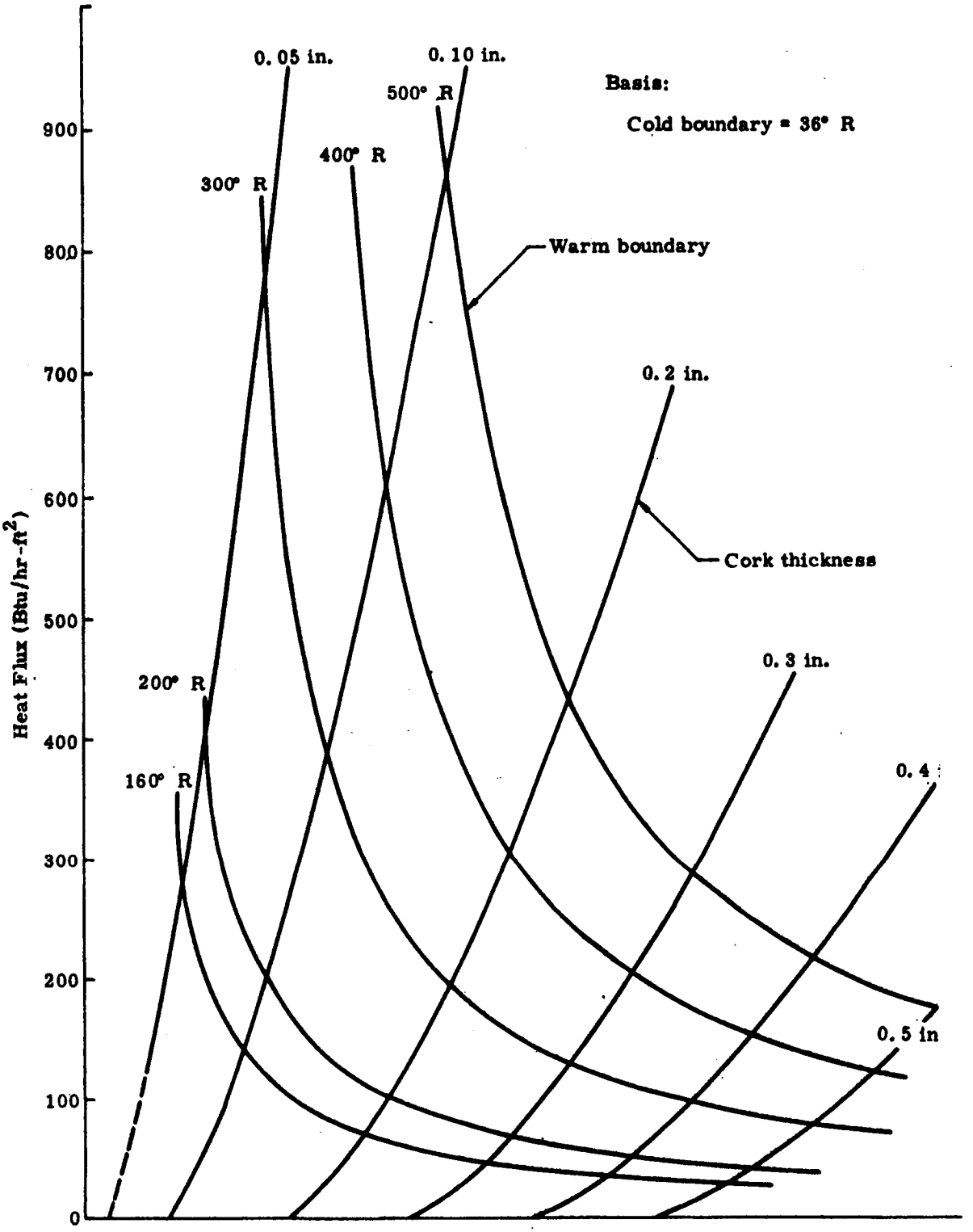

Fig. II-20. Heat Flux Across Corkboard Insulation on LH_2 Tankage

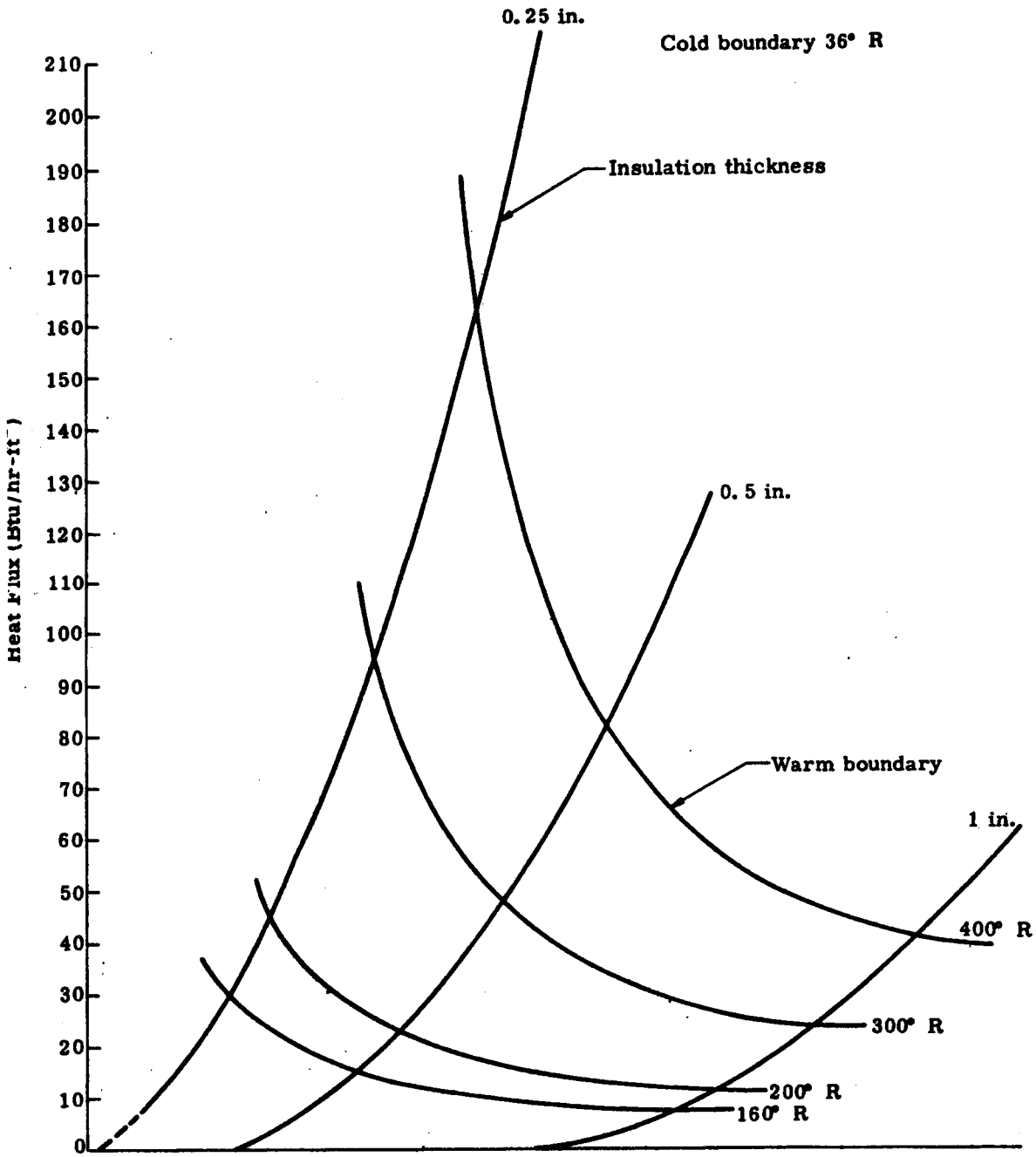

Fig. II-21. Heat Flux Across Typical Polyurethane Foams on LH_2 Tankage

III. OPTIMUM DESIGN CONSIDERATIONS

This chapter illustrates the results of insulation optimum design studies, chiefly those appearing in the appendices of this report, and shows their influence on the practical design problems treated in Chapter IV.

The results of Appendix E are presented first to show effects of the various thermal efficiencies of insulation blankets selected for investigations and effects of variations of thermal efficiency within each type of insulation blanket selected. These effects are expressed in terms of mission penalties incurred during the space storage phase of the missions relative to those for ideal insulation. It is assumed that the mission penalty due to heating through the blanket can be evaluated independent of other sources of heating in the storage phase as well as other phases of the mission, e. g., ground hold. It is shown that the penalty for not achieving a high degree of insulation efficiency in the blanket may not be great for many classes of spacecraft and missions. Those classes include large spacecraft for which duration of cryogenic storage is not large and for which subsequent velocity change requirement is not large.

Effects of other sources of heating and their respective insulation weights on optimum proportions of each insulating component are then shown by considering them simultaneously in an optimum design analysis. It is shown that even though each insulating component is considered to function independent of other components, their respective optimum insulation proportions are affected by their collective contributions to heating and inert weights. However, it is also shown that these cross effects are in many cases not dominant, so that each insulating component can be optimized independently with close approximation for a wide range of mission parameters.

Finally an illustrative example of the method presented in Appendix F for the optimum design of structural supports is given for the typical spherical tank upon which the design efforts presented in Chapter IV were concentrated.

A. EFFECTS OF INSULATION EFFICIENCY ON MISSION PERFORMANCE

Effects of the thermal efficiency parameter $k_i \rho_i$ (product of insulation's conductivity and density) of a storage tank's insulation blanket on mission performance is demonstrated for two of the types of missions analyzed in Appendix E. The first type of mission is Case III of

Appendix E wherein the objective is to retain during storage as high a percentage of cryogenic mass as possible relative to the initial total mass of the storage stage. Subsequent utilization of the cryogenic is not a relevant parameter in this case. The second type of mission considered is Case II of Appendix E wherein the objective is to maximize inert mass fraction (not including insulation mass) for a stage that is to be subsequently accelerated to a prescribed velocity change by utilizing for propellant the stored cryogenic. The following assumptions are made for both types of storage missions:

(1) The storage tanks are spherical but a correction factor, C_2, can be employed to treat nonspherical tanks.

(2) The propellant is liquid hydrogen stored at a temperature of 36° R.

(3) The temperature difference across the insulation blanket is a uniform value of 424° R.

(4) Factors representing ullage space and trapped propellant are as shown on the graphs of mission penalties as they vary with the parameters.

(5) Other sources of space heating during other than the space storage phase of the mission have no effect on optimum proportions of the insulation blanket as determined for the space storage phase of the mission.

The effects of insulation efficiency, $k_i\rho_i$, and other parameters, on the mission penalty factor P_F for the first type of mission are given by Eqs (25) and (26) of Appendix E as

$$P_F = 1 - \frac{F_{max}}{F_{ideal}} = 2\sqrt{\frac{C_3}{1 - C_4}} \qquad (1)$$

where

$$C_3 = \frac{k_i\rho_i \Delta T \theta}{H_V \rho_f^2 r^2} \left[3 (1+C_1) (1+C_2)\right]^2 \qquad (2)$$

and the symbols are defined therein. Equation (1) represents penalties

when the blanket is of optimum proportions. Figure III-1 shows Eq (1) graphically where P_F is the ordinate, $k_i\rho_i$ is abscissa and tank radii and storage times are parameters. Ranges of $k_i\rho_i$ for NRC-2, Linde and Marshield are shown as hatched areas in Fig. III-1, extending from their ideal values on the left to conservative estimates of their practicably achievable values on the right. Tank radii, r, and storage times, θ, shown in Fig. III-1 represent the limits of design requirements for this program.

The curves show clearly that rather large variations from the ideal value of $k_i\rho_i$ for each type of insulation do not as greatly change the mission penalty, the penalty being proportional to $\sqrt{k_i\rho_i}$. The more important observation is, however, that in the range of short storage times and large tank size the mission penalties are very small so that especially in that range it is not so important to achieve the lowest possible value of $k_i\rho_i$, and in that range the penalty for utilizing the potentially high reliability of Marshield is more acceptable.

Approximately the same trends are shown in Fig. III-2 for the second type of mission, maximizing inert mass fractions for prescribed velocity changes subsequent to storage. The mission penalty in this case is given by Eqs (19) and (21) of Appendix E.

$$P_{\lambda_I} = 1 - \frac{\lambda_{I_{max}}}{\lambda_{I_{ideal}}} = \frac{1 - R}{R - C_4}\sqrt{\frac{4C_3R}{1 - C_4}} \qquad (3)$$

where

$$R = \exp\left(-\frac{\Delta V}{gI_{sp}}\right) \qquad (4)$$

Figure III-2 also shows mission penalty as the ordinate and $k_i\rho_i$ of the insulation blanket as the abscissa. The same trends and conclusions as those for the first case apply to Fig. III-2, but it should also be noted that when $R > 0.6$ and approaches unity the adverse effects of high $k_i\rho_i$ are even further reduced from those of the first case (Fig. III-1).

In summary, it is shown that for extended storage of cryogens in small tanks and large subsequent velocity changes, great emphasis should be placed on achieving the lowest possible value of $k_i\rho_i$, since the change in mission penalty for a given change in $k_i\rho_i$ is then large. For short storage times, large tanks and small velocity changes, the change in mission penalty for the small change in $k_i\rho_i$ is not so large and the emphasis on achieving very low values of $k_i\rho_i$ can be correspondingly decreased.

B. COLLECTIVE EFFECTS OF HEATING AND INSULATION WEIGHTS ON COMPONENT OPTIMUM DESIGN

Appendixes E and F give optimum proportions of the blanket and structural supports for the space storage phase of the missions as obtained independent of one another, as well as of heating during the ground hold and boost phases of the missions. Those approaches are only approximate, as will be shown in this section, since each component's optimization depends on all contributions to heating and insulation weight.

This section shows the more complete approach that should be taken in optimizing the insulating components, and the results are carried out to an extent where the degree of approximation is assessed for not using the more complete approach. The nomenclature used is the same as that in Appendixes E and F except where new nomenclature is defined as used.

Consider Case III of Appendix E where ratio F of the cryogenic mass after storage to the initial (preground-hold) mass of the storage stage is to be maximized by properly proportioning the insulation system. When many sources of heating and insulating components are present the fraction F is given by

$$F = (1 - C_4)\left(1 - \lambda_I - \lambda_B - \lambda_G - \sum_{m=1}^{n} \lambda_{i_m}\right) - \lambda_{BO_B} - \lambda_{BO_G} - \sum_{m=1}^{n} \lambda_{BO_m} \tag{5}$$

where

λ_B = the mass fraction of the blanket used for in-space insulation

λ_G = the mass fraction of an insulation used for ground hold and boost insulation

λ_{i_m} = the mass fraction of the mth of n other insulating components

λ_{BO_B} = the in-space boiloff mass fraction due to heat passing through the in-space blanket

λ_{BO_G} = the ground hold and boost boiloff mass fractions due to heat passing through the λ_G insulation.

λ_{BO_m} = the mass fraction of boiloff due to heat passing through the mth insulating component.

λ_I = the inert mass fraction of all other inert masses.

For conservation of mass,

$$\lambda_{f_o} + \lambda_I + \lambda_B + \lambda_G + \sum_{m=1}^{n} \lambda_{i_m} = 1 \tag{6}$$

where λ_{f_o} is the initial propellant mass fraction (top-off value).

The individual components of heating can be related to their respective insulating mass fractions by

$$\lambda_{BO_B} = \frac{C_{3_B} \lambda_{f_o}^2}{\lambda_B} \tag{7}$$

$$\lambda_{BO_G} = \frac{C_{3_G} \lambda_{f_o}^2}{\lambda_G} \tag{8}$$

and

$$\lambda_{BO_m} = \frac{C_m}{\left(\lambda_{i_m}\right)^{P_m}} \tag{9}$$

Boiloff components λ_{BO_B} and λ_{BO_G} are related to the initial propellant mass fractions as shown because they depend on the tank size (see Appendix E for λ_{BO_B} which is also the general form for λ_{BO_G}) and it is assumed that the other components of boiloff are not dependent upon the initial propellant mass fraction as was assumed in Appendix F for structural supports. A general form of Eq (23) in Appendix F was assumed for all λ_{BO_m} components. The term C_m used in Eq (9) is a

generalization of the C_5 term in Eq (23) of Appendix F for an m^{th} penetration and the P_m term is a generalization of n in Eq (23) for an m^{th} penetration. It should be noted that the boiloff components are not coupled to one another except through λ_{f_o}. It has been tacitly assumed also that λ_B is not effective in performing λ_G's function which only applies to some of the systems treated in this study. The assumption that λ_G is not effective in λ_B's function is generally a close approximation.

Mass fraction F is maximized by setting equal to zero the derivative of F with respect to the sum of all insulation mass fractions, λ_T:

$$\frac{dF}{d\lambda_T} = 0 = \frac{\partial F}{\partial \lambda_G}\frac{d\lambda_G}{d\lambda_T} + \frac{\partial F}{\partial \lambda_B}\frac{d\lambda_B}{d\lambda_T} + \frac{\partial F}{\partial \lambda_{i_1}}\frac{d\lambda_{i_1}}{d\lambda_T} + \cdots + \frac{\partial F}{\partial \lambda_{i_n}}\frac{d\lambda_{i_n}}{d\lambda_T}. \tag{10}$$

Since

$$\lambda_T = \lambda_B + \lambda_G + \sum_{m=1}^{n} \lambda_{i_m} \tag{11}$$

$$\frac{d\lambda_G}{d\lambda_T} = \frac{d\lambda_B}{d\lambda_T} = \frac{d\lambda_{i_m}}{d\lambda_T} = 1. \tag{12}$$

It is therefore seen that equations

$$\frac{\partial F}{\partial \lambda_G} = \frac{\partial F}{\partial \lambda_B} = \frac{\partial F}{\partial \lambda_{i_m}} = 0 \tag{13}$$

are simultaneous conditions for maximizing F. The general approach for determining the optimum values of each insulation mass fraction then involves the simultaneous solution of Eqs (6), (7), (8), (9) and (13).

By neglecting C_{3_B} and C_{3_G} terms and products of $C_{3_B}\,\lambda_{f_o}/\lambda_B$ and $C_{3_G}\,\lambda_{f_o}/\lambda_G$ when compared to unity, the following optimum mass fractions are determined:

$$\lambda_{i_m} = \left\{ \left(p_m C_m \right) \left(1 - C_4 + 2 \left[\sqrt{C_{3_B} (1 - C_4)} + \sqrt{C_{3_G} (1 - C_4)} \right] \right)^{-1} \right\}^{\frac{1}{1 + P_m}} \quad (14)$$

$$\lambda_B = \left(1 - \lambda_I - \sum_{m=1}^{n} \lambda_{i_m} \right) \sqrt{\frac{C_{3_B}}{1 - C_4}} \left(1 - \sqrt{\frac{C_{3_G}}{1 - C_4}} \right) \quad (15)$$

$$\lambda_G = \left(1 - \lambda_I - \sum_{m=1}^{n} \lambda_{i_m} \right) \sqrt{\frac{C_{3_G}}{1 - C_4}} \left(1 - \sqrt{\frac{C_{3_B}}{1 - C_4}} \right) \quad (16)$$

It is observed first that Eq (14) differs from Eq (33) of Appendix F for optimum structural supports only by the last term in the denominator which closely approximates the ground and space blanket's mass fractions. A large error would not be made in dropping those terms for the range of parameters and blanket insulations considered in this program. It is further noted that Eq (14) applies to components other than supports when their boiloff-mass fraction equation is of the form of Eq (9). Equation (15) is observed to be exactly equal to Eq (23) of Appendix E if the mass fractions $\sum_{m=1}^{n} \lambda_{i_m}$ are included in λ_I and C_{3_G} is considered zero. Thus, the effect of the supports and other penetrations of the type represented by Eq (9) is only to increase λ_I and accordingly decrease λ_B. The same effect relative to λ_G is noted in Eq (16). The C_{3_G} term in Eq (15) essentially represents the ground blanket mass fraction and it is seen to decrease the optimum value of λ_B further. Values of λ_B derived from Appendix E are therefore conservative. For the designs in Chapter IV, the ground insulation was specified by the assumption that no condensing is allowed. The λ_G term was then fixed and simply added to λ_I of the stage when using Eq (15) to determine λ_B. However, should very long ground hold conditions be considered, additional ground insulation would be required and the optimum amount would be given by Eq (16).

It is noted also that for cases where spacing material is added between multiradiation shields only for the purpose of augmentation in the ground hold condition, λ_G may be considered the spacer mass fraction and optimized accordingly. Thus, Eqs (14), (15) and (16) represent optimum tradeoff values of the penetrations, space insulation blanket and ground hold insulation blanket for cases where each may be varied freely. It is seen that their interaction is, in general, not severe but could be important for some situations. The above trends can be expected to be typical of Cases I and II of Appendix E, also.

C. EXAMPLE ANALYSIS OF STRUCTURAL SUPPORT OPTIMUM DESIGN

The example mission, tankage and structural support specifications are those on which most of the design effort reported in Chapter IV was based:

Tank:

1. Spherical configuration, 125-in. dia.
2. Contents, LH_2 at 36° R and temperature difference across insulation of 424° R; LH_2 heat of vaporization is 194 Btu/lb.
3. Trapped propellant fraction, C_4 is 0.01.

Mission:

1. Type of mission in Case III in Appendixes E and F; namely, maximize propellant mass fraction available after storage.
2. Storage duration, θ, is 720 hr.

Supports:

1. Titanium; density, ρ_s, is 285 lb/cu ft conductivity, k_s is 2.80 Btu/ft-° R-hr, yield strength is 120,000 psi.
2. NRC-2 insulation on supports for which $k_i \rho_i$ is 2.5×10^{-5} Btu-lb/ft^4-° R-hr.
3. Six cruciform supports rotated 45° from longitudinal axis of stage will be used as shown in the designs of Chapter IV.
4. Axial load factor, n_x, is 6g, normal factor, n_y, is 1g and 1g inertia load on supports is 26,000 lb.

5. Factor of safety is 1.4 based on ultimate stress.

6. Supports should be corrugated to minimize their dynamic response and prevent their excessive static deflections.

The load per support leg, P, is then

$$P = \frac{26,000\,(1.414)\,(1.4)\,(6+1)}{12} = 30,000 \text{ lb.}$$

The cross-sectional area of each support must then be

$$Bt_s = \frac{30,000}{120,000} = 0.25 \text{ in.}^2$$

where B and t_s are respectively the support elements' width and thickness as used in Appendix F. It will be assumed that the straps will be made of material that is 0.032 in. thick and 7.8 in. wide to provide sufficient width for forming a square wave corrugation that will keep their dynamic response low. With the insulation lying only over the crests of the corrugation as shown in Chapter IV, the effective thickness for heat transfer calculation will then be 0.064 in.

The problem is then to determine the optimum length support; that is, the distance from their intersection to their ends. To utilize the optimum design curves of Appendix F for this problem it is first necessary to determine the value of β^{n+1}/nA using Eq (35) of Appendix F and the above specifications:

$$\frac{\beta^{n+1}}{nA} = \frac{2.8(424)\,(720)\,144}{0.99\,(0.064)^2\,(285)\,194} = 5.45 \times 10^5$$

Entering Fig. F-3 of Appendix F at the above value of β^{n+1}/nA it is seen that

$$\frac{t_s}{l} = 1.6 \times 10^{-3}$$

and

$$\frac{2\rho_i t_i}{\rho_s t_s} = 0.15$$

The optimum support length is then 40 in. and the corresponding insulation thickness is 0.91 in., using 1.5 lb/cu ft for the insulation density. The value of β for these proportions can then be read from Fig. F-2 of Appendix F as

$$\beta = 8.0 \times 10^{2}$$

For that value of β, Fig. F-1 of Appendix F shows $q/k_s \Delta T$ is 1.6×10^{-3}, or

$$q = 2.8\ (424) \times 1.6 \times 10^{-3}$$

$$= 1.9 \text{ Btu/ft-hr}$$

or

$$q = 0.618 \text{ Btu/hr/support leg.}$$

Thermal stress considerations. A thermal stress analysis of these supports was made for the purpose of determining whether a problem exists. It was assumed in the analysis that one end of each support member was attached to a rigid shroud and the other end to a rigid aluminum LH_2 tank. The results show that total thermal strains in titanium supports of the above length on the 125-in. radius tank are approximately 1.16×10^{-3} of which 0.16×10^{-3} is due to tank shrinkage upon filling with LH_2 and 1.0×10^{-3} is due to shrinkage of the supports themselves. Rather than sustain the resulting 18,500-psi thermal stress it was decided to mount the intersection of the cruciform supports on diaphragms attached to the shell surrounding the tank. The diaphragms would permit radial deflection of the support intersections to alleviate the thermal stress condition while providing stiff support against any translation of the tank relative to the surrounding shell.

D. ILLUSTRATIONS

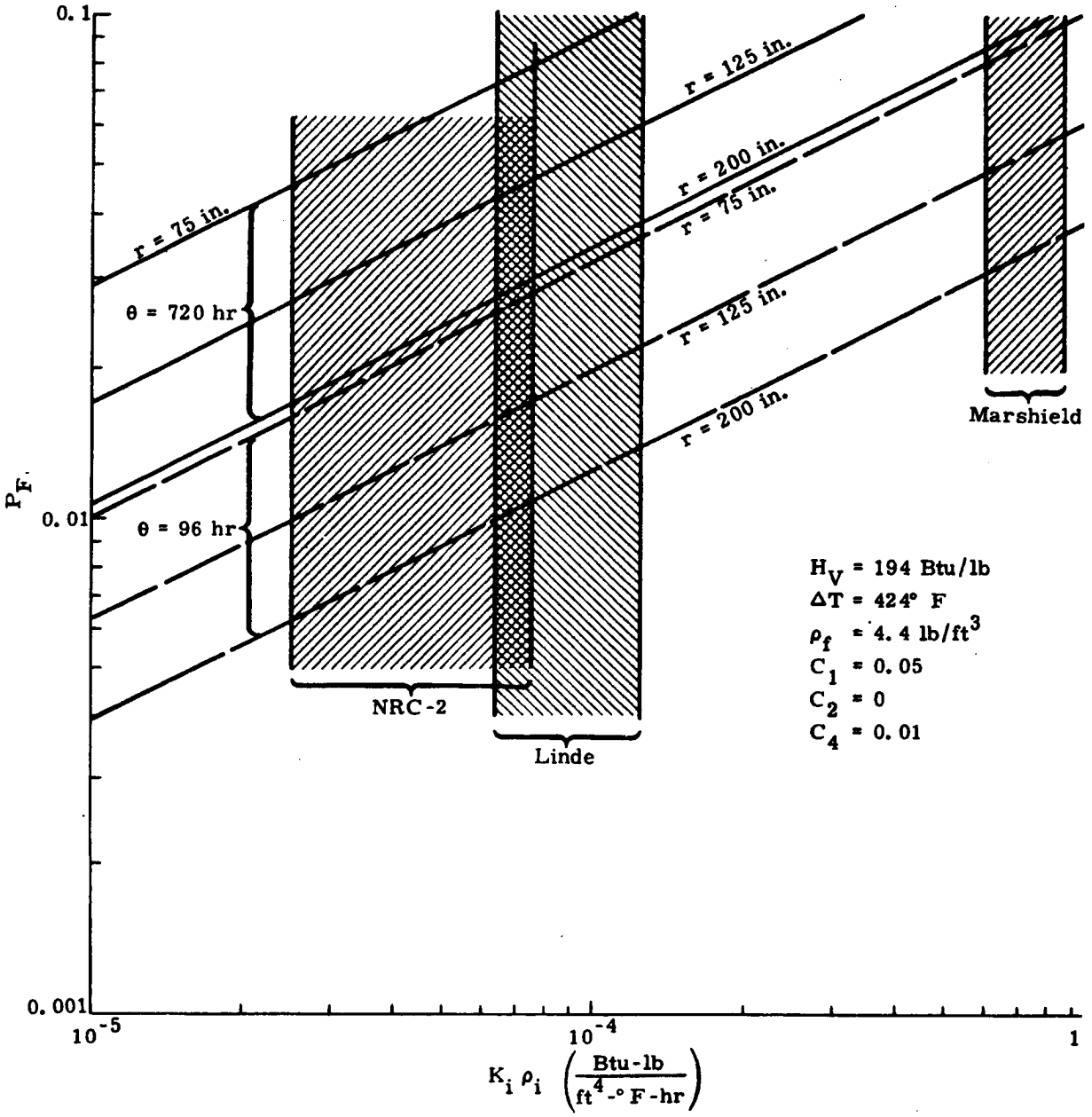

Fig. III-1. Penalty in Stored Fuel Versus $K_i \rho_i$ as Function of Storage Time (θ) and Tank Radius (r)

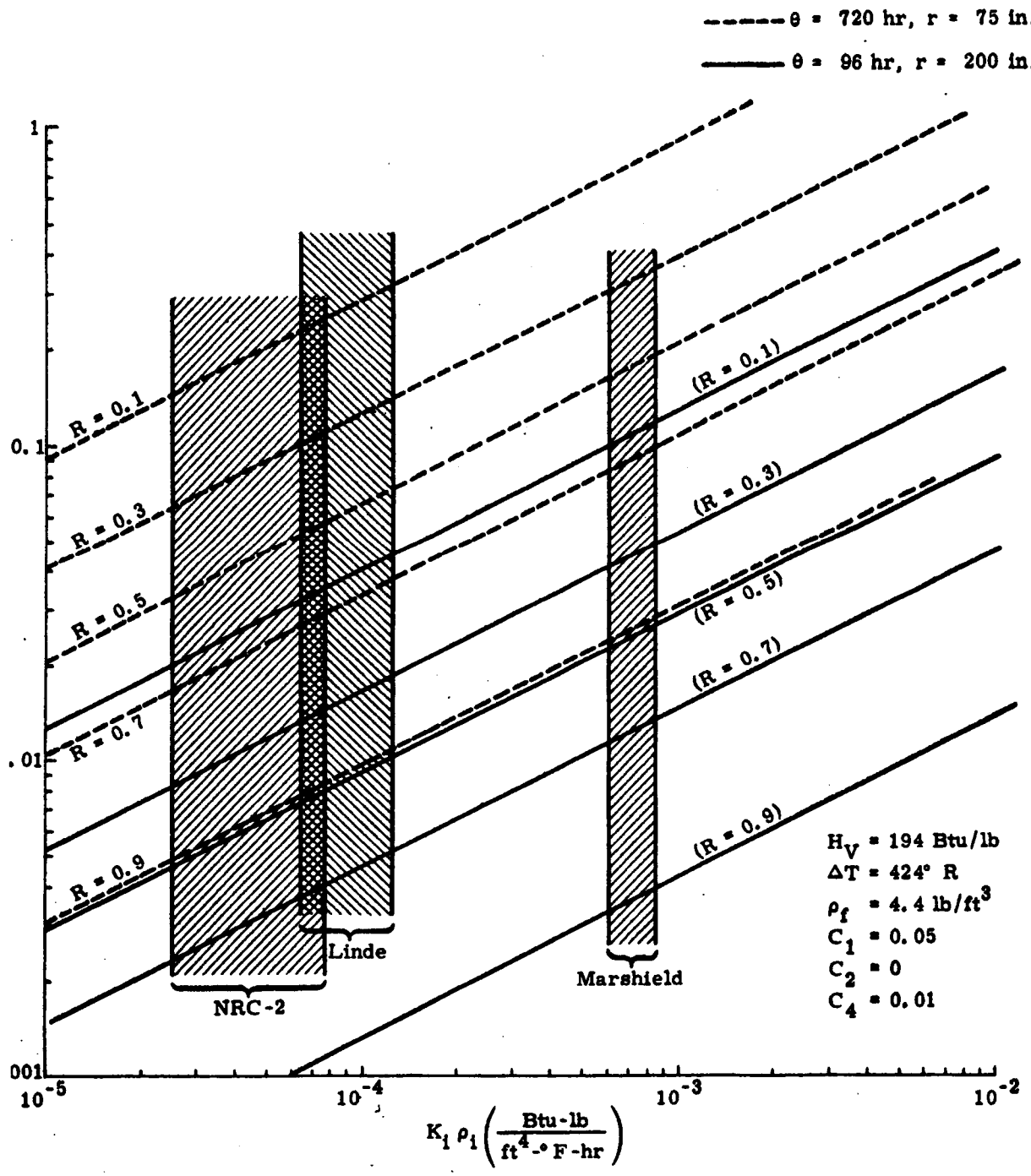

Fig. III-2. Payload Penalty Versus $K_i \rho_i$ as Function of R $\left(R = \exp\left[-\frac{\Delta V}{gI_{sp}}\right]\right)$

IV. DEVELOPMENT OF DESIGN SOLUTIONS

The primary design effort has been concentrated on a 250-in. diameter spherical tank. This direction of approach is the result of considering that the major objective of this program is a rather general one of developing design solutions for integrating several contending types of insulation systems for a wide range of tankage configurations. The objective required many cycles of development and comparison among the various insulation concepts. For the development of each system to be unbiased and effective in showing the relative advantages of the variou insulation systems developed they required the same design basis. Accordingly, the one shape and size of tank was emphasized, and it was considered that the large (250-in. diameter) spherical tank presents all the major design problems that are encountered in the other configurations. The principal exception to this latter consideration is that problems of an integral tank, one for which the cylindrical barrel section would form the primary outer structure of a stage, are not encountered in the spherical tank investigation. A smaller portion of the design effort was therefore devoted to this special problem and the results are presented after those from the spherical tank investigation. A typical adaptation of the design solutions developed for the spherical tank is given for the toroidal tank.

Variations in tank size from the 250-in. diameter one investigated (within the bounds of the configuration requirements) are not expected to have great influence within any one of the design concepts but can be expected to have the following general effects:

(1) Reduce boiloff percent with increasing diameter as shown in Chap ter III. This is due chiefly to reducing the ratio of surface area t volume.

(2) Increased boost inflation forces with increasing tank size due to increased resistance to evacuation and membrane forces' dependence on product of pressure and radius.

(3) Heat leak through tank supports will decrease slightly percentage wise, with increasing tank size if the supports are loaded primarily by the cryogenics inertia forces during boost. This may be seen by considering either square (rod-like) or cylindrical sup port members in the formulas of Appendix F.

The designs in this chapter are generally based on the design criteria of Chapter II. The insulation blanket thicknesses for all cases are based on optimum design for a 30-day storage, but the supports shown are not sized for any specific storage time. However, example calculations are shown for sizing the supports, in Section C of Chapter III.

While a relatively large number of systems were examined in some detail during the course of this study, only those systems considered to have good performance potential as well as practicable design features are presented and discussed in detail in this chapter.

The discussion of each system follows although not necessarily in their final rated order except that the first design is the higher rated one.

A. SPHERICAL TANKS

1. Passive System--NRC-2 with Sealed Mylar Honeycomb Subinsulation

a. General system description

The overall concept and details of this system are shown in Fig. IV-1. The design concept consists of bonding and surface sealing a thickness of mylar honeycomb to the tank wall over which a blanket of air-filled NRC-2 is installed. The concept evolved from a belief that an insulation system devoid of requirements for pre-evacuation or for purging before tank filling would be inherently reliable, require no complicated launch pad procedures, exhibit acceptable performance in all mission phases and therefore be extremely attractive.

(1) Insulation blankets. The double gores of the insulation blanket (henceforth called gores) would be pre-made or tailored prior to installation. They would consist of nearly full length (one-half circumference long) gores of 70-100 layers, their ends being cut off at the manhole station and near the suction line at the bottom. The gores' maximum widths are at the equator of the tank where they would be approximately 5-1/2 ft wide. The long edges of each gore would, in section, have 5-in. long saw teeth or fingers formed by separating the layers of the blanket into groups of 10 or more layers. The layer-groups would then be permanently held together by binding the edges with a mylar strip which forms the outline of the edge and then stitching together each mylar finger with the group of layers enclosed. The stitching would be done intermittently along the edges by ultrasonic welding techniques. Other methods of stitching should also be considered in a development program. Each gore would have a small circular cutout at its equator to permit its installation over one of the 12 trunnion fittings. As shown in section D-D, the finger edges are scalloped to provide edge area for venting of the gases within the insulation.

(2) Insulation attachment design.

(a) Subinsulation. A 1/2-in. layer of 3/8-in. Hexcell Mylar Honeycomb (MHC) is shown bonded to the tank in Fig. IV-1 with one

of the mylar-to-metal adhesives recommended earlier. In addition, while the bond cures, the MHC would be secured to the tank by a pretensioned winding of fiber glass yarn in a manner similar to that reported in Ref. II-10. The mylar honeycomb outer surface would then be sealed with an "ALUMISEAL" type laminate film by bonding the film to the honeycomb with one of the mylar-to-mylar adhesives recommended earlier.

Portions of the mylar honeycomb must be cut away to accommodate the anchors which are shown as the attachment devices for the primary NRC-2 insulation blankets. Section F-F shows how the seal would be effected at the areas where the anchors pierce the honeycomb.

(b) Primary insulation--NRC-2. The 12 preformed NRC-2 gores of the insulation blanket are shown secured to the outer surface of the subinsulation by a system of anchors and 3/16-in. diameter nylon ropes. Each anchor consists of two oval-shaped 3/32-in. rings which are welded to the tank and to each other and to a circular plate at the level of the honeycomb. Welded to the top of the circular plate is shown a smaller ring (or eye) to which the rope-end, snap clamps attach. These anchors occur only under the sawtooth-type joints. It is estimated that a total of 72 anchors would be required--6 under each of the 12 longitudinal blanket seams. The 12 blanket sections would be preattached to the nylon ropes by folding the blanket laterally around the rope as shown in section D-D (Fig. IV-1). These lateral folds occur six times for each section. The blanket and rope would be secured together by a large number of plastic clips which squeeze the blanket around the rope. The plastic clip ends would be prevented from spreading apart by plastic screw type (or other) fasteners which pass completely through the two folded layers of the blanket. The folds are cut away at the blanket edges (see section D-D) to permit the formation of the sawtooth edge.

(c) Seam or blanket juncture design. For all longitudinal seams, the juncture would be made by interleaving the adjacent preformed fingers. For the top and bottom dome caps, however, an extreme overlap would be used (10 to 12 in.) to provide sufficient exposed edge area and at the same time minimize the heat leak by a long conduction path.

The dome caps are shown in Fig. IV-1 as preformed units. The edges would be folded over a circular piece of nylon rope and fastened to the rope with plastic clips as described earlier. The edges would be scalloped to expose portions of the rope as shown on Section A-A. The edges of the dome cap would be tied to the main anchor-rope system by the use of small nonmetallic Y-shaped pieces having holes in each section of the Y. These Y-shaped pieces would be connected to the main anchor ropes at the time of blanket makeup by a small

length of cord which is secured to one hole in the Y-shaped piece. The other holes in the top Y-shaped pieces would be used to anchor one of upper dome cap net ropes, and one of the lower outer net ropes, as well as alternate sections of the exposed edge rope of the cap. At other stations down the length of the section, the Y-shaped pieces would be used primarily as guides for the outer net ropes. The upper dome cap is shown held to the tank by an outer net system of 1/8-in. diameter nylon ropes. At the top of the upper dome cap, the net ropes are shown tied to a small floating ring.

The lower dome cap is shown as a preformed unit which includes the engine-feed line collar (see section B-B). This would be accomplished by laying up precut gore sections on a die and welding them together ultrasonically.

The lower dome cap is shown held to the tank in a manner similar to that of the upper dome cap except that two floating rings (section J-J) are used to secure the net ropes.

In addition, each exposed section of the dome cap edge rope is shown secured to the main anchor rope system to resist the greater otherwise unsupported inertia forces of the bottom cap.

Periodically down the length of the suction line collar, circular net ropes are tied to the longitudinal net ropes mainly to resist boost inflation forces.

(3) Penetration insulation design.

(a) Tank support system (see Fig. IV-2). The mylar honeycomb subinsulation height will be varied to match the varying support height above the tank from trunnion to weld point. The honeycomb seal sheet will then be bonded on the lateral surface of the supports and sealed at the trunnions. Preformed foam blocks would be used to fill in the corrugations in each support strap providing a smooth sealing surface. The area under each support strap would be insulated with patches of NRC-2, and the support straps would be prevented from bending when this space is cryopumped by a series of phenolic blocks. The outer surface of each support would be covered by the main gore sections up to the small trunnion cutouts when efficient design indicates the support legs should be short; when they should be long, they would be outside of the gore and insulated independently. The supports were designed according to the methods of Appendix F and are corrugated to prevent buckling or excessive bending.

b. Performance summary

(1) Weights.

Item	Thickness	Weight (lb)	Weight (lb/sq ft)	Comments
Basic insulation--NRC-2	1.3 in.	226.5	0.166	NRC-2 (70 layers/inch), ρ = 1.53 lb/ft^3
Mylar honeycomb subinsulation	0.5 in.	119.5	0.0875	3/8-in. Hexcell MHC, ρ = 2.1 lb/ft^3
"ALUMISEAL" sheet for MHC	2 mils	30.0	0.022	Mylar-Al foil laminate
Bond for MHC and seal	--	21.2	0.0155	
Anchors, nylon ropes and plastic clips		35.0	0.0256	See note (1)
Local spacers under anchor ropes		5.4	0.00396	240 ft by 3 in.
Tank supports, suction and vent line insulation	1.0 in.	11.5	0.00842	Insulated line L/D = 8
End cap overlap insulation		3.2	0.00234	12-in. overlap
Totals		452.3	0.331	

$$\text{Installation factor} = \frac{0.331}{0.166} = 1.995$$

NOTES:

1. 72 anchors--8 lb; 305 ft of 3/16-in. diameter rope at 1 lb/100 ft; 640 ft of 1/8-in. diameter net rope at 0.6 lb/100 ft; and 260 ft of plastic clips at 0.072 lb/ft.
2. Installation factor is ratio of basic insulation blanket weight to total insulation system weight.

(2) Thermal performance.

Ground hold. The equilibrium ground hold heat transfer was determined by graphical iteration using the performance curves given on Figs. II-3, II-12, and II-21. Since tank wall and hydrogen film resistances are negligible, the condition that must be satisfied for equilibrium is

$$\dot{Q}_{\text{boundary layer}} = \dot{Q}_{NRC} = \dot{Q}_{MHC}$$

For large tank radii, $\dot{Q}/A$ may be substituted for $\dot{Q}$ without appreciable error. The results of the iterative calculation indicate that an equilibrium heat flux of 27 Btu/hr-ft^2 would exist for internal tankage (i. e., heat transfer from ambient air by natural convection only). For integral tankage using this insulation system, and for a wind velocity of 40 knots, this heat flux would rise to approximately 30. 5 Btu/hr-ft^2.

Ascent flight. For all system concepts, the total integrated heat leak through boost plus a soak period until orbit equilibrium conditions are established was assumed a constant at 64 Btu/ft^2. While this value in itself may be conservative for certain trajectories or configurations, it was considered to be sufficiently accurate to use as a constant value for the purpose of comparing systems. The major difference between insulation system performances during ascent flight is the actual heat transferred to the propellant during the aero-heating period of the flight, the maximum surface temperatures reached and the percent of the total heating which is absorbed by the insulation. For example, the heat transfer data for the typical trajectory elements shown on Fig. II-1 are based on an uninsulated tank wall with an adiabatic inner wall. In this case all the aerodynamic heating (less a small amount reradiated) results in raising the temperature of the aluminum wall due to its thermal capacity. No heat is assumed transferred into the interior. For a realistic case, however, some of the heat absorbed by the walls or insulation during the boost period would be transferred into the cold propellant before it could be reradiated away. In addition, the majority of the heat absorbed in the insulation during boost will ultimately reach the propellant whether it is transferred there during the aero-heating period or not.

Earth orbit flight. The ideal orbit heat leak to the propellant is herein defined as that heat leak which a perfectly insulated tank (no penetrations or seams) would experience when insulated to a thickness consistent with minimizing overall penalty for a given mission. The mission selected for system comparison is a 30-day orbital storage mission. While this mission choice is somewhat arbitrary, and while it is true that some mission choices favor higher heat leak, lower weight

systems, the screening and comparison process is not significantly affected by this choice. Once the ideal heat leak is established, the other heat leaks are presented in terms of a percentage of this value in order to highlight the magnitude of the thermal degradation which results from the inclusion of penetration and installation heat leaks.

The ideal heat leak for the NRC-2 passive system occurs at an insulation thickness of 1.3 in. (see Fig. IV-3, curve (a) or Eq 14 of Appendix E). The following table summarizes the orbit heat leak contributions:

Orbit* Heat Leaks--NRC-2 Passive System

Item	Insulation Thickness (in.)	k (460-36 °R) (Btu/ft-°R-hr)	Heat Flux ($Btu/hr-ft^2$)	Heat Leak (Btu/hr)	Lengths	Heat Leak (Btu/hr-ft)	Notes
Basic blanket (ideal)	1.3	1.28×10^{-5}	0.05	68.25			
Tank supports	1.0			23.1	44 in.		(1)
Suction line	1.0			3.64	32 in.		(2)
Vent/pressurization line	1.0			0.51	18 in.		(3)
Sawtooth edges				4.6	300 ft	0.01535	(4)
Anchor rope attachments				14.4	240 ft	0.06	(5)
End cap overlaps				1.25	25 ft	0.05	(6)
Total			0.0848	115.75			

$$\frac{\dot{Q}_{total}}{\dot{Q}_{ideal}} = \frac{115.75}{68.25} = 1.697$$

* Equilibrium shell temperature = 460° R

NOTE (1) Based on the analytical approach given in Appendix F and Section III-C.

NOTE (2) Based on the analytical approach given in Appendix G, a warm boundary temperature of 530° R, 4-in. diameter--35 mil--Ti pipe, insulated to an L/D = 8.

NOTE (3) Based on Appendix G, warm boundary temperature = 460° R, a 2.25-in. diameter.

NOTE (4) Estimate only--based on 4- to 5-in. finger length.

NOTE (5) Estimate only--based on local compression of NRC-2 with spacers to 300 layers/in. over 14 to 15% of tank area.

NOTE (6) Estimate only--based on 11- to 12-in. overlap.

General rating considerations. This insulation system once installed would require no further attendance, and hence has been labeled a passive system. The advantages of not having to purge or pre-evacuate the insulation prior to filling the tank could potentially far outweigh any theoretically determined thermal performance degradation due to lack of assurance of rapid space evacuation. There are many attractive features of this system as listed below, but some of the obvious disadvantages, also listed, should not be overlooked. The table lists some of the factors for consideration in the rating of this system.

NRC-2 Passive System

Advantages	Disadvantages
1. No pre-evacuation required.	1. Venting of insulation during boost required.
2. No purging required.	2. Space evacuation of insulation required.
3. No leak detection or other complicated installation or launch pad procedures required.	3. Outgassing of condensed water vapor and frost likely to increase space evacuation time. *
4. Ground-hold performance--good.	4. Subinsulation seal integrity must be maintained during ground hold and boost--however, leak in seal could be confined to one honeycomb cell.
5. Subinsulation may retard or prevent hydrogen gas leakage into main blanket.	
6. Integrity of MHC bond on tank not required if fiber glass yarn or seal remains intact.	

*This could be alleviated by purging with dry gaseous nitrogen.

2. Helium Purged NRC-2 System

a. General description

This system (Fig. IV-4) would consist of a 1.3-in. layer of NRC-2 insulation installed adjacent to the bare tank wall. The system feature

which permits the elimination of the subinsulation and thus allows direct contact of the blanket with the tank wall (even at liquid hydrogen temperatures) is the replacement of the liquefiable air in the insulation with the noncondensible helium gas.

(1) Insulation blanket design. Twelve gore-shaped blanket sections would be manufactured with the trunnion cutouts, the sawtooth joints preformed on the longitudinal edges, and the anchor ropes preinstalled as described for the passive NRC-2 system. (For an alternative design approach, the extreme ends of the gores would also be provided with the sawtooth edges for mating with the dome caps.) In addition, each gore section would be prefitted with two sections of a flexible purge duct as shown in Section G-G of Fig. IV-4. Patches of NRC-2 insulation would then be taped over the purge ducts with the ends partially scrolled.

The upper and lower dome caps would have different design features. The upper dome cap would have a straight section of purging duct over the central portion of the cap. The dome cap edges would be fitted with the rope by folding over the scalloped edges and fastening periodically with the plastic clips as in the passive system. (The alternative design would utilize a sawtooth edge for mating with the gore ends as shown in Section E-E of Fig. IV-5.)

The lower dome cap design would incorporate a preformed suction line collar as an integral part of the cap. The purging duct would be circular in this case to avoid interference with the suction line collar.

(2) Attachment method. Patches of NRC-2 insulation would be installed under the supports before positioning the gore sections. As with the passive NRC-2 system, the gore sections would be attached to the tank by snapping the anchor-rope end clamps to the six ring-type anchors welded along meridian lines (see Section F-F, Fig. IV-4). The sawtooth edges would then be joined along these lines. The upper and lower dome caps would be installed overlapping the gore section ends, and the edges would be clipped to the anchor lines as described previously for the passive NRC-2 system.

The boost inflation force restraining net system would be installed next using the Y-shaped guides as shown in the overall view of Fig. IV-4 Finally the insulated main purge and feeder line manifolds would be tied to the main anchor-rope loop-type feeder ropes (preinstalled) and the restraining net ropes, respectively. Where the net ropes pass under the main manifold lines, additional stabilizing ropes could be tied across the manifold.

(3) Blanket juncture design. All longitudinal seams would be effected by mating adjacent sawtooth edges as shown in Section F-F. The edges are shown scalloped at the interior points in Section G-G to permit easy bleeding of the purge gas out through the seams. The dome cap junctures would be made by an extreme overlap to minimize the heat leak.

(4) Penetration design.

Supports. The entire support system would be covered by the gore sections with the exception of the small trunnion cutouts. The lower surfaces of the supports would be insulated from the tank surface by patches of NRC-2 as mentioned earlier. Should efficient design require long supports, they would be exterior to the blanket and insulated separately.

The pressurization/vent line. The pressurization/vent line penetration would be insulated by a preformed collar of NRC-2 with a taped-on spiral overwrap of NRC-2 at the collar-main-blanket juncture.

b. Performance summary

One of the attractive features of this system is evident in the weight table presented below. The estimated system weight shown is low because essentially a single component, inherently lightweight, insulation material would be used.

(1) Weights

Item	Thickness or Number	Weight (lb)	Weight (lb/sq ft)	Comments
Basic insulation	1.3 in.	226.5	0.166	70 layers/in.; $\rho = 1.53$ lb/ft^3
Purge ducts	(2) per gore	13.2	0.00967	150 ft; 0.088 lb/ft
Purge duct patches	(2) per gore	41.5	0.0304	150 ft; 20 in. wide
Tank support, suction and vent line insulation		11.5	0.00843	
Anchors, nylon ropes and plastic clips		35	0.0256	See NRC-2 passive system
Local spacers under ropes		5.4	0.00396	
Purge manifolds		13	0.00953	92 ft; 0.14 lb/ft
Total		346.1	0.254	

Installation factor = $\frac{0.254}{0.166} = 1.53$

(2) Thermal performance.

Ground hold. The ground hold performance of this system is relatively poor since the thermal conductivity of the helium purge gas is from one half to one order of magnitude higher than that for air depending upon the temperature range involved. The equilibrium ground hold heat flux was estimated at 158.5 Btu/hr-ft^2 from Figs. II-3 and II-11.

Ascent flight. See Table V-1.

Earth orbit.

Item	k (460-36° R) (Btu/ft-hr-° R)	Thickness (in.)	Heat Flux (Btu/ft^2-hr)	Heat Leak (Btu/hr)	Length, L	$\dot{Q}$/L (Btu/hr-ft)	Notes
Basic insulation	1.28×10^{-5}	1.3	0.05	68.25			See Fig. IV-3
Tank supports		1.0		23.1	42 in.		Appendix F
Suction line		1.0		3.64	L/D = 8		Appendix G
Pressurization/ vent line		1.0		0.51	L/D = 8		Appendix G
Sawtooth joints				3.07	300 ft	0.01535	(1)
Purge duct patches				9.0	150 ft	0.06	(2)
Anchor-rope attachments				14.4	240 ft	0.06	(3)
Total			0.0894	121.97			

$$\frac{\dot{Q}_{total}}{\dot{Q}_{ideal}} = \frac{121.97}{68.25} = 1.787$$

NOTES

(1) See notes--passive NRC-2 system.
(2) Estimate only--partial scroll both edges.
(3) See notes--passive NRC-2 system.

General rating considerations. Ideally, vacuum jacketed multilayer insulation systems possess higher potential than this system for thermall protecting cryogenic tankage from the adverse thermal environments in all phases of a mission. However, vacuum jacket development problems, as well as other factors which will be subsequently discussed, have led to serious consideration of this purged multilayer insulation system.

The helium filled multilayer insulations are estimated to have very poor ground hold performance because of the replacement of air in the insulation with a gas of extremely high thermal conductivity such as helium (required for insulation temperatures close to that of liquid

hydrogen). It does not appear to be a very attractive alternative to the vacuum bag systems. However, it is felt that poor ground hold performance, need not and should not lead to poor overall mission performance, particularly for a vehicle whose primary mission is a space one. The relatively high rating of this system given in Chapter V results, in part, from the belief that the ground hold period without topping for this class of vehicle would be short on the order of several minutes. Naturally, the longer the required ground hold period without topping, the lower this system would fall in the ratings. At some point, the concept as presented would no longer be applicable and the system would devolve into a combination system wherein a subinsulation would be used under perhaps a nitrogen purged NRC-2 blanket.

Admitting the use of a reasonably short ground hold after topping, the helium purged NRC-2 system would appear to possess the following advantages and disadvantages.

Advantages	Disadvantages
1. Vacuum bag development not required.	1. Venting of helium gas during ascent flight required.
2. Leak detection procedures are eliminated.	2. Space evacuation of insulation required.
3. Single component--lightweight system (no subinsulation required).	3. Development of efficient purge techniques required.
	4. No subinsulation is present which could suppress hydrogen gas leakage into insulation during space storage.
	5. Relatively poor ground hold performance.
	6. Requirement to purge complicates launch pad operations.

While one of the disadvantages listed above is the requirement for space evacuation, one of the tests conducted during the course of this program was encouraging in this regard. This test, reported in Appendix D, involved evacuation of a helium purged multilayer insulation installed directly on a cylindrical tank filled with liquid hydrogen. The blanket was pumped along one circumferential edge, and an acceptable pressure level was attained at a station four feet from the blanket edge in a very short time. The open edge was not representative of an actual installation, of course, but the impedance of a typical installation may also permit acceptable evacuation times (less than one day) to be attainable.

3. Multiple Bag, Pre-evacuated (or on site evacuation) NRC-2 Over Sealed Mylar Honeycomb Subinsulation

a. General description

This system (Fig. IV-6) would consist basically of a sealed subinsulation attached to the tank over which would be bonded a number of gore-shaped NRC-2 insulation sections. Each NRC-2 gore section would be encased in a vacuum jacket, evacuated, leak detected and checked out prior to bonding to the subinsulation.

As an alternative to this pre-evacuation concept, the gore sections could be prefitted with evacuation ducts (similar in concept to the purge ducts shown for the helium purged NRC-2 system). The insulation system could then be evacuated after installation on the tank or on site at the launch complex.

Another version of this system could utilize a concept that has received some attention at NASA-Lewis wherein the NRC-2 blanket is perforated. Cryopumping of the insulation would begin upon fueling the tank; the perforations give molecular communication paths to the colder inner layers of the blanket. The time required for attaining a suitable vacuum and the equilibrium pressure level of such a system remains to be demonstrated. Its potential is therefore unknown.

The mylar honeycomb subinsulation would be installed in a manner similar to that discussed for the NRC-2 passive system. The mylar honeycomb would have to be sealed and permitted to cryopump because during ground hold and boost essentially this would be the only thermal protection for the tank. That is, the NRC-2 gores in their evacuated condition would be very thin and afford little protection on the ground.

(1) Blanket design. The 12 gore sections would be made up of 90 layers of NRC-2 with the precut trunnion holes. The gore sections would be made oversized in all directions to effect section junctures by scrolling the edges. The edges would be stitched together to prevent inner layers from slipping. The entire gore would be encased and sealed in a vacuum jacket fitted with a vacuum port.

As an alternative design, the evacuation duct would be installed as shown in Section E-E of Fig. IV-6 before encasing the gores in the vacuum jacket.

The lower dome cap would be a separate pre-evacuated piece with the preformed suction line boot as an integral part. The upper dome cap would likewise be a pre-evacuated piece with mylar tape eyelets bonded around the edges to accept the tie-down rope.

(2) Installation method. The gore sections would be bonded directly to the sealed surface of the mylar honeycomb, the edges being free to be subsequently scrolled and loosely taped down. The bottom dome cap would be slipped over the suction line, overlapping the gore ends by a foot or more. The lower portion would be bonded to the honeycomb subinsulation while the upper ends would be taped to the gore sections between the scrolls.

The upper dome cap would not be bonded to the subinsulation, thus making it removable for access to the manhole cover. Instead, it would be held in place by an interlacing rope fed through mylar tape loops bonded to both the dome cap edge and upper portions of the gore sections.

A lightweight nylon rope net would be placed over the entire tank surface for additional restraint in case of bond failure.

(3) Blanket juncture. The longitudinal edge junctures would be effected by complete scrolling of the adjacent edges as indicated. The dome cap would overlap the gores' edges by a wide margin as shown.

(4) Penetrations. The penetrations would be handled in the same manner as described for the passive NRC-2 system.

b. Performance summary

(1) Weights

Item	Thickness	Weight (lb)	Weight (lb/sq ft)	Comments
Basic insulation--NRC-2	1.3 in.	226.5	0.166	70 layers/in.; $\rho = 1.53 \frac{lb}{ft^3}$
Mylar H/C subinsulation	0.5 in.	119.5	0.0875	3/8-in. Hexcell MHC; $\rho = 2.1 \frac{lb}{ft^3}$
Vacuum bag for NRC-2	2 mils	60	0.044	Mylar--Al foil laminate
Mylar H/C seal	2 mils	30	0.022	Mylar--Al foil laminate
Bond for H/C, seal and vacuum bag to seal		41	0.03	
Scroll insulation weight		41.5	0.0304	5-in. overlap for scrolls

Item	Thickness	Weight (lb)	Weight (lb/sq ft)	Comments
Nylon net ropes	1/8-in. diameter	4	0.00293	650 ft of 1/8-in. diameter rope
Tank support, suction and vent line insulation	1 in.	11.5	0.00843	
Total		534	0.391	

$$\text{Installation factor} = \frac{0.391}{0.166} = 2.355$$

(2) Thermal performance

Ground hold. The pre-evacuated NRC-2 insulation alone would be ineffective on the ground since its thickness would be reduced to about 30 mils. The equilibrium ground performance thus would be primarily that of the cryopumped mylar honeycomb. From Figs. II-3 and II-21, the extimated ground hold heat flux would be 105 Btu/hr-ft^2.

Ascent flight. See Table V-1.

Earth orbit.

Item	k (460-36° R) (Btu/ft-hr-°R)	Thickness	Heat Flux (Btu/hr-ft^2)	Heat Leak (Btu/hr)	Length, L	Q/L	Notes
Basic insulation (ideal)	1.28×10^{-5}	1.3 in.	0.05	68.25			See Fig. IV-3
Tank supports				23.1	42 in.		Appendix F
Suction line				3.64	L/D = 8		Appendix G
Pressurization/vent line				0.51	L/D = 8		Appendix G
Scrolls				6.75	300 ft	0.0225	(1)
Total			0.075	102.25			

$$\frac{Q_{total}}{Q_{ideal}} = \frac{102.25}{68.25} = 1.50$$

NOTE:
(1) Estimate only.

General rating consideration. Fundamentally, this system is a combination of system concepts. While evacuation of the main insulation material (NRC-2) would be required, the degree of vacuum in the NRC-2 would not be important for the ground hold or ascent flight performance, since the sealed, cryopumped subinsulation serves as the main thermal protection.

The unique feature of this system concept is complete encasement of

both sides of each insulation gore section in a vacuum jacket, and pre-evacuation of each prior to installation. It is believed that evacuation and leak detection of these individual gores would be far easier if done before installation. Evacuation could even be performed in a vacuum chamber where the blanket would not be compressed giving less resistance to achieving a high vacuum. In addition, the vacuum jackets could be tailored so as to minimize the wrinkling of the vacuum jacket which is suspected as being the cause of leaks. Some evidence indicates that the wrinkles cause small cracks in the aluminum layer of the Zero-Perm bag whereupon it becomes ineffective as a barrier. Finally, handling and installation of the relatively stiff pre-evacuated gores may prove easier than the more or less bulky unevacuated ones.

In general, then, this system concept appears to possess the following advantages and disadvantages:

Advantages	Disadvantages
1. No venting of insulation during ascent flight is required.	1. NRC-2 insulation is ineffective during ground hold or boost.
2. Pre-evacuation may make evacuation and leak detection easier.	2. Subinsulation seal integrity must be maintained during ground hold boost.
3. Individual gores may be easier to install.	3. Leaks could develop in NRC-2 gores during installation, or in subsequent handling.
4. Sealed subinsulation may inhibit hydrogen leakage into main blanket.	4. Requires effective vacuum bag sealing.
5. Leaks into NRC-2 gores after installation will not necessarily result in air liquefaction in the NRC-2.	5. Reduced insulation efficiency if vacuum bag does not allow full recovery of insulation.

4. Evacuated NRC-2 with Spacers--Unit Vacuum Bag

a. General description

This system would consist of a blanket of NRC-2 insulation installed adjacent to the tank wall and completely enshrouded in a flexible, plastic film type of vacuum jacket. Since the basic NRC-2 insulation has very little resistance to external bearing pressure, its thickness when evacuated would become too small to provide thermal protection on the launch pad or during ascent flight. Therefore, fiber glass cloth or fiber glass mat spacers are specified between the inner one-third of the layers of the NRC-2 insulation.

(1) Blanket design. The 12 gore sections of the blanket would be manufactured in a manner similar to that for the passive NRC-2 system (i. e., with anchor ropes, feeder ropes, etc., installed) except that the extreme ends of the gore, the sawtooth edge shown in Section E-E of Fig. IV-5, would be provided instead of a straight edge cut.

The lower dome cap would be made up by laying up and overlapping precut pieces of aluminized mylar (and spacers in the inner layers) on a form shaped with the contours of the suction line--bottom dome section. The upper edges of this section would then be grouped to form a sawtooth edge for mating with the lower gore sawtooth edges as shown in Section J-J.

The upper dome cap would likewise be premade on a form, and its edges bound to form a sawtooth edge for mating with similar edges on upper gore end, see Section C-C of Fig. IV-5.

(2) Installation method. Installation of the complete blanket would be effected using the anchor and rope system in a manner identical to that described earlier for the NRC passive system. The exception to this would be that the upper dome cap and the lower dome cap with its integral suction line boot are not overlapped with the gore ends but rather are mated by interconnecting the sawtooth edges as described above. The bottom cap would, in addition, be taped to the gores because otherwise the joints would tend to disconnect. The upper dome cap is not shown taped since the inertia forces, the interconnected edges, and the outer net ropes tend to keep it positioned. This feature would facilitate access to the manhole cover once the vacuum jacket is removed.

After the light restraining net is installed, the vacuum bag would be applied over the insulation in sections. Sections would be sealed to one another by pinch-type joints formed by the Alumiseal tape in Section C-C of Fig. IV-5. Other methods of sealing this joint may be devised. The sealing would be effected along meridian lines, circumferentially at the manhole cover station, circumferentially just above the suction line station, at the trunnion fittings, and at a warm location down the suction line. The section encompassing the suction line insulation and a portion of the lower dome would be preformed in the same manner as the suction line insulation sleeve (or boot). Therefore, little or no gathering of the vacuum bag material would be required to effect the seal on the suction line.

The vacuum bag material assumed here is the Zero-Perm Vapor Barrier type, but bag development programs hopefully will result in developing this or other materials into a more reliable form.

b. Performance summary

(1) Weights

Item	Thickness	Weight (lb)	Weight (lb/ sq ft)	Comments
Basic insulation	2.0 in.	480	0.352	Spacers in inner layers, ρ = 2.11 lb/ft^3
Vacuum bag	2 mils	30	0.022	Mylar-Al foil laminate
Tank support, suction and vent line insulation	1 in.	13.65	0.01	
Anchors, ropes and plastic clips		35	0.0255	See NRC-2 passive notes
Complete spacers under ropes		4.5	0.0033	
Total		563.15	0.412	

$$\text{Installation factor} = \frac{0.412}{0.352} = 1.17$$

(2) Thermal performance

Ground hold. The basic thermal data for establishing the equilibrium ground hold heat flux for this system was taken from the experimental data reported in Ref. II-3. The spacers were assumed to exist in the first 40 to 50 layers only. The estimated performance of the evacuated and compressed NRC-2 with partial spacers is given in Figs. II-16a and II-16b. These figures and Fig. IV-8 were used to predict a ground hold heat flux of 48.6 Btu/hr-ft^2.

Ascent flight. See Table V-1.

Earth Orbit.

Item	k (460-36° R) (Btu/ft-hr-° R)	Thickness (in.)	Heat Flux (Btu/ft^2-hr)	Heat Leak (Btu/hr)	Length, L	Q/L	Notes
Basic insulation (ideal)	2.81×10^{-5}	2.0	0.0715	97.5			See Fig. IV-3
Tank supports		1.0		24	41 in.		Appendix F
Suction line		1.0		3.76	L/D = 8		Appendix G
Pressurization/vent line		1.0		0.52	L/D = 8		Appendix G
Sawtooth joints				3.07	300 ft	0.01535	(1)
Anchor-rope attachments				14.4	240 ft	0.06	(2)
Total			0.105	143.25			

$$\frac{Q_{total}}{Q_{ideal}} = \frac{143.25}{97.5} = 1.47$$

NOTES:

(1) and (2) See previous NRC-2 passive system notes.

General rating considerations. In order to utilize the lightweight NRC-2 insulation for a ground evacuated condition and avoid the necessity of using a sealed subinsulation, some method of endowing the NRC-2 with an inherent thickness when under external pressure must be provided. This is accomplished in this system concept by the use of fiber glass cloth spacers (or other) between some or all of the layers. Admittedly, this is similar to the Linde SI concept with two important exceptions. First, with the Linde SI, each foil must be separated or a dead thermal short exists, and second, the Linde SI lateral thermal conductivity is much higher making penetrations and junctures more difficult to insulate.

In this system, only a sufficient number of layers need be provided with spacers to give acceptable (depending on mission and operational requirements) ground hold performance. Additional spacer material only increases the deadweight when in space.

As with all ground evacuated systems, the development of a good vacuum bag material or composite is still the major problem.

The advantages and disadvantages of this system are summarized as follows:

Advantages	Disadvantages
1. No venting of insulation during ascent flight is required.	1. Vacuum bag development required.
2. Penetration insulation and gore section junctures easier to effect than evacuated Linde SI--lower lateral thermal conductivity.	2. Complicated leak detection procedures required.

3. Insulation density may be kept low by use of partial spacers.	3. Air liquefaction in blanket if leak occurs. 4. Hydrogen gas can diffuse into blanket

5. Evacuated Linde Superinsulation-Unit Vacuum Bag

a. General description

Except for the basic insulation material and thickness, this system concept (Fig. IV-5) and its design features would be identical to the preceding "Evacuated NRC-2 with Spacers" system. It is assumed that basic material for this case is Linde SI-62 which, despite its high density, appears to offer the best overall performance of the Linde superinsulations. Its high density results in a lower optimum thickness for Linde SI-62 than for the lower density NRC-2 insulations (see Table V-1).

In view of the fact that the spherical tank design features for the Evacuated Linde SI system and the Evacuated NRC-2 with spacers system would be essentially identical, only Fig. IV-5 is shown to present both systems. For discussion of design features, refer to previous system writeup (Section IV. A. 4).

b. Performance summary

(1) Weights.

Item	Thickness	Weight (lb)	Weight (lb/ sq ft)	Comments
Basic insulation	0.85 in.	532	0.39	SI-62, ρ = 5.5 lb/ft^3
Vacuum bag	2 mils	30	0.022	Mylar-Al foil laminate
Tank support, suction and vent line insulation		20.6	0.0151	
Anchors, ropes and plastic clips		35	0.0265	
Total		617.6	0.452	

Installation factor = $\frac{0.452}{0.39}$ = 1.16

(2) Thermal performance

Ground hold. The heat flux through evacuated Linde SI-44 compressed under one atmosphere is presented on Fig. IV-7. As noted on that figure, the performance of Linde SI-62 under identical conditions may be approximately determined. The equilibrium ground hold heat flux for the Linde SI-62 system was determined from Figs. IV-7 and II-3 to be 13 Btu/hr-ft^2.

Ascent flight. See Table V-1.

Earth orbit.

Item	k (460-36° R) (Btu/ft-hr-°R)	Thickness (in.)	Heat Flux (Btu/hr-ft^2)	Heat Leak (Btu/hr)	Length L	Q̇/L (Btu/hr-ft)	Notes
Basic insulation (ideal)	1.5×10^{-5}	0.85	0.0897	122.5			See Fig. IV-3
Tank supports		0.85		25.4	40 in.		
Suction line		0.85		3.655	L/D = 8		
Pressurization/ vent line		0.85		0.53	L/D = 8		
Sawtooth joints				14.6	300 ft	0.0487	(1)
Anchor-rope attachments				33.8	260 ft	0.13	(2)
Total			0.147	200.5			

$$\frac{\dot{Q}_{total}}{\dot{Q}_{ideal}} = \frac{200.5}{122.5} = 1.64$$

NOTES:

(1) and (2) Estimates only.

General rating considerations. The primary advantage of the basic Linde SI type of material is its potential ability to provide high thermal performance during ground hold under evacuated conditions. The relatively large bulk of spacer material causes the Linde SI to retain at least one-quarter of its original thickness even under a crushing pressure of 1 atm. The spacer material keeps the foils spaced in the compressed condition even though the spacing distance is reduced. The reduced spacing distance actually is advantageous since the molecular heat transport regime occurs between foils at a lower vacuum pressure level.

The advantage of high ground hold thermal performance is not easy to assess in a general study. If the ground hold period is short, it has very little influence on the optimum design. If the ground hold period (without topping) is long, it can have a significant effect on the system optimization regardless of whether the space mission is long or short. A general method for performing this tradeoff study is indicated in Section B of Chapter III.

In general, the advantages and disadvantages of this system are identical to those of the previous system (NRC-2 with Spacers) with the exception that the insulation of penetrations, joining of adjacent sections and termination of blanket sections are much more difficult due to the higher lateral thermal conductivity of the basic material.

6. Helium Purged Marshield

a. General description

The basic materials (aluminum foils and separators) which go into manufacturing one type of Marshield insulation (Fig. IV-8) have been described previously in Section II.C. The system would consist of a shield of 20 layers of aluminum foils, and dimpled, impregnated fiber glass cloth separators literally hung on the tank piece by piece.

(1) Insulation materials. The reflecting foils of the Marshield would be typically 3- to 4-mil thick aluminum foils polished on both sides. These foils would be cut and formed into doubly curved panels of various sizes as indicated in Fig. IV-8 (typically 3 ft x 2 ft). At their four corners and at the centers of each edge, a circular flareout with a precut hole provides for overlapping and connecting adjacent intersecting foils and insertion over the support pins where they occur.

The separator sheets (foil spacer sheets) would be cut similarly into panels of the same size and form as the foil panels. The spacer sheets are shown double-dimpled on 1-in. square centers with 1/8-in. deep dimples. The square pattern is staggered from front-to-back side. The alternating dimples provide a foil spacing of 1/4 in. for the design shown. The spacing may be varied by varying dimple depth. The spacing may be determined by performance level desired or by simply the volume available for shield installation.

(2) Installation method. Low conduction, nonmetallic support pins would be attached to the tank by bonding them to the tank initially and welding retaining clips around the wide base as shown. A circular row of 12 support pins would be located around the periphery of the manhole cover, and 24 would be located around the equator.

The Marshield separator panels and foil panels would be installed one at a time over the support pins. At foil and spacer panel intersections, the precut holes would be aligned and fastened together with small metal clips (see Detail E of Fig. IV-8).

A lightweight restraining net is shown installed over the shield. This would be primarily a safety feature to prevent sagging of the lower half of the shields or to carry helium gas pressure buildup in the shield during ascent flight. While it would be expected that rapid venting of

the helium purge gas should pose no problem, it might be necessary to partially seal the shield to maintain a slightly positive purge pressure on the ground. In this eventuality, the restraining net might be necessary during flight.

(3) Penetrations

Tank supports. The Marshield would be terminated at the tank end of the supports. Patches of NRC-2 insulation are shown placed under the supports. The outer support surface would be insulated with NRC-2 insulation which would be faired into the Marshield terminations by interleaving the NRC-2 plys with the foils and separators, and securing the ends by taping.

Suction line. It has been estimated that the Marshield basic materials could be preformed or molded into shapes having the required curvature for piecing together the Marshield insulation into a bottom dome-suction line juncture. The ends of the suction line collar would then be staggered and several of the outer layers bent inward to block some of the radiation to the foil ends. The bending would be accomplished by slitting the edges (or notching them) and overlapping the material.

b. Performance summary

(1) Weights

Item	Thickness or Number	Weight (lb)	Weight (lb/ sq ft)	Comments
Basic insulation	2.5 in.	1400	1.025	See note (1)
Support pins	36	0.8		See note (2)
Tank support, suction and vent line insulation		14.2	0.0104	NRC-2 insulation
Net ropes		4	0.00293	650-ft, 1/8-in. nylon rope
Totals		1419	1.04	

$$\text{Installation factor} = \frac{1.04}{1.025} = 1.015$$

NOTE (1). Ten (3 mils) Al foils, ten (5 mils), 1/8-in. deep dimpled separators; $\rho = 4.93\ \text{lb/ft}^3$.

NOTE (2). 0.4-in. diameter fiber glass or phenolic pins.

(2) Thermal performance

Ground hold. The estimated equilibrium ground hold heat flux for this system is 130 Btu/hr-ft^2. The probable heat transfer conditions within the helium purged shield have been discussed in Section II. C. 1. (c). The ground hold heat flux was determined from Fig. II-3 and the following relationship which was derived by using an empirical relationship for effective conductivity that included convection:

$$\dot{Q}/A_{\substack{\text{He purged}\\ \text{Marshield}}} = \frac{8.91 \times 10^{-3}}{\delta_i} \left[T_w^{1.675} - 404 \right]$$

where

T_w = outer wall temperature of Marshield

δ_i = Marshield thickness (in.)

Ascent flight. See Table V-1.

Earth orbit.

Item	k (460-36° R) Btu/ft-hr-°R	Thickness (in.)	Heat Flux Btu/hr-ft^2	Heat Leak (Btu/hr)	Length, L	Notes
Basic insulation	1.53×10^{-4}	2.5	0.311	425		See Appendix B
Tank supports		1		26.4	40 in.	NRC-2
Suction line		2.5		4.81	L/D = 8	Marshield + NRC-2
Pressurization/vent line		1		0.70		NRC-2
Shield joints				0		
Support pins				13.2		
Totals			0.3445	470.1		

$$\dot{Q}_{total}/\dot{Q}_{ideal} = \frac{470}{425} = 1.11$$

General rating considerations. It was realized before conducting the design study that the thermal performance of this insulation material would not match that of the Linde and NRC insulations. The main impetus for consideration of its development lies in certain unresolved or potentially unsolvable problem areas inherent in the other systems. Some of these problem areas involve questions concerning the ability to attain the ideal performance assumed in the comparison. Should the attainment of ideal performance prove unfeasible or impractical, the Marshield concept would attain even higher stature.

Currently experimental thermal data have not been obtained for this insulation material.

The main advantages and disadvantages of this system concept are considered to be:

Advantages	Disadvantages
1. Positive structural attachment.	1. High lateral thermal conductivity and low solidity of foils poses problems with exposed edges.
2. Predictable, reliable performance once basic data is known.	2. Relatively poor estimated performance for all mission phases.
3. Efficient purging of insulation should be easily achieved.	3. Volume requirements for shield are high.
4. Venting of purge gases during ascent should pose no problems.	4. Sensitive to handling damage.
5. Space evacuation to desired pressure level should be achieved quickly.	5. Optical properties of foil surfaces must be maintained.
6. Hydrogen gas diffusion from tank and other outgases should be quickly removed from shield.	6. Difficult to form contours at penetrations.

B. TOROIDAL TANK INSULATION SYSTEM DESIGN

The toroidal tank (Fig. IV-9), being internally supported, can utilize most of the features developed for the insulation systems of the spherical tanks. The primary difference between the toroidal and spherical tanks is, of course, their shapes. The toroidal tanks present some relatively adverse characteristics for installing an insulation system mostly due to smaller radii of curvature for equal outside radii. The volume-to-area ratio is smaller for the toroidal than for the spherical tanks which will lead to some insulation inefficiencies, and the insulation will have more joints per unit surface area than the spherical tanks if equal gore widths are considered in each case.

An installation advantage relative to the sperical case is that roving (fiber glass yarn) about the subinsulation and the nets for the main blanket can be easily installed about the smaller circumference.

The structural support problem appears to be basically the same here as for the spherical tanks. Therefore, strap or rod-like supports would be designed using the methods given in Appendix F.

1. System General Description

The system presented in Fig. IV-9 is fundamentally an adaptation of the passive NRC-2 system presented in Fig. IV-1. The subinsulation would be mylar honeycomb and would be applied as discussed in Section A-1 of this chapter.

a. NRC-2 insulation blanket

Twelve gores would be fabricated with all edges provided with sawteeth for joining with adjacent gores. Their lengths would be approximately equal to the tank's smallest circumference and their widths equal to one-twelfth of the largest circumference. Six gores would have precut holes through which the center attachment of the outer trunnion supports would fit. Six additional holes with radial serrations would also be cut along the inner horizontal circumference of the blanket for installing the inner support members. Four anchor ropes are shown installed horizontally in each gore--two close to the fingers at the gore ends as shown in the detail of the typical gore.

The manhole cap would be manufactured as a single circular piece with sawtooth edges and eyelets on its outer surface for lacing to the main blanket. The gore with the manhole opening would have mating sawtooth edges with radial serrations forming flaps to accommodate interleaving the edges of the manhole cover and main blanket.

The two gores which would otherwise join at the suction line penetration are shown with cutouts and a flapped, sawtooth edging in Section B-B to interleave with the sawtooth edging of the suction line boot. The suction line boot would be made up as a separate preformed sleeve and slipped over the suction line before installation.

Separate insulation sleeves would also be fabricated for the six inner rod supports.

b. Installation method

In some respects, the use of the anchor-rope attachment system for the toroidal tank should be even more reliable than for the spherical tank. This would result from each gore being wrapped fully around the small circumference of the tank and anchored by two anchors close to the short edges of the gores. The seam of the mating short edges is shown to occur at the inner radius, but this placement is arbitrary. In addition, the gores would be anchored at two intermediate stations

along their lengths. All anchors would be positioned under the saw-tooth seams as on the other designs. Adjacent fingers would then be mated along all edges, except where the suction line boot joins the gores.

The suction line boot would be held on primarily by interleaving the gore flaps with the sawteeth of the boot edge and taping each pair together as they are mated. The boot would be restrained from boost inflation by a separate sleeve-type net tied at several places to the main restraining net lines passing around the tank.

The manhole cap would then be laced securely in position after being interleaved with the blanket in a manner similar to the suction line juncture. The main net for restraining boost loads would then be tied around the entire insulation blanket.

The inner rod supports would be insulated by butting the end of its preformed sleeve against the turned-up, serrated flaps of the holes in the blanket. The abutting edges would be secured by tape. The joint would then be further insulated by spirally overwrapping with NRC-2 strips that would be also secured by taping.

C. CYLINDRICAL TANK INSULATION SYSTEM DESIGN

While some of the insulation systems developed for spherical shaped tankage are adaptable to cylindrical-type tankage, the cylindrical shape does pose some unique design problems. Two basic forms of cylindrical tankage must be considered: internally supported and integral cylindrical tanks. The internally supported cylindrical tanks present design problems quite similar to internally supported spherical tanks. The primary difference is the presence of large lateral surfaces (depending upon L/D) having single curvature, and more latitude in the design of the tank supports. The lateral surfaces of the internally supported tank can be insulated by most of the techniques evolved in this study, and the blanket junctures and penetration insulation can be effected by methods similar to those shown for the spherical tankage. However, variations in the tank support method from that shown for the spherical tanks may be considered. For example, strap-type supports may be employed on the lower portion of the tank, with upper supports being used to restrain the tank against the smaller lateral loads.

The differences between the internal spherical tank and the integral cylindrical tank are much greater. The insulation system in this case becomes split between internal surfaces and quasi-external surfaces. The tank support systems are the fore and aft interstage sections which now carry the upper stage inertia loads and bending moments as well

as the inertia loads of the propellant. This support structure, of necessity, is a continuous cylinder and heavier than straps designed by propellant inertia loads, and its potential heat leak is thus higher. In addition, the insulated tank barrel must now be protected by a secondary structure, a shroud, against exposure to the boost ambient environment (heating, aerodynamic loads, etc.).

Thus, optimization of the structure-insulation system for the integral tank case involves some additional factors which were not present for the internally supported tanks. These include:

(1) Insulation system weight and performance as affected by shroud design or installation method.

(2) Weight of shroud as a function of attachment method, meteoroid protection potential, and interaction with the external portion of the insulation system.

(3) Interstage weights as a function of insulated skirt length, and upper stage weight and configuration.

(4) Effects of fluid line routing on weight and performance, particularly in the case of bipropellant tankage.

A generalized study of the detailed or even optimum design of integral tankage might be performed that includes the above additional factors, but such a study was considered beyond the scope of this program.

1. System General Description

Figure IV-10 presents the passive NRC-2 system as applied to the integral cylindrical tank. This insulation system was selected not only because it was rated number one, but because inherently it possesses several advantages over the other systems when considering this particular design. First, being a passive system, no other operations are required once the cinching shroud has been attached. Second, local compression of the insulation by the shroud during ground hold and ascent phases is thermally acceptable since the subinsulation is adequate by itself to accomplish the thermal protection function. Third, the vital vacuum jacket of an evacuated system would be vulnerable to chafing or tearing with cinching shroud concept. Fourth, a helium purged insulation system used in conjunction with this cinching shroud concept would exhibit poor ground hold performance, and possibly be subject to local air liquefaction at locally compressed areas. Finally, the use of sealed foam subinsulation on the external surfaces may tend to partly dampen the effects of external pressure oscillations on the shroud.

a. Insulation blanket design

(1) Subinsulation. The tank domes would be covered with sealed mylar honeycomb which would be bonded on and, in addition, would be held to the tank by pretensioned fiber glass roving attached to the small Z-shaped clips near the barrel dome juncture (see Detail D of Fig. IV-10).

The external surface of the barrel section would be covered with bonded-on, sealed polyurethane foam, likewise held on by pretensioned fiber glass roving under the seal layer.

(2) NRC-2 gores. Twelve full-length, straight-edge gores for the barrel section would be fabricated with preformed sawtooth longitudinal edges and installed anchor ropes and Y-clips as described previously for System 1 (Section IV.A.1).

Twelve upper and twelve lower dome gores would be fabricated much as the gores described for the spherical tanks except that the lower end shape would be slightly different with no trunnion cutouts present, and the anchor ropes would be located to permit close fitting of the gores around the barrel-dome junctures (see Detail D). The remainder of the gores would form the insulation blankets for the interior surface of the upper and lower skirts. The skirt ends of the lower portion of the gore would be scalloped, fitted with anchor ropes to permit attachment to the skirts by clips located approximately 5 ft from the barrel-dome juncture (see Detail E). The manhole cap would be fabricated as a single piece as described for System 1.

The lower dome cap would be fabricated with a suction-line boot as an integral part as described previously for the passive system.

(3) Installation method. The barrel section gores would be installed by snapping the anchor rope end clamps to the 12 rows of anchor ring eyes. The gore edges would then be mated by interleaving the sawtooth (or finger) edges. These gores extend beyond both the fore and aft barrel-dome junctures to provide insulation for the external surfaces of the interstage skirts.

The dome gores would be installed also by the anchor rope system, the lower ends being reversed and brought along the internal surfaces of the skirts and attached as shown in Detail E. The upper and lower dome caps and their restraining nets would be installed by attaching the nets to the Y-clips (see Detail D) as described for the spherical passive system (Section IV.A.1).

With the barrel section insulation blanket in place, the shroud sections can be installed and cinched to the required tension.

b. Shroud design

The shroud is designed to exert 2 psi crushing pressure on the insulation during ground hold and ascent flight as discussed in Chapter II under design requirements. The corrugated sections of the shroud are titanium to assure retention of modulus and therefore spring tension throughout ascent heating.

The lower end of the shroud abuts on the shroud clocks during ascent as shown in Fig. IV-10. It is further restrained from longitudinal motion relative to the tank by the depressed leaf springs and friction forces. Upon reaching orbit the joints in the corrugated shroud are exploded, permitting the shroud to expand to the limits of the short cables connecting the shroud segments. The predepressed leaf springs would aid in deploying the shroud and keeping it concentric with the tank and accordingly free of the insulation while deployed in space. Further, the leaf springs may be designed to restrain the shroud against longitudinal forces arising in-space acceleration.

Small fairing blocks are shown attached to the forward ends of the shroud corrugations in Fig. IV-10. Their purpose is to prevent air from being rammed down the outstanding segments of the corrugations during ascent. The small blocks would be attached to the outer groove of the corrugations. These fairing blocks may not be required, or other devices may be used for the same purposes, depending upon payload configuration.

Many of the details shown for the integral tankage shown in Fig. IV-10 should be considered only nominal, since their complete definition would depend upon precise specification of the design requirements of the booster, payload and mission.

D. ILLUSTRATIONS

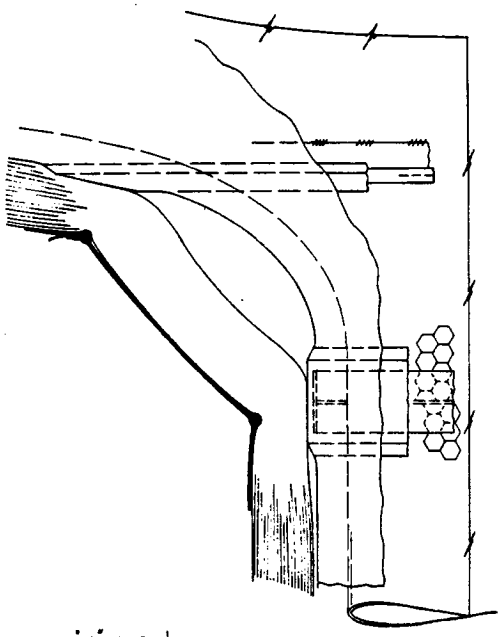

SECT. J-J SCALE 1

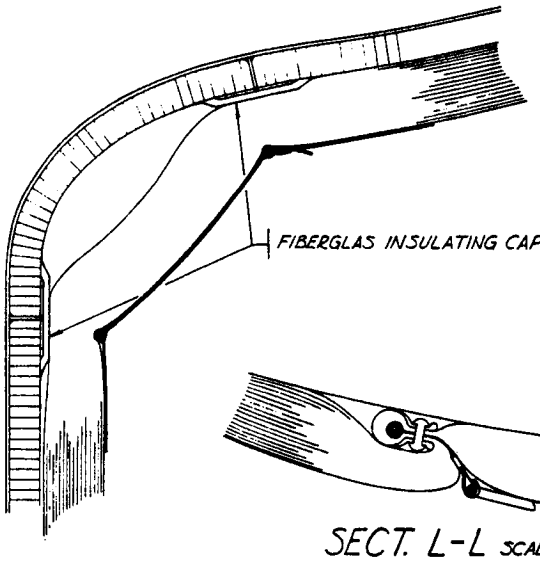

SECT. L-L SCALE 1
BOOT ATTACHMENT (TYP.)

PLAS

RESTRAINI

'y' CLIP

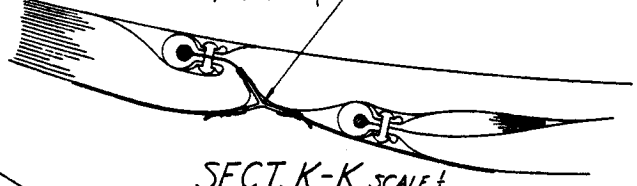

SECT. K-K SCALE 1

SECT. B-B SCALE 1/2
SUCTION LINE BOOT-ARRANGEMENT SHOWN ON DWG 4 MAY BE CONSIDERED AS ALTERNATE

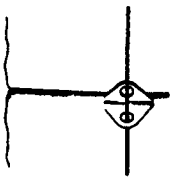

DETAIL
SCALE 1
TYP. 'y' CLIP USED FOR RESTRAININ

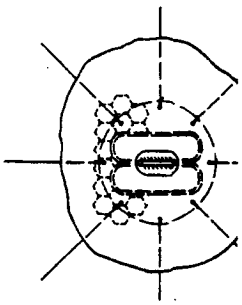

SECT. G-G S
TYP. ANCHOR (BLANKET

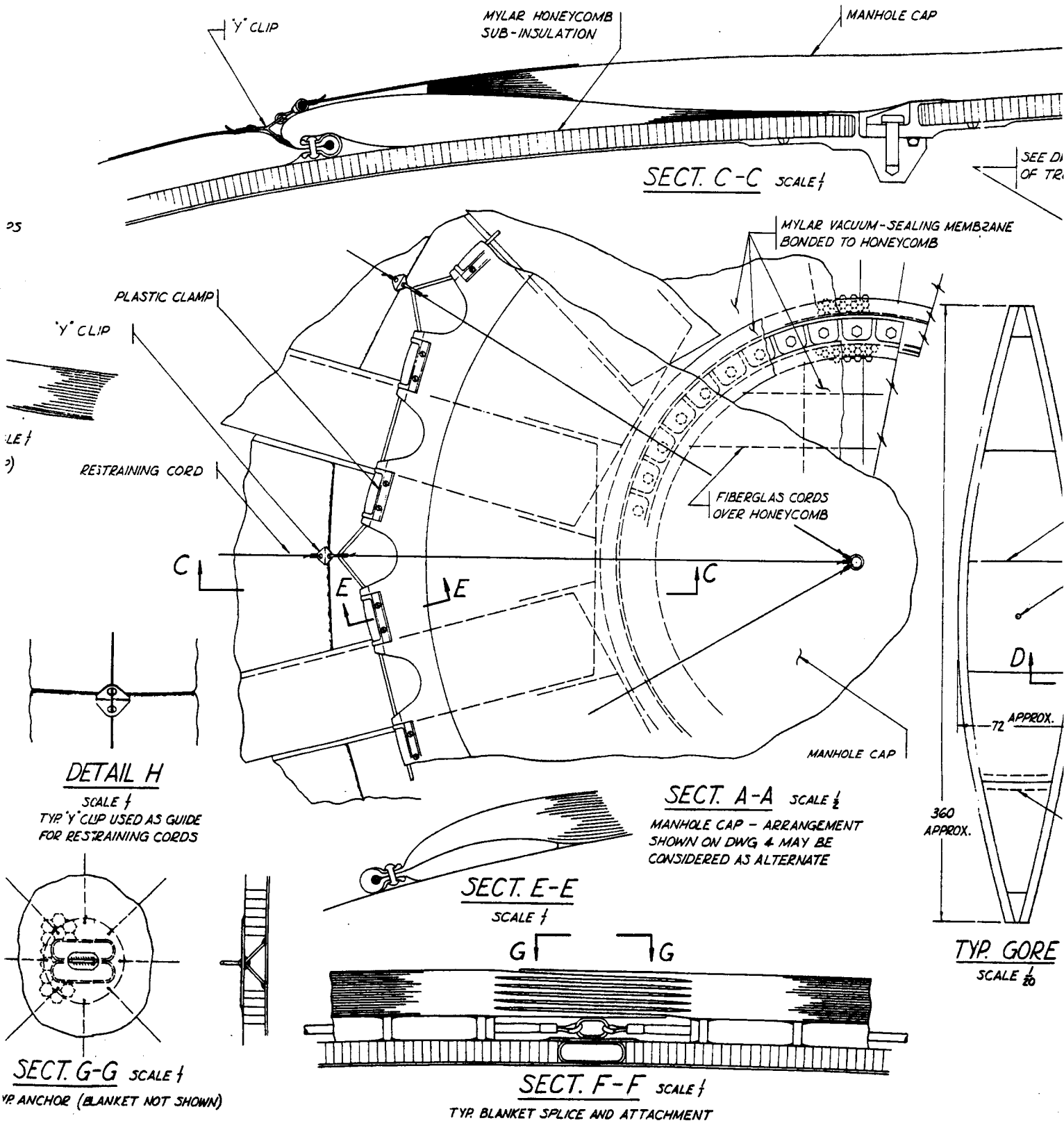
'Y' CLIP
MYLAR HONEYCOMB SUB-INSULATION
MANHOLE CAP
SECT. C-C SCALE 1/
MYLAR VACUUM-SEALING MEMBRANE BONDED TO HONEYCOMB
PLASTIC CLAMP
'Y' CLIP
RESTRAINING CORD
FIBERGLAS CORDS OVER HONEYCOMB
C
E
E
C
MANHOLE CAP
DETAIL H
SCALE 1/
TYP 'Y' CLIP USED AS GUIDE FOR RESTRAINING CORDS
SECT. A-A SCALE 1/2
MANHOLE CAP - ARRANGEMENT SHOWN ON DWG 4 MAY BE CONSIDERED AS ALTERNATE
D
72 APPROX.
360 APPROX.
TYP. GORE
SCALE 1/20
SECT. E-E
SCALE 1/
G
G
SECT. G-G SCALE 1/
YP. ANCHOR (BLANKET NOT SHOWN)
SECT. F-F SCALE 1/
TYP. BLANKET SPLICE AND ATTACHMENT

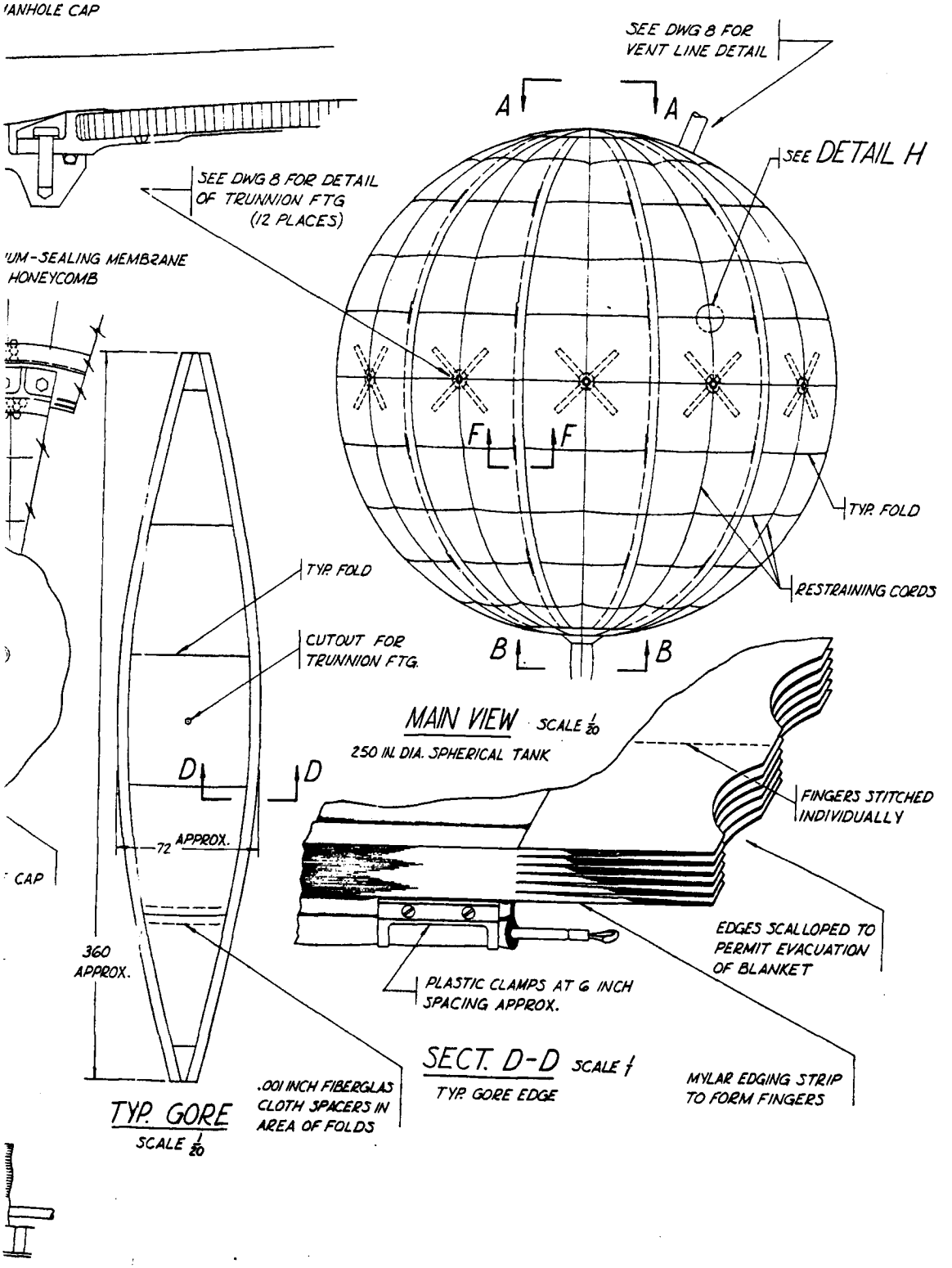

Fig. IV-1. NRC-2 Passive System

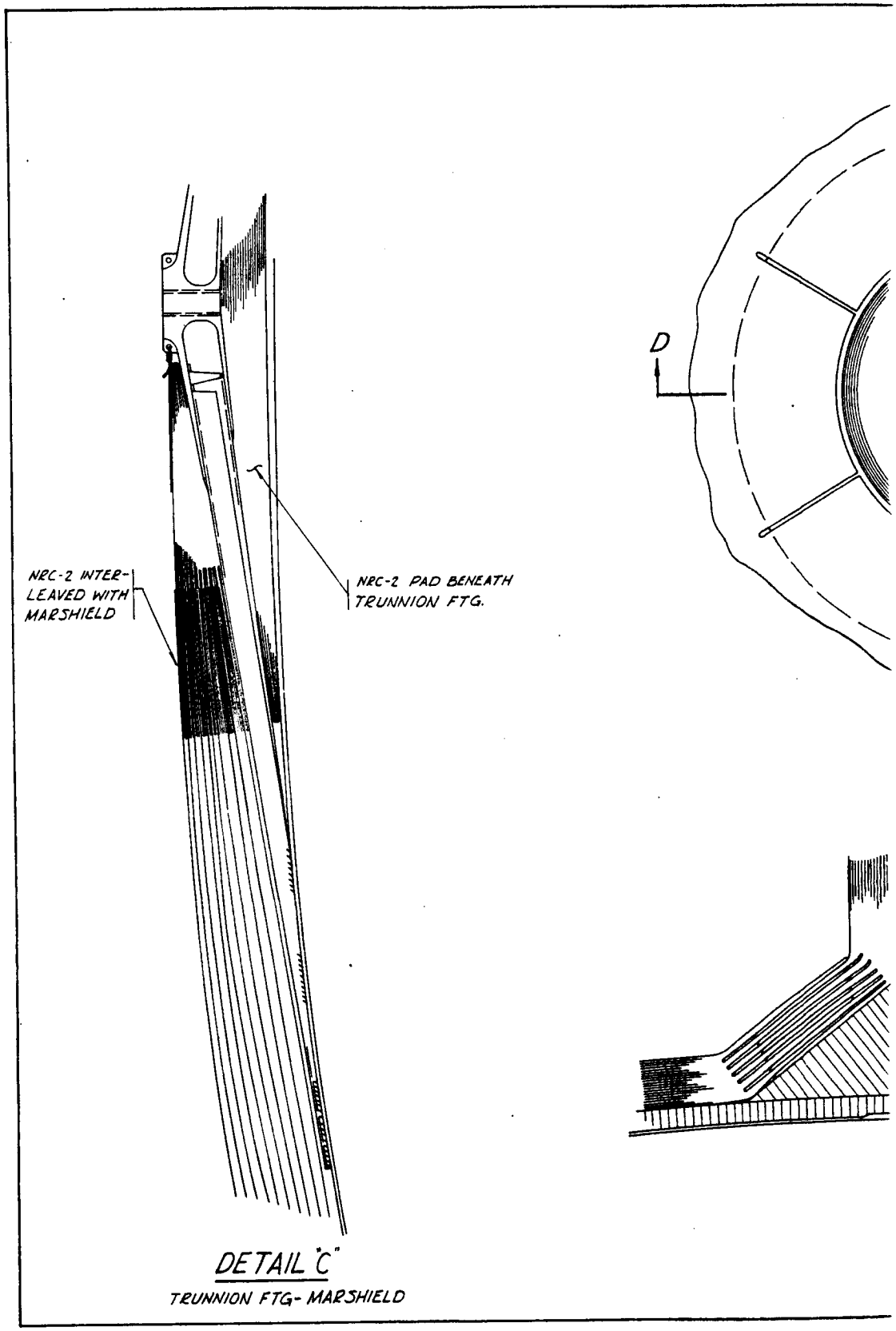

DETAIL "C"

TRUNNION FTG- MARSHIELD

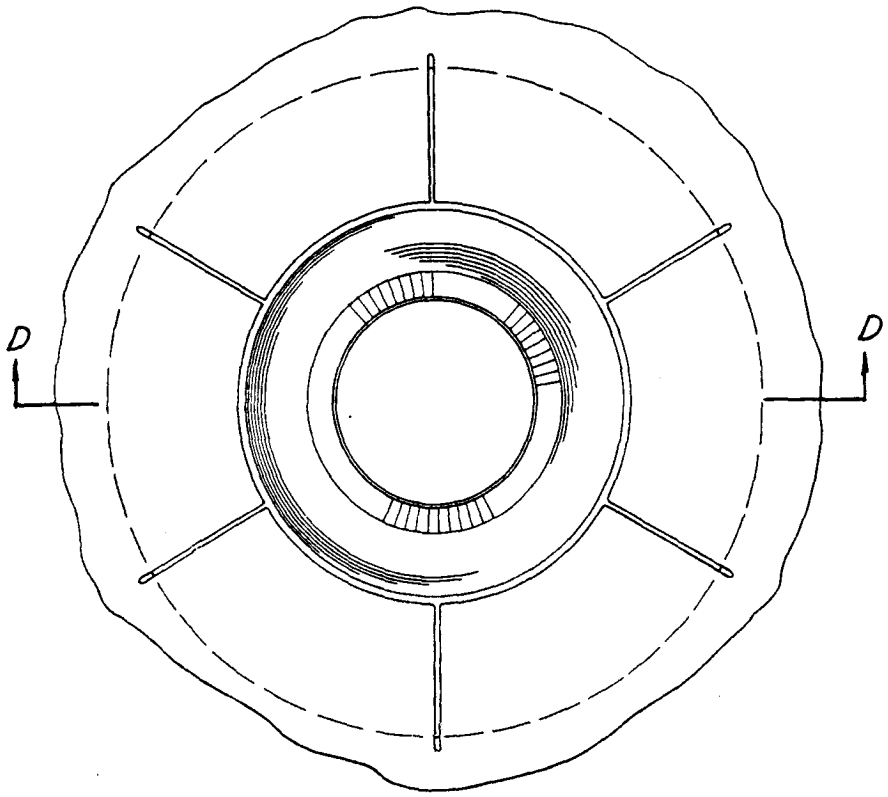

DETAIL B
TYP. VENT LINE

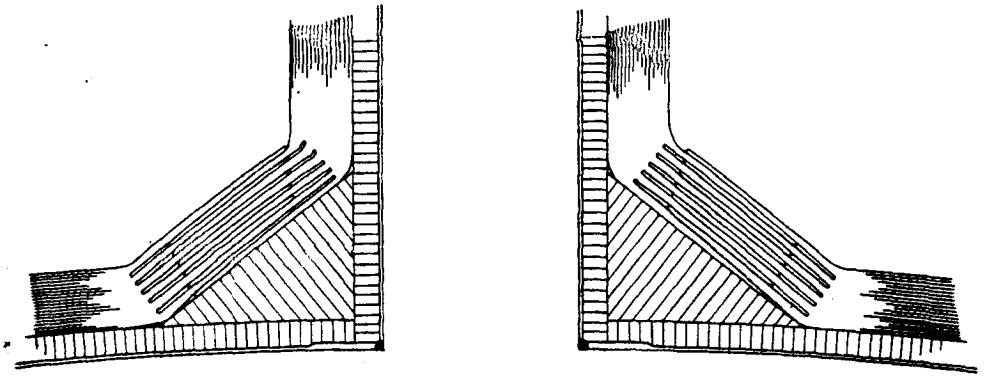

SECT. D-D

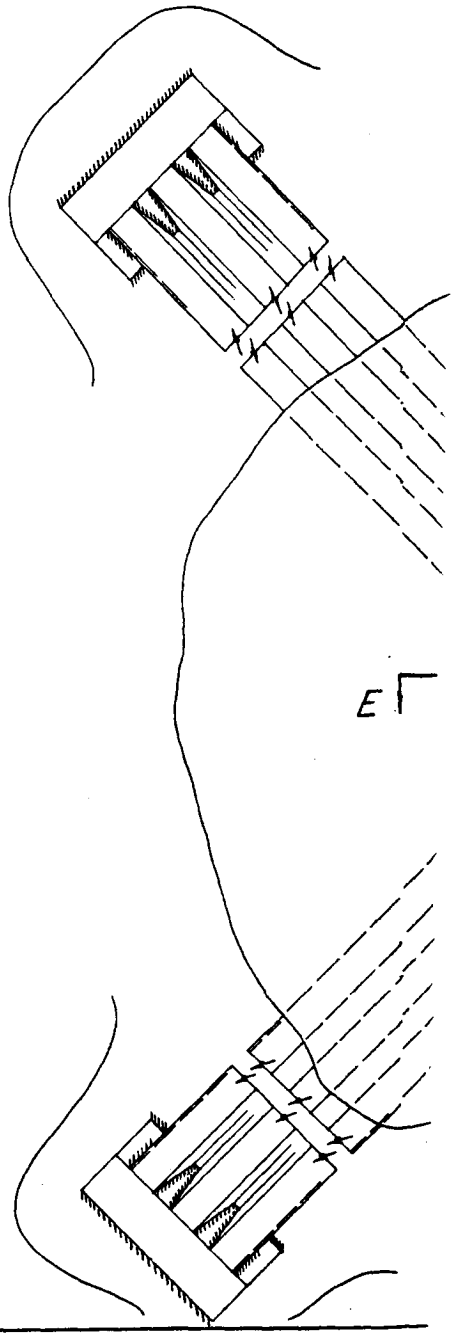

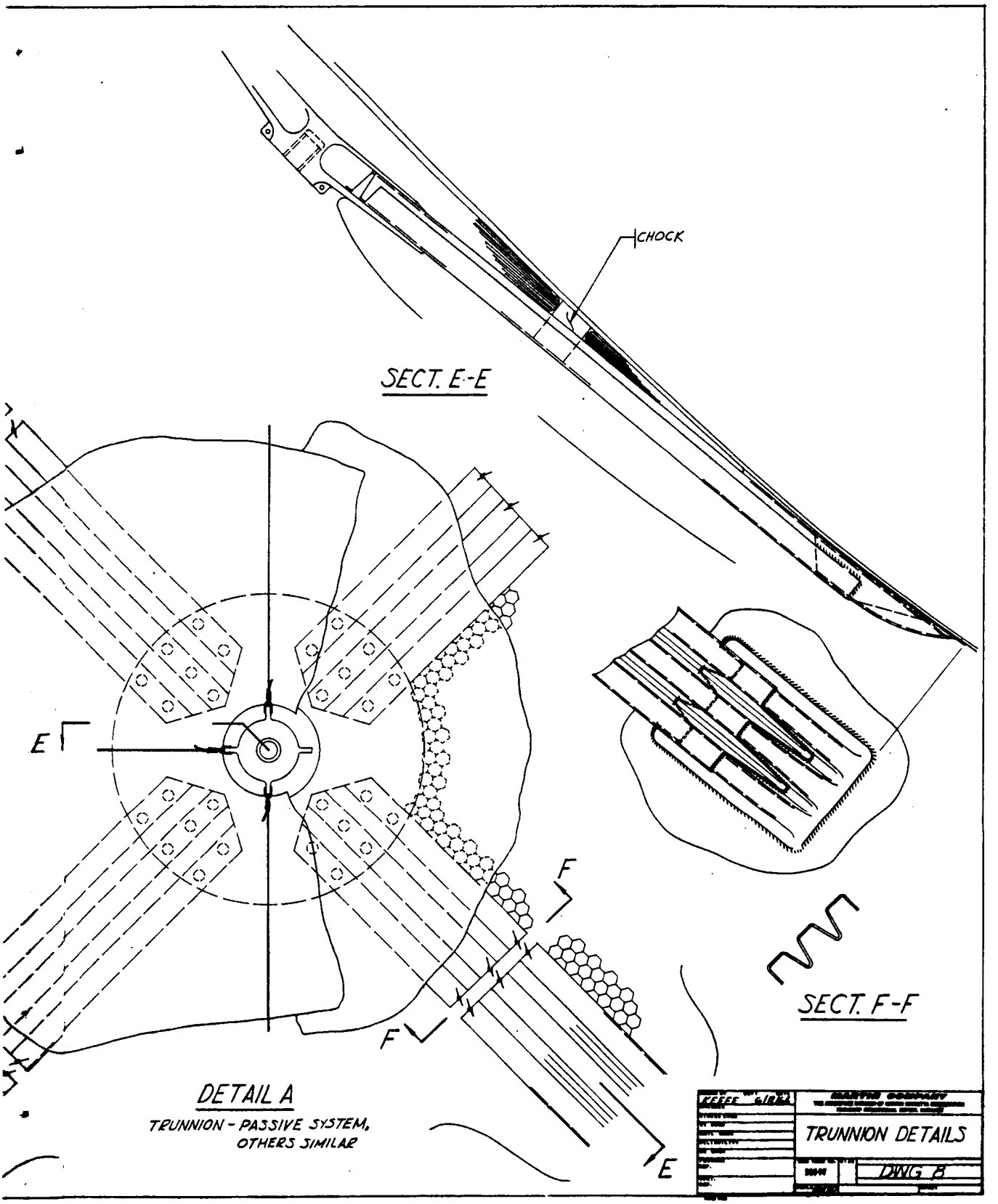

Fig. IV-2. Trunnion Details

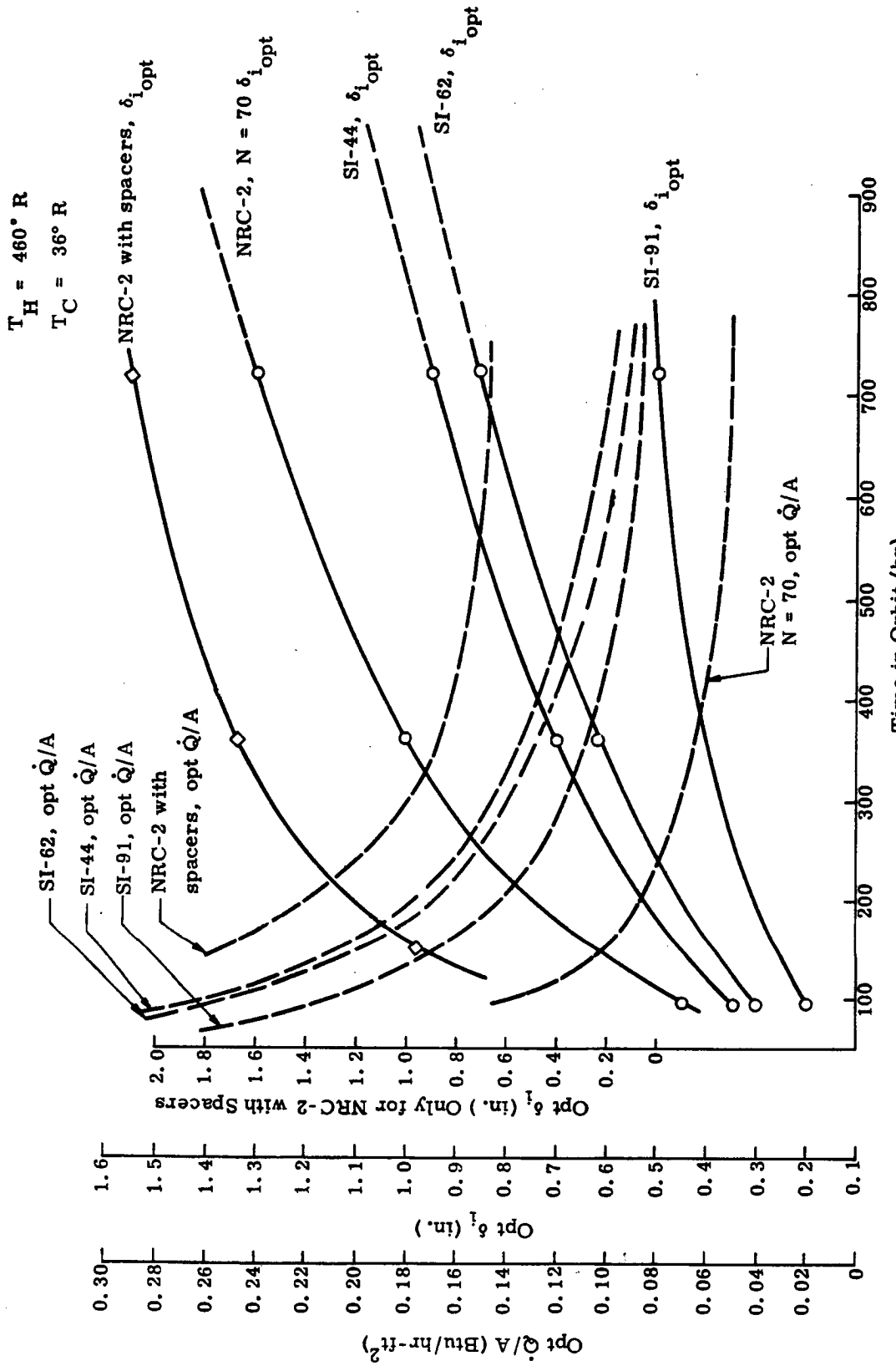

Fig. IV-3. Optimum Insulation Thickness for Orbit Condition Liquid Hydrogen Propellant Storage Mission

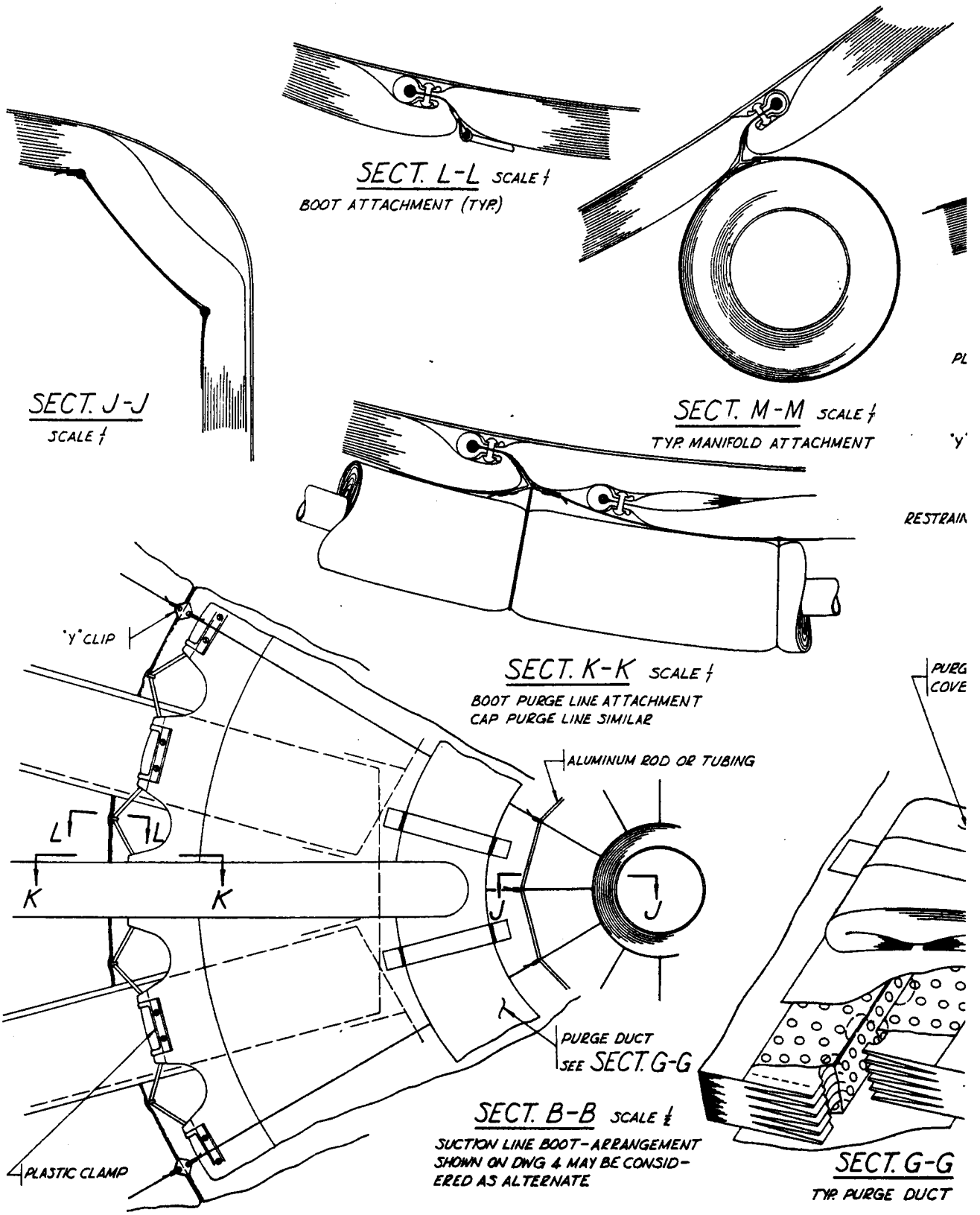
SECT. L-L SCALE 1
BOOT ATTACHMENT (TYP.)
SECT. J-J
SCALE 1
SECT. M-M SCALE 1
TYP. MANIFOLD ATTACHMENT
SECT. K-K SCALE 1
BOOT PURGE LINE ATTACHMENT
CAP PURGE LINE SIMILAR
"Y" CLIP
ALUMINUM ROD OR TUBING
PURGE DUCT
SEE SECT. G-G
SECT. B-B SCALE 1
SUCTION LINE BOOT-ARRANGEMENT
SHOWN ON DWG 4 MAY BE CONSIDERED AS ALTERNATE
PLASTIC CLAMP
SECT. G-G
TYP. PURGE DUCT
RESTRAIN
PURG
COVE

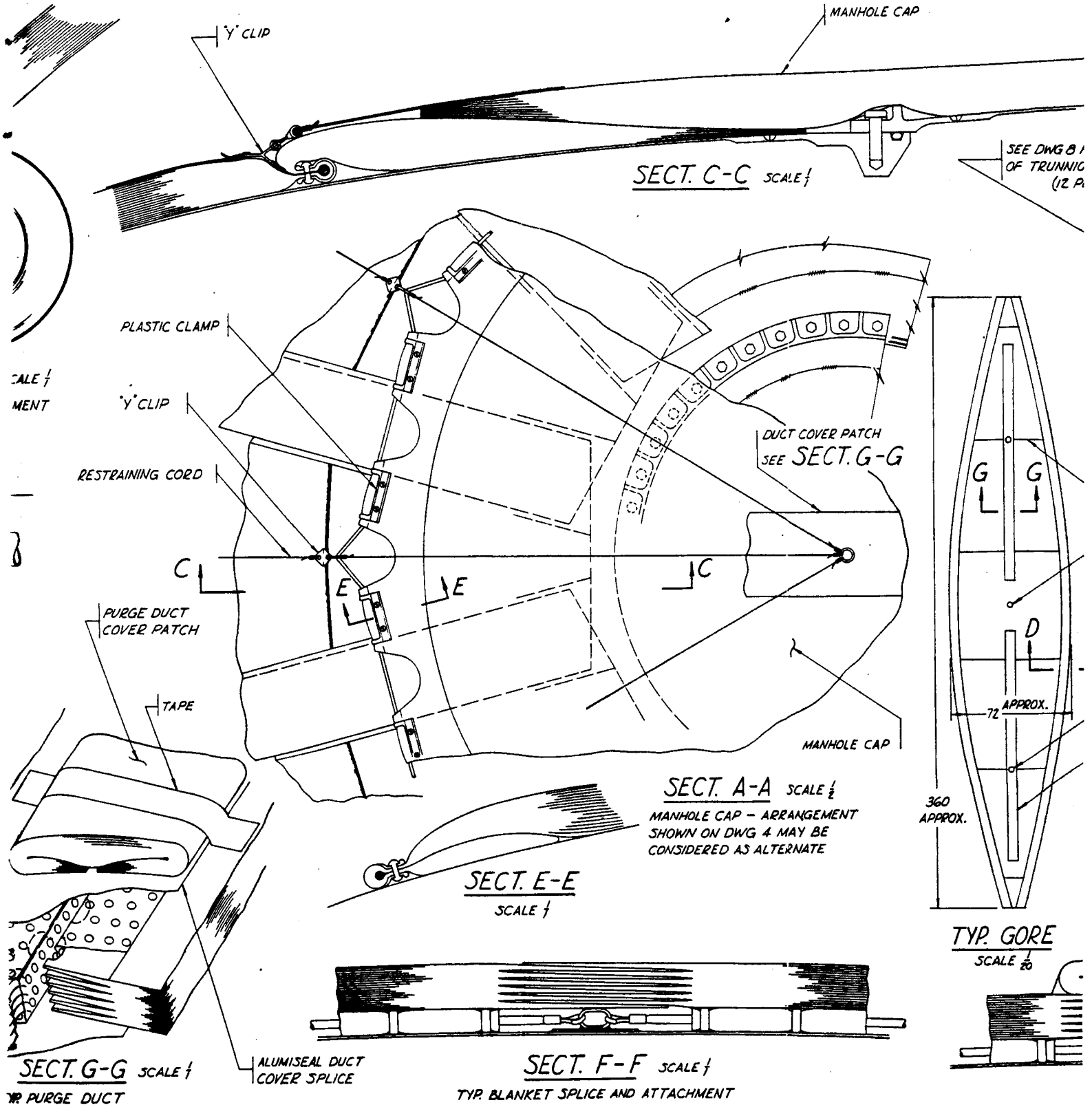
'Y' CLIP
MANHOLE CAP
SECT. C-C SCALE 1/
SEE DWG 8 /
OF TRUNNIC
(12 P
PLASTIC CLAMP
'Y' CLIP
RESTRAINING CORD
DUCT COVER PATCH
SEE SECT. G-G
C
C
E
E
G
G
D
72 APPROX.
360 APPROX.
PURGE DUCT
COVER PATCH
TAPE
MANHOLE CAP
SECT. A-A SCALE 1/2
MANHOLE CAP - ARRANGEMENT
SHOWN ON DWG 4 MAY BE
CONSIDERED AS ALTERNATE
SECT. E-E
SCALE 1/
TYP. GORE
SCALE 1/20
SECT. G-G SCALE 1/
TYP. PURGE DUCT
ALUMISEAL DUCT
COVER SPLICE
SECT. F-F SCALE 1/
TYP. BLANKET SPLICE AND ATTACHMENT

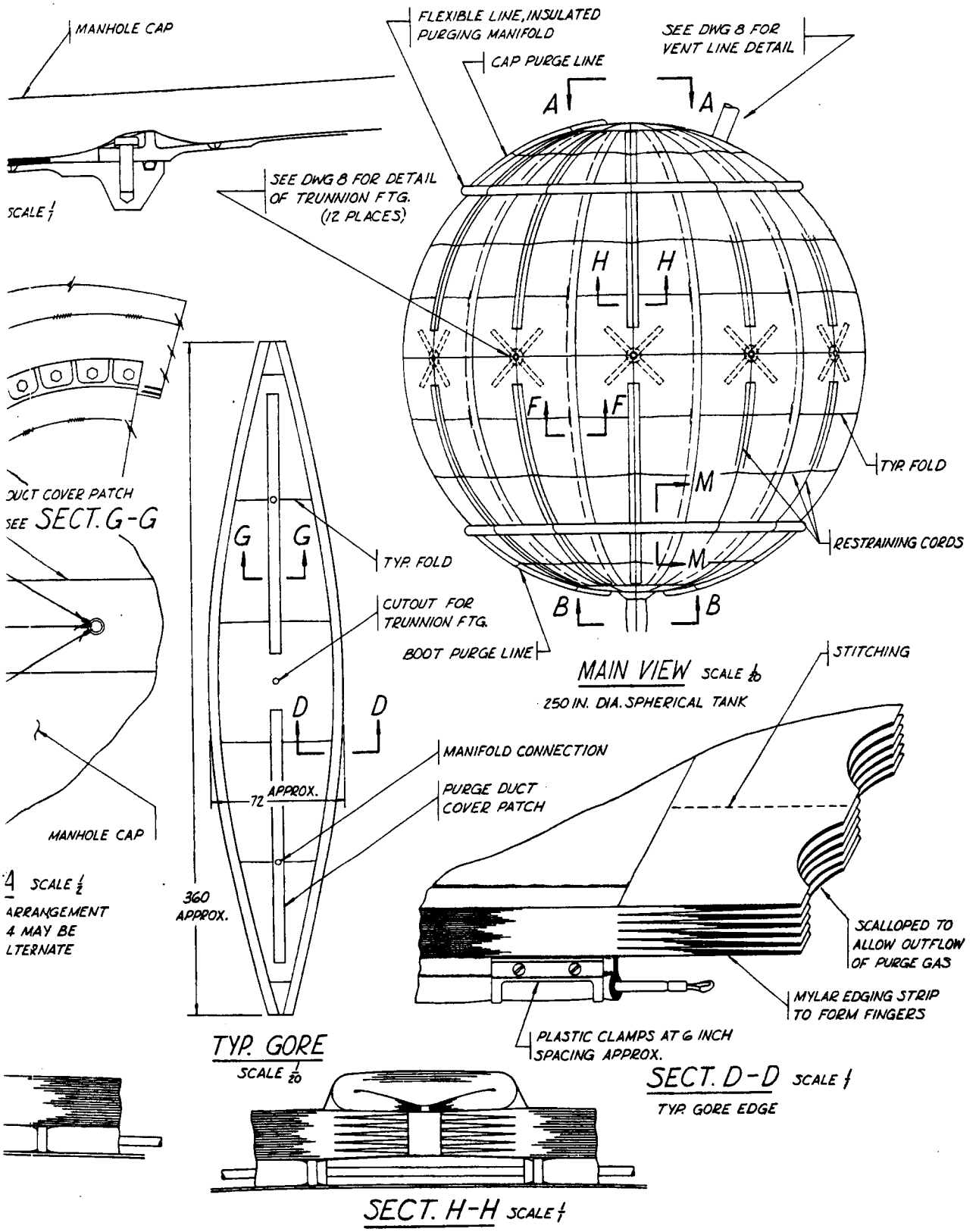

Fig. IV-4. NRC-2 Purged System

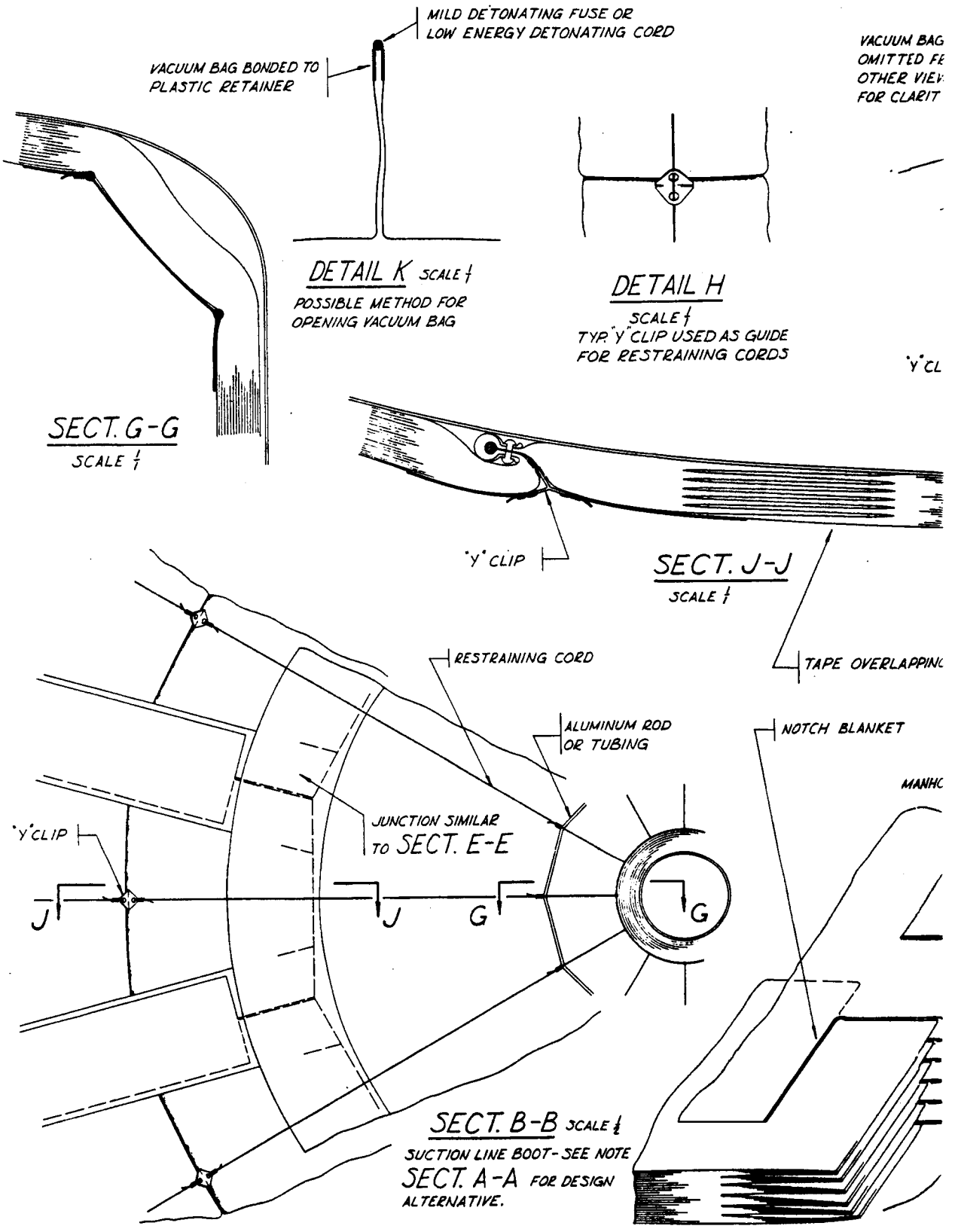
MILD DETONATING FUSE OR
LOW ENERGY DETONATING CORD
VACUUM BAG BONDED TO
PLASTIC RETAINER
VACUUM BAG
OMITTED FE
OTHER VIEV
FOR CLARIT
DETAIL K SCALE 1
POSSIBLE METHOD FOR
OPENING VACUUM BAG
DETAIL H
SCALE 1
TYP. "Y" CLIP USED AS GUIDE
FOR RESTRAINING CORDS
"Y" CL
SECT. G-G
SCALE 1
"Y" CLIP
SECT. J-J
SCALE 1
RESTRAINING CORD
TAPE OVERLAPPIN
ALUMINUM ROD
OR TUBING
NOTCH BLANKET
MANHC
JUNCTION SIMILAR
TO SECT. E-E
"Y" CLIP
J
J
G
G
SECT. B-B SCALE 1
SUCTION LINE BOOT - SEE NOTE
SECT. A-A FOR DESIGN
ALTERNATIVE.

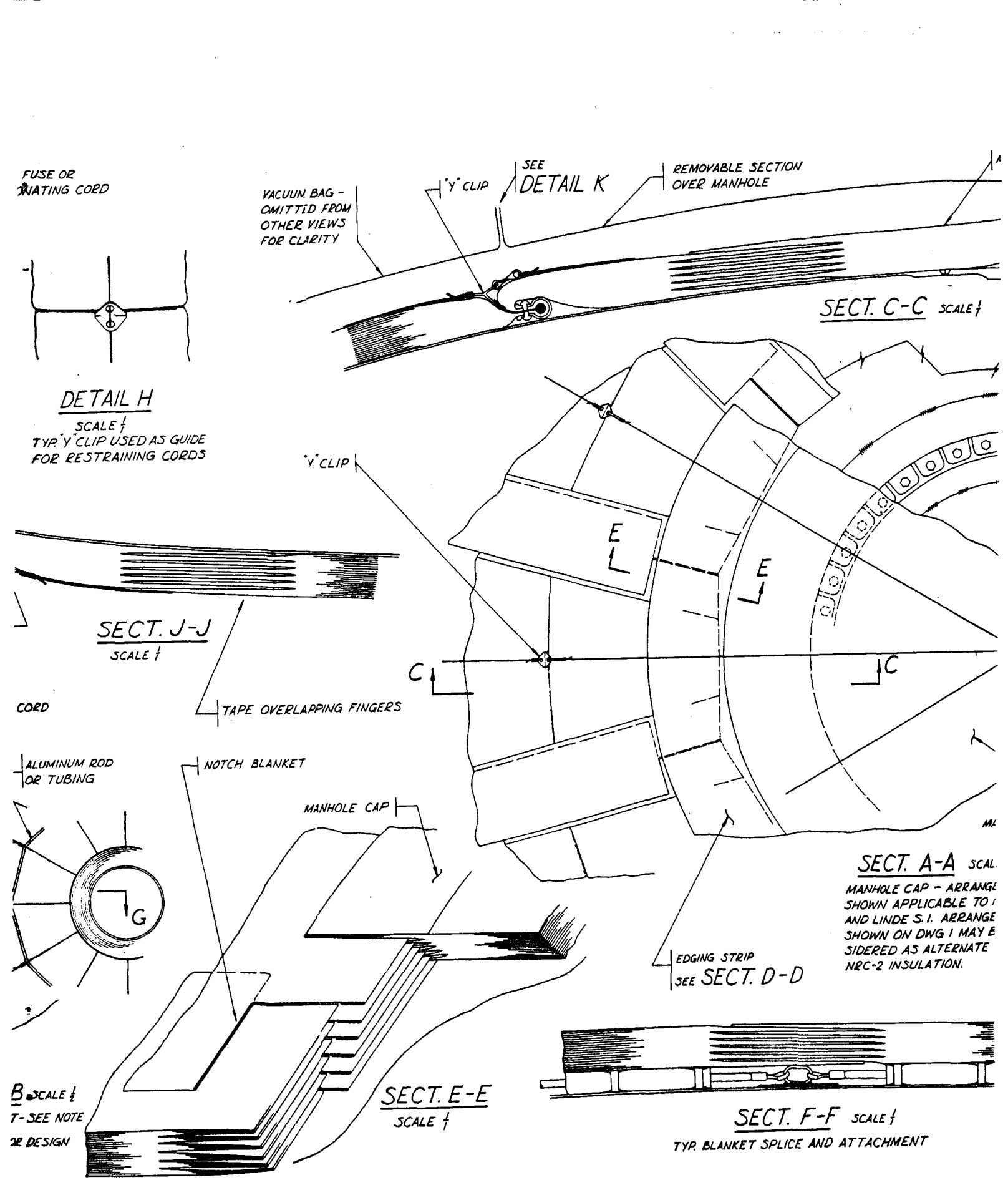
FUSE OR
HEATING CORD
DETAIL H
SCALE 1/1
TYP. "Y" CLIP USED AS GUIDE
FOR RESTRAINING CORDS
VACUUM BAG - OMITTED FROM OTHER VIEWS FOR CLARITY
"Y" CLIP
SEE DETAIL K
REMOVABLE SECTION OVER MANHOLE
SECT. C-C SCALE 1/1
"Y" CLIP
E
E
C
C
SECT. J-J
SCALE 1/1
CORD
TAPE OVERLAPPING FINGERS
ALUMINUM ROD OR TUBING
NOTCH BLANKET
MANHOLE CAP
G
B SCALE 1/2
T - SEE NOTE
2R DESIGN
SECT. E-E
SCALE 1/1
EDGING STRIP
SEE SECT. D-D
SECT. A-A SCAL
MANHOLE CAP - ARRANGE
SHOWN APPLICABLE TO
AND LINDE S.I. ARRANGE
SHOWN ON DWG 1 MAY E
SIDERED AS ALTERNATE
NRC-2 INSULATION.
SECT. F-F SCALE 1/1
TYP. BLANKET SPLICE AND ATTACHMENT

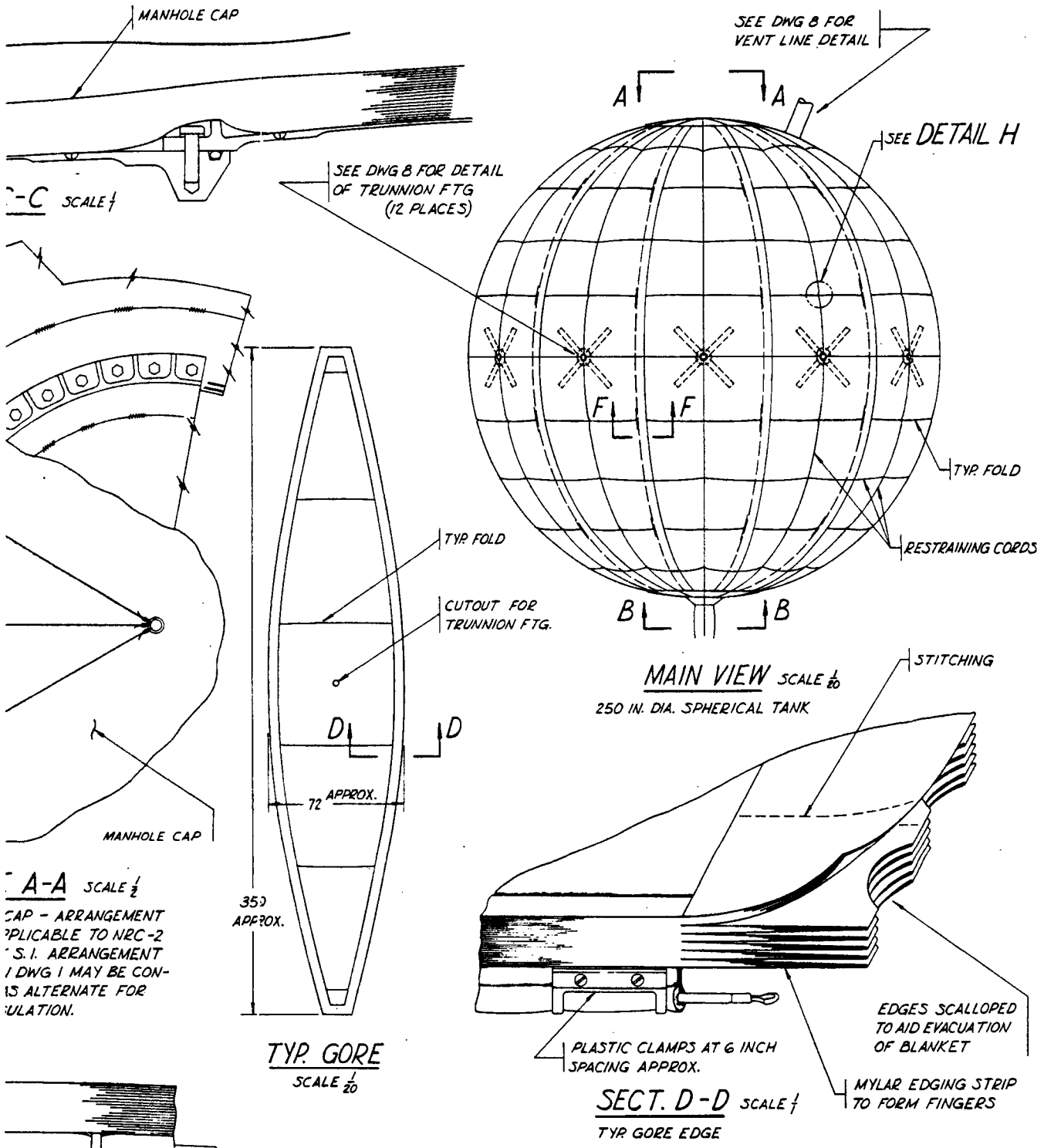

Fig. IV-5. NRC-2 with Spacers

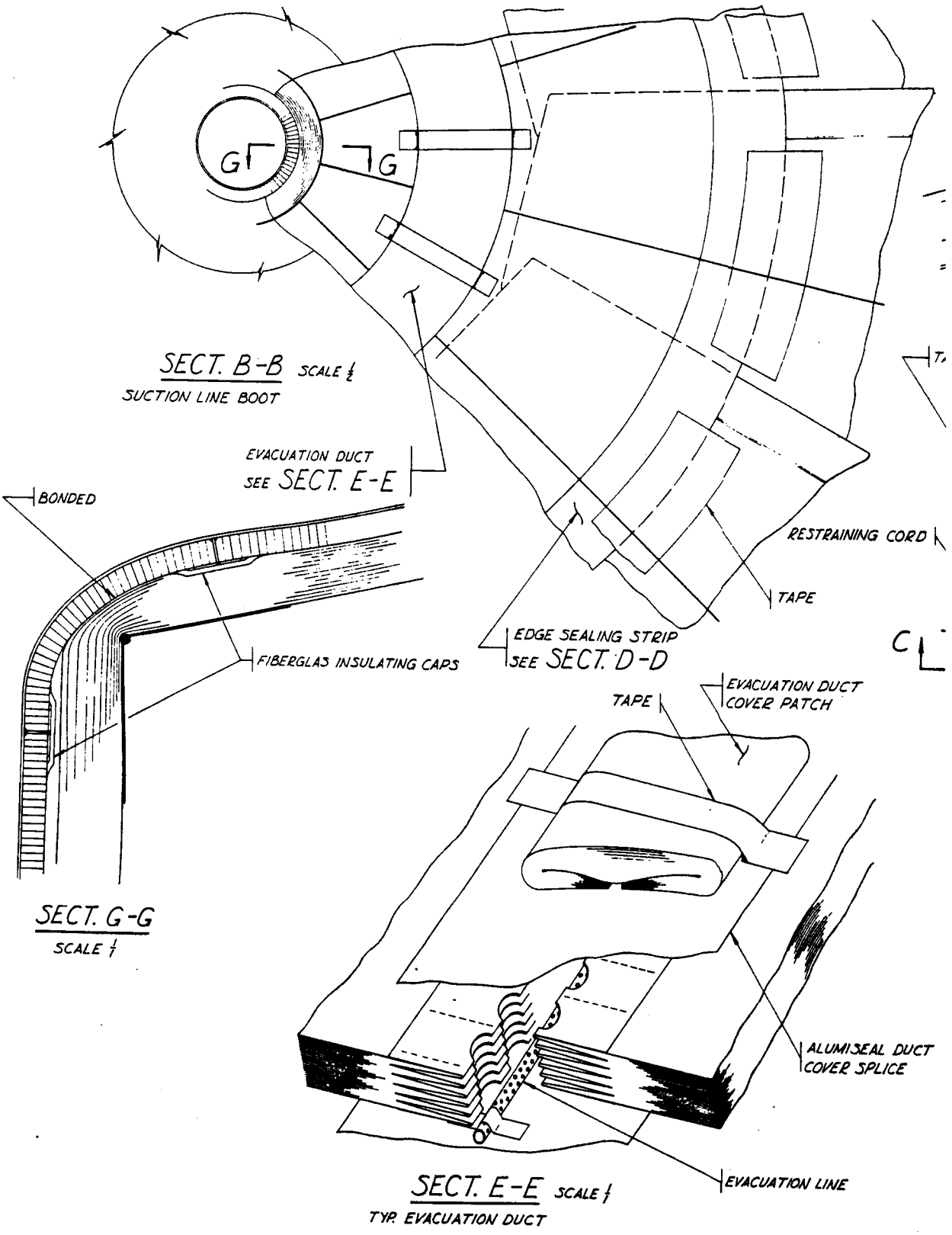
G
G
SECT. B-B SCALE ½
SUCTION LINE BOOT
EVACUATION DUCT
SEE SECT. E-E
BONDED
FIBERGLAS INSULATING CAPS
SECT. G-G
SCALE 1
RESTRAINING CORD
TAPE
EDGE SEALING STRIP
SEE SECT. D-D
TAPE
EVACUATION DUCT
COVER PATCH
ALUMISEAL DUCT
COVER SPLICE
EVACUATION LINE
SECT. E-E SCALE 1
TYP. EVACUATION DUCT

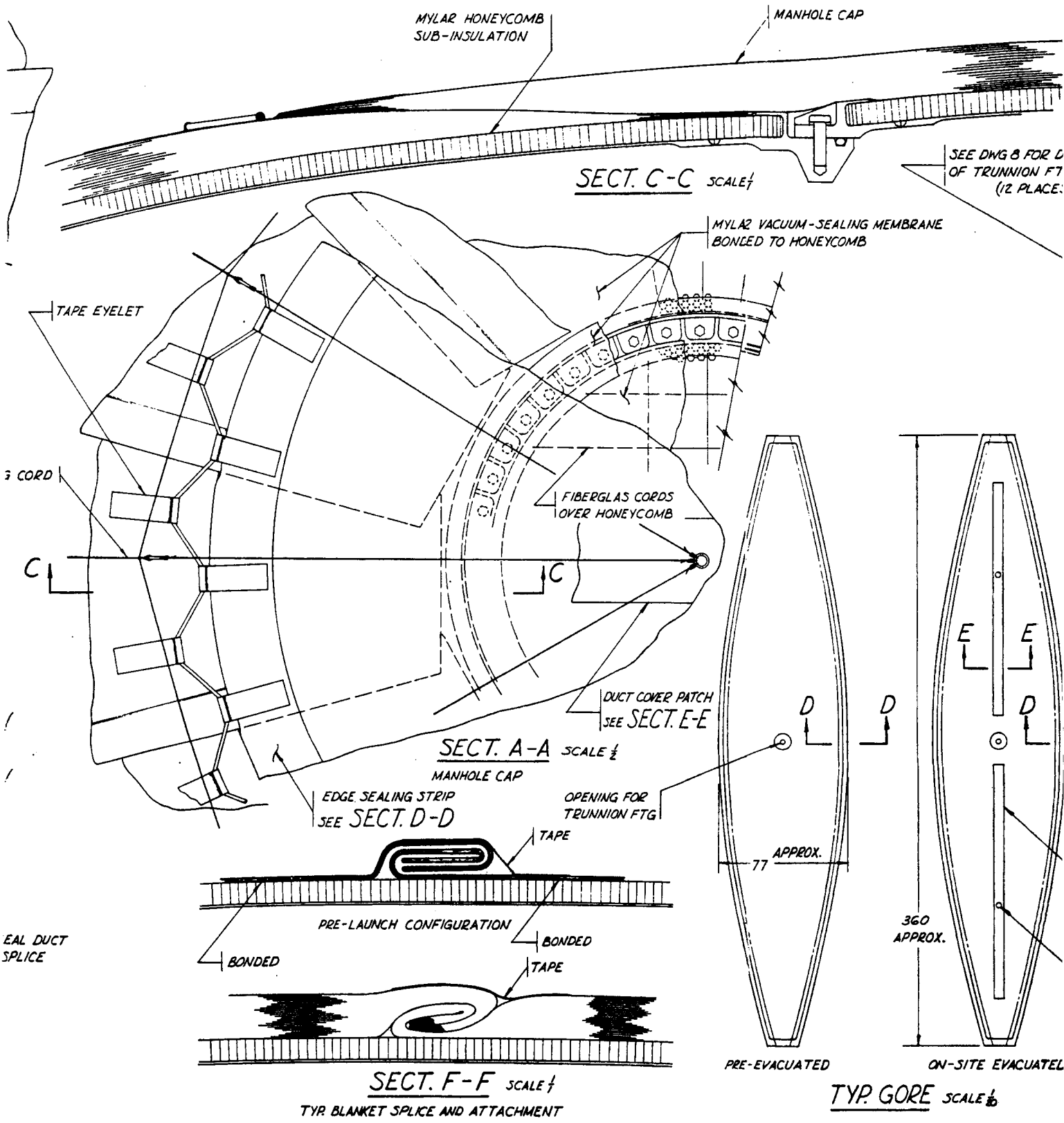
MYLAR HONEYCOMB SUB-INSULATION
MANHOLE CAP
SECT. C-C SCALE
SEE DWG B FOR D
OF TRUNNION FT
(12 PLACES
MYLAR VACUUM-SEALING MEMBRANE BONDED TO HONEYCOMB
TAPE EYELET
FIBERGLAS CORDS OVER HONEYCOMB
C
C
DUCT COVER PATCH SEE SECT. E-E
SECT. A-A SCALE
MANHOLE CAP
EDGE SEALING STRIP SEE SECT. D-D
OPENING FOR TRUNNION FTG
D
D
D
E
E
APPROX.
77
360 APPROX.
PRE-EVACUATED
ON-SITE EVACUATEL
TYP. GORE SCALE
TAPE
PRE-LAUNCH CONFIGURATION
BONDED
BONDED
TAPE
SECT. F-F SCALE
TYP. BLANKET SPLICE AND ATTACHMENT

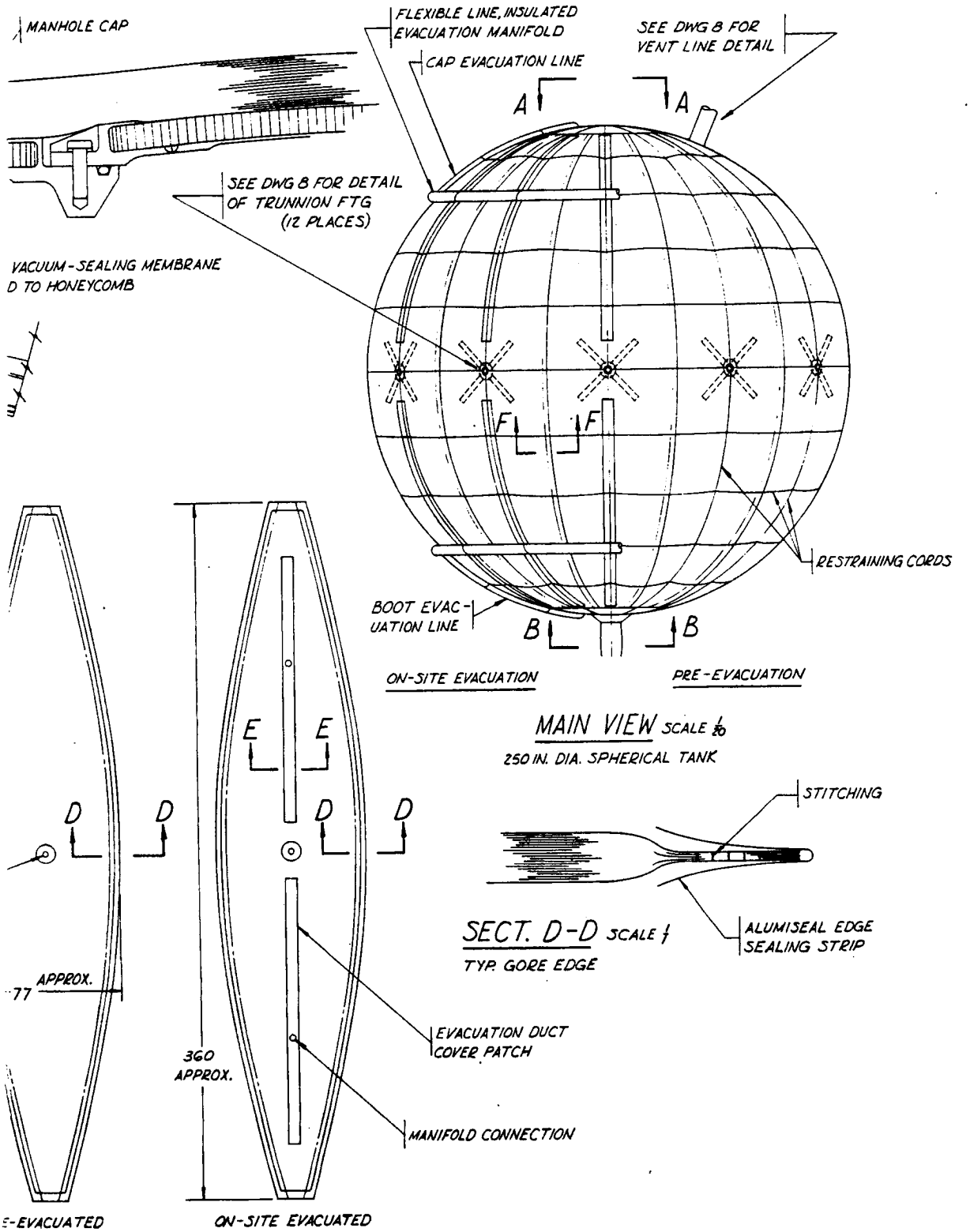

Fig. IV-6. NRC-2 Ground Evacuated System

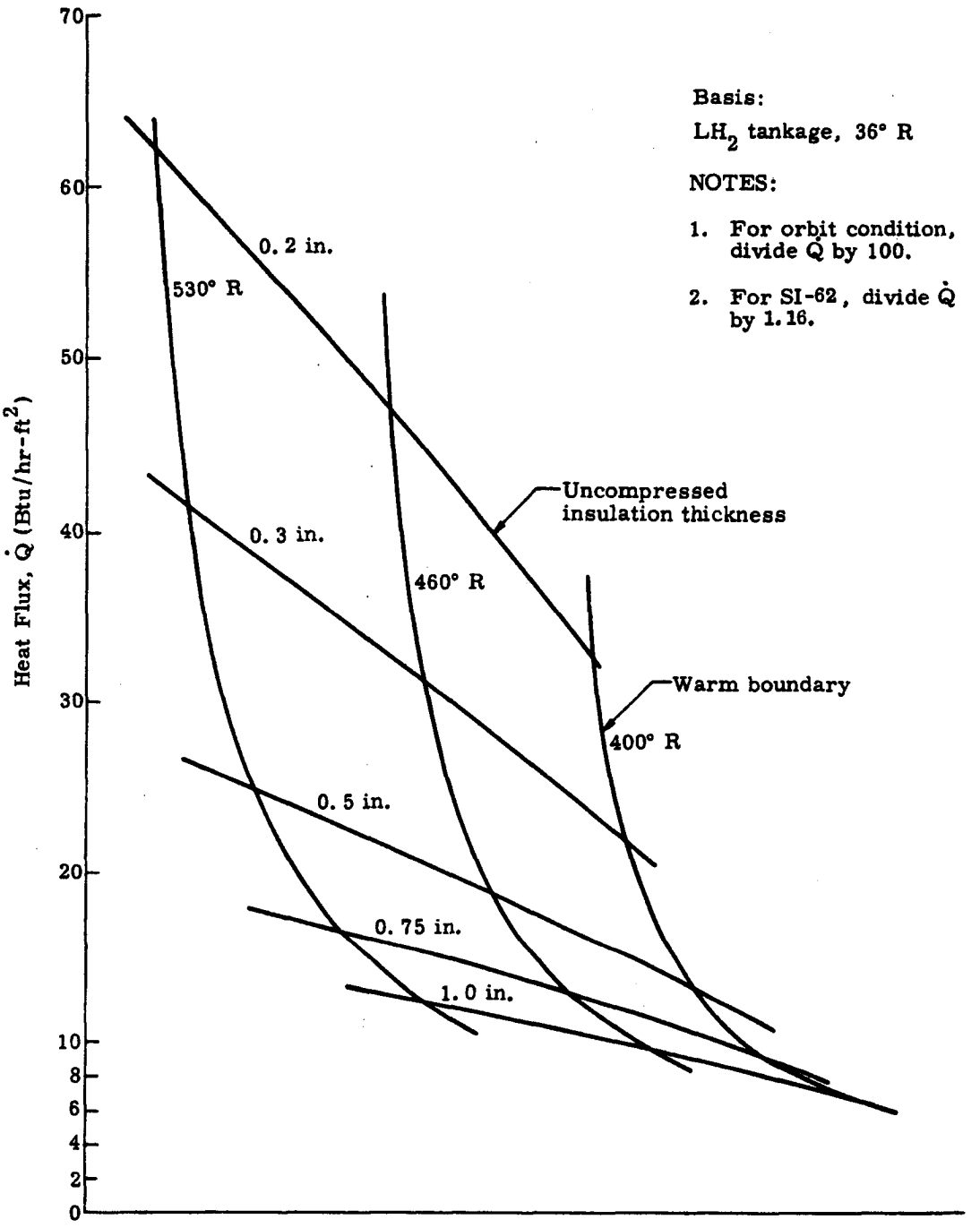

Fig. IV-7. Heat Flux Across Evacuated Linde SI-44 at Launch Pad Conditions

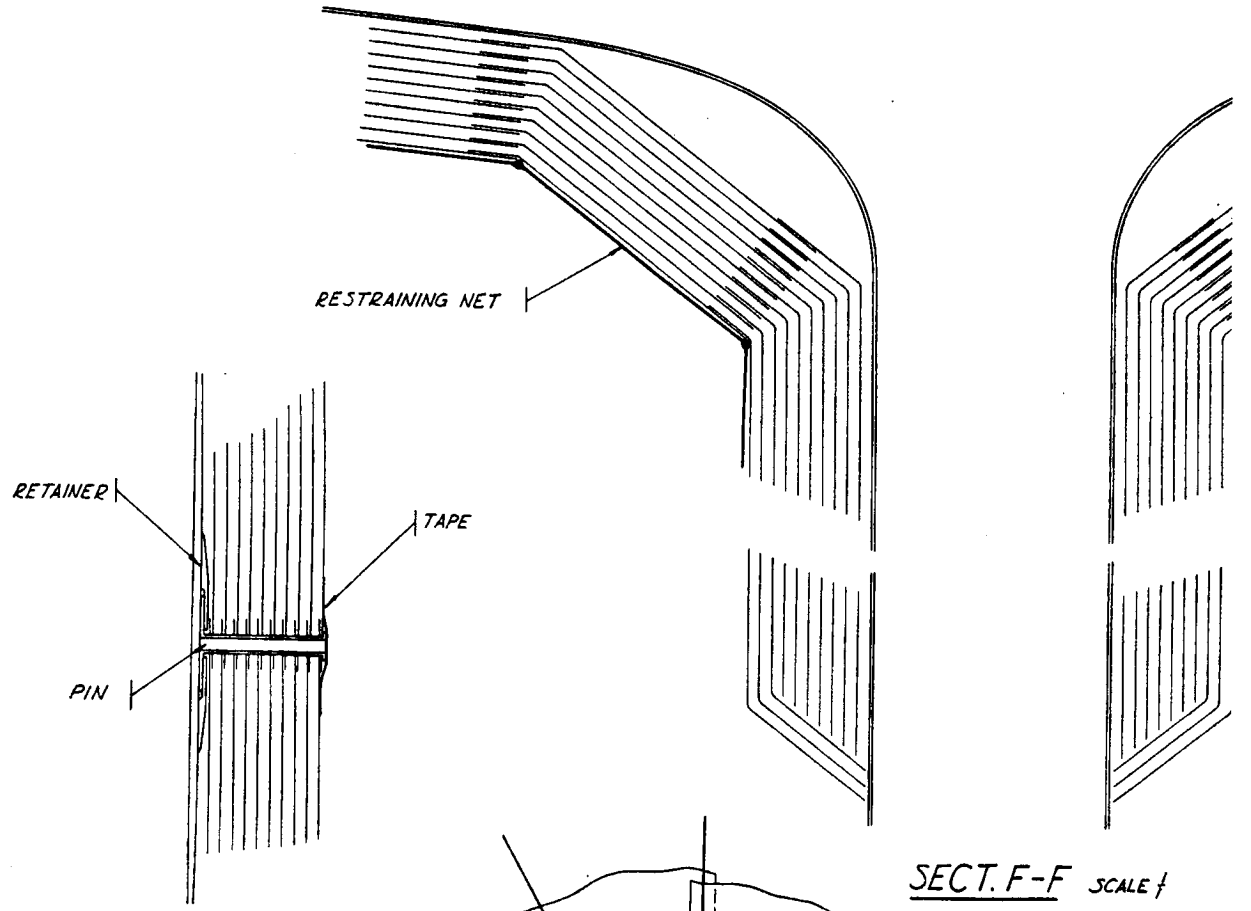

SECT. G-G SCALE 1

SECT. F-F SCALE 1

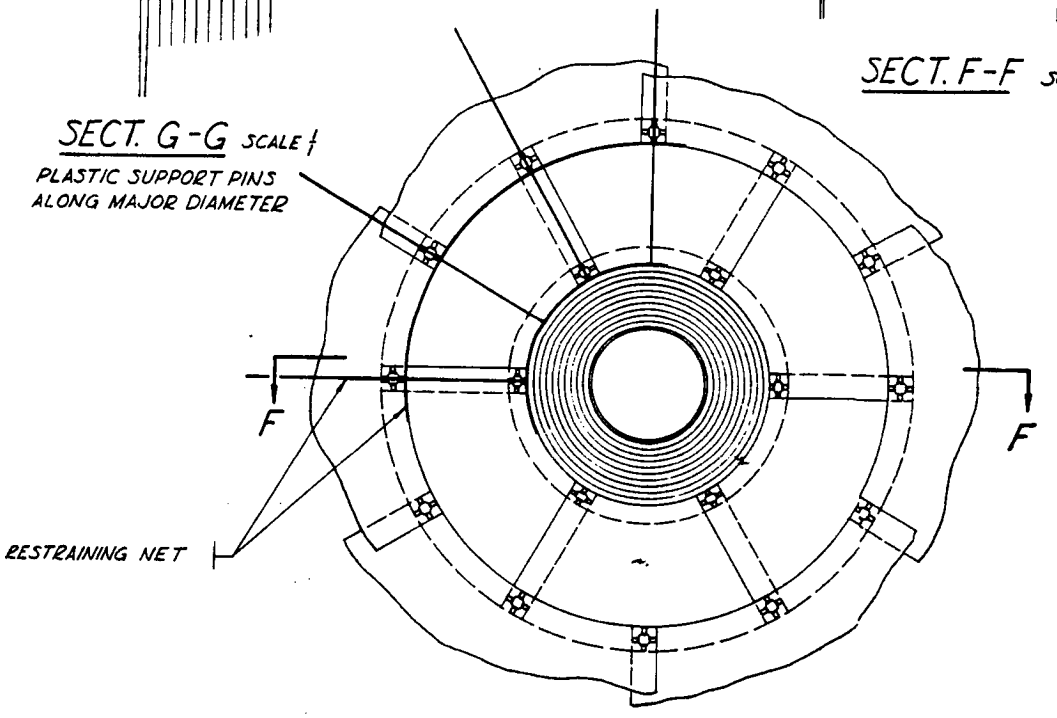

SECT. B-B SCALE 1/2

SUCTION LINE

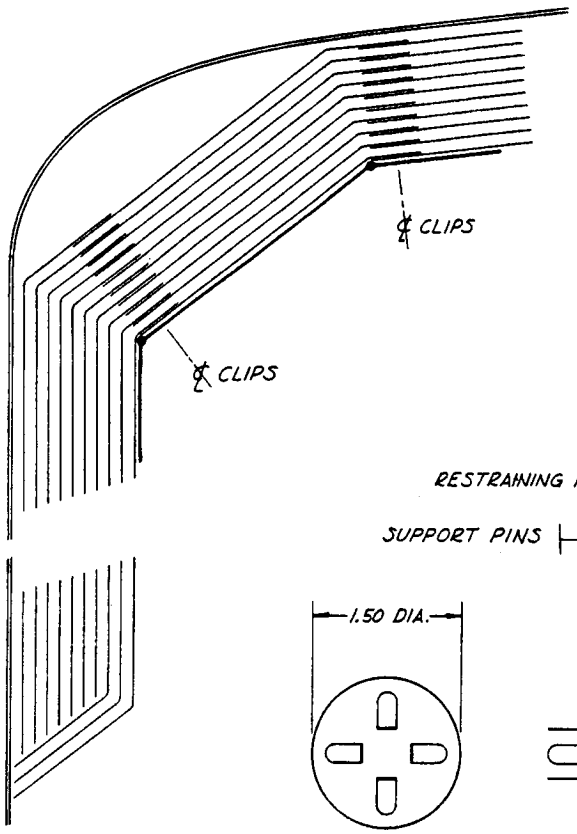

SECT. F-F SCALE 1

TYP. CLIP SCALE 2

.005 ALUM. ALLOY

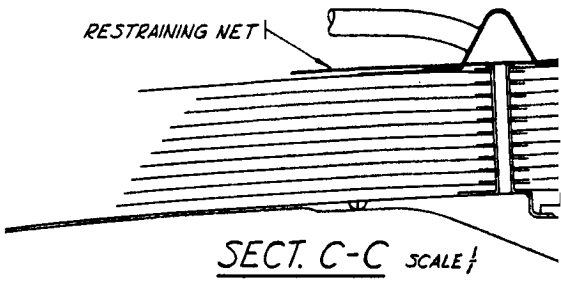

SECT. C-C SCALE 1

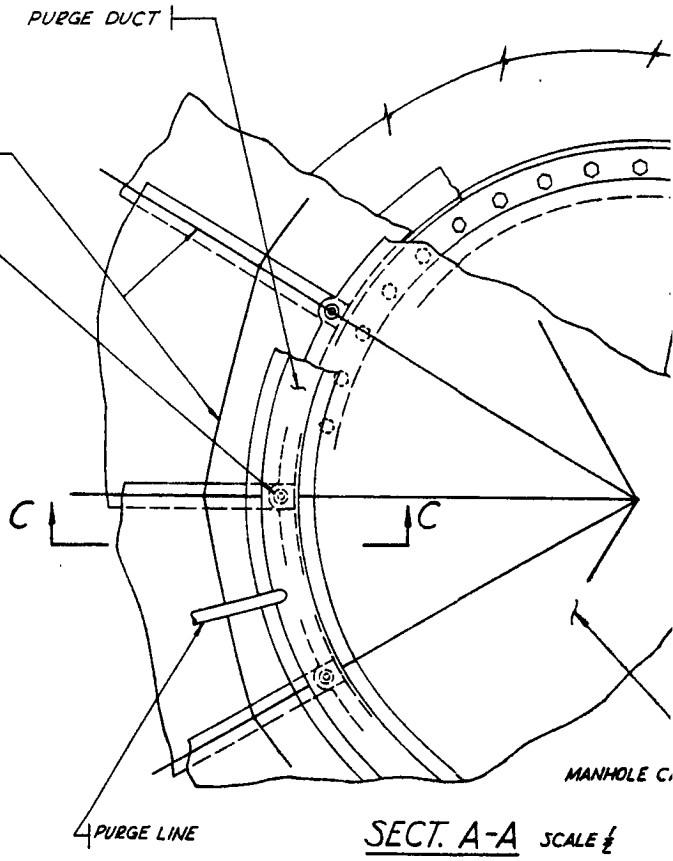

SECT. A-A SCALE 1

MANHOLE CAP

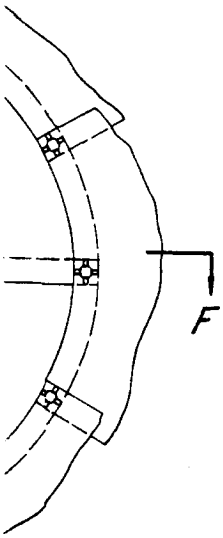

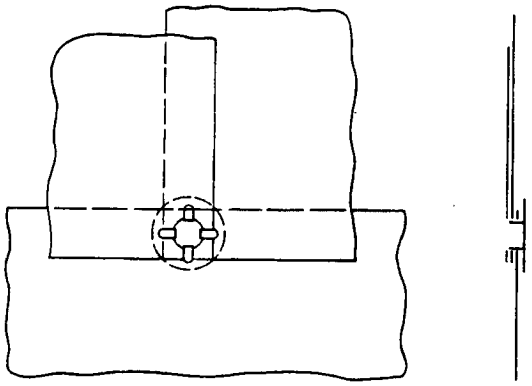

DETAIL E SCALE 1

CLIP INSTALLATION – TYP. FOR EACH SET OF OVERLAPPING PLIES

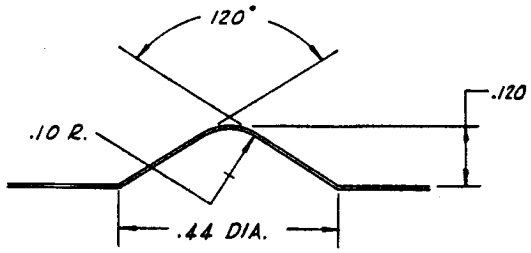

DETAIL D SCALE 10

TYP. DIMPLE

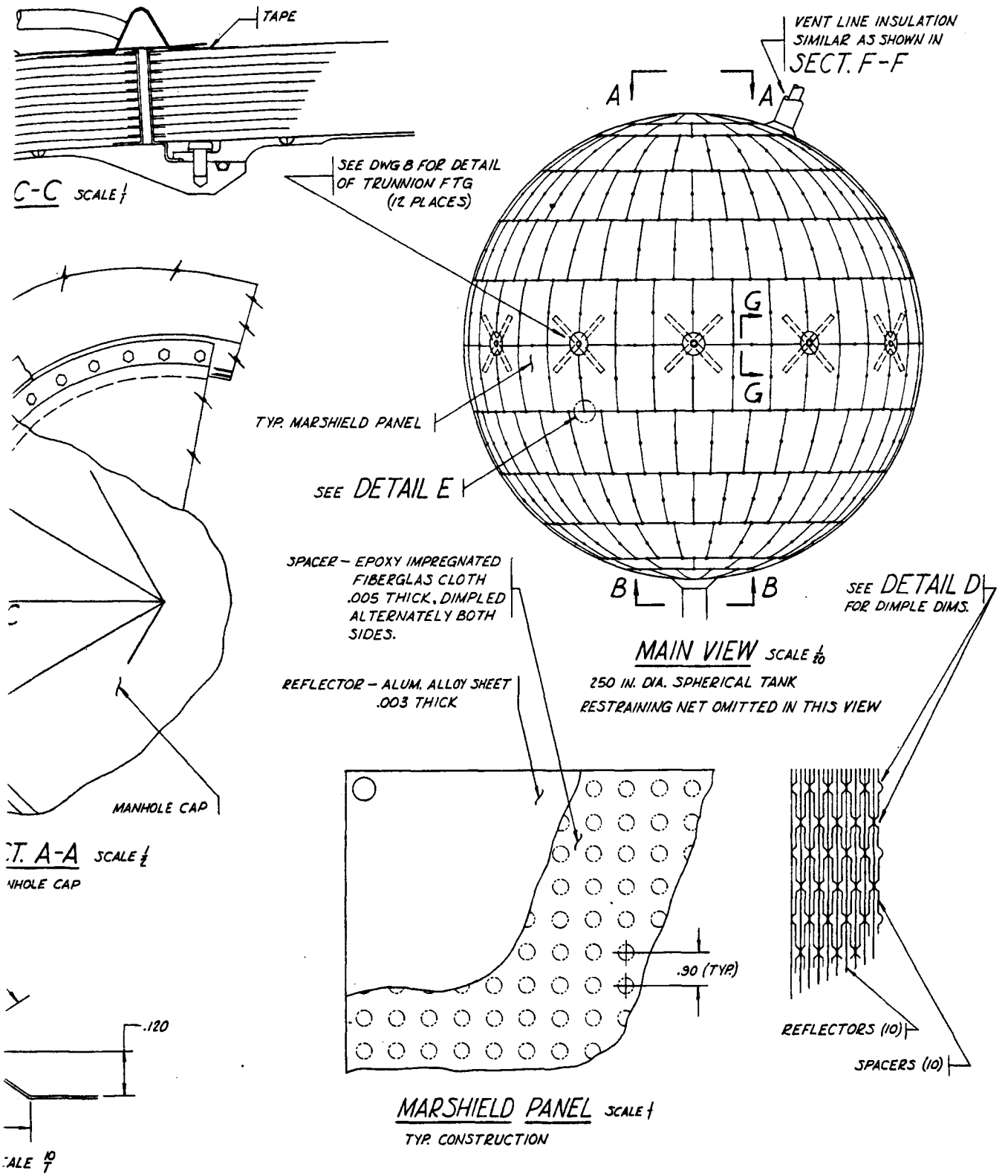

Fig. IV-8. MARSHIELD Purged

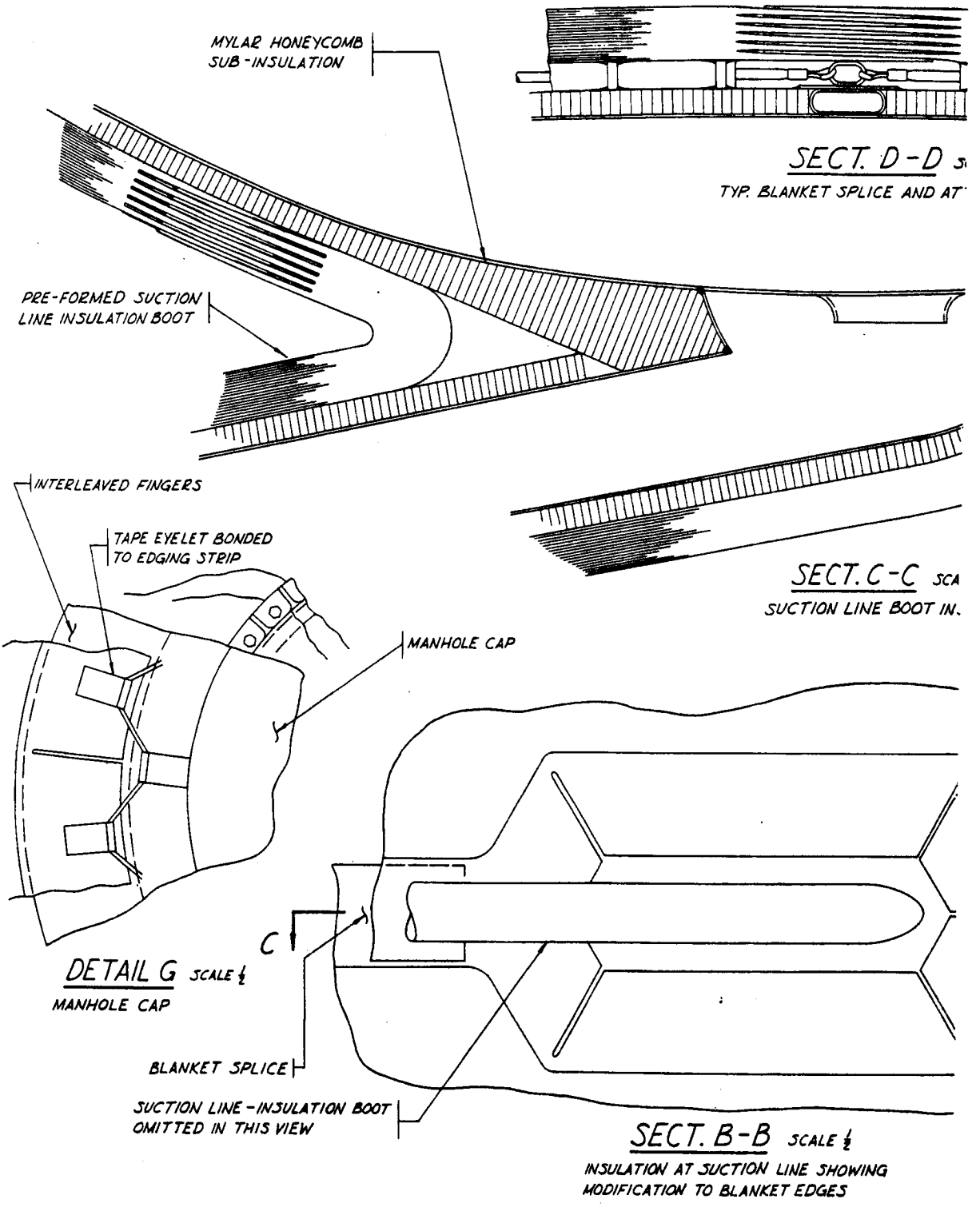

SECT. D-D S

TYP. BLANKET SPLICE AND AT

SECT. C-C SCA

SUCTION LINE BOOT IN.

DETAIL G SCALE ½

MANHOLE CAP

SECT. B-B SCALE ½

INSULATION AT SUCTION LINE SHOWING MODIFICATION TO BLANKET EDGES

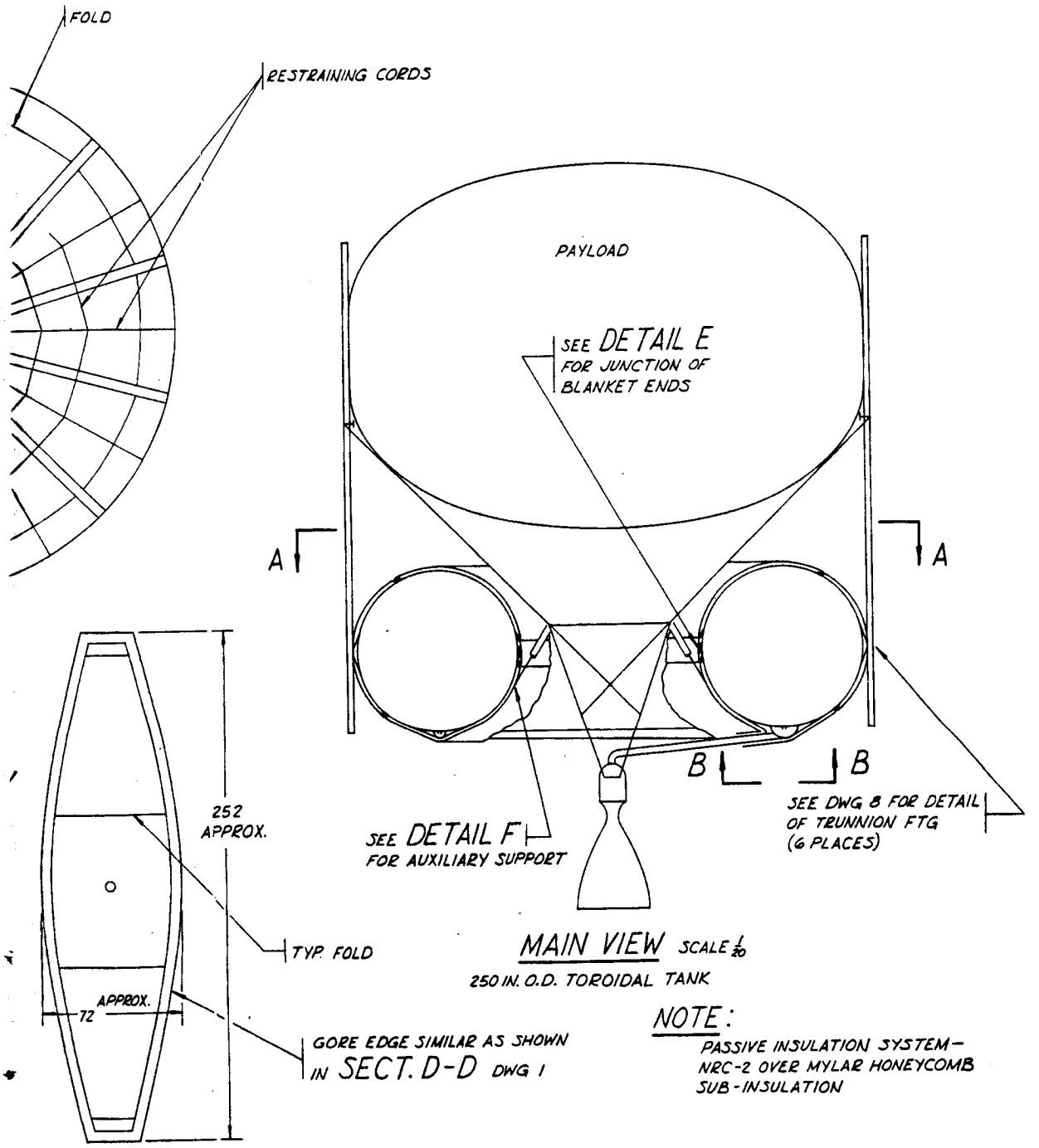

Fig. IV-9. Toroidal Tank

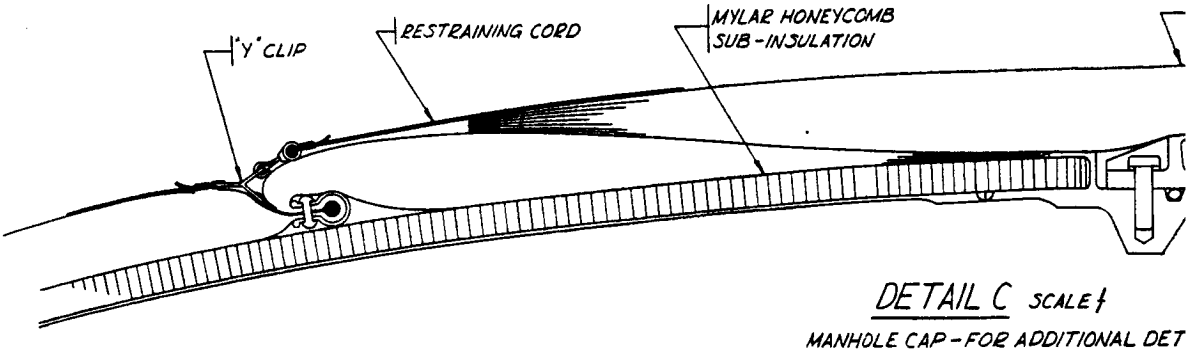

DETAIL C SCALE 1

MANHOLE CAP - FOR ADDITIONAL DET SEE SECT. A-A DWG 1

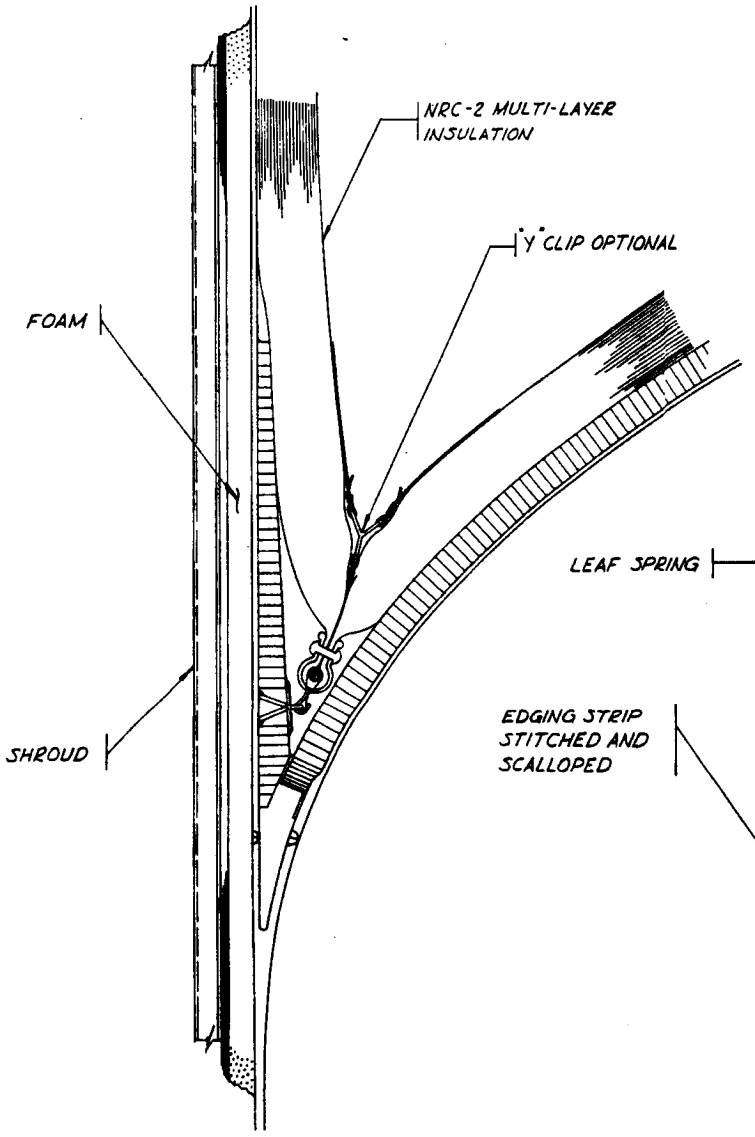

DETAIL D SCALE 1

TYP. UPPER AND LOWER DOME

DETAIL E SCALE 1

UPPER SKIRT SHOWN, LOWER SIM

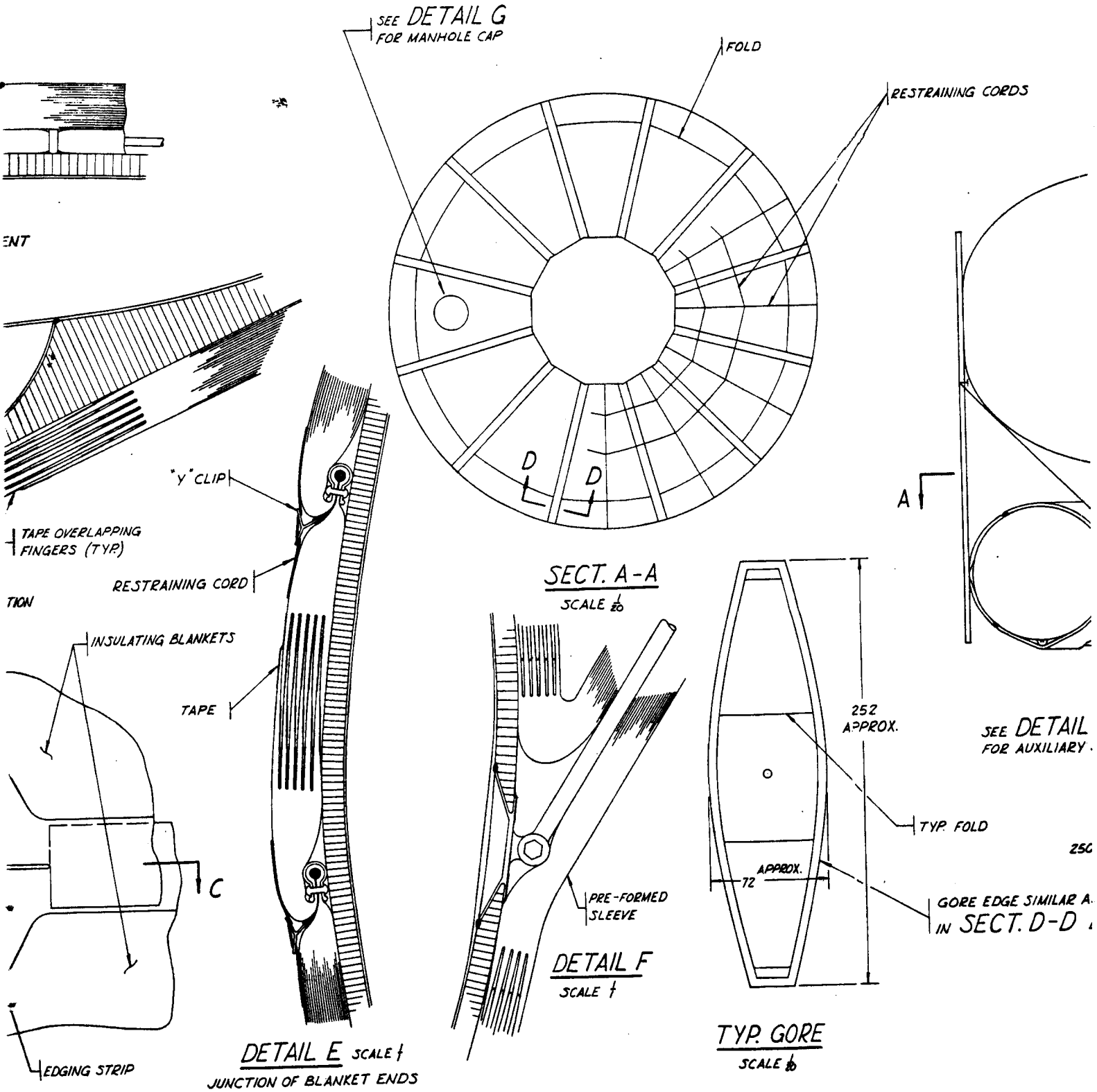
SEE DETAIL G
FOR MANHOLE CAP
FOLD
RESTRAINING CORDS
D
D
SECT. A-A
SCALE 1/20
A
SEE DETAIL
FOR AUXILIARY
"Y" CLIP
TAPE OVERLAPPING
FINGERS (TYP.)
RESTRAINING CORD
INSULATING BLANKETS
TAPE
C
EDGING STRIP
DETAIL E SCALE 1
JUNCTION OF BLANKET ENDS
PRE-FORMED
SLEEVE
DETAIL F
SCALE 1
252
APPROX.
TYP. FOLD
APPROX.
72
GORE EDGE SIMILAR A
IN SECT. D-D
TYP. GORE
SCALE 1/10

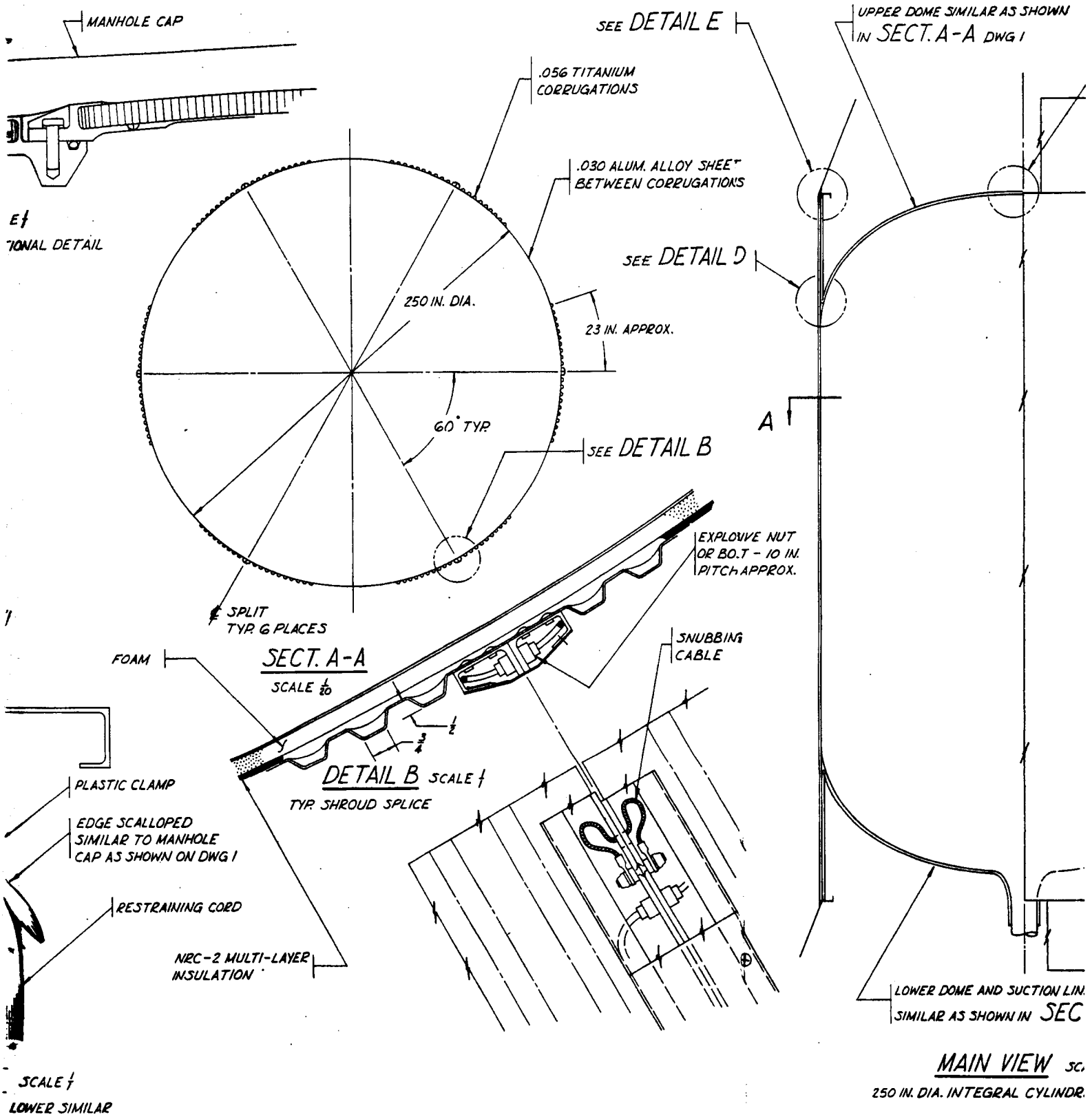
MANHOLE CAP
E
TIONAL DETAIL
.056 TITANIUM CORRUGATIONS
.030 ALUM. ALLOY SHEET BETWEEN CORRUGATIONS
250 IN. DIA.
23 IN. APPROX.
60° TYP.
SEE DETAIL B
SEE DETAIL E
UPPER DOME SIMILAR AS SHOWN IN SECT. A-A DWG 1
SEE DETAIL D
A
EXPLOVVE NUT OR BO.T - 10 IN. PITCh APPROX.
SPLIT TYP. 6 PLACES
FOAM
SECT. A-A
SCALE 1/20
SNUBBING CABLE
1/2
3/4
DETAIL B SCALE 1
TYP. SHROUD SPLICE
PLASTIC CLAMP
EDGE SCALLOPED SIMILAR TO MANHOLE CAP AS SHOWN ON DWG 1
RESTRAINING CORD
NRC-2 MULTI-LAYER INSULATION
SCALE 1
LOWER SIMILAR
LOWER DOME AND SUCTION LIN
SIMILAR AS SHOWN IN SEC
MAIN VIEW SC
250 IN. DIA. INTEGRAL CYLINDR

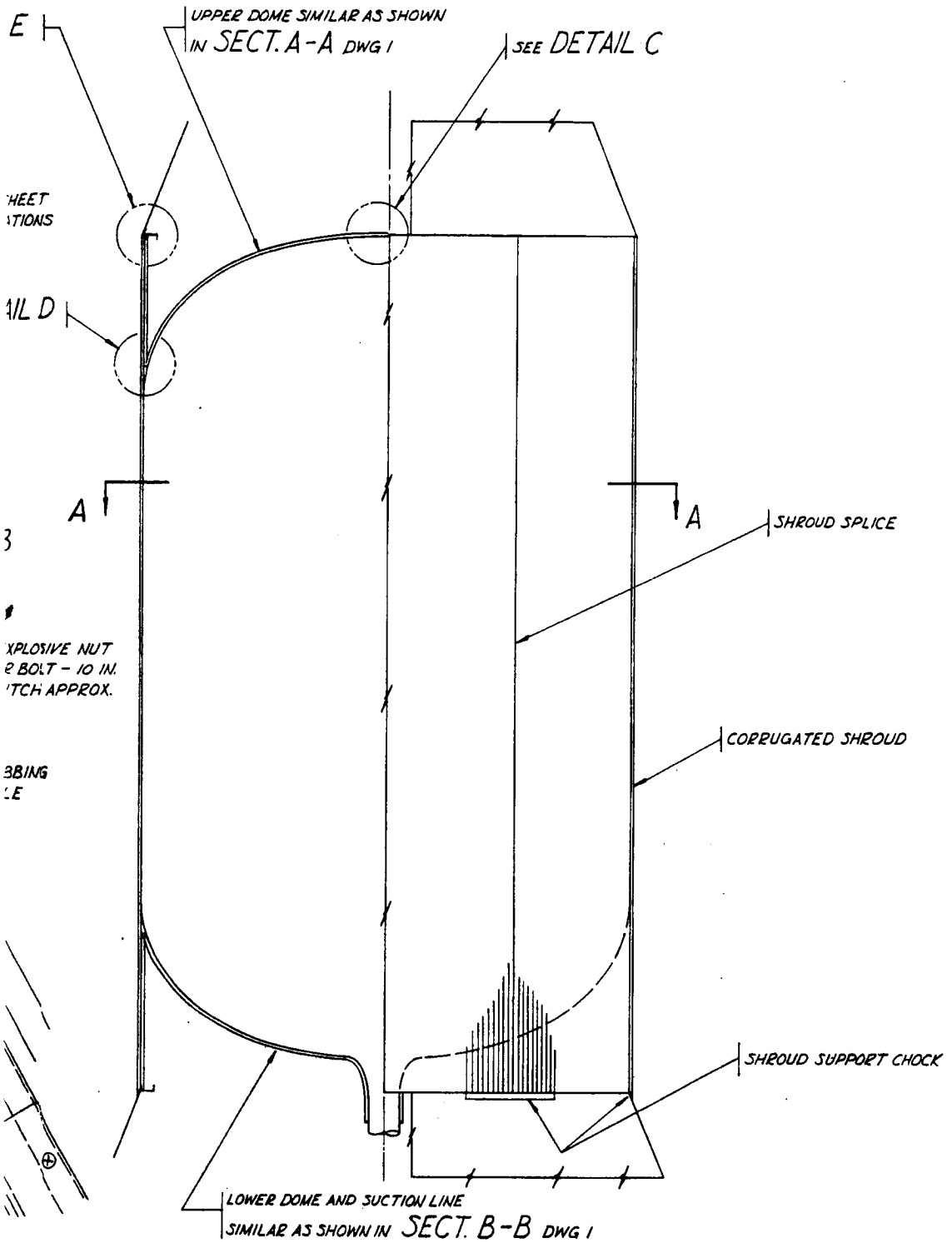

MAIN VIEW SCALE 1/50

250 IN. DIA. INTEGRAL CYLINDRICAL TANK

Fig. IV-10. Integral Cylinder

V. EVALUATION OF CONCEPTS

The logic and bases for rating the selected systems are presented herein. The bases for selection are certainly influenced by the state of development of each system and certain system components, the ground rules of the study and the evaluator's natural preferences. Recognizing these factors, the ratings were made by providing key project personnel from different specialty areas (i.e., thermal, structural, design, manufacturing, quality, etc.) with basic performance data on each of the six contending system approaches. They were then permitted freedom to weight and rate each of the systems for the items given in the last seven columns of Table V-1. The results presented are a compilation of those results.

The performance data used for the rating process were derived from the data presented in Table V-1, Columns 2 through 14. The basic tank geometry assumed was the 250-in. diameter spherical tank emphasized in Chapter IV, and the mission was arbitrarily selected as a 30-day orbital storage of liquid hydrogen. While Table V-1 presents data based only upon a 2-min ground hold after topping, the data supplied the evaluators (given in Table V-2) included data on the same systems' performance with a 60-min ground hold.

Many of the columns in Table V-1 are self-explanatory. The basic insulation weight per square foot of tank surface area (Column 3) is that for the space insulation only. The additional weights such as sub-insulation, vacuum bags, seals, attachment devices, etc., are included in the installation weight factor, Column 4. These weight items are tabulated in Chapter IV.

The total heat input, ascent flight and soak for Column 7 is assumed constant as shown. Since this will vary with trajectory and location of the stage in the boost vehicle, its effect has been removed from Column 14, and from the percent penalty data given in Table V-2. This was done because too heavy a weighting of this item can favor a poorer performing system like Marshield.

Columns 14 and 2 of Table V-1 and Table V-2, respectively, emphasize the fact that from an absolute payload penalty or percentage payload penalty standpoint, there is not a large difference between most contending systems, except Marshield.

The 530-lb weight spread in Column 14 among the first five systems is significant when converted to equivalent booster take-off weight, but this difference is theoretical and based upon all systems operating at the design pressure in the insulation. Any significant deviation from this condition in practice could quickly eradicate that difference.

TABLE

Comparison of Ins

① Final Rated Position	② System Description	③ Basic Insulation Weight of Tank Surface (lb/ft^2)	④ Installation Weight Factor	⑤ Total Insulation Weight (lb/ft^2)	⑥ Ground Hold Heat Flux ($Btu/hr\text{-}ft^2$)	⑦ Ascent Flight and Soak Heat $\int Q/Ad\theta$ (Btu/ft^2)	⑧ Ideal Orbit Heat Flux ($Btu/hr\text{-}ft^2$)	⑨ Ratio, Total/Ideal Orbit Heat Leak	⑩ 30-Day Mission Boiloff b/o, Orbit/Total	⑪ Total Insulation System Weight, (lb)	⑫ Total Hydrogen Boiloff Weight, Including Ascent (lb)
1	NRC-2 Passive	0.166	1.995	0.331	27	64	0.05	1.697	2.17 4.48	452	88
2	He purged NRC-2	0.166	1.53	0.254	158.5	64	0.05	1.787	2.82 4.74	346	93
3	He purged Marshield	1.025	1.015	1.04	110	64	0.311	1.11	8.81 11.25	1419	222
4	Pre-evac NRC-2 over mylar H/C	0.166	2.355	0.391	105	64	0.05	1.50	1.915 4.31	534	85
5	Unit bag NRC-2 with spacers	0.352	1.17	0.412	48.6	64	0.0715	1.47	2.68 5.01	563	99
6	Unit bag Linde SI	0.39	1.16	0.452	13	64	0.0897	1.64	3.75 6.05	618	1197

Ground rules for table:

Ground hold --560° R, internal tankage
Orbit --460° R, equilibrium average
Tank --250 in dia sphere, 1365 sq ft surface, 19,800 lb, LH_2
Insulation thicknesses--see system discussions Chapter IV

LEV-1

nsulation Systems

) al ygen off ght, ding ght)	(13) Total Insulation and Boiloff Weight, Including Ascent (lb)	(14) Total Insulation and Boiloff Weight Excluding Ascent (lb)	(15) Efficiency 30 Points	(16) Thermal Reliability 20 Points	(17) Structural Reliability 20 Points	(18) Manufacturing, Quality and Installation 14 Points	(19) Service, Maintenance, and GSE Requirements 6 Points	(20) Development 10 Points	(21) Total 100 Points Maximum
5	1338	885	27	17.25	15.2	12.5	5.62	8.63	86.2
9	1285	835	25.3	15	15.75	8.75	4	5.75	74.55
5	3644	3195	7.9	20	20	10.95	3.7	4.85	67.4
4	1388	938	23.3	12.75	17	7	3.25	3	66.3
3	1556	1106	21.1	11.25	17.75	7	2.4	2.5	62
7	1815	1365	19.8	10.5	17.5	6.3	2.4	2.5	59

TABLE V-2

Systems and Respective Performance Penalties
for 30-Day Storage and Listed Ground Hold Times
(P = ratio of actual to ideal weight
of fuel after orbital storage)

System	2-Min Ground Hold		60-Min Ground Hold	
	% Penalty	P	% Penalty	P
He purged NRC-2	3.34	1.00	7.63	0.564
Pre-evacuated NRC-2 over mylar honeycomb	3.75	0.891	6.62	0.650
Unit bagged NRC-2 with spacers	4.42	0.756	5.75	0.748
Unit bagged Linde SI	4.94	0.677	5.30	0.812
He purged Marshield	12.78	0.262	16.3	0.264
Passive NRC-2	3.55	0.941	4.30	1.00

In view of this tenuous difference among most of the attractive systems, except Marshield, it is important that the selection be based on more substantial differences than those shown by theoretical performance calculations. Hence, the rating process was set up to reflect the experience and judgment of a number of people involved with the study as to other factors as listed in Columns 15 through 20 in Table V-1. These results, of the rating process, are presented in Columns 15 through 21 of Table V-1.

It is noted that while the ratings for most systems varied, there was unanimous agreement on the highest rated system--the NRC-2 passive system.

There are as many reasons for the high rating of the NRC-2 passive system as there were evaluators. It probably reflects a general belief in the inherent thermal reliability of a system which requires neither purging nor evacuation for its operation; a passive one. It is also felt that when the pressure level to which the space environment will reliably evacuate a given configuration has been established, the minimum performance level can be guaranteed. If frosting or moisture condensation proves troublesome, purging of the insulation with dry gaseous nitrogen is inexpensive and would improve the evacuation characteristics--see Appendix D.

The low rating given for structural reliability is a result of concern for nondestructive venting of the air purged insulation during the boost period. While the helium purged systems have a similar problem, preliminary tests indicate that they should vent more easily.

The use of a sealed subinsulation such as the mylar honeycomb at first appeared inherently unreliable. However, recent success in the application of sealed foams to hydrogen tanks (Ref. II-10) and reported success in the similar use of mylar honeycomb in some Saturn Program work is encouraging. Particularly significant is the fact that reliance need not be placed upon a bond between the tank and honeycomb at liquid hydrogen temperatures to hold the subinsulation in place, since the pretensioned fiber glass roving is a redundant feature of the system.

Development of a good seal for the subinsulation could serve to alleviate the requirement for development of an absolutely leak free tank since it could act as a trap for the diffusing gas, or could be developed as a means of ducting the gas overboard before it enters the NRC-2 insulation.

The use of a bonded and sealed mylar honeycomb subinsulation also tends to minimize the effects of air liquefaction due to a small seal leak by confining it to a single honeycomb cell.

Finally, lead time required for the development of this passive system should be the least since development of neither vacuum bagging nor purging technology is required.

The second and third rated systems are purged insulation concepts--NRC-2 and Marshield, respectively. These high ratings for the purged systems again reflect a general belief that their reliability will be high since they do not depend on ground evacuation of the insulation by either vacuum pumping or cryopumping to make the insulation function properly and prevent liquefaction of air on the exterior surface.

In addition, the evacuation tests discussed in Appendix D indicate that the helium purge gas is readily removed from multilayer insulations installed adjacent to the hydrogen filled tanks--at least under ideal conditions.

The reasons for the high rating of the Marshield system despite its poor thermal efficiency are obvious from Table V-1. That is, the performance level, once established, should be highly repeatable and the structural attachment method is certain. In addition, the Marshield performance is less sensitive to penetration and attachment method heat leaks. Some optimism for increased thermal performance is, perhaps, also present in the Marshield rating.

The lower rated systems are all vacuum jacketed one which rely on ground evacuation to ensure acceptable ground hold and ascent flight performance. The pre-evacuated NRC-2 over a sealed mylar honeycomb subinsulation system appears least sensitive to failure to achieve low insulation pressure--at least for ground hold and ascent flight operation. However, since very low insulation pressures are required

for efficient space operation, the low pressures must be achieved either before liftoff or else the vacuum jacket must be opened upon entry into orbit in order or permit space evacuation.

The results of current attempts to evacuate vacuum jacketed multilayer insulations on the ground do not give confidence in the reliability of this approach. Further vacuum bag material developments may improve this situation considerably. These ratings reflect what is believed to be the state of the art.

In summary, pending analyses of the results of the experimental screening tests recommended in the next chapter, it appears that the NRC-2 passive system could adequately and reliably insulate a liquid hydrogen tank for missions considered within the scope of this study.

VI. RECOMMENDED PERFORMANCE TEST PLAN

At the present state-of-the-art, all the designs discussed in Chapter IV and rated in Chapter V appear capable of satisfactorily performing the task of isolating such a cryogenic as liquid hydrogen from the thermal environment of an earth orbit for periods of from 4 to 30 days, as well as remaining intact through launch and boost. However, the designs and ratings are at best preliminary since they are based on data, concepts and theoretical evaluations that, in many instances, are unproved. Many features of each system or, at least, each basic category of system (evacuated, purged and passive) now require experimental investigation or developmental testing before their development is either discontinued or extended through final performance testing. The recommended plan for experimental screening and subsequent performance testing of systems designed in this or other programs is given in this chapter. The plan begins with a screening specimen design and test planning phase, Phase I; continues with specimen fabrication and testing phase, Phase II; and concludes with Phase III in which two of the more promising insulation systems are selected, installed on large scale test tanks and performance tested.

A. PHASE I--SCREENING SPECIMEN DESIGN AND TEST PLANNING

The purpose of the screening tests is to determine economically whether basic requirements of an insulation system, as discussed in Chapter II, can be met by each of the candidate systems. In so doing, sufficient experimental data should be provided for screening out certain of the systems from future development and the selection of the two more promising systems. To accomplish this, representative screening specimens of each system should be designed to provide representative data on their performance when subjected to simulated mission environment.

1. Specimen Design

Certain full-scale dimensions must be produced in the screening specimens to properly evaluate such properties of each candidate system as effectiveness of structural attachments, space and ground evacuation resistance and structural response to the rapid pressure drop during boost. Also, actual temperature of liquid hydrogen should be produced inside the specimens along with close simulation of the exterior thermal environment of launch, boost and space. Such measures are felt to be very important to proper evaluation since scaling laws are uncertain for many of the problem areas that are to be resolved for each of the candidate systems.

The type specimen recommended for the screening tests is shown in Figure VI-1. The basic tank shown would be used for all the candidate systems throughout all phases of their testing. A candidate system would be installed on the tank only once in this plan and would then be tested in various testing apparatus to provide data on the systems performance through all phases of a mission. The shape and size of the basic tank shown in Fig. VI-1 satisfies requirements for simulation of the response of each system including structural forces and evacuation distances, and it is adaptable to tests for evaluating effects of penetrations that would be installed on the test article when it would function as a calorimeter.

Table VI-1 gives a complete list of the structural and thermal tests including penetration evaluation required to screen or qualify each of the more promising structure-cryogenic insulation systems listed therein. The Discussion of Systems presented earlier indicated that not all of these tests are either required or applicable to every system. For example, no boost inflation tests are required for the evacuated insulation systems, except should a combination of approaches be employed. In the design of the screening and qualification test article, however, it was deemed desirable to use the same shape for all specimens, and that shape should satisfy all screening test simulation requirements.

The acceleration, mechanical vibration and acoustic vibration tests all require that means for fastening the test article to the apparatus be incorporated in the design. Since it is planned that many of these tests will be performed with liquid hydrogen in the test article as discussed later in this section, the orientation of the specimen during these tests must be considered in order to properly locate attachment points, vents and fill lines, etc. In addition, the attachment points must not increase the heat leak to the extent that hydrogen liquid level in the tank cannot be maintained for the test duration. The vent system must also be capable of withstanding the vibratory loads.

Simulation of the boost inflation forces in the insulation, restraining nets and/or insulation attachment methods requires simulation of full scale radii of curvature. This aspect of testing has dictated the lenticular cross section of the test specimen design and the side bar installation as shown in Fig. VI-1.

The ground-hold and space thermal tests require the incorporation of a fill and vent system for the hydrogen testing which also must perform as inlet and outlet lines for the cold gaseous helium testing in the vacuum chamber as discussed under test planning. The helium cryostat output must be fed into and out of the space chamber. This is best accomplished by passing both inlet and outlet lines through the same space chamber port. Thus, the specimen design incorporates a

standpipe passing down the length of the specimen in order to permit the inlet and outlet to enter the specimen at the same end. This has an additional benefit, for in the vibration tests one end must be free to permit attachment to the shaker head.

Since the screening specimens will be used for evaluating penetrations, provisions should be made for mechanical attachment points for the penetrations on the lateral surface of the tanks. Simple bosses with tapped bolt holes or bayonet joints should therefore be installed. The penetrations themselves will be of two categories: structural supports and tubular lines. They should have fittings for attachment to the tanks.

The various insulation systems shown in Table VI-1, with their respective methods of installation, must be carefully adapted to the tank and penetrations for screening and qualifying tests. The adaptations should emphasize proper representation of the more critical aspects of each system and installation method. For systems in which space evacuation is critical, special emphasis should be given to properly proportioning blanket volume to pumping area and distances, for instance. Where vacuum bagging is involved, the problems of bag leaks should be circumvented by not using flight-type bagging. Instead extra heavy bags would be used to simulate conditions that will be achieved if flight-type vacuum bags are successfully developed. In all adaptations to the tank the method of structurally securing the systems should be carefully simulated to ensure proper, representative response of the insulation during structural testing. The recommended specimen is believed to be adequate for this simulation.

As will be discussed later, the penetration tests should be performed only after space thermal performance qualification of the systems. The insulation would then be pierced to attach the penetration and the juncture would be insulated employing the established design techniques. Provisions for the penetration attachment will therefore be incorporated in the basic adaptation of each system to the screening and qualifying specimens.

2. Test Plan

The screening tests are planned so that tests on similar systems will be grouped as shown in Table VI-1. Test results on basic problems common to the group will then apply throughout the group and possibly eliminate repetitive testing. For this reason, the vacuum bagged systems are in Group I, the purged systems are in Group II, and the systems involving neither are in Group III.

The proper sequence of testing for each group and systems within are determined to increase the probability of their early elimination

from further testing. The sequences shown in Table VI-1 reflect tentative decisions. The arrows between tests in Table VI-1 show tests that are conducted either simultaneously or immediately following for purposes of conserving testing fluids or space chamber test time.

The testing sequences shown are based on current knowledge of the systems. In general it is desirable to subject each system to a sequence of testing environments which parallels that which an actual stage would experience. However, testing time and money are saved by breaking this order for certain systems. In other cases, it may be possible to eliminate one or more systems by a judicious selection of one or two tests to be run first.

As may be noted in Table VI-1, the penetration tests are tentatively scheduled to follow space thermal performance testing. This sequence is for the purpose of minimizing this type of testing by not performing it until the system has survived other tests. Once a system has survived other tests it will be used essentially as a calorimeter to evaluate space performance of the penetration. The major penetrations, such as structural supports and suction lines, will be installed in the specimens as previously discussed, and evaluated for their space performance, one at a time, in the space chamber. This testing will provide quantitative data on the penetration's contribution to the entire system's heat load and the effectiveness of juncture insulation designs.

As the test program proceeds, the results may suggest alternate, more attractive approaches.

Details of some of the testing plans are presented now under the headings of Structural, Ground Thermal Space Performance, and Penetration testing.

a. Structural tests

Ideally, it would be proper to combine and/or program acoustic vibration, acceleration and altitude environments as they occur during boost. However, it is planned to conduct the vibration and acoustic tests simultaneously and conduct the acceleration and rapid pressure drop tests separately. The vibration and acoustic tests on the specimens should be performed while they are filled with liquid hydrogen because increased brittleness in the cold condition is of major importance. The acceleration test, where strength is of major importance, should be conducted under the more stringent condition of the specimens being uncooled where strength is decreased.

Vibration. A test fixture should be designed and fabricated to support the test specimens; the fixture should be designed to be resonant free below 150 cps. Vibration tests would first be conducted in three

planes while the specimen is not filled with liquid hydrogen. Resonant surveys would be conducted at a low vibration level to determine whether adverse resonances exist in the fixture-test specimen combination. If they exist it should be noted and fixes should be employed to ensure a valid evaluation of the insulation and attachment. Sine sweep tests should then be conducted at a 6.0-g level from 20 to 150 cps in the direction of each of the three major axes using a vibration exciter system. Sweep rates should be one octave per minute and made up and down in frequency. Visual observations should be made throughout the test and an examination for failures should be made after the test. Stroboscopic techniques could be employed to aid visual observations. If critical frequencies exist, these could then be examined more thoroughly.

After this vibration survey, the specimen should be vibrated at the 6.0-g level, 20 to 150 cps, in the longitudinal direction while filled with liquid hydrogen and simultaneously subjected to the acoustic environment. Longitudinal vibrations are felt to be the more severe. In this final test the vibration levels of 6 g from 20 to 150 cps would be applied by sweeping up and down in frequency at the rate of 1 octave/min. Simultaneously a random acoustic input of 150 db would be applied simulating boost noise. The insulation system should then be inspected for damage. If damage affecting thermal performance has occurred which cannot be visually detected, it will be determined in subsequent thermal performance testing.

Acoustic. Acoustic testing should be conducted only in combination with the vibration environment. These tests would be performed as stated in the vibration section.

Acceleration. The test specimen would be mounted in the same fixture used for vibration testing and that assembly mounted on a centrifuge arm. Acceleration tests should be conducted in each of three major planes at a level of 6.6 g measured at the cg. Visual observation should be made after the tests to determine if damage has occurred. Damage affecting thermal performance of the insulation which is not visible will be detected during the thermal performance tests.

Rapid pressure-drop test. Only the non-vacuum-bagged specimens would be subjected to this test. The test specimens should have a radius equal to that of the barrel section of a complete tank, and insulation blanket proportions should simulate the area to edge-length ratios of practical insulation blanket installations. Therefore, it is expected that inflating forces developed during decompression will accurately simulate full-scale conditions. The test would be conducted in a vacuum chamber while the specimen is cooled with gaseous helium for the reasons discussed later in this section.

Pressures within the purged and unevacuated blankets should be monitored with pressure transducers in this phase of testing and the specimens observed visually for any damage resulting from the test. The pressure drop profile specified by NASA as typical of a boost trajectory, if of interest, should be simulated by the space chamber.

b. Ground thermal performance

The major objective of these tests is to determine how well each of the promising insulation systems performs the job of preventing excessive boiloff of the cryogenic fluid under simulated prelaunch or launch pad conditions. Knowledge of the heat transfer for this ground-hold condition is extremely important since a requirement for a long ground-hold after topping can incur significant payload penalty or mission velocity increment penalty. The effects of ground-hold performance should be included in the final evaluation of the systems.

Since heat transfer measurement is the test objective and since liquid hydrogen is the cryogenic propellant being considered here, the question arises as to whether it would be safer, more economical or even feasible to test with a more inert fluid (i.e., either liquid or gas). As presented earlier, the ground-hold performance of the systems varies over a large range (a factor of 30 or more). Since the heat fluxes are relatively high, estimates were made to determine the feasibility of ground testing with a cold gas (such as helium). These estimates indicate that this approach is not advisable because of relatively high temperature drops across the gas film next to the tank. For example, these temperature drops can be as high as 40° to 50° F for the higher heat flux systems (250 to 300 Btu/ft^2-hr). More important, the equilibrium heat flux established would not be representative of the system, and accurate comparison of the systems could not be made.

Consideration was given to the use of several liquefied gases, liquid helium and liquid neon, to aid in reducing the safety hazards associated with hydrogen testing. Liquid helium would be satisfactory to simulate the heat transfer aspects, but the cost is excessive and its low heat of vaporization (8.8 Btu/lb versus 193 Btu/lb for LH_2) would make it impossible to keep enough liquid in a test specimen for most of the systems. Liquid neon (50°R) might adequately simulate the heat transfer aspects, but, aside from cost and its heat of vaporization being one fifth that of LH_2, it is 17 times heavier than liquid hydrogen. This would make handling and supporting of both the test specimen and the complete system tank a major operation. The only realistic alternative is testing with liquid hydrogen.

The test tank, fully insulated, would be suspended from a load cell for this phase of the testing. The cell would be used for measuring the

weight change due to boiloff of the liquid hydrogen. The output of the load cell would be recorded on a suitable readout system, whose accuracy would not degrade the load cell accuracy. A test setup is shown in Fig. VI-2 that would be suitable for the tests.

After suspending the test tank in the test fixture, a vacuum jacketed liquid hydrogen fueling line should be connected to it and a storage reservoir. The fueling line and test tank should be purged with gaseous nitrogen making several volume changes to assure reduction of undesirable gases to a nonhazardous percentage. The purging gases would exit the test tank through the tank vent and would be directed to a venting stack not directly coupled to the test tank. Direct coupling of the venting stack to the test tank would cause problems with the weighing system. The juncture of the tank vent and the venting stack would be equipped with a manifold ring through which nitrogen would pass and hydrogen gas vented to minimize air aspiration up the vent stack and possible moisture freeze out on the test tank vent line. The test article would then be filled to a nearly-full level with liquid hydrogen.

Upon completion of the fueling operation, the recording system should be energized and the boiloff rate determined as previously described. Upon completion of the boiloff test, the tank could be prepared for and subjected to the cold vibration and acoustic tests while in its cooled condition.

c. Space thermal performance

It is only necessary to accurately simulate tank wall temperature in this phase of the testing. The high performance insulation systems being tested in this phase will have such high thermal resistance that, regardless of the nature of the subinsulation, tank wall or fluid in the tank, the insulation alone is controlling the heat transfer for all practical purposes. Thus, cold gaseous helium at liquid hydrogen temperatures can be used with negligible loss in the accuracy to establish the heat flux. That is, the thermal resistance of the cold gaseous helium film is a negligible fraction of the overall thermal resistance of the heat transfer circuit. Table VI-2 shows the estimated heat fluxes, helium film and insulation resistances, and film temperature drops for typical test conditions for both the NRC-2 and a Linde superinsulation.

Items 2 and 3 in Table VI-2 are presented to show that even for conditions where the design pressures in the insulations have not been reached, the film temperature drops are not sufficient to prevent measuring the heat transfer with good accuracy. The helium film coefficients were estimated by conservatively assuming the heat transfer at the wall was by natural convection. In practice, however, there would be some flow of helium gas through the test

article, and the film resistances would be even lower than those given. Figure VI-3 presents the natural convection capability of the cold gaseous helium film as a function of film temperature. This figure is based on the following

$$\frac{\dot{Q}}{A} = h_f (\Delta T)_f \tag{17}$$

where

$\frac{\dot{Q}}{A}$ is heat flux

h_f is a film coefficient defined by

$$h_f = 0.13 \frac{K_f}{L} \left(N_{GR_f} N_{Pr_f} \right)^{1/3} = F(T_f) (\Delta T_f)^{1/3} \tag{18}$$

K_f is helium thermal conductivity at the film temperature, T_f

L is the characteristic dimension

N_{GR} is Grashof number based on film temperature

N_{Pr} is Prandtl number based on film temperature

$F(T_f)$ is some function of the film temperature

ΔT_f is the temperature difference across the film

$$F(T_f) = \frac{\dot{Q}}{A (\Delta T_f)^{1.333}} \tag{19}$$

Since a space chamber must be utilized to perform this phase of the test program, the use of cold gaseous helium in place of liquid hydrogen has several distinct advantages. These advantages are safety, cost and the use of facilities which otherwise would not be available. Most space chambers are located in confined facilities which contain other valuable equipment in close proximity. Tanks containing liquid hydrogen cannot be tested in most space chambers for safety reasons. The use of helium does not pose any safety problems. In addition, when testing with hydrogen, the propellant is lost through boil-off representing a large cost item. On the other hand, many space chambers have a closed loop cold

gaseous helium circuit for use in the cryo-pumping panels. If the heat load to the test article is within this circuit's capability, it can be used to provide the cryogenic environment within the tank for no appreciable additional cost for cyrogenic fluids. The only coolant cost for using this system is the helium make-up required for the small losses in the system and small amounts of inexpensive coolants in the heat exchanger of the helium cryostat.

Space thermal performance tests on the basic insulation systems and the penetrations should therefore be conducted in a space simulator using gaseous helium cooled to 18° K by a cryostat. The fully insulated test specimen would be placed in the chamber and the helium lines routed to the filling and vent ports of that tank. The lines would be connected to the cryostat in such a manner as to provide a closed-loop system; that is, a circulating system will be established so that the output of the cryostat will flow through the test specimen and return to the intake of the cryostat. Flow through the specimen should be measured with a highly accurate venturi flowmeter since it will be small. Flow through the specimen should be regulated to produce a minimum temperature rise in the helium consistent with accuracy of the gas temperature measuring instruments used. Total heat entering the tank can then be calculated knowing the flow rate and temperature rise in the gaseous helium.

While the above recommendations are primarily for determining steady-state performance of the insulation systems, some indication of the length of time and heating involved between storage initiation and steady-state should be obtained by monitoring pressures in the blanket during that period. Since aerodynamic heating would not be simulated, heat transferred during ascent would not be simulated. Ascent ambient pressures would be simulated, however, so that from the end of the ascent period to the beginning of the steady-state period pressures within the insulation will be somewhat representative and can be monitored. Knowing these pressures and the relationship between pressure and effective thermal conductivity through the basic blanket, heat transferred through it can be integrated for the transient period. The steady-state part of the space thermal test will give data on the additional heating due to direct conduction through seams, joints and penetrations. That heating rate multiplied by the transient time period can be added to the integrated heating through the basic insulation to approximate total heating during the transient period.

It is noted that the above discussed transient heating and evacuation period is affected by temperature of the gas within the blanket which in turn depends on aerodynamic heating during ascent. This discrepancy in the simulation will then of course limit the applicability of any data collected during the transient period.

d. Effects of penetrations

One of the major objectives of the current program has been to analytically assess the thermal effects of major penetrations through and discontinuities in the insulation system. These items include: fill, drain and suction lines; pressurization and vent lines; instrumentation conduits; insulation structural supports; manhole access; insulation blanket terminations, splices, or joints; propellant tank supports; and others. Without penetrations in the tank, the ideal heat leak to the tank through basic multilayer cryogenic insulation is very low and readily computed assuming the design pressure is achieved in the insulation. This very fact of high efficiency for the insulation over main tank areas causes penetrations to assume major heat leak proportions. For example, information developed in previous chapters indicates that the penetrations can easily double the ideal heat leak for the space condition even when these penetrations are carefully designed and properly insulated.

It is highly desirable, therefore, in this test program to attempt to isolate these various heat leaks, one at a time, to assess their magnitude. It is not desirable to determine these with any accuracy during the ground thermal tests, because at these conditions the insulation efficiency is not high and the penetration heat leak contribution is a much smaller percent of the overall heat leak. Therefore, this determination is made during the space thermal testing of the screening specimens, when it is important. It is felt that this testing can be performed much more economically on the screening specimens and with as much accuracy as if they were similarly tested on the large scale tanks.

The heat leaks through tank structural supports, insulation structural attachments, blanket terminations, splices, joints, scrolls, etc., are, in general, very difficult to predict analytically, and certainly require experimental verification to determine the validity of analytical models.

It is felt that the penetration tests should not be run on any system until it has been proved to be a candidate for selection for performance testing; i.e., it should have passed all other tests indicated in Table VI-1. Typical penetrations should then be installed on the specimens with both the penetration and its juncture with the specimen properly simulating an actual installation. Using the specimen as a calorimeter and its previous unpenetrated space performance data for calibration the specimen with the installed penetration should be tested in simulated space environment. The various penetrations should thus be tested one at a time to determine their individual contributions to heating.

B. PHASE II--SCREENING SPECIMEN FABRICATION AND TESTING

Since the recommended plans for testing are described above in Section A, only some recommendations for screening specimen fabrication are discussed here.

At least two aluminum tanks similar to the preliminary design shown in Fig. VI-1 should be made for use in screening and qualifying the cryogenic insulation systems. Their tolerances are not critical, other than the mating of details at the weld joints. Details required for the tanks are simple sheet metal parts that should be made from layouts and setups, requiring a minimum of assist tools.

The most stringent requirement in the tank fabrication is the need for maximum probability of leak-free welds. To satisfy these requirements, details should be matched by hand fitting, to ensure good joints, and electron beam welding will be utilized where possible. The use of gas tungsten arc welding should be employed where electron beam welding is not accessible. Prior to proof-testing, all welds should undergo dye penetrant checks.

Testing of the tanks prior to any insulation installation should be accomplished by hydrostatic and helium tests. The hydrostatic test should consist of pressure testing to 40 psi over a two-minute period, followed by leak testing at ambient conditions using a helium mass spectrometer with a rated sensitivity of 2×10^{-10} cc/sec. In this final test, the tank should be subjected to thermal shock, using an existing vacuum chamber and thermally exercising the unit.

Installation of the insulating systems on the test tank should be in general accordance with the method shown in Fig. VI-1 where the system under investigation is installed over the lateral surfaces of the tank, the insulation of the ends being standard for all systems. It is expected that all systems being investigated will present difficult fabrication problems requiring some processes development work. Whatever those problems may be, it is emphasized that the installation should duplicate, insofar as possible, the principal characteristics of the system as installed on a large tank. For instance, the tank recommended is sufficiently large to install a gore of the systems treated in Chapter IV. The edge treatment can therefore be simulated on the screening specimen while maintaining typical edge length-to-blanket area ratios. Further, the large curvature of the tank will permit accurate evaluation of the methods for resisting inflation of the blankets during boost decompression. Therefore, those methods recommended should be closely simulated in the installation.

It is to be expected that as fabrication and testing of the screening specimens proceed, the design details of the systems will evolve. Both fabrication and testing of the systems should reveal better methods of installation since most of these systems have never before been made.

C. PHASE III--PERFORMANCE TESTING

Upon completion of the screening and development tests of Phase II, the remaining systems should be rerated accounting for any pertinent data developed in the test program. The two higher ranking systems

should then be selected for testing as complete, insulated, spherical-tank systems. Their designs should be modified to incorporate any beneficial developments in installation techniques made to that point.

It is recommended that the two higher ranking systems then be installed on a tank whose size and shape is near or equal that of one intended for actual flight. In lieu of the existence of such planned tanks it is recommended that the systems be installed on a spherical tank of at least 150 in. diameter including accurate simulation of the usual penetrations including their own insulation and treatment of their juncture with the tank. It is felt that the use of a spherical tank will give ample opportunity for encountering the important problems of the insulation systems while keeping the size of the tank and the required test facilities to a minimum.

The recommended program for testing the two complete systems is summarized below:

1. Structural Tests

The complete system should be in a test fixture such as illustrated in Fig. VI-4. Acoustic excitation should be applied at a level of 150 db, with a spectrum shape simulating booster noise, for a period of 5 min. The excitation should be directed at the test fixture that simulates typical skin-stiffener construction and permits some attenuation similar to that which would exist under actual conditions. Visual inspection of the insulation should be made at the conclusion of the test. Any damage affecting thermal performance which is not visible will be detected during the thermal performance tests.

Present data show that the acoustic environment is critical--that is, previous tests have been performed on multilayer insulation showing no damage from vibration, while some chafing resulted from acoustic excitation. Typical tank supports can be expected to dynamically isolate the tank from mechanical vibrations above 20 cps. Neither is the static acceleration condition expected to be critical. Therefore, acoustic testing should be sufficient to adequately test the structural properties of the installations.

2. Ground Thermal Performance

The full scale tanks should then be subjected to ground performance tests. The procedure outlined in the small scale test applies to the full scale systems except that larger apparatus will be required.

3. Space Performance

a. Rapid pressure drop

The full scale tank insulation (if nonevacuated systems are selected for complete systems) should be subjected to the rapid pressure drop of a specified boost trajectory. These tests will require a large space

chamber with a high pumping rate capacity. The specimens may be mounted on an engine mount-type support structure shown in Fig. VI-5. Pressures within the blankets should be monitored with pressure transducers and ionization vacuum gages to determine the degree of evacuation obtained and the time for pump-down to thermally acceptable values of evacuation. Gaseous helium should be used as the refrigerant during these tests for the reasons discussed earlier.

The results of the rapid decompression should be monitored by visual observation for obvious structural failures, as well as by means of the pressure and temperature instrumentation.

b. Space performance

If no obvious insulation failures occur as the result of the rapid pressure drop tests, the space performance evaluations of the complete system should follow. Liquid hydrogen temperature at the tank wall should be maintained by use of gaseous helium flowing in a closed-cycle cryostat. Heat transferred to the complete tank can be evaluated by measuring the helium flow and its temperature rise across the tank. The steady state temperature of the outside insulation surface and the wall temperatures of the tank will be measured by the use of thermocouples. It is expected that essentially room temperature can be passively maintained on the outer surface of the insulation and this will be a sufficient simulation of the thermal environment of space.

TABLE VI-1

Screening and Qualification Test Plan

Group	System	Testing Order (1)	(2)	(3)	(4)	(5)	(6)	(7)	(8)	(9)
I	(1) Evacuated NRC with spacers (with and without double bag)	(e)	(f)	(g)→	(b)-(c)	(a)	(h)→	(k)		
	(2) Evacuated NRC over cork, foam or honeycomb (with or without double bag)	(f)-(e)	(j)	(g)→	(b)-(c)	(a)	(h)→	(k)		
	(3) Evacuated Linde SI	(e)	(g) →	(b)-(c)	(a)	(h)→(k)				
II	(4) He purged NRC-2	(i)	(g)→	(b)-(c)	(d) →	(h)	(k)	(a)		
	(5) He purged Linde SI	(i)	(b)-(c)	(d) →	(h)→	(k)				
	(6) He purged Marshield	(i)	(g) →	(b)-(c)	(d) →	(h)→(k)		(a)		
	(7) He purged gap under NRC-2	(i)	(g) →	(b)-(c)	(d) →	(h)→(k)		(a)		
III	(8) Unpurged NRC-2 over foam or honeycomb	(j)	(g) →	(b)-(c)	(d)→	(h)→(k)		(a)		
	(9) Alternate systems	Order to be determined.								

Tests

(a) 6.6 g steady accel.
(b) 6.0 g mech. vibration (20-150 cps)
(c) 150 db acoustic vibration
(d) Boost inflation
(e) Checkout of vacuum bag unit
(f) Checkout of indiv. evac. bags
(g) Ground performance
(h) Space performance
(i) Development of purge methods
(j) Development of subinsulation system--attachment (or bonding) and sealing methods
(k) Penetration tests

☐ represents items which may not have to be duplicated

→ indicates tests which will be run immediately following another or combining with it.

TABLE VI-2

Insulation Resistances

Item	Insulation	Insulation Apparent k (Btu/ft-hr°R)	Insulation Thickness (in.)	Heat Flux ($Btu/ft\text{-}hr^2$)	R_i Insulation Resistance	Film ΔT	R_{film}, Film Coefficient	Film Resistance	$\frac{R_{film}}{R_i}$
1	NRC-2	1.28×10^{-5}	1.3	0.05	8455	0.0485	1.03	0.971	0.000115
2	NRC-2	1.28×10^{-4}	1.3	0.50	845.5	0.275	1.82	0.55	0.000649
3	NRC-2	1.28×10^{-3}	1.3	5.0	84.55	1.597	3.17	0.3155	0.00373
4	LINDE SI-91	0.85×10^{-5}	0.5	0.0865	4900	0.073	1.187	0.842	0.000172

* Table is based upon:

Warm Boundary 460° R
Cold Boundary 36° R
NRC-2--70 layers/in.

D. ILLUSTRATIONS

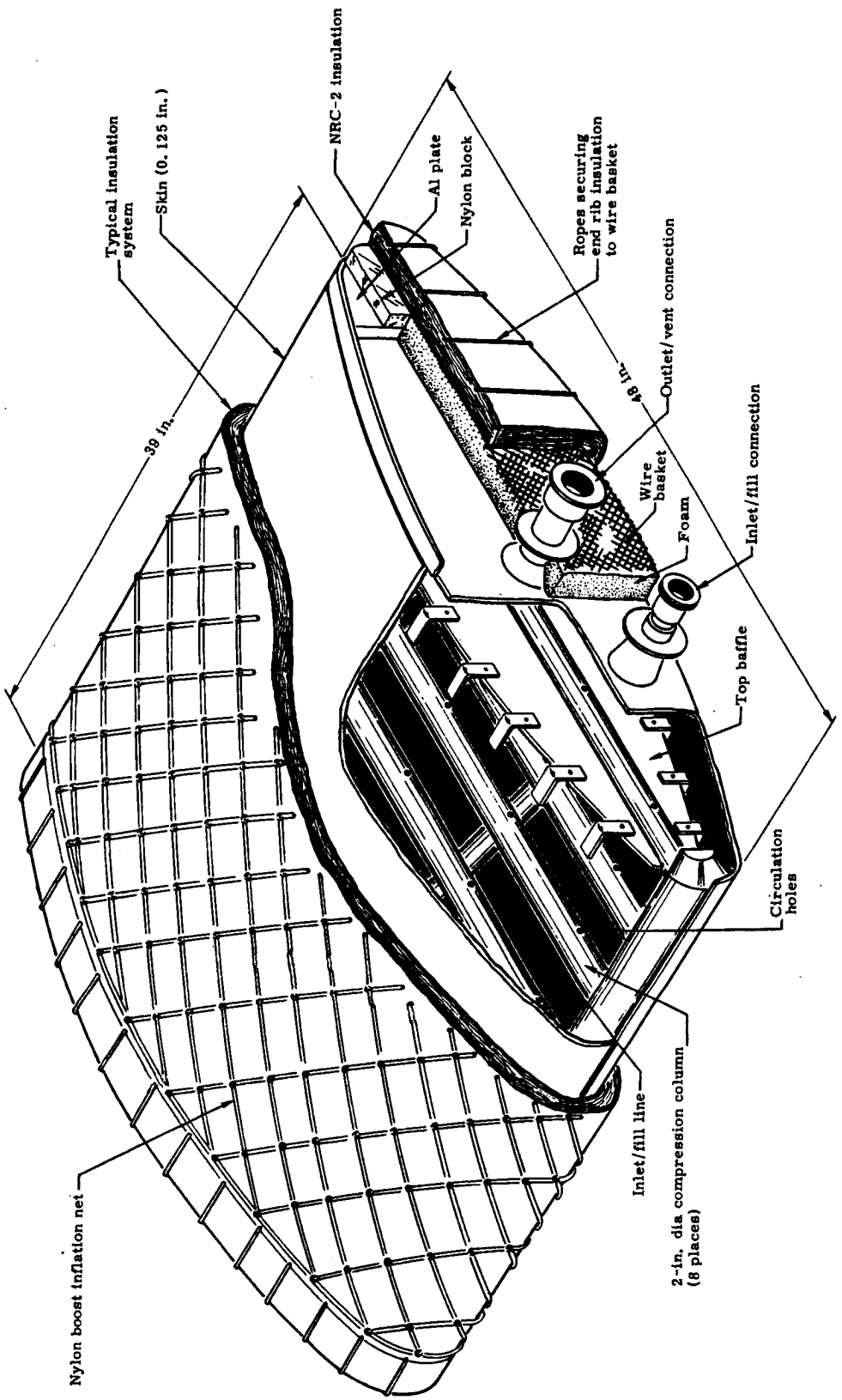

Fig. VI-1. Screening Test Specimen

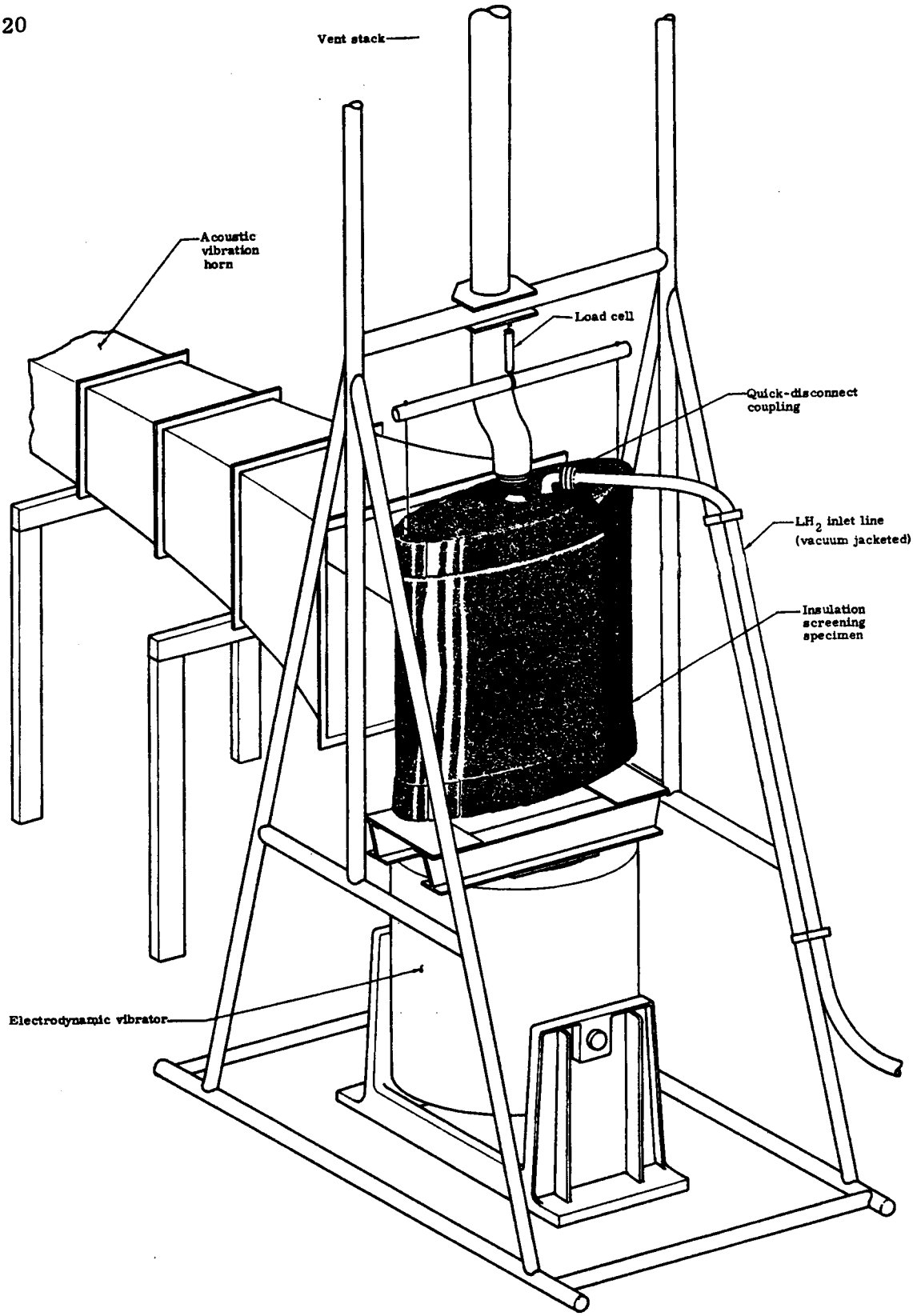

Fig. VI-2. Test Apparatus, Ground Thermal and Vibration

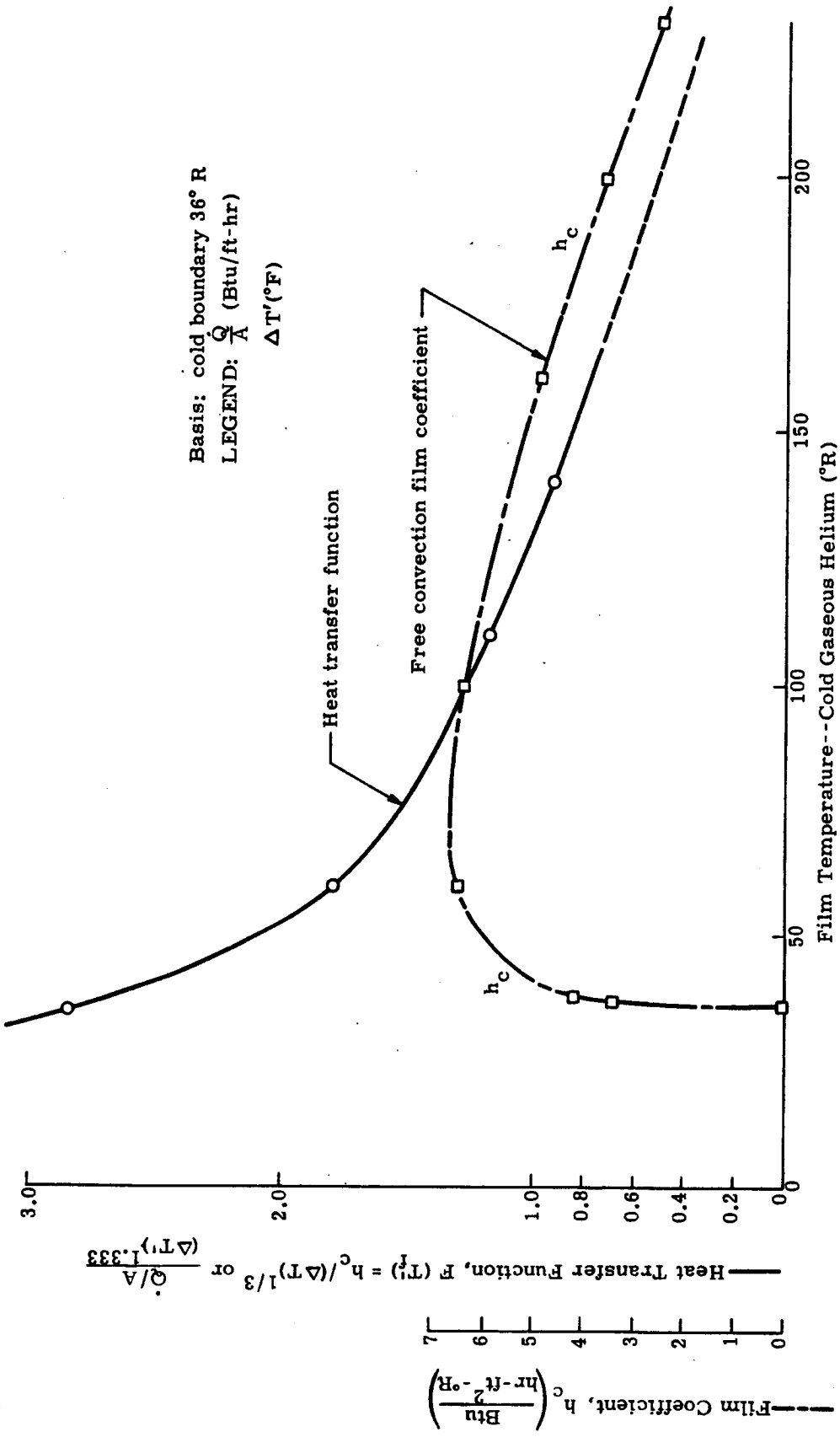

Fig. VI-3. Free Convection Heat Transfer by Gaseous Helium

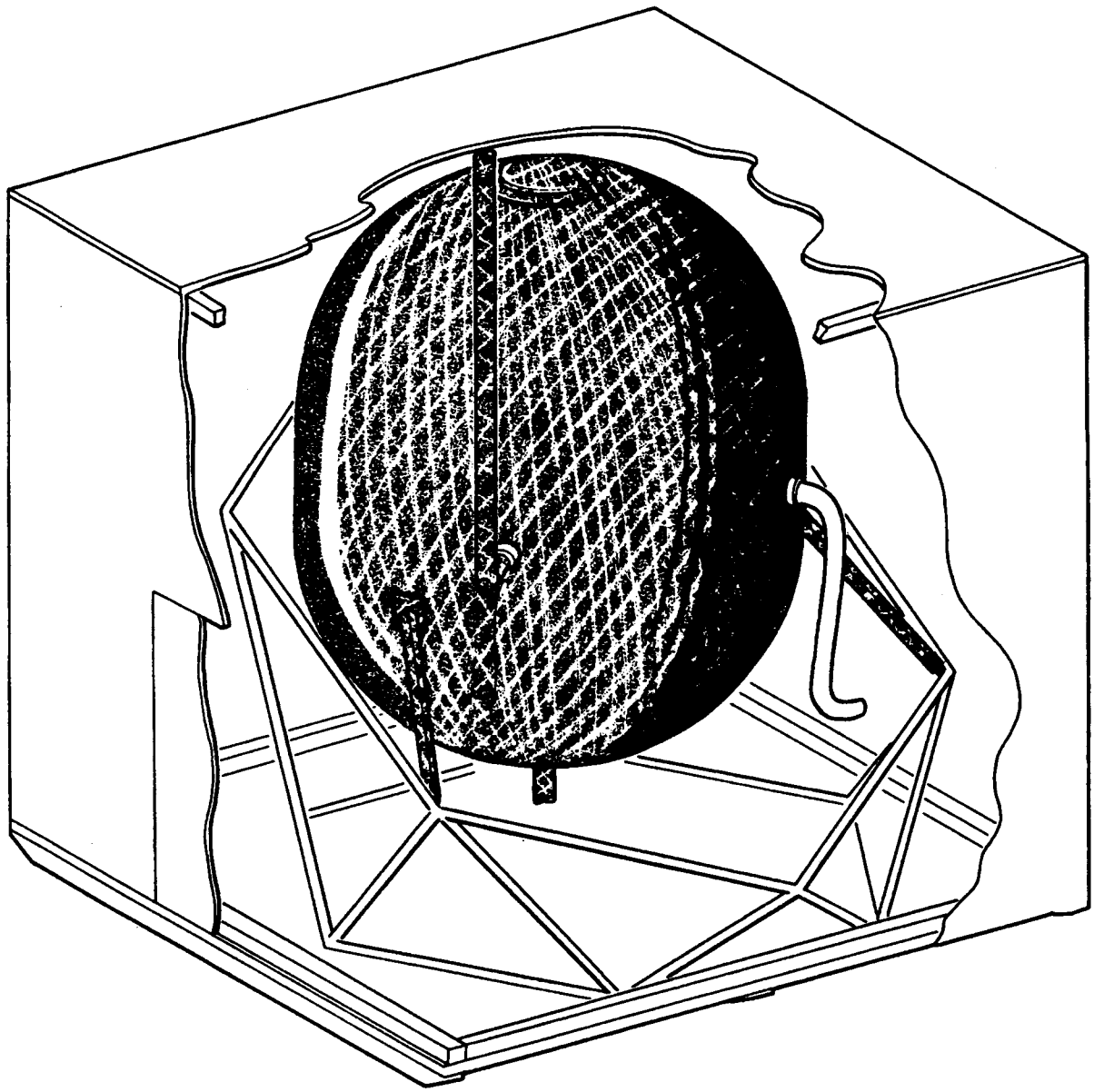

Fig. VI-4. Performance Test Setup, Ground Hold Condition

Fig. VI-5. Space Thermal Test, Complete System Concept

APPENDIX A

METEOROID TESTS

APPENDIX A

METEOROID TESTS

The design solution of the meteoroid problem for a space vehicle currently depends upon statistical data on the meteoroid environment to which the vehicle will be exposed and the effects of their hypervelocity impacts upon the vehicle's surface. By a review of data on the meteoroid environment and consideration of demonstrated efficiency of the multilayer insulations as energy absorbers, it appears that the meteoroid problem is relatively unimportant in the design of storage tanks for the 30-day duration specified for this study.

Figure 1 shows the various current semiempirical estimates of the meteoroid flux rate and particle size relationships. Included in Fig. A-1 are the "pessimistic" and "optimistic" limits as drawn in NASA TN-D-1504 (Ref. 1) along with the S-55 satellite data which tends to justify the current trend toward acceptance of the "optimistic" limit. Also shown in Fig. 1 are the revised flux rate estimates of Whipple and Watson (Ref. 2) based upon improvements in meteoroid data by the measurement of luminous efficiency in the artificial meteoroid experiments of Trailblazer 1 (Ref. 2). Both the Whipple and Watson predictions agree closely in the area of the larger meteoroids; however, Whipple's modified curve shows closer agreement with the higher frequency rates of encounter of the smaller meteoroids as indicated by the microphonic satellite data of Ref. 3. Hence, Whipple's 1963 modified estimate of the meteoroid flux rate has been selected as the model to be used in this study. It demonstrates a mean velocity of 22 km/sec.

Using the Whipple flux rate model, and assuming a Poisson probability distribution, the design meteoroid curves of Fig. A-2 were constructed. The curves indicate the largest meteoroid to be encountered (the design meteoroid) as a function of exposure factor and any desired probability of not encountering a meteoroid larger than the indicated design value. Shown in Fig. A-2, as an example, is the exposure factor for the target tank prescribed for this study, a cylindrical tank 400 in. in diameter, having an L/D ratio of 1.75. At 30 days exposure time the exposure factor is 182,000 sq ft-days. Assuming 0.001 as the design probability of encounter for the vehicle, the design meteoroid is seen to be one having a mass of 1.2×10^{-2} gm.

Several techniques have been proposed for estimating meteoroid damage to a structure. However, most of these techniques have been based upon either meteoroid penetration in semi-infinite plates, single plates of finite thickness, or upon the behavior of meteoroids intercepting multiple plate bumper shields. The meteoroid problem to be evaluated for multilayer insulations is similar to the multiple plate shield wherein

the meteoroid is fragmented by the outer shield, since any multilayer insulation installation must include a shroud or outer structure to provide protection from aerodynamic conditions during boost.

To establish the required bumper thickness, reference is made to the results of Nysmith & Summers double sheet penetration experiments (Ref. 4). Using these results and assuming a spherical projectile, the total thickness of a double sheet structure with a sheet separation distance of eight projectile diameters between plates of equal gage, the total thickness required becomes

$$t_b = 0.356 \left(\frac{1}{\rho_p}\right)^{1/3} \left(mv^2\right)^{1/3}$$

where v is in km/sec. However, it is pointed out that a more efficient bumper shield is obtained by having a 0.25 to 0.75 weight distribution between the outer and inner plates. Hence, an efficient fragmentation shield or bumper thickness is obtained by the use of

$$t_f = \frac{0.356}{4} \left(\frac{1}{\rho_p}\right)^{1/3} \left(mv^2\right)^{1/3}$$

For meteoroids having velocities on the order of 22 km/sec this results in fragmentation bumper thicknesses of approximately 0.030 in., which is entirely compatible with, or less than, design minimums of shrouds or structural skins of realistic vehicles. It is, therefore, assumed that the above shroud thickness will be provided and it remains to determine the extent to which multilayer insulation will resist penetration by the resulting fragmentation particles of the design meteoroid.

It is pointed out in Ref. 4 that the fragmentation particles resulting from the hypervelocity projectile penetration of the bumper have a residual velocity of approximately 60% of the impact velocity. Hence, the velocity of the fragmentation particles impinging on the multilayer insulation from the design meteoroid would be of the order of 13 km/sec.

For the present investigation, the conservative assumption is made that the meteoroid is principally iron. Existing data from shaped charge experiments developed and calibrated by Aberdeen Proving Grounds Ballistic Research Laboratory are applicable to the present problems. A selected BRL shaped charge fired in a vacuum closely approximates the fragmentation particle velocity that the multilayer insulation would experience, 13 km/sec. The development and calibration of this charge is described in Ref. 5.

As explained in Ref. 6, the BRL small cylinders of brittle cast iron are cast into an explosive charge and, when fired in a vacuum, a cluster of iron particles is projected all of which are 100 μ or less in diameter and travel at a velocity in the range of 12 km/sec. The total iron mass is 0.6 gm, but not all of that mass reaches the standard target. A shutter and aperture arrangement is used to screen out particles of other velocities. The particle size distribution in the debris that impinges on the target is said in Ref. 6 to be characteristic of the products of fragmentation that an iron meteoroid would have. Although there seems to be no specific data on the extent that the present design meteoroid would fragment in passing through a 0.030-in. aluminum sheet, it was presumed that the 100 μ fragments of the BRL shaped charges may be in the proper range. Therefore, a series of experiments was conducted in which the above described shaped charge was fired at specimens of Linde SI and NRC-2 multilayer insulations.

The multilayer specimens tested are shown in Fig. A-3. The results of the experiments are tabulated below:

Specimen Number	Cover Plate	Insulation	Penetration
1	0.014	Linde SI (t = 0.0005)	4th layer unpenetrated
2	none	Linde SI (t = 0.0005)	8th layer unpenetrated
3	none	Linde SI (t = 0.0005)	6th layer unpenetrated
4	0.014	NRC (t = 0.00025)	Cover plate unpenetrated
5	none	NRC (t = 0.00025)	12th layer unpenetrated
6	none	NRC (t = 0.00025)	(No results--misalignment)

Although no other quantitative analysis of these data has been attempted it was noted that the Linde SI is approximately four times more efficient (on a weight basis) as an energy absorber than is the aluminum cover plate and that the NRC is approximately nine times more efficient. Assuming the dispersion area of the charge to be representative of fragmentation dispersion caused by the design meteoroid impacting the shroud, it is also noted that the particles caused only negigible degradation of the insulation since the fragments produced only a small pattern of pin holes as they penetrated the layers.

REFERENCES

1. Zender, George, and Davidson, J. R., "Structural Requirements of Large Manned Space Stations" NASA TN D-1504, August 1962.

2. Whipple, F. L., "On Meteoroids and Penetrations," Proceedings of the 9th Annual Meeting of the American Astronautical Society, 15-17 January 1963.

3. Davidson, John, and Sandorff, Paul, "Environmental Problems of Space Flight Structures" NASA TN D-1493, January 1963.

4. Nysmith, C. R., and Summers, J. L., "An Experimental Investigation of the Impact Resistance of Double Sheet Structures at Velocities of 24,000 Feet per Second" NASA TND 1431, October 1962.

5. Richards, L. G., and Holloway, L. S., "Study of Hypervelocity Microparticle Cratering" B. R. L. Memorandum Report ;No. 1286, June 1960.

6. Richards, L. G., and Gehring, J. W., Jr., "Hypervelocity Microparticle Impact on Thin Foils," B. R. L. Technical Note No. 1380, February 1961.

ILLUSTRATIONS

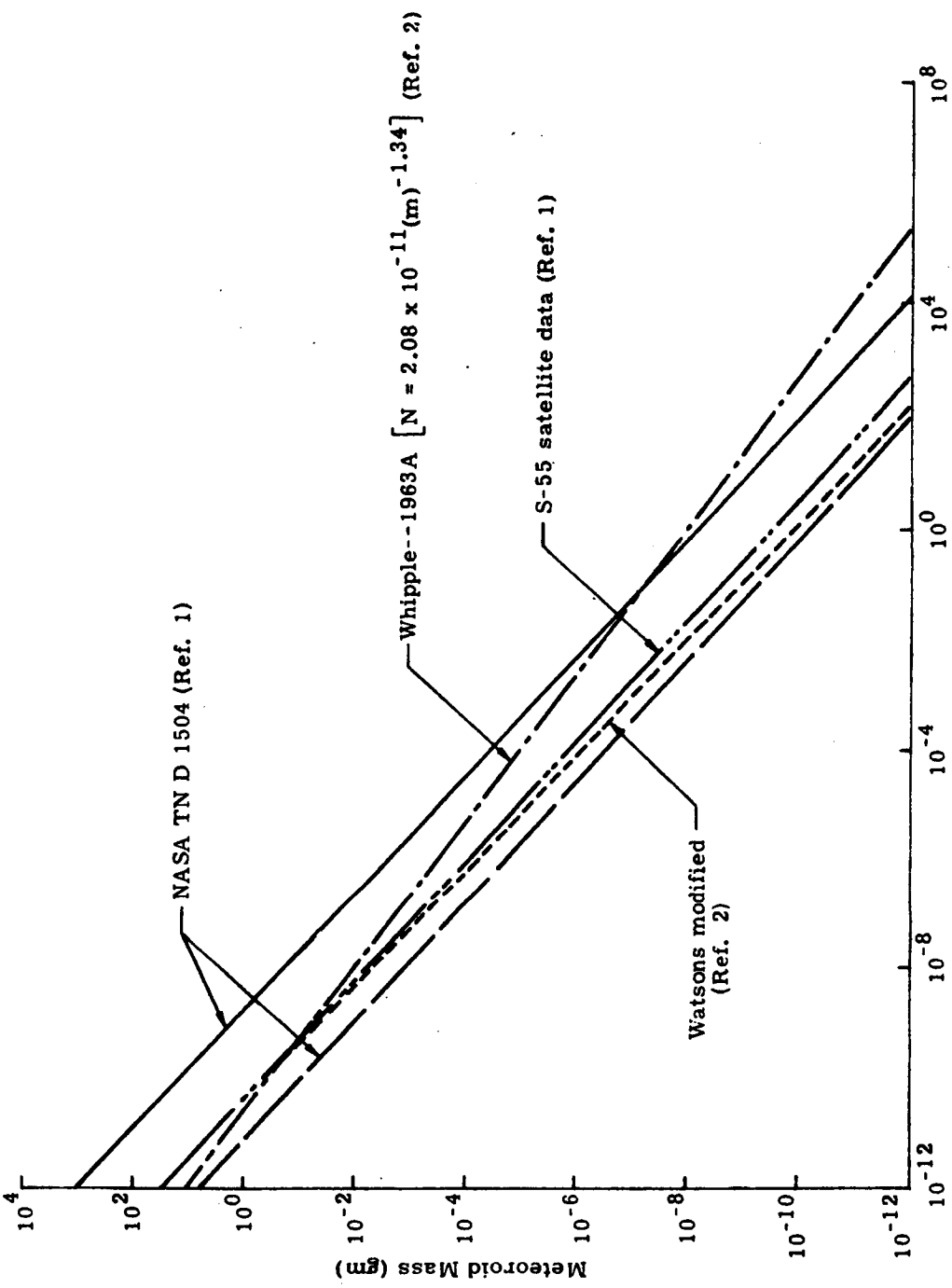

Fig. A-1. Meteoroid Flux Densities

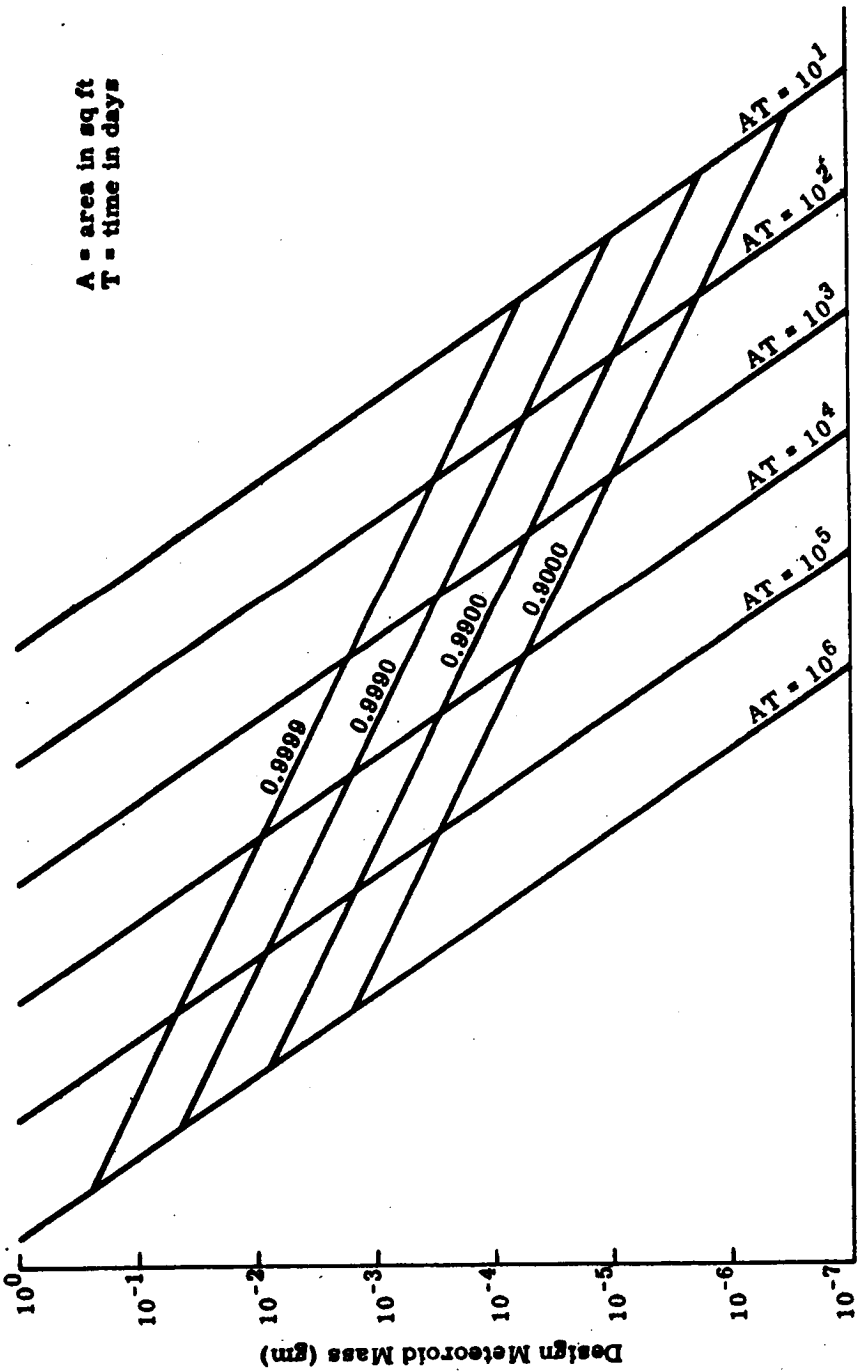

Fig. A-2. Design Meteoroid Mass and Probability of Encounter Versus Exposure Factor (AT)

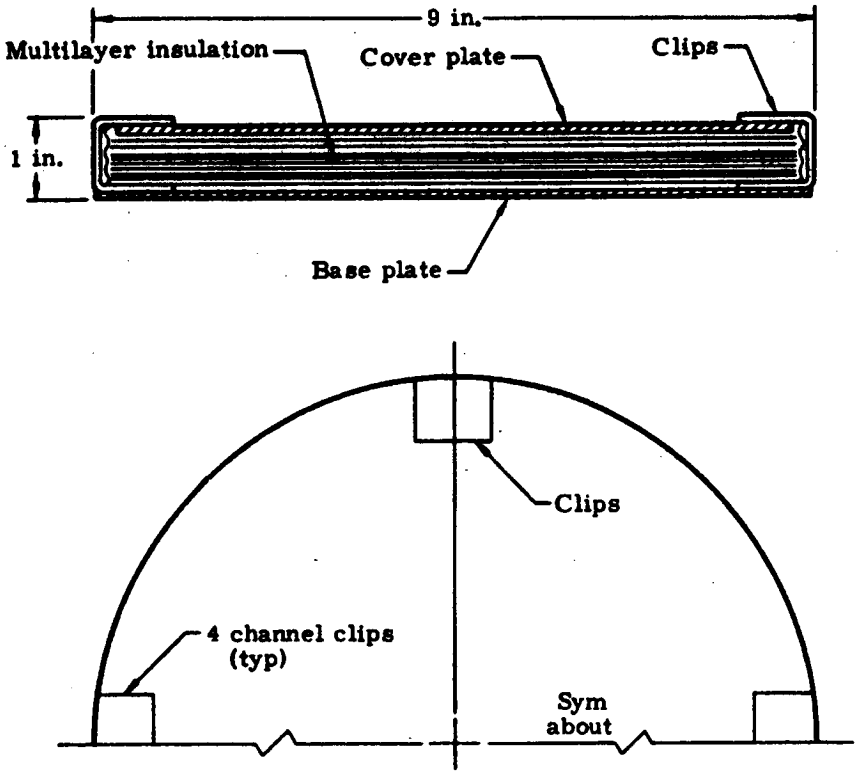

Sample	Cover Plate	Filler
1	0.014	Linde - 60 layers (t = 0.0005)
2	None	Linde - 60 layers (t = 0.0005)
3	None	Linde - 60 layers (t = 0.0005)
4	0.014	NRC-2 - 60 layers (t = 0.00025)
5	None	NRC-2 - 60 layers (t = 0.00025)
6	None	NRC-2 - 60 layers (t = 0.00025)

Fig. A-3. Meteoroid Barrier Specimens

APPENDIX B
MARSHIELD ANALYSIS

APPENDIX B

MARSHIELD ANALYSIS

The Marshield concept, as discussed in Chapter II, is based on the use of multiple radiation barriers stacked in the form of a shield over the surface to be thermally protected. Marshield insulations differ from current multilayer insulations (i.e., Linde SI and NRC-2) in that the radiation barriers (or foils) are smaller in number, each having sufficient thickness to be somewhat more rigid and they are much more widely spaced. The various methods by which the foil spacing may be accomplished have been detailed in Chapter II. The considerations which led to its initial development, and the reasons for its attractiveness as a space insulation have also been developed in Chapter II of this report.

The basic idea of using multiple radiation shields is certainly not a new one--even for space applications. Multiple shadow shields and radiation barriers have been proposed by many authors as protection devices for cryogenic tankage in space. However, practical schemes for installing these devices on a flight-type cryogenic tankage have not been in evidence.

A. HEAT TRANSFER ANALYSIS

Marshield, like other multilayer-type insulations, depends upon the removal of the gas (air) from between its radiation barriers for good thermal efficiency. As in most cryogenic insulation materials, the rate of heat transfer in Marshield could be by three modes--radiation, gaseous conduction and solid conduction. At normal atmospheric pressure levels, the gaseous conduction mode completely dominates the other two modes. As the gas pressure is lowered, a point is reached where the mean free path of the gas molecules becomes much larger than the spacing between the foils. From this point, the heat transported by the residual gas is directly proportional to the pressure level. If the pressure level can be reduced to 10^{-4} torr (mean free path in air $\approx$ 20 in.) or below, the contribution of gaseous conduction to the total can essentially be neglected (Marshield foil spacings of 1/8 to 1/4 in. are anticipated).

The apparent normal thermal conductivity ($k_{a\perp}$) (i.e., perpendicular to the foils) is then composed chiefly of two components, that is:

$$k_{a\perp} = \bar{k}_r + \bar{k}_s$$

$\bar{k}_r$ = radiation component

$\bar{k}_s$ = solid conduction component

The minimization of the solid conduction component will be now considered. In Linde-type multilayer insulations, the foil spacing is maintained by continuous spacers of a low conductivity material such as fiber glass paper, mats or fabrics. In the NRC-2 insulation, the foil spacing is maintained by the crinkles in the metalized plastic film. In either case, the solid conduction is limited by minimizing the direct contact area and by contact thermal resistance.

The optimum apparent thermal conductivity for these insulations does not occur when minimum solid conduction is attained. The reason for this is that the radiation component can only be decreased by increasing the number of foils used per inch. Thus the increase in spacer material contact results in an increasing conduction component with increasing number of foils per inch. The combined result of these two opposing trends is that the optimum apparent thermal conductivity occurs at the number of layers per inch where the radiation and solid conduction components are approximately equal.

In the case of Marshield, only a limited number of radiation barriers are practical because of the volume required to contain the rather widely spaced foils. The minimum radiation component is nearly established once the number of foils is selected and the best surface optical property (lowest emissivity) is obtained. The Marshield thermal performance may then be improved only by minimizing the solid conduction contribution to the total thermal performance.

Solid conduction can be reduced by:

(1) Limiting the direct contact area between foils and spacer materials and/or themselves.

(2) Lengthening the effective conduction length between foils either by physically providing a long path or by increasing the contact thermal resistance.

(3) The use of low thermal conductivity spacer materials.

The use of discrete spacers or blocks of low conductivity material between foils is theoretically attractive for several reasons. The spacers may be formed of low density materials, and the contact area and path length could be varied to establish optimum thermal performance designs for various mission conditions. The optimum performance values occur at rather large foil spacing distances which make this approach appear impractical. It has therefore been discarded in favor of another spacer concept for several practical reasons.

The form of Marshield employing continuous, dimpled spacers is utilized in the system design shown in Fig. IV-8. The spacer material is fiber glass cloth (4 or 5 mils thick) which is made rigid by impregnating with a resin (e.g., polyurethane, phenolic, epoxy, etc.) and curing. The cloth at the time of impregnation is laid on a die having dimple forms in both directions and staggered. The finished rigid spacer panel has 1/8-in. high dimples on both sides which provide a foil separation distance of 1/4 in. Since the dimples are staggered from one spacer side to the other, the effective conduction path between foils is much longer than 1/4 in. (i.e., dimples are on 1-in. centers, see Fig. IV-8). The difficulty with analyzing this Marshield form lies in the inability to specify precisely what this effective conduction path is for two reasons. First, radiation heat transfer is occurring across the spacer panel and will tend to shorten the effective length. Secondly, while the potential contact area can be controlled by the dimple design, the effect of contact resistance on the effective path length is difficult to estimate.

The following equations were developed for approximating the heat transfer chiefly for the dimpled-type spacers but are used for other cases in the following paragraphs.

As was shown previously the apparent thermal conductivity of the Marshield can be expressed as:

$$k_a = \bar{k}_r + \bar{k}_s \tag{1}$$

Thus, the heat transfer across the shield is

$$\frac{\dot{Q}}{A} = \frac{k_a (T_H - T_c)}{\delta_i} = \frac{(\bar{k}_r + \bar{k}_s)(T_H - T_c)}{\delta_i} \tag{2}$$

T_H = warm boundary temperature

T_c = cold boundary temperature

δ_i = shield thickness

1. Case I--Dimpled Fiber Glass Spacers, Separating Polished Aluminum Foils

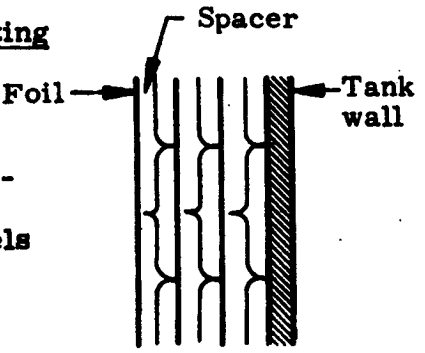

In practice the fiber glass spacers will exhibit some transmittance particularly if thin gage fiber glass cloth is used. In this analysis, the transmittance is assumed to be zero, and some accounting for it is taken care of by assuming the spacer panels to be nearly "black." The heat transfer through N foils and spacers is estimated to be given by

$$\left(\frac{\dot{Q}}{A}\right)_N = \frac{\sigma(1-\tau)}{(N_f+N_s)}\left(\frac{\epsilon_f\epsilon_s}{\epsilon_f+\epsilon_s-\epsilon_f\epsilon_s}\right)\left(T_H^4 - T_c^4\right) + \frac{\tau k_s (T_H - T_c)}{(N_f+N_s)\ell_{eff}} \quad (3)$$

(This equation is strictly valid only if the emissivity of the tank wall is equal to that of the foil)

where

ϵ_f, ϵ_s = emissivities of foil and spacer

N_f, N_s = numbers of foils and spacers

τ = ratio of contact area to total area

k_s = thermal conductivity of spacer material

ℓ_{eff} = effective path length for conduction

σ = Boltzmann constant

Typical values assumed for Marshield performance calculations are as follows:

T_H = 460° R		τ =	0.003 to 0.005
T_c = 36° R		k_s =	0.12 to 0.35 Btu/ft-hr-°R
ϵ_f = 0.05		$N_f = N_s$ =	8 to 10
ϵ_s = 0.85 to 1.0		ℓ_{eff} =	0.25 to 0.75 inch

For example, the most optimistic (underlined) assumptions result in,

$$\left(\frac{\dot{Q}}{A}\right)_N = \frac{3.79}{(N_f+N_s)} + \frac{2.44}{(N_f+N_s)} \quad \frac{\text{Btu}}{\text{hr - ft}^2} \quad (4)$$

or for 10 foils, the heat transfer is estimated at:

$$\left(\frac{\dot{Q}}{A}\right)_{20} = \frac{3.79}{20} + \frac{2.44}{20} = 0.3115 \quad \frac{\text{Btu}}{\text{hr - ft}^2}$$

Note in Eq (4) that even for optimistic assumptions, the conduction contribution is as important as the radiation contribution to the heat transfer.

2. Case II--Dimpled Fiber Glass Spacers Aluminized on One Side, Separating Polished Aluminum Foils

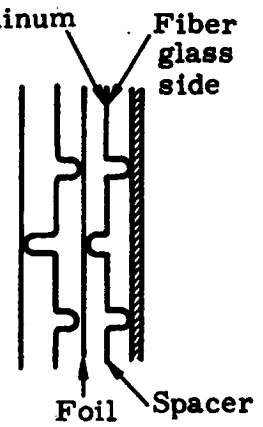

The aluminizing of one side of the fiber glass spacer results in the effective emissivity of half the gaps being different from the other half. This effect is included in Eq (5), below, by computing the effective emmissivity of each type of gap and taking the reciprocal of the sum of the reciprocals of these computed values as the overall effective emissivity of the stack. The heat transfer for this case is estimated to be given by:

$$\left(\frac{\dot{Q}}{A}\right)_N = \frac{\sigma(1-\tau)}{N_{eff}} \left[\frac{\epsilon_{eff_1} \cdot \epsilon_{eff_2}}{\epsilon_{eff_1} + \epsilon_{eff_2}}\right] (T_H^4 - T_c^4)$$

$$+ \frac{\tau k_s (T_H - T_c)}{(N_f + N_s)\ell_{eff}} \qquad (5)$$

where

$$N_{eff} = \frac{N_f + N_s}{2}$$

$$\epsilon_{eff_1} = \frac{\epsilon_f}{2 - \epsilon_f}$$

$$\epsilon_{eff_2} = \frac{\epsilon_f \epsilon_s}{\epsilon_f + \epsilon_s - \epsilon_f \epsilon_s}$$

ϵ_f = emissivity of aluminum foil and aluminized side of spacer.

For the same assumptions as in the previous example, the aluminizing of one side of the spacer theoretically would reduce the radiation component by about 32%. The effective path length for conduction would also be reduced somewhat, however, due to the metallizing process.

3. Case III--Dimpled Fiber Glass Spacers Aluminized on One Side, Separating Undimpled Fiber Glass Sheets Aluminized on One Side

In this case the aluminum foils are replaced by fiber glass panels which are aluminized on one side as are the spacers. This is similar in concept to the NRC-2 insulation. If the emissivity and absorptivity for each side are assumed equal (i.e., $\epsilon_1 = \alpha_1$ and $\epsilon_2 = \alpha_2$), but

different ($\epsilon_1 \neq \epsilon_2$), then Eq (3) adequately expresses the heat transfer. If not, then the heat transfer would be expressed by the following equation:

$$\left(\frac{\dot{Q}}{A}\right) = \sigma(1-\tau)\left\{\frac{\epsilon_1\left(\frac{\alpha_1\epsilon_2}{\alpha_2\epsilon_1}\right)^{(N_f+N_s)} T_H^4 - \epsilon_1 T_c^4}{\left(1-\alpha_1+\frac{\alpha_1}{\alpha_2}\right)\left[\frac{1-\left(\frac{\alpha_1\epsilon_2}{\alpha_2\epsilon_1}\right)}{1-\left(\frac{\alpha_1\epsilon_2}{\alpha_2\epsilon_1}\right)}\right]}\right\}^{(N_f+N_s)} + \frac{\tau k_s (T_H - T_c)}{(N_f+N_s)\ell_{eff}} \qquad (6)$$

where ϵ_1 = aluminized side.

4. Case IV--Aluminum Foils Separated by Discrete Spacers

This case may be analyzed by the use of Eq (3) if the spacer emissivity, ϵ_s, is replaced with the foil emissivity, ϵ_f. The effective emissivity reduces to $\frac{\epsilon_f}{2-\epsilon_f}$ for this case.

B. WEIGHT OF MARSHIELD

The aluminum foils used in samples of Marshield manufactured to date have been about 3 mils thick. These appear to have sufficient rigidity to serve the intended purpose although greater foil thicknesses could be considered, depending upon the application. The impregnated fiber glass cloth spacers used have ranged in thicknesses from 4 to 10 mils. The smaller gages, however, appear to possess sufficient rigidity to provide adequate foil separation and be self-supporting. The dimpling increases the spacer area by only 5 to 6%. Hence, the density of a typical Marshield employing continuous dimpled spacers is given by:

$$\rho_{MS} = \frac{t_f \rho_f N_f + t_s \rho_s N_s (1.06)}{(N_f+N_s)\delta_d + N_f t_f + N_s t_s} \qquad (7)$$

where

δ_d = dimple height

ρ_f, ρ_s = foil density, spacer material density

N_f = N_s (generally)

For example, for 3-mil aluminum foils, 5-mil spacers, and 1/8-in. dimple height, the density would be 4.14 lb/cu ft.

C. COMPARISON WITH OTHER MULTILAYER INSULATION PERFORMANCE

The general index of performance for cryogenic insulations is the product of apparent thermal conductivity and density, $\bar{k}_a\rho$. The following comparison is made between MARSHIELD with continuous, dimpled spacers and typical Linde and NRC insulations each with a temperature difference of 530 - 36° R.

Type	$\bar{k}_a\rho \times 10^5$	Range (ideal) (530 - 36° R)
Linde SI	7.5 to 10	(150 to 35 foils/inch)
NRC-2	2.5 to 7	(40 to 150 foils/inch)
Marshield (continuous spacers)	80 to 100	(4 foils per inch)

Use of the previously discussed concept of Marshield with discrete low density spacers will theoretically give $\bar{k}_a\rho$ values lower than shown in the table above, but as was pointed out this approach appears less practical than the continuous spacer approach.

The effects of employing an insulation such as Marshield having higher $\bar{k}_a\rho$ values than the current multilayer insulations are discussed in Chapter III. It is sufficient to say that certain types of missions could possibly be performed efficiently with Marshield as the insulation for the cryogenic tankage, particularly if the attainment of the ideal performance assumed for the other multilayer insulations proves impossible or impractical to achieve.

D. EXPERIMENTAL DATA

Samples of Marshield have been manufactured and structurally tested as mentioned in the foregoing report. To date, however, no thermal test data has been obtained. Data on its thermal performance should be obtained before any further development of the concept is made.

APPENDIX C

BOOST DECOMPRESSION TESTS

APPENDIX C

BOOST DECOMPRESSION TESTS

Rapid ambient pressure drop during boost presents the problem of providing sufficient venting of the gases in a nonvacuum-bagged system to prevent excessive pressure differences across the insulation, whether it contains air or a purgant. Such pressures could rupture the insulations or require excessively heavy nets or other structural devices to carry them. The problem is inherent in the insulation systems which are either purged or unevacuated during the ground-hold condition. A typical ambient pressure drop versus time and maximum rate of pressure change are shown in Fig. C-1. Tests for this condition are deemed necessary for development and proof testing of future systems as the result of two pilot tests that were made using NRC-2 blankets conducted under NAS 8-5268.

Two NRC recommended seams as shown in Fig. C-2 were tested at the Martin Company. These seams, the "scroll" and the "cuff" are designed on the basis of thermal performance; presenting cold surface to cold surface at the joint and shadowing the ends of the layers from external radiation.

In the first test, a longitudinal scrolled splice was made in accordance with recommendations by wrapping a blanket of insulation around a 12-in. diameter cylinder and scrolling the longitudinal lap. The lap was intermittently taped at about 4-in. spacings to secure it structurally. The ends of the specimen were cinched tightly. When the specimen was subjected to a simulated boost pressure drop, the outer foil ripped near taping points and the scroll unrolled. The results of this test and the apparatus used are shown in Fig. C-3.

In the second test, a longitudinal seam on a cylindrical blanket was scrolled and taped as above but the bottom circumferential edge was cuffed with only the upper circumference being cinched. When this model was subjected to the same boost pressure transient, neither the cuff nor the scroll failed but the blanket released its gases very slowly.

Two scaling factors in these tests are worthy of note: (1) the wrapped cylinder was only 12-in. in diameter, and (2) the ratio of the volume of trapped air to the length of seam was necessarily lower than can be anticipated for the full scale tank. Both of these items mitigated the bursting effects of rapid pressure drop in the tests. The problem can, therefore, be expected to be much more pronounced in a full-scale system.

Because of this problem, practical designs should incorporate such schemes as nets, "presqueezing" the blankets and other schemes such

as the interleaved joints shown in Chapter IV of the report. Their effectiveness should be fully evaluated in a testing program as recommended in Chapter VI. The size and shape of the specimens should be carefully designed to properly simulate the source of the problem and the structural response if a smaller than full scale tank is tested.

C. ILLUSTRATIONS

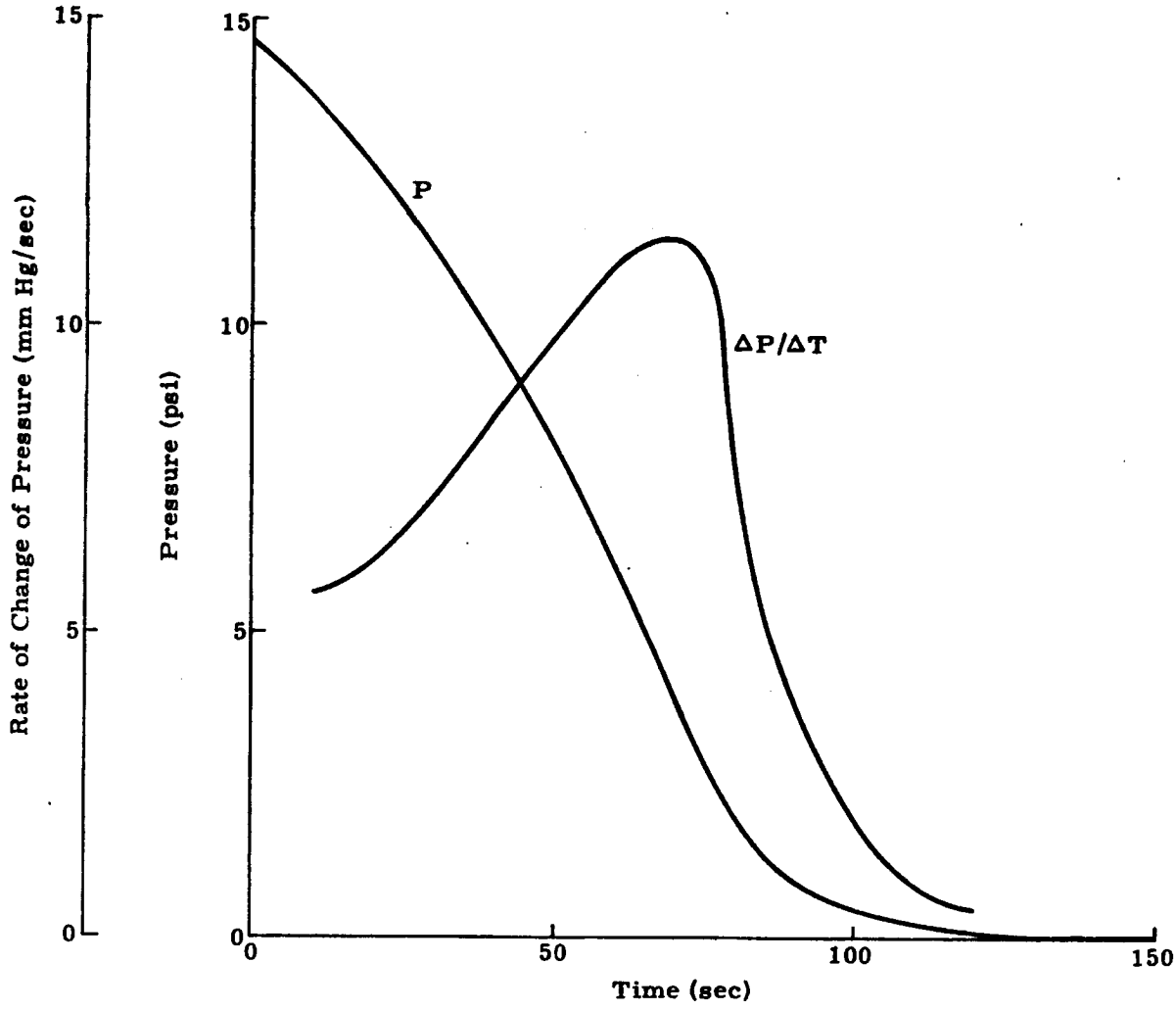

Fig. C-1. Saturn Pressure-Time History

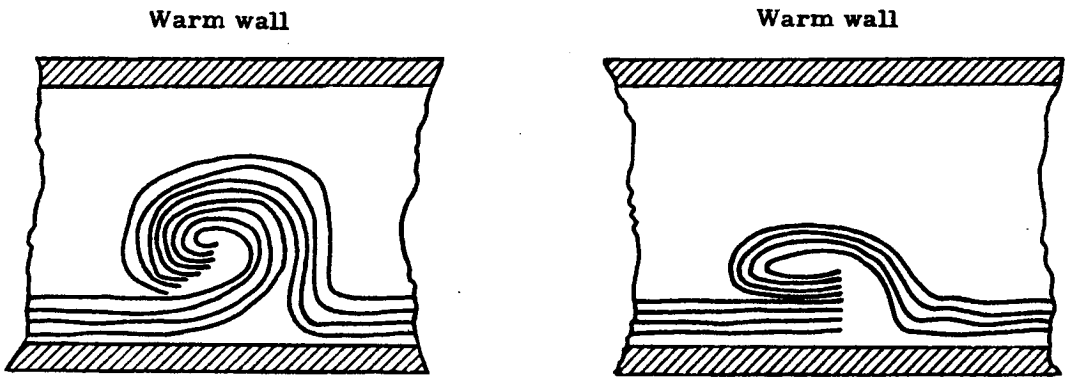

Fig. C-2. NRC Recommended "Scrolls" and "Cuffs"

Fig. C-3. Rapid Pressure Drop Test

APPENDIX D
EVACUATION TESTS--PART A

APPENDIX D

EVACUATION TESTS--PART A

It was realized early in this study that knowledge of pressure-time characteristics during evacuation of multilayer type insulations might be required to form a rational basis for selecting or discarding various approaches and ideas. For example, it was suspected, but not known, that the evacuation of Linde SI might take much longer than NRC-2--either by an active ground pumping system or by letting the space environment do the pumping. Also, it was expected that the Linde SI material would have a serious outgassing* problem--much more so than NRC-2 insulation. Data was required in such areas as the effects of gas temperature and of the nature of gas (e.g., type of purgant), on the insulation evacuation and of insulation bulk density on evacuation time. Therefore, a limited experimental program was planned.

The program was set up to first determine the nature of the problem of evacuating a blanket of multilayer insulation; the length of time required to pump down these insulations under controlled, relatively ideal conditions; the extent of the outgassing problem; the effect of gas temperature in the pump down process; and the characteristic pressure distribution at points remote from the evacuation point.

Only free, unscrolled edges of the blanket were subjected to evacuation because of the limited scope of this study, but it is felt that some useful data was obtained.

A. TEST APPARATUS

The test vessel, see Figs. D-1 through D-3, consisted of two concentric stainless steel cylinders. The inner cylinder, which had 10-in. OD, supported the insulation blanket in the vacuum space and contained the cryogenic liquid. The outer cylinder, which was 12-in. ID, connected directly to an optical baffle cold trap which in turn connected directly to the diffusion pump. The diffusion pump was an NRC 1500, and the roughing pump was a Kinney KS-47. This combination of pumps made it possible to evacuate the system to 10^{-6} and 10^{-7} torr in a very short period of time. The pressure on both ends of the insulation was monitored continuously by two Phillips gages, the readings from which were recorded as a function of time, thus making it possible to plot time versus pressure drop curves for all the different insulation schemes. The associated subsystems made it possible to purge the insulation with either helium or nitrogen prior to evacuation, and to fill the inner vessel with either liquid nitrogen or liquid hydrogen prior to evacuation.

*Gases absorbed on insulation materials and tank walls, either chemisorbed or physisorbed.

B. TEST PROGRAM AND RESULTS

Table 1 lists the tests that were run during the program. Discussion of each test or procedure follows Table 1. The bottom gage readings are not discussed since in all instances, they dropped very rapidly to 10^{-7} torr and below. The bottom gage readings are presented in Table 2. The pressure readings discussed are those of the top gage which was located 4 ft from the exposed edge of the insulation wrap.

Table 2 gives a summary of the results of the evacuation test runs. Selected points on the pressure-time history curves are given (all times given in minutes). All test runs except the empty cavity ones are summarized graphically in Figs. D-4 through D-7. Only the top gage readings are presented.

TABLE 1

Table of Tests Conducted

Test No.	Insulation Configuration	Purgant	Inner Vessel Fluid	Test Purpose and Procedure	Comments
1	None	Air	None	Basic pressure-time history of the empty cavity (annulus) was established for both gage positions. Four separate runs made to determine repeatibility of pressure-time curves.	Repeatibility was demonstrated. (See Table 2.)
2	1-in. NRC-2 type insulation clear, hand crinkled, 1/4-mil tedlar used 125 layers per inch circular wrap-open edge	Air	None	Pressure-time history. At both probe positions. One run made.	See Table 2 and Fig. D-4.
3	Same as above.	Air	Liquid nitrogen	Pressure-time history. Three runs made on three consecutive days. (See notes following table.)	See Fig. D-5. This test setup equivalent to NRC-2 passive system.
4	Same as above.	Dry gaseous nitrogen	Liquid nitrogen	Pressure-time history. (See notes.)	See Fig. D-6.
5	1-in. Linde SI-44 65 layers per inch circular wrap-open edge.	Air	None	Pressure-time history.	See Table 2 and Fig. D-4.
6	1-in. Linde SI-44 65 layers per inch circular wrap-open edge.	Air	Liquid nitrogen	Pressure-time history. One run conducted.	See Table 2 and Fig. D-5.
7	Same as above.	Dry gaseous nitrogen	Liquid nitrogen	Pressure-time history. Two runs conducted. (See notes.)	See Table 2 and Fig. D-6.
8	Same as above.	Helium	Liquid nitrogen	Pressure-time history. One run conducted.	See Table 2 and Fig. D-7.
9	Same as above.	Helium	Liquid nitrogen	Pressure-time history. One run conducted.	See Fig. D-7 and Table 2.
10	Same as Test 6.	Air	Liquid hydrogen	Pressure-time history. Cavity vented for 2 hr after fill.	See Table 2, Notes and Fig. D-5.
11	1-in. Linde SI-91 105 layers per inch.	Air	None	Pressure-time history at higher layer density.	See Table 2 and Fig. D-4.
12	Same as above.	Dry gaseous nitrogen	Liquid nitrogen	Pressure-time history at higher layer density.	See Table 2 and Fig. D-6. Compare with Test No. 7, Run No. 2.

TABLE 2

Evacuation Test Data

Test No.	Run No.	Configuration Description	Gage	Pressure-Time History*							Final+ Pressure (torr)	Comments
				10^{-1} torr	10^{-2} torr	10^{-3} torr	10^{-4} torr	10^{-5} torr	10^{-6} torr	10^{-7} torr		
1	1	Empty	Top	6	7.5		11	13			2×10^{-6}	120 min to final pressure rdg
	2	Cavity	Top	5.0	6.5		9.8	11.5			2×10^{-6}	120 min to final pressure rdg
	3		Top	4.5	7		10.5	12			2×10^{-6}	120 min to final pressure rdg
	4		Top	5.5	7.5		12.3	14.5			2×10^{-6}	120 min to final pressure rdg
	1		Bottom	6	7		8.8	9.5	48	80	$< 10^{-7}$	
2		NRC-2, air										
	1	None	Top	25	41	42					2×10^{-4}	At 120'--slightly negative slope
	1	None	Bottom	20	37	37.5	38.8	41.5	78		10^{-7}	
3		NRC, air										
	1, 2, 3	LN_2	Top		See Fig. D-5							See notes--page D-5
		LN_2	Bottom	11.8	18.5		20	20	27	27	10^{-7}	
4		NRC-2, GN_2										
	1	LN_2	Top		See Fig. D-6						2×10^{-5}	
	1	LN_2	Bottom								10^{-7}	
5		Linde SI-44										
	1	Air, none	Top	6	8	77					2×10^{-4}	283 min to final pressure
	1	Air, none	Bottom	6	8	10	16	370			10^{-5}	Slightly negative slope at final pressure rdg
6		Linde SI-44, air										
	1	LN_2	Top	10	24.5	26	32				1×10^{-4}	Leveled out at final rdg
	1	LN_2	Bottom	10.5	14	15	15	24	180		5×10^{-7}	Negative slope at final pressure rdg
7		Linde SI-44, GN_2										
	1	LN_2	Top	72	115	116	118				2×10^{-5}	GN_2-
	1	LN_2	Bottom	38	67	68	68.5	74	92		5×10^{-7}	Water contaminated (see notes pg D-5)
	2	LN_2			See Fig. D-6						2×10^{-5}	Dry GN_2
8		Linde SI-44, He										
	1	LN_2	Top	1.8	2.3	2.5	4.6				4×10^{-5}	125' level at final rdg
	1	LN_2	Bottom	1.5				3.75	7.5	125	1×10^{-7}	Level at final rdg
9	1	Linde SI-44, He										
	1	LH_2	Top		See Fig. D-7						5×10^{-6}	
		LH_2	Bottom								10^{-7}	
10		Linde SI-44										
	1	Air, LN_2	Top	20	28.5	29					3×10^{-4}	Leveled out at final rdg
	1	Air, LN_2	Bottom	17			20.5	35	208		10-6	Leveled out at final rdg
11	1	Linde SI-91										
		Air, none	Top	28	148						2.8×10^{-3}	Negative slope at 240 min
12	1	Linde SI-91										
		Dry GN_2	Top	7	11.5	13.5	28				1×10^{-4}	Leveled out at final rdg
		LN_2	Bottom							48	10^{-7}	Negative slope at final rdg

*All times are in minutes
+ Last reading taken

NOTES:

Test No. 2. The air in the insulation was essentially at room temperature. When comparing these results with later tests where a cryogenic fluid was in the inner vessel (and thus lower blanket temperatures existed), the impedance appeared to be lower at the lower temperatures.

Test No. 3. The inner vessel was filled with liquid nitrogen just prior to turning on the vacuum pump. During the first day the pressure at the remote station (4-ft from the chamber) dropped to 3×10^{-4} torr in approximately 1 hr and could be reduced no further. The diffusion pump was turned off overnight with the roughing pump left on. The next morning the pressure had risen to the roughing pump limit (about 50 to 70 microns). Upon turning on the diffusion pump, the pressure dropped more rapidly to about 4×10^{-5} torr in 20 min and could not be reduced further during the remainder of the day (6 hr). The same procedure was followed the second night. On the third day, when the diffusion pump was turned on, the pressure again quickly dropped to an even lower level of 3×10^{-6} torr in 25 min and could not be further reduced by another day of pumping (about 6 hr). The bottom gage for all runs dropped to below 10^{-7} torr in approximately 25 min. These results indicate that the introduction of the liquid nitrogen caused condensation and freezing of some of the water vapor initially in the air. This continued to outgas until the final pressure attained was the vapor pressure of the ice at some low temperature.

Test No. 4. The dry gaseous nitrogen was purged into the annulus from the bottom to top prior to filling the inner vessel with liquid nitrogen. The system pumped down initially to a much lower pressure with dry nitrogen as the purge gas than it did with moist air as the purgant (about 2×10^{-5} torr in 1/2 hr).

Test No. 5. This test can be directly compared with Test No. 2. Note the increased evacuation times for the Linde SI insulation under these conditions.

Test No. 6. This test is comparable to Test No. 3 except that only one run was conducted. The pressure dropped to slightly below 1×10^{-4} torr in just over 1/2 hr and could not be reduced further by 5 to 6 hr of pumping. Again failure to reduce the pressure level over this time period indicates that outgassing of the water vapor was taking place.

Test No. 7. In the first run, the nitrogen purge gas was contaminated with water vapor resulting in a limit pressure of approximately 3 x

x 10^{-5} torr being reached after 2 hr. In the second run, a limit pressure of 2 x 10^{-5} torr was reached after 30 min using dry gaseous nitrogen. This was more consistent with the comparable Test No. 4 using NRC-2 insulation.

Test No. 8. This is the first test wherein helium was used as a purgant. The results indicate that this purgant can be removed easier than air under similar conditions, however, the level to which the system must be evacuated is considerably lower for equal performance.

Test No. 9. The results of this test indicate that the use of helium purge with insulations at near liquid hydrogen temperatures is much more advantageous than its use at a higher temperature (e.g., see Test No. 8 where liquid nitrogen temperatures prevailed). A pressure level of below 10^{-5} torr was reached in approximately 45 min and an ultimate pressure level of 5 x 10^{-6} torr in about 2 hr. Note that during the diffusion pump warm up time, the pressure level was being reduced by cryopumping within the insulation.

Test No. 10. This test was basically a rerun of Test No. 6. The exception was that after the liquid nitrogen was transferred to the inner tank, the cavity was vented to the atmosphere for 2 hr. The objective was to determine whether the condensation and freezing of the water vapor in the air originally trapped in the blanket tended to draw more air into the insulation due to the lowering of the pressure by the condensation process. As had been concluded from some previous exploratory tests, the test results confirm that this process is basically limited to the original volume of air in the insulation blanket.

Test No. 11. This test was conducted to determine the difference in pump down characteristics between the Linde SI-44 at 65 layers per inch and Linde SI-91 at 105 layers per inch--i.e., compare this test with Test No. 5. The results indicate the higher density Linde SI types are as anticipated more difficult to evacuate than the lower density ones at identical conditions (see Fig. B-4 for this comparison).

Test No. 12. This test was conducted to determine if the evacuation time differential between higher density and lower density multilayer insulations experienced in Test No. 11 would exist for lower blanket temperatures and purgants other than air. This test of SI-91 is comparable to that for SI-44 in Test No. 7, Run No. 2. Figure D-6 presents the comparison of the pressure-time histories of these two Linde insulations as well as the NRC-2 test at identical conditions. It can be noted that the differential evacuation time at the colder, nitrogen purged conditions of this test is much lower than for the previous tests of Linde SI-44 and SI-91 where air at room temperature was the insulation purgant.

C. EVALUATION OF RESULTS

The tests indicate that with air in the insulations at room temperature there is a significant difference in pump down time between the NRC-2 insulation and the Linde SI types. However, when the insulation temperature is reduced by the introduction of a cryogenic fluid into the tank, there appears to be very little difference in the pump down times to a given pressure level. This is apparently true whether the purgant is air or gaseous nitrogen.

Unfortunately, the test offers no direct comparison of the two insulations at liquid hydrogen temperatures, but it is unlikely that the test results would be significantly different for the NRC-2 insulation from results given for the Linde SI in Test No. 9.

One fact evident from the test results is that helium should not be used as a purgant except when the insulation is adjacent to a liquid hydrogen tank. Tests Nos. 7 and 8 indicate that the helium is not easier to remove from the insulation than gaseous nitrogen when the fluid in the tank is liquid nitrogen. Since helium exhibits higher heat transfer characteristics in the molecular regime than nitrogen gas, the purge gas choice would have to be nitrogen for these conditions.

While realistic edge and seam treatments were not simulated in these tests, the 4 ft long annular cavity does represent a high impedance path. The results are encouraging, however, for even in those tests where considerable outgassing was taking place (as in tests Nos. 3 and 6), acceptable pressure levels were reached. Since outgassing is time dependent, those pressure levels would ultimately have been reduced. The use of a desiccant or purging with dry air could undoubtedly improve these situations.

Although not attempted in this program, the employment of adsorbents (as are used in some vacuum jacketed lines) could also aid the evacuation process.

For a given type of insulation, the greater the number of layers per inch employed (i.e., density), the longer the evacuation time to a given pressure level, and the higher the final pressure reached (at least within the limits of the test time).

In summary the test results indicate that:

(1) NRC-2 insulations are easier to evacuate than the Linde SI types at room temperature.

(2) Linde SI-91 is more difficult to evacuate than Linde SI-44 insulation.

(3) Evacuation of multilayer insulations is much easier when temperature gradients exist across them, that is when the average temperature level in the insulation is well below room temperature.

(4) The use of purge gases to replace air in the insulation makes evacuation of these insulations much easier.

(5) When using a purge gas, it is better to select a purge gas which has a liquefication temperature close to the cold boundary temperature.

D. ILLUSTRATIONS

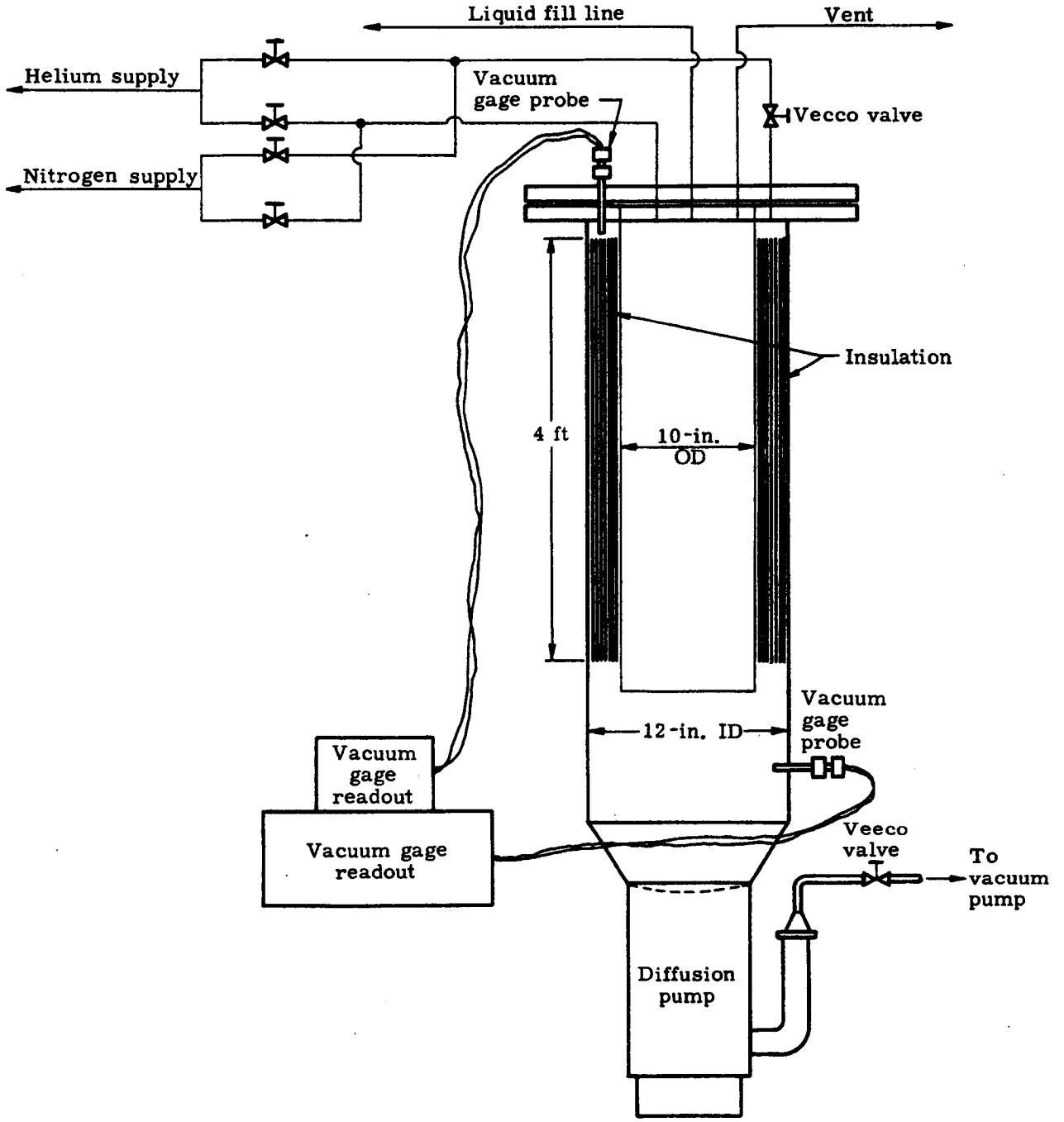

Fig. D-1. Insulation Pump Down

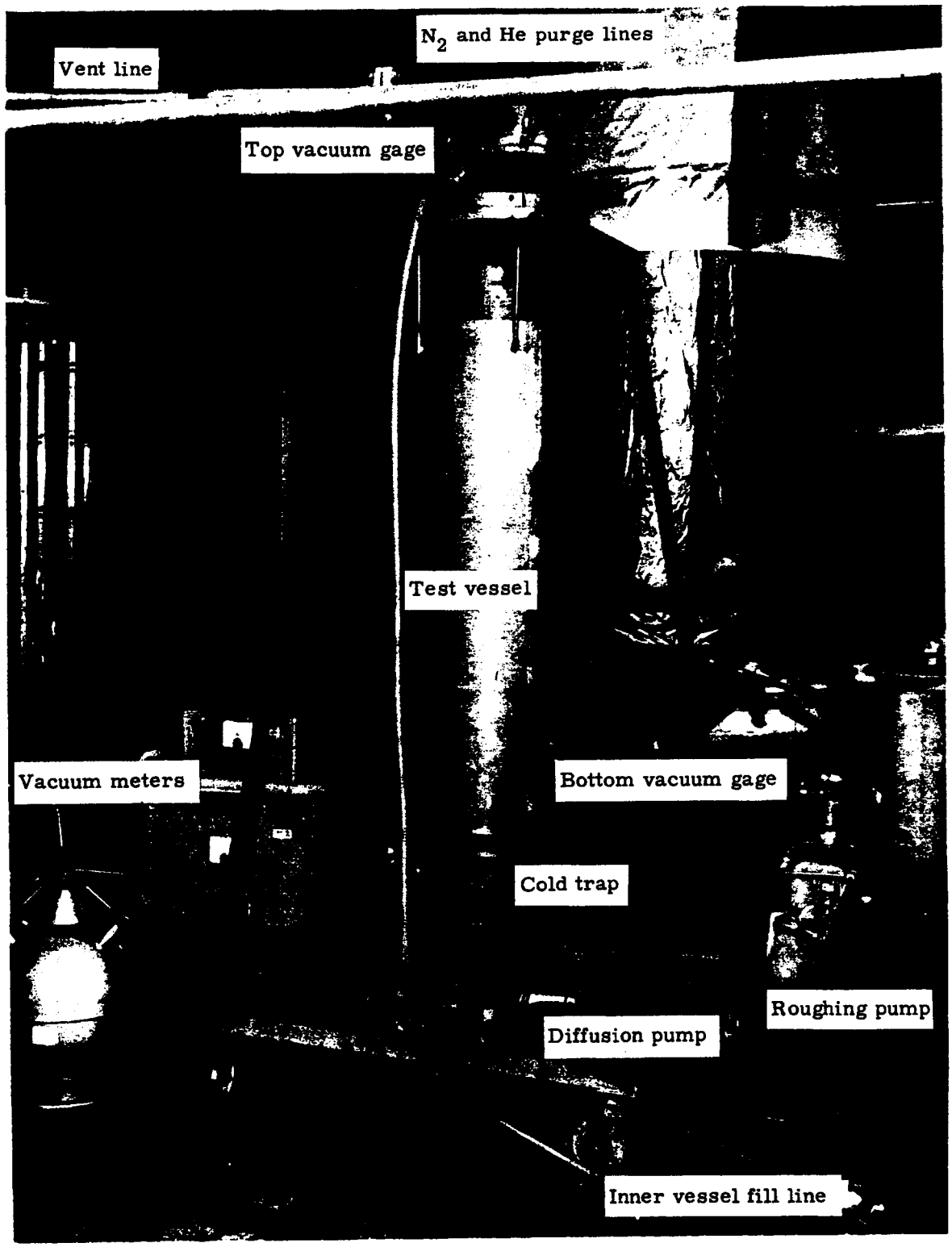

Fig. D-2. Overall Test Setup

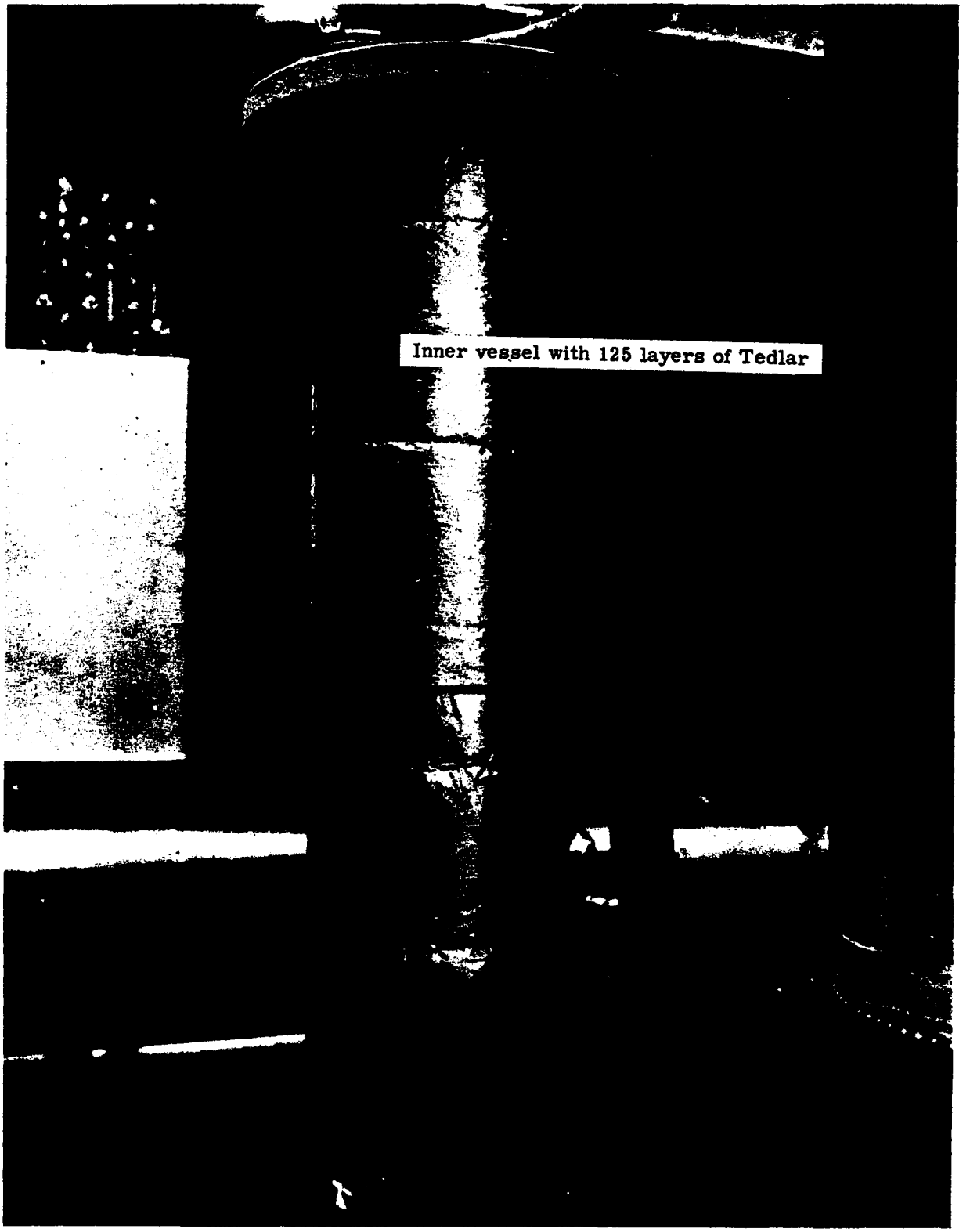

Fig. D-3. Inner Vessel Insulated with NRC-2

NOTE:

1. Purgant--air
2. Liquid--none
3. Insulation--as noted

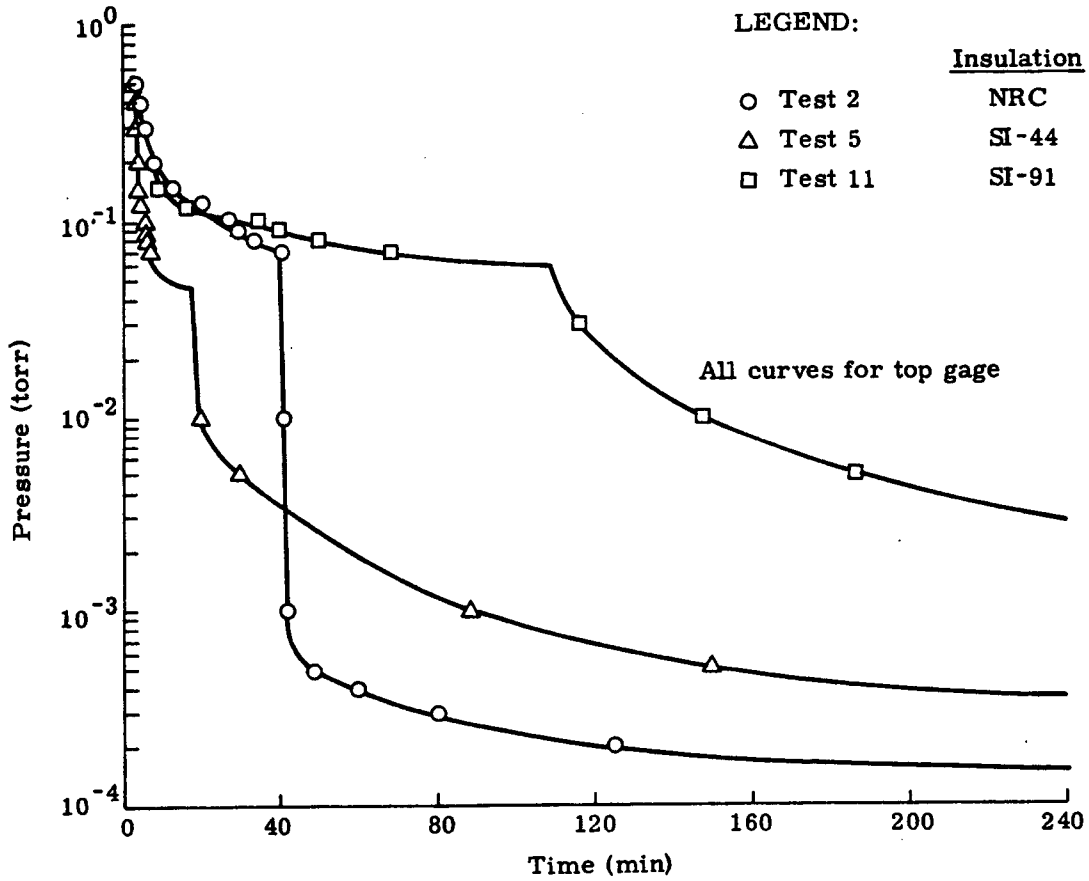

Fig. D-4. Time Versus Pressure Profile (Tests 2, 5, 11)

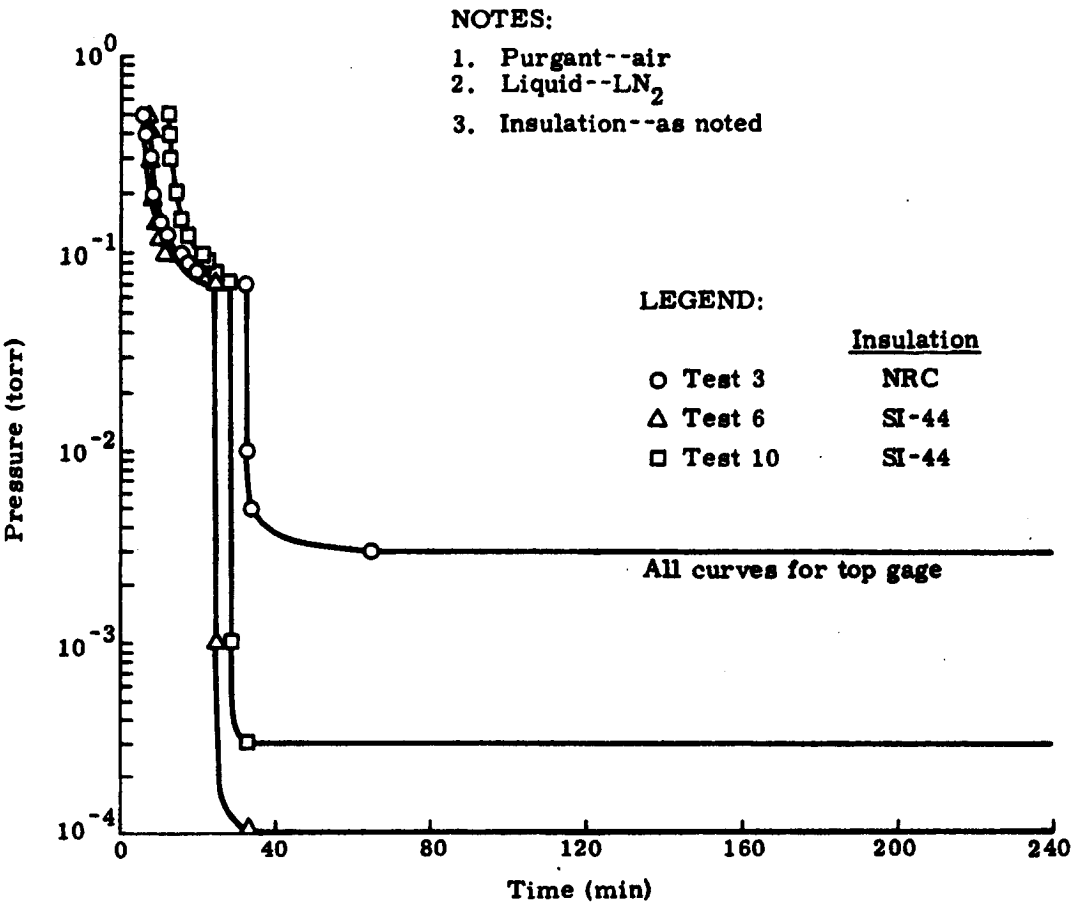

Fig. D-5. Time Versus Pressure Profile (Tests 3, 6 and 10)

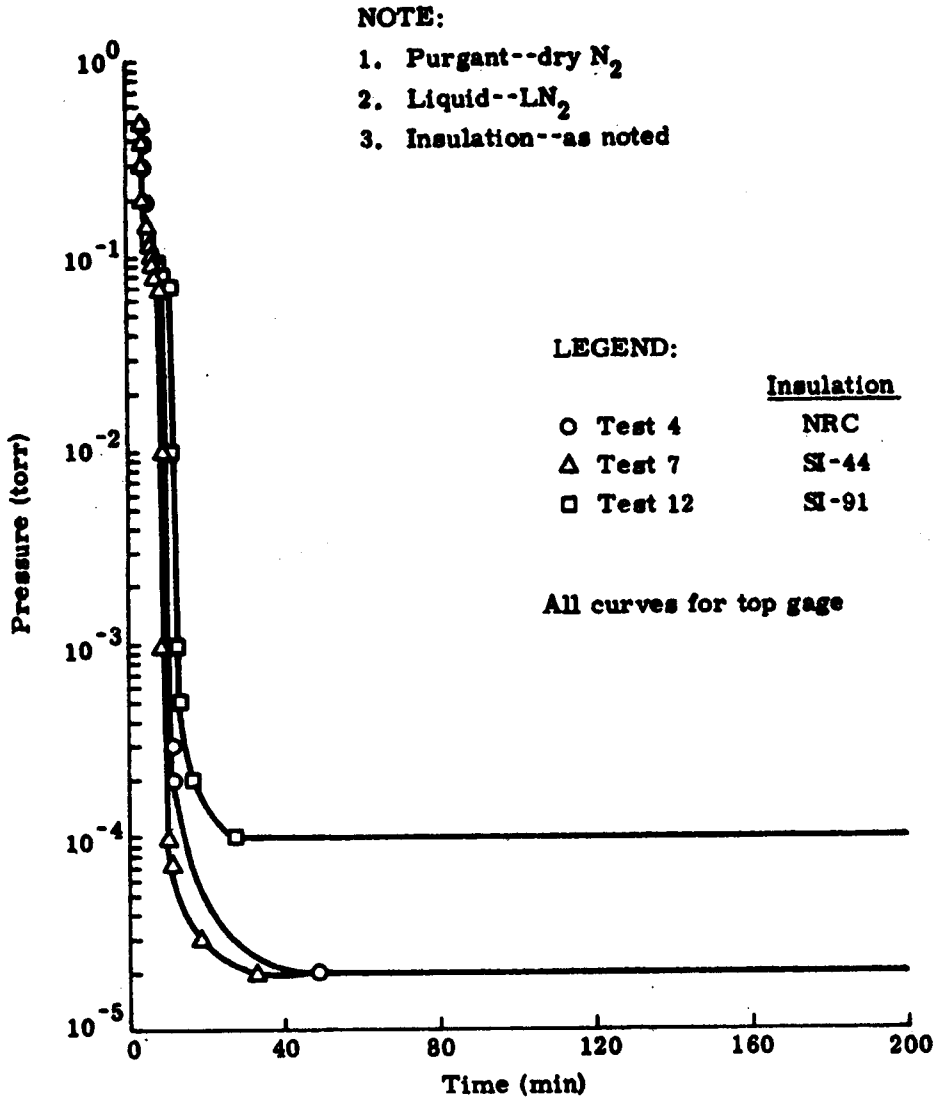

Fig. D-6. Time Versus Pressure Profile (Tests 4, 7, 12)

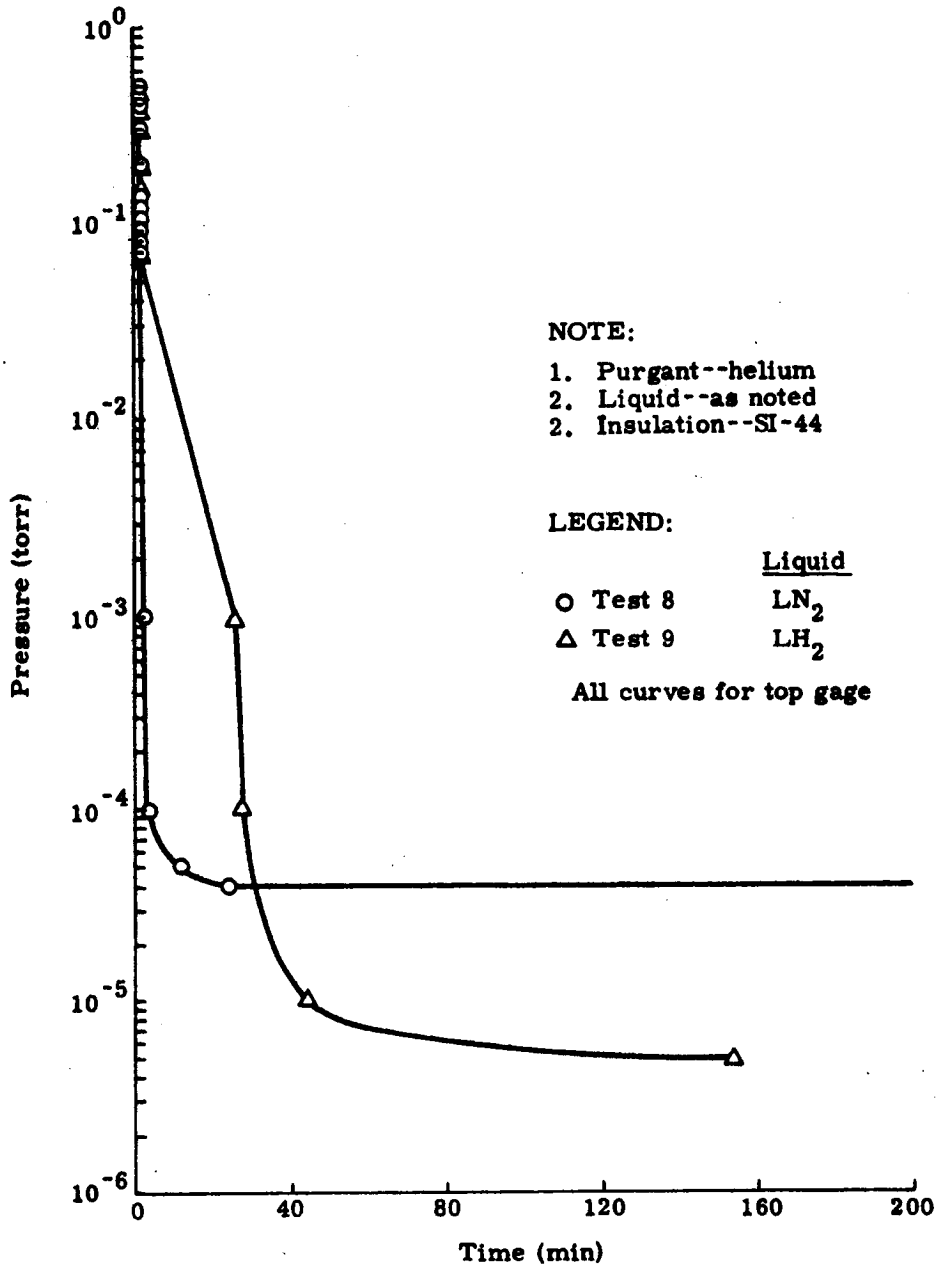

Fig. D-7. Time Versus Pressure Profile (Tests 8 and 9)

APPENDIX E

OPTIMUM INSULATION BLANKET FOR ORBITAL STORAGE OF CRYOGENS

APPENDIX E

OPTIMUM INSULATION BLANKET FOR ORBITAL STORAGE OF CRYOGENS

The efficiency with which an orbiting stage containing a cryogen can perform its mission may be significantly affected by the proportions of insulation weight and boiloff of the cryogen. Therefore, mission optimization analyses are required in forming a basis for selection of appropriate types and amounts of insulation for thermal protection of cryogenic fluids in the environment of orbital storage. Such analysis should include consideration of the various types of missions that may be performed subsequent to the storage phase; e.g., acceleration of a spacecraft that is integrated with the tankage, or indepdendent use of the cryogen by a separate spacecraft. The analysis should make clear the effects of such parameters as insulation efficiency, tankage size and thermal exposure on the potential efficiency with which each type of mission can be performed.

This type of information can be used to determine appropriate amounts of insulation that should be applied in the various cases. In addition, it should also be used to influence such decisions as, for example, whether for a given mission, an insulation of higher reliability and fabricability should be selected over one of higher thermal efficiency, or whether development of highly efficient insulations and/or techniques for their joining and attachment is warranted in certain applications.

The following analyses were performed to provide the required information:

(1) Case 1--insulation required on tankage integrated with a spacecraft to maximize the velocity increment when the stage is fired subsequent to storage phase for specified inert-to-initial weight ratios of the stage.

(2) Case 2--insulation required on tankage integrated with a spacecraft to mazimize ratio of inert to initial weight of stage when it is fired subsequent to the storage phase and the velocity increment is specified.

(3) Case 3--insulation required on tankage that is separate from the spacecraft utilizing the cryogen to maximize the ratio of final cryogen weight to initial stage weight.

In each case the insulation weight is treated separately from the other inert weights of the system. It is assumed throughout that the tankage is exposed to uniform and constant-rate heat transfer over its surface during

the entire storage phase, that all heat transfer to the cryogen during storage results in boiloff, that launch and boost heating and associated boiloff can be specified independently, and that effects of boiloff subsequent to storage are negligible.

The performance maximization analyses for these three cases are accurate for situations in which the tank weights or other inert weights are not strongly dependent on changes in propellant weights (e. g., large, low pressure tankage); the important differentials up to that level of accuracy have been included.

The methods of analysis are described in the following sections where resulting equations and their graphs are presented. The results show the optimum amounts of insulation in each case as they vary with insulation and cryogenic physical properties, the exposure, the tanks size and properties, stage properties and the mission parameters. Effects of important parameters on potential efficiency with which the missions can be performed are also shown.

The results show clearly that for large tankage sizes, large inert mass fractions and short durations of storage of LH_2 in near earth orbits the performance of the insulation system can be an order of magnitude worse than performance forecasts for superinsulations $\left(K\rho = 10^4 \ \frac{\text{Btu-ft}^2}{\text{lb-}^\circ\text{F-hr}}\right)$ without incurring severe penalties in mission performance. For small tankage sizes and inert mass fractions but long storage durations the converse is true.

A. NOTATION

A = surface area of tank

C_1 = fractional part of fuel volume W_{f_0}/ρ_f devoted to ullage space and cryogen boiled off during launch and boost

C_2 = dimensionless fraction by which the surface area of an equal volume spherical tank must be increased to give surface area of a nonspherical tank

C_3 = see Eq (4)

C_4 = fractional part of cryogen that is trapped or otherwise not usable

F = ratio of weight of cryogen available after storage to weight of stage at storage initiation

g = acceleration due to gravity

H_V = heat of vaporization for cryogenic

I_{sp} = specific impulse of propellant

k_i = conductivity of insulation

$P_{\Delta v}$ = velocity increment penalty fraction, see Eq (13)

P_{λ_I} = payload penalty fraction, see Eq (19)

P_F = available cryogen penalty fraction, see Eq (25)

r = tank radius

R = see Eqs (6) and (7)

t_i = insulation blanket thickness

ΔT = temperature difference across insulation

ΔV = increment of velocity for the stage

W_{BO} = weight of cryogen boiled off during storage

W_i = weight of insulation

W_{f_0} = weight of cryogen in tank at storage initiation

W_0 = weight of stage at initiation of storage

W_I = inert weight of stage, less insulation weight

λ_{BO} = ratio of cryogen boiloff to stage weight with no boiloff

λ_i = insulation--initial mass fraction, W_i/W_0

λ_{f_0} = ratio of weight of cryogen to weight of stage at initiation of storage period

λ_I = inert--initial mass fraction W_I/W_0

ρ_f = density of cryogen

ρ_i = density of insulation

θ = exposure or storage time

B. ANALYSIS

The weight of cryogen boiled off during orbital storage due to steady, uniform heat transfer through a constant thickness insulation blanket over the entire surface area of the tankage is given by

$$W_{BO} = \frac{k_i \rho_i A^2 \Delta T \theta}{W_i H_V} \tag{1}$$

where the symbols are those defined in Section A.

The tankage area is related to weight of cryogen it contains by the expression

$$A = \frac{3W_{f_0}}{\rho_f r} (1 + C_1)(1 + C_2) \tag{2}$$

Combining Eqs (1) and (2) to obtain boiloff mass fractions in terms of initial cryogenic mass fraction λ_{f_0} and insulation mass fraction λ_i gives

$$\lambda_{BO} = C_3 \frac{\lambda_{f_0}^2}{\lambda_i} \tag{3}$$

where

$$C_3 = \frac{k_i \rho_i \Delta T \theta}{H_V \rho_f^2 r^2} \left[3 (1 + C_1)(1 + C_2)\right]^2 \tag{4}$$

and the respective λ's indicate W_{BO}, W_{f_0} and W_i have been divided by the stage weight W_0 at storage initiation. Equation (3) will be used in the three cases to be optimized where it is assumed that all heat transfer is through the insulation blanket.

The velocity increment for Cases 1 and 2 is

$$\Delta V = g I_{sp} \ln \left[\frac{W_0 - W_{BO}}{W_0 - (1 - C_4) W_{f_0}} \right] \tag{5}$$

or

$$R = \frac{1 - (1 - C_4)\,\lambda_{f_0}}{1 - \lambda_{BO}} \tag{6}$$

where

$$R = \exp\left(-\Delta V / g\, I_{sp}\right) \tag{7}$$

R is usually defined as the stage's inert-to-initial mass fraction but here boiloff is included. The total weight of the stage at initiation of storage, W_0, is

$$W_0 = W_{f_0} + W_I + W_i$$

or

$$1 = \lambda_{f_0} + \lambda_I + \lambda_i \tag{8}$$

Combining Eqs (3), (6) and (8) then gives the following relationship for R, λ_I and λ_i

$$R = \frac{1 - (1 - C_4)(1 - \lambda_I - \lambda_i)}{1 - \dfrac{C_3}{\lambda_i}(1 - \lambda_I - \lambda_i)^2} \tag{9}$$

1. Case 1--Insulation Required for Maximizing Velocity Increment

This case applies to those instances for which inert weights of the stage including such items as payload and structural weight are specified independent of the insulation system. The proper insulation blanket weight to maximize the velocity increment is required. The tank radius, r, is treated as a parameter, but is not varied in the differentiation. The relationship between insulation weight and inert weight for maximizing the velocity increment is then obtained by setting equal to zero the partial derivative of R with respect to λ_i in Eq (9). The resulting relationship is

$$\lambda_{i_{opt}} = \frac{C_3 (1 - \lambda_I)^2 (1 - C_4)}{1 - C_4 + C_3 (2 - C_4 - \lambda_I)} \left(1 + \frac{1}{1 - \lambda_I} \sqrt{\frac{1}{C_3}\left(\lambda_I + \frac{C_4}{1 - C_4}\right) + \frac{1}{(1 - C_4)^2}}\right) \tag{10a}$$

Since C_3 is negligibly small relative to unity and λ_I for ranges of C_3 parameter within the scope of this study, Eq (10a) is approximated by

$$\lambda_{i_{opt}} = C_3 (1 - \lambda_I)^2 + (1 - \lambda_I) \sqrt{C_3 \left(\frac{C_4 + (1 - C_4)\,\lambda_I}{1 - C_4}\right)} \tag{10b}$$

If the quantity $(1 - \lambda_I)\sqrt{C_3}$ is negligible relative to $\sqrt{\lambda_I}$, Eq (10b) simplifies further to

$$\lambda_{i_{opt}} \simeq (1 - \lambda_I)\sqrt{C_3\left(\frac{C_4 + (1 - C_4)\lambda_I}{1 - C_4}\right)} \tag{11}$$

The penalty in velocity increment is

$$P_{\Delta v} = 1 + \frac{\ln\left[1 - \frac{C_3}{\lambda_i}(1 - \lambda_I - \lambda_i)^2\right] - \ln\left[C_4 + (1 - C_4)(\lambda_I + \lambda_i)\right]}{\ln\left[C_4 + (1 - C_4)\lambda_I\right]} \tag{12}$$

where, by definition,

$$P_{\Delta v} = 1 - \frac{\Delta V}{\Delta V_{ideal}} \tag{13}$$

The quantity ΔV_{ideal} is the velocity increment for the specified inert mass fraction, λ_I, if no insulation weight is present and no boiloff occurs.

Figure E-1 shows graphically values of the insulation mass faction, λ_i, as calculated from Eq (10b) with C_3 and λ_I as parameters. A typical value of C_4 is used in Fig. E-1.

Figure E-2 shows the penalty $P_{\Delta v}$ as calculated from Eq (12) with C_3 and λ_I as parameters. The same value of C_4 as is used in Fig. E-1 is used in Fig. E-2.

The optimum thickness of insulation blanket that would be used to achieve the indicated minimum penalties is obtained as follows by noting $t_i = \lambda_i W_o / A\rho_i$;

$$t_i\Big|_{opt} = \frac{\lambda_i r \rho_f}{3\rho_i (1 - \lambda_I - \lambda_i)(1 + C_1)(1 + C_2)} \tag{14a}$$

or

$$t_i = \sqrt{\frac{k_i \Delta T \theta}{\rho_i H_V} \left[\frac{C_4 + (1 - C_4) \lambda_I}{1 - C_4} \right]} \qquad (14b)$$

where λ_i in the denominator of Eq (14a) has been assumed negligible relative to $1 - \lambda_I$.

2. Case 2--Insulation Required for Maximizing Payload

This case applies to those instances where the velocity increment for the stage is specified independent of the insulation system. The proper insulation weight to maximize payload is required. As in Case 1, tank radius r is treated as a parameter (included in C_3). The required relationship between the optimum insulation and the specified velocity increment is determined by setting equal to zero the partial derivative of λ_I with respect to λ_i. It is assumed that maximizing the inert-initial mass fraction λ_I maximizes payload capability. The relationship between λ_I and λ_i is obtained from Eq (9) as

$$\lambda_I = 1 - \frac{(1 - C_4) \lambda_i}{2 C_3 R} \left[1 + \frac{2C_3 R}{1 - C_4} - \sqrt{1 - \frac{4 (1 - R) C_3 R}{(1 - C_4)^2 \lambda_i}} \right] \qquad (15)$$

Performing the maximization of λ_I gives

$$\lambda_{i_{opt}} = \frac{2C_3 R}{1 - C_4} \left(\frac{1 - R}{1 - C_4} \right) \left[1 + \sqrt{1 + \frac{1 - C_4}{4C_3 R}} \right] \qquad (16)$$

when $\frac{C_3 R}{1 - C_4}$ is negligibly small relative to unity. When $\sqrt{\frac{4C_3 R}{1 - C_4}}$ is also negligibly small relative to unity, Eq (16) reduces to

$$\lambda_{i_{opt}} = \frac{1 - R}{1 - C_4} \sqrt{\frac{C_3 R}{1 - C_4}} \qquad (17)$$

It is noted that when R is approximated by neglecting λ_i in Eq (9), Eq (17) then is identical to Eq (11).

Substituting from Eq (16) for λ_i in Eq (15) and neglecting $\frac{2C_3 R}{1 - R}$ relative to unity gives the following equation for the maximum inert weight

$$\lambda_{I_{max}} = \frac{R - C_4}{1 - C_4} - \frac{1 - R}{1 - C_4} \sqrt{\frac{4C_3 R}{1 - C_4}} \qquad (18)$$

The penalty in payload is defined as

$$P_{\lambda_I} = 1 - \frac{\lambda_{I_{max}}}{\lambda_{I_{ideal}}} \tag{19}$$

where $\lambda_{I_{ideal}}$ is the inert mass fraction if no insulation is necessary and no boiloff occurs;

$$\lambda_{I_{ideal}} = \frac{R - C_4}{1 - C_4} \tag{20}$$

The minimum penalty in payload is then

$$P_{\lambda_I} = \frac{1 - R}{R - C_4} \sqrt{\frac{4C_3 R}{1 - C_4}} \tag{21}$$

Figure E-3 shows the insulation mass fraction as calculated from Eq (16) with C_3 and R as parameters. (The value of C_4 assumed is shown in Fig. E-3.) Figure E-4 gives the penalty P_{λ_I} resulting from Eq (21) with C_3 and R as parameters. The optimum insulation thickness that would be used in this case is calculated by Eq (14) using values of λ_i from Eqs (16), (17) or Fig. E-3.

3. Case 3--Insulation Required to Maximize Cryogenic Mass Fraction After Storage

When the post-storage utilization of the cryogen is independent of the inert weight of the storage stage and the stage is used only once, the performance optimization reduces to that of maximizing the ratio of final weight of cryogen to initial weight of stage. That mass fraction, F, is

$$F = (1 - C_4)\,\lambda_{f_0} - \lambda_{BO} \tag{22a}$$

or

$$F = (1 - C_4)(1 - \lambda_I - \lambda_i) - \frac{C_3 (1 - \lambda_I - \lambda_i)^2}{\lambda_i} \tag{22b}$$

It is assumed that the stage's inert mass fraction λ_I can be determined independent of the insulation requirements; therefore λ_I is treated as a constant in the following equation. Setting the derivative of F with respect to λ_i equal to zero gives

$$\lambda_{i_{opt}} = (1 - \lambda_I) \sqrt{\frac{C_3}{1 - C_4}} \tag{23}$$

where C_3 is assumed negligible relative to unity. Equation (14) would also be used to compute insulation thickness in this case. It is noted that C_3 can be increased by n, the number of times the tank would be reused for storage of the same period, if launch and transfer losses are negligible.

The maximum value of the performance fraction F is then

$$F_{max} = (1 - \lambda_I)(1 - C_4)\left(1 - 2\sqrt{\frac{C_3}{1 - C_4}}\right) \tag{24}$$

where Eq (23) has been used for $\lambda_{i_{opt}}$ and, consistent with this use, C_3 was assumed negligible relative to unity; and the penalty is defined by

$$P_F = 1 - \frac{F_{max}}{F_{ideal}} \tag{25}$$

is

$$P_F = 2\sqrt{\frac{C_3}{1 - C_4}} \tag{26}$$

The value of F_{ideal} is taken from Eq (22) when λ_i and boiloff are zero.

ILLUSTRATIONS

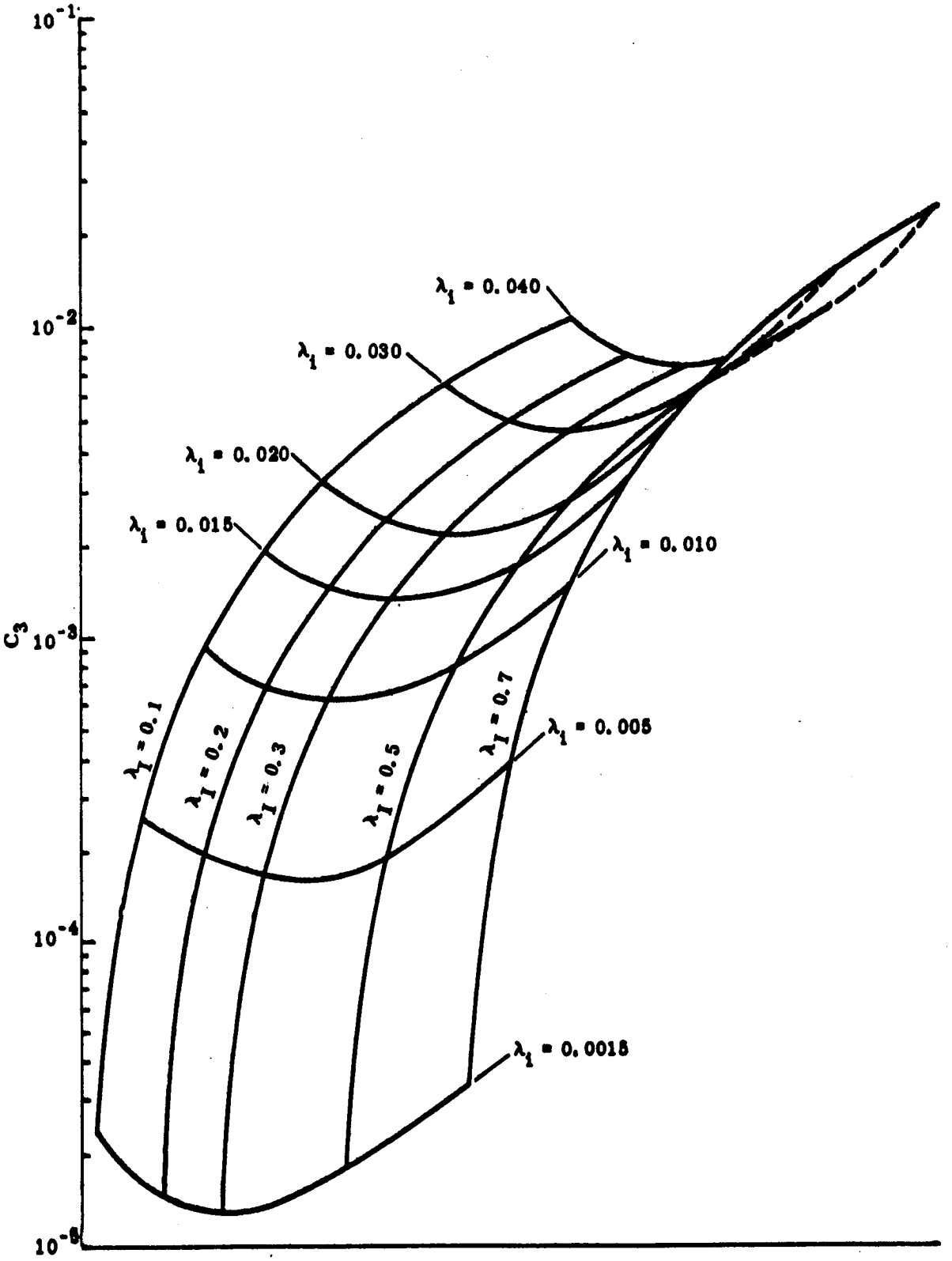

Fig. E-1. Optimum Insulation Mass Fraction, λ_1, for Specified Inert Mass Fraction, λ_I, to Maximize ΔV; $C_4 = 0.01$

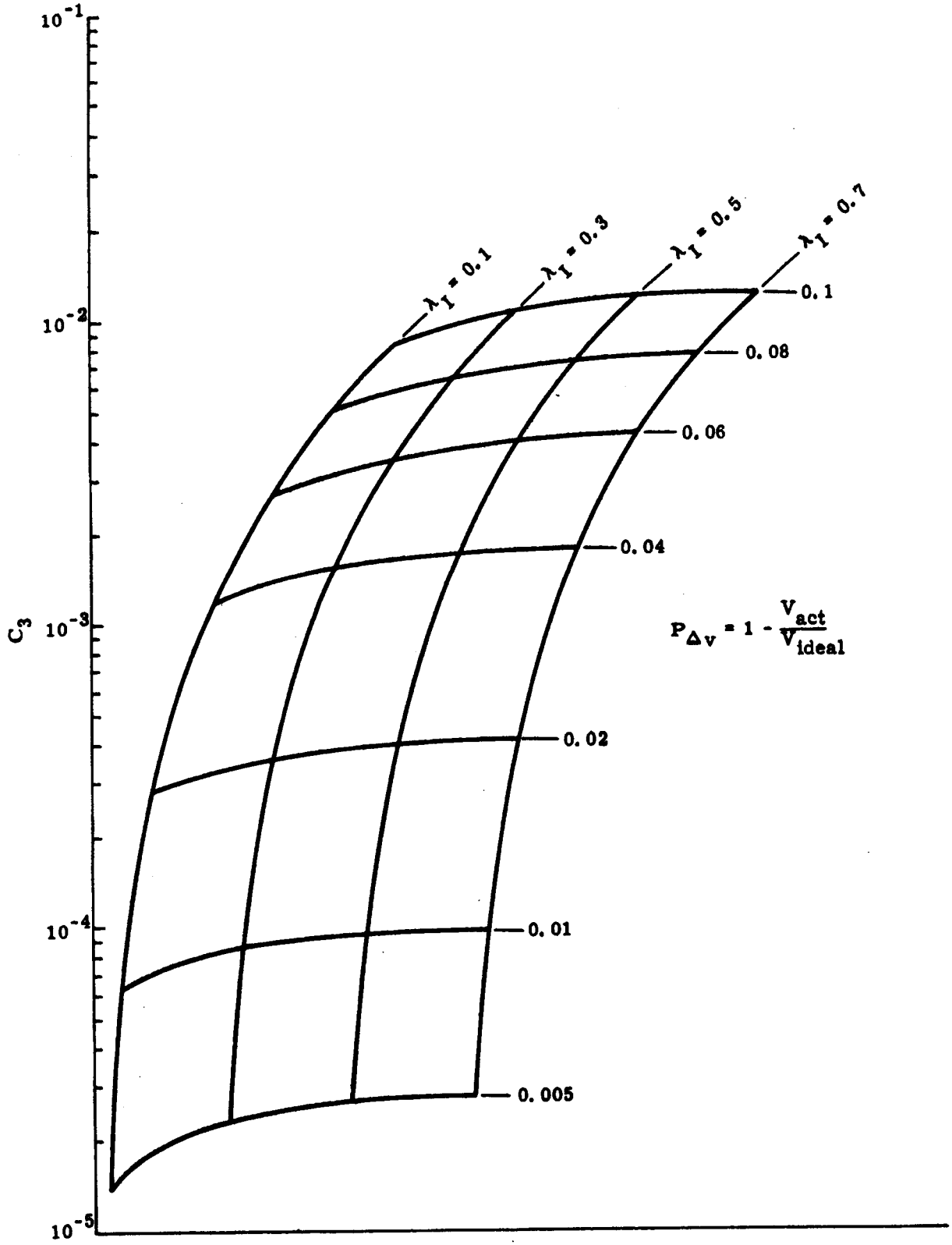

Fig. E-2. Minimum Δv Penalties When λ_I is Specified; $C_4 = 0.01$

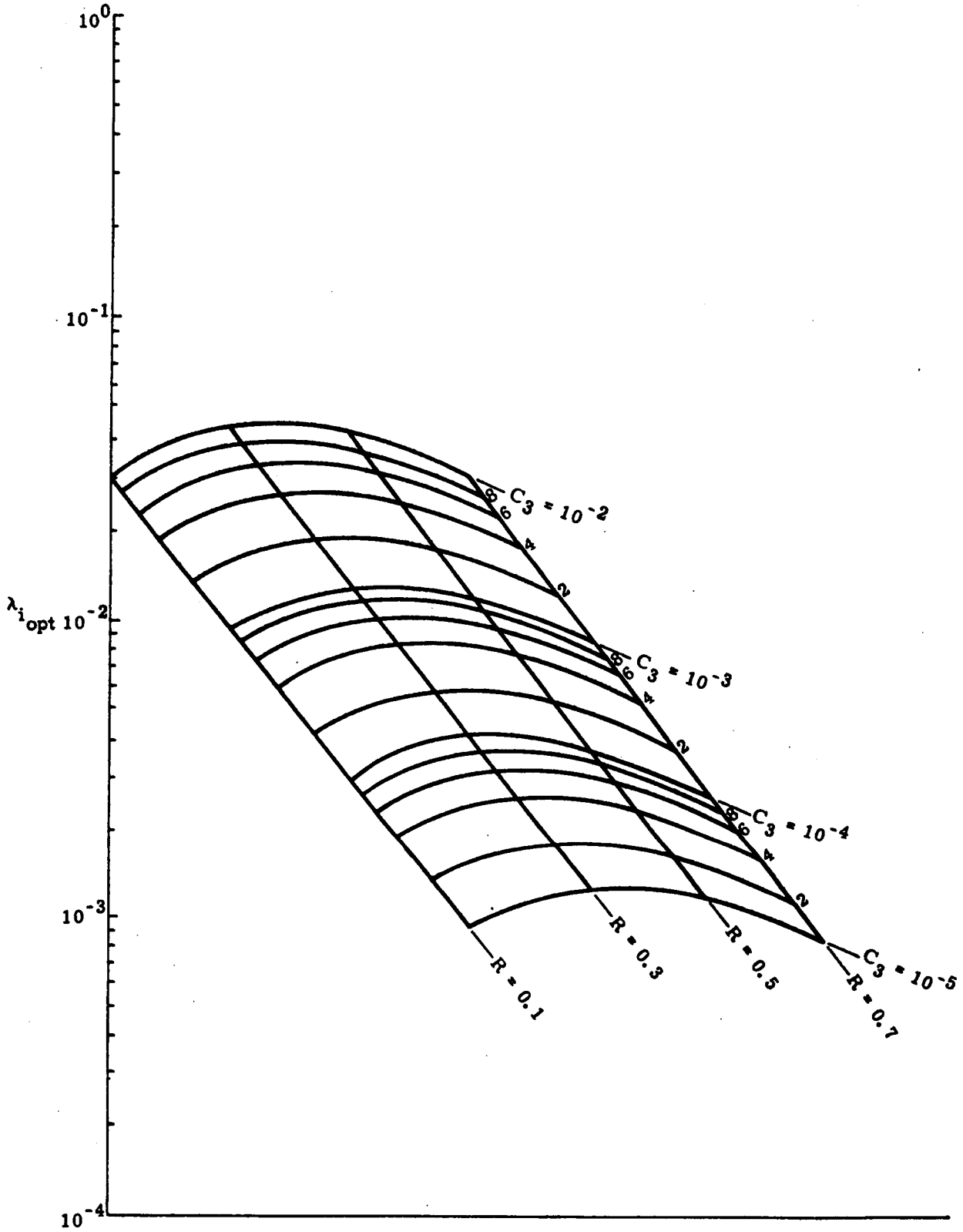

Fig. E-3. Optimum Insulation Mass Fraction, λ_i, as Function of C_3 for Specified ΔV; $R = \exp(-\Delta V/gI_{sp})$; $C_4 = 0.01$

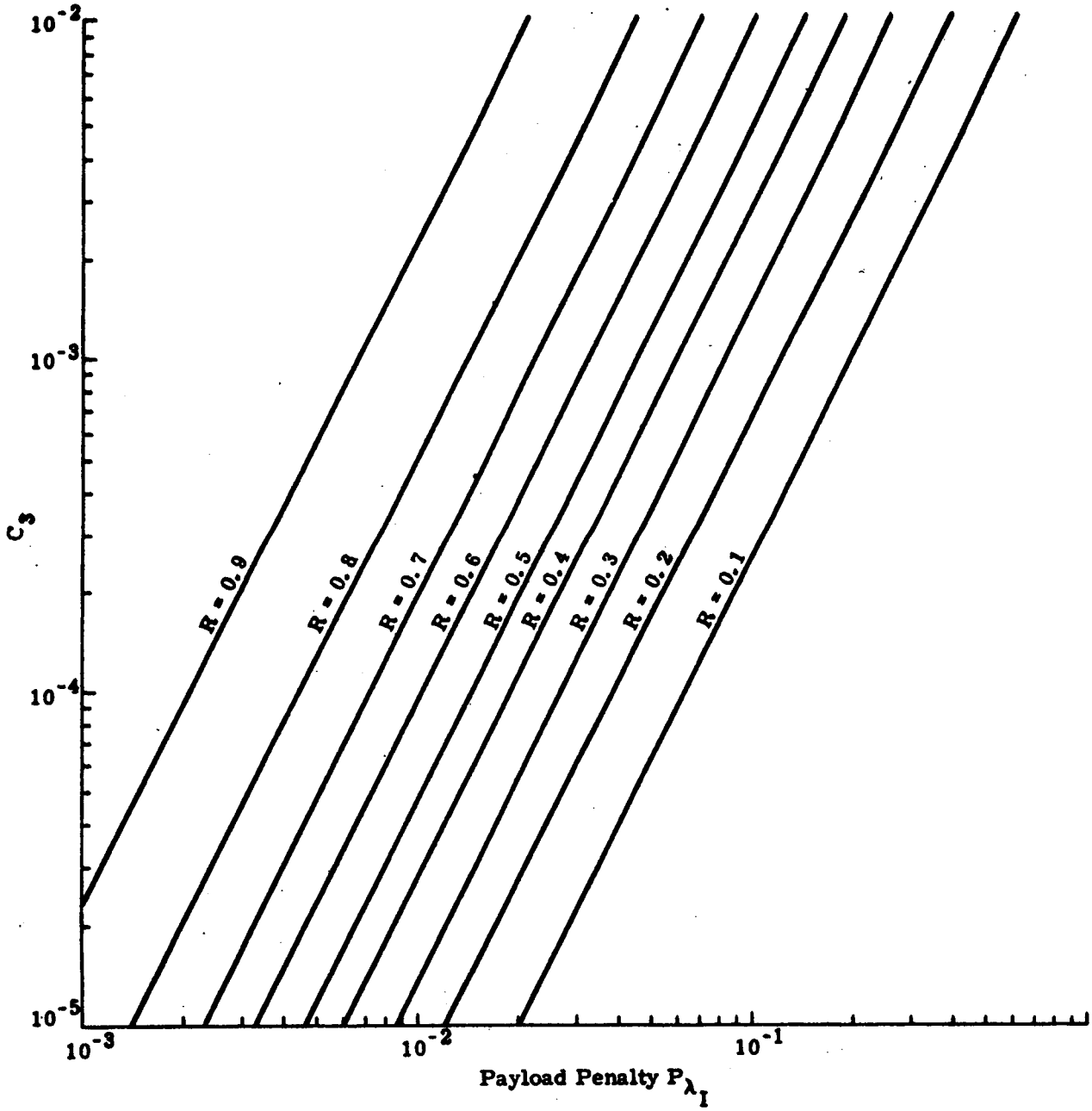

Fig. E-4. Payload Penalty, P_{λ_I} Versus C_3 and R; R = exp $(-\Delta V/gI_{sp})$, C = 0.01

APPENDIX F
HEAT TRANSFER AND OPTIMUM DESIGN ANALYSIS FOR STRUCTURAL SUPPORTS

APPENDIX F

HEAT TRANSFER AND OPTIMUM DESIGN ANALYSIS FOR STRUCTURAL SUPPORTS

Skirt or strap-like structural members for supporting a cryogenic propellant tank can transfer excessive heat to the tank if they are either too short or inadequately insulated over their surfaces. It is clear that such members should be insulated to some extent over their surfaces, and that if they are too long, their structural weight becomes excessive--as severe a detriment as an excessive heat leak. Therefore, heat transfer in insulated structural members of the skirt or strap-like category requires analysis, and the results should be used to prepare design information on optimum structural and insulation proportions of the members.

The required heat transfer analysis is presented in this appendix for the case of a constant thickness strap or segment of a cylindrical skirt with constant but unequal thicknesses of insulation over their two surfaces. Constant but not necessarily equal temperatures are assumed over the lateral surfaces and ends. It is also assumed that the insulation conducts no heat parallel to the direction of heat transfer in the structural member which is a justifiable approximation only for insulations such as NRC-2.

The solution is then specialized for the case of equal temperature over the surfaces and hot end of the members as well as equal insulation thicknesses on the two surfaces. This solution is used in an optimization analysis to determine proper insulation-to-structural weight ratios and structural thickness-to-length ratios. The optimization analyses are performed for three different types of spacecraft missions. It is assumed that cross-sectional areas of the structural members will be specified independently by other considerations.

Results of the optimization analysis are presented in the form of equations and easy-to-use design curves. The results can be used directly to obtain optimum proportions for this type of structural member and its insulation knowing only independently specified mission, cryogenic propellant, insulation and structural parameters.

An index of insulation efficiency is also derived at the end of this Appendix for use in choosing the more appropriate structural material for this application. The index shows that titanium is the most effective structural metal for this application and that it is not much less effective than plastics.

The approach used is not generalized for other type supports such as rods or wires, but the same methods of analysis apply in those cases.

A. HEAT TRANSFER ANALYSIS

The following sketch shows schematically heat flow q_x in a differential element of a support having length ℓ and unit width. The support is subjected to temperatures T_H at its hot end, T_C at its cold end and temperatures T_{i_1} and T_{i_2} on the other surfaces of its insulation. The insulations are of thicknesses t_{i_1} and t_{i_2}, respectively, and have conductivity k_i. The structural member is of thickness t_s and has conductivity k_s.

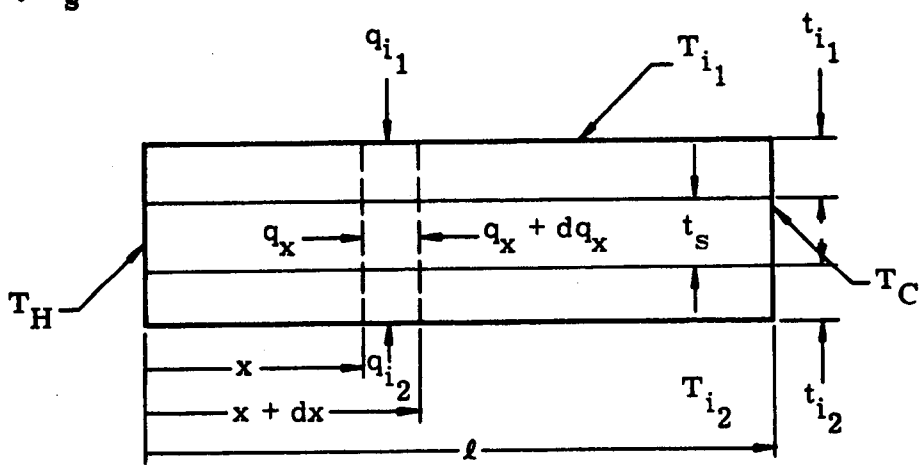

The problem is to determine heat flow, q, at $x = \ell$.

For steady state conditions, heat flow q_x plus that entering over the differential element $(q_{i_1} + q_{i_2})\,dx$ must be equal to that at $x + dx$, $q_x + dq_x$. Therefore

$$\frac{dq_x}{dx} = q_{i_1} + q_{i_2} \tag{1}$$

since

$$q_{i_1} = \frac{k_i}{t_{i_1}} \left(T_{i_1} - T\right) \tag{2}$$

$$q_{i_2} = \frac{k_i}{t_{i_2}} \left(T_{i_2} - T \right) \tag{3}$$

and

$$q_x = -k_s t_s \frac{dT}{dx} \tag{4}$$

Therefore,

$$\frac{k_i}{t_{i_1}} \left(1 + \frac{t_{i_1}}{t_{i_2}} \right) \left[\frac{T_{i_1} \left(1 + \frac{t_{i_1}}{t_{i_2}} \frac{T_{i_2}}{T_{i_1}} \right)}{1 + \frac{t_{i_1}}{t_{i_2}}} - T \right] = - \frac{k_s t_s}{\ell^2} \frac{d^2 T}{d\xi^2} \tag{5}$$

where

$$\xi = \frac{x}{\ell} .$$

Setting

$$\overline{T}_i = \frac{T_{i_1} \left(1 + \frac{t_{i_1}}{t_{i_2}} \frac{T_{i_2}}{T_{i_1}} \right)}{1 + \frac{t_{i_1}}{t_{i_2}}} \tag{6}$$

Eq (5) becomes

$$\frac{d^2 (\overline{T}_i - T)}{d\xi^2} = a^2 (\overline{T}_i - T) \tag{7}$$

where

$$a^2 = \frac{k_i \ell^2 \left(1 + \frac{t_{i_1}}{t_{i_2}} \right)}{k_s t_s t_{i_1}} \tag{8}$$

The solution to Eq (7) is by classical methods,

$$T^* = \frac{1 - \bar{T}^* \cosh a}{\sinh a} \sinh a\xi + \bar{T}^* \cosh a\xi \tag{9}$$

where

$$T^* = \frac{\bar{T}_i - T}{\bar{T}_i - T_C} \tag{10}$$

and

$$\bar{T}^* = \frac{\bar{T}_i - T_H}{\bar{T}_i - T_C} \tag{11}$$

The heat flow at $x = \ell$ is then given by

$$q\Big|_{\xi=1} = \frac{k_s t_s}{\ell} \left.\frac{dT^*}{d\xi}\right|_{\xi=1} (\bar{T}_i - T_C)$$

$$= \frac{k_s t_s}{\ell} (\bar{T}_i - T_C) \frac{a}{\sinh a} (\cosh a - \bar{T}^*) \tag{12}$$

When

$T_{i_1} = T_{i_2} = T_H$, $\bar{T}_i = T_H$ and $\bar{T}^* = 0$ in which case

$$q\Big|_{\xi=1} = \frac{\frac{k_s t_s}{\ell} (T_H - T_C)\, a}{\tanh a} \tag{13}$$

When

$$t_{i_1} = t_{i_2} = t_i$$

$$q\Big|_{\xi=1} = \frac{\frac{k_s t_s}{\ell} (T_H - T_C) \frac{\ell}{t_s} \sqrt{2 \frac{k_i t_s}{k_s t_i}}}{\tanh \frac{\ell}{t_s} \sqrt{2 \frac{k_i t_s}{k_s t_i}}} \tag{14}$$

If k_i/t_i is very small (no conduction through the insulation), Eq (14) becomes the familiar conduction equation,

$$q = \frac{k_s t_s}{\ell} (T_H - T_C) \tag{15}$$

The above equations may be applied generally when heat transfer in the plane of the insulation is small as it is judged to be in insulations such as NRC-2 but not in Linde SI. Equation (14) is felt to be a good approximation to boundary conditions and geometries of practicable cryogenic tank supports insulated with NRC-2, and it is used in the following optimum design analysis.

B. OPTIMUM DESIGN ANALYSIS

For the purpose of determining optimum ratios of length-to-thickness and insulation-to-structural weight for the skirt or strap supports, Eq (14) of the previous section is used in the form

$$q = \frac{2 k_s (T_H - T_C) \sqrt{\frac{\alpha}{\frac{t_s}{\ell}\beta - 1}}}{\tanh 2 \frac{\ell}{t_s} \sqrt{\frac{\alpha}{\frac{t_s}{\ell}\beta - 1}}} \tag{16}$$

where

$$\alpha = \frac{k_i \rho_i}{k_s \rho_s} \tag{17}$$

and

$$\beta = \frac{W_{si}}{\rho_s t_s^2} = \frac{\ell}{t_s} \left(1 + \frac{2 \rho_i t_i}{\rho_s t_s}\right) \tag{18}$$

W_{si} is the total weight of a unit width strip of the support of length ℓ and ρ_s and ρ_i are densities of the structural member and insulation, respectively. It is again noted that this analysis is for the case of equal temperatures, T_H, over the hot end of the support and outer surfaces

of its insulation and that the insulations on the two surfaces are of equal thickness; also, there is no lateral conduction of heat in the insulation.

To perform the optimization a relationship is required between the weight of the structural supports and the heat transferred through them. But, first it is necessary to determine the best proportions of the supports for any given support weight; namely, the proportions that will minimize heat transfer per unit weight of support. The optimum proportions are obtained graphically in Fig. F-1 where $\bar{q} = \frac{q}{k_s (T_H - T_C)}$ is plotted against β for various values of t_s/ℓ. A value of α representative of NRC-2 insulation over a titanium structural member is used in Fig. F-1. It is seen in Fig. F-1 that the optimum t_s/ℓ values at each value of β form the envelope that minimizes $\bar{q}$ at those values of β. Those optimum values of t_s/ℓ and $1 + \frac{2 \rho_i t_i}{\rho_s t_s}$ are plotted against β in Fig. F-2 for use in design. It has been assumed in the preparation of Figs. F-1 and F-2 that the structural thickness t_s will be specified by structural strength considerations, independently; therefore, length ℓ and insulation thickness t_i can be found knowing t_s and the optimum value of β for a particular mission.

Optimum design analysis of the support structure for several types of cryogenic space storage missions is performed by assuming that in the vicinity of the optimum support weight, heat transfer to the cryogen is given by the following equation for a curve tangent to the $\bar{q}$, β curve in Fig. F-1:

$$\bar{q} = A \beta^{-n} \tag{19}$$

where values of n for the specific value of α used in Fig. F-2 are given in Fig. F-2. Values of the constant A in Eq (19) are not necessary to a design problem and are not given.

Assuming all heat that enters the cryogenic tank through the structural supports results in boiloff, that boiloff weight W_{BO} is

$$W_{BO} = \frac{AB\, k_s (T_H - T_C)\, \theta}{H_V \beta^n} \tag{20}$$

where

B = the width of the supports; the circumference for a cylindrical skirt or Nb when straps are used

N = the number of strap supports

b = the width of the straps

H_V = the cryogenic's heat of vaporization

θ = exposure time.

The total weight of the structural supports and their insulation is then

$$W_s = B\, W_{si} \tag{21}$$

Assuming the total cross-sectional area, S, of the supports will be specified independently by strength considerations,

$$S = Bt_s \tag{22}$$

Combining Eqs (20), (21) and (22) then gives the following relationship between boiloff mass fraction, λ_{BO}, and structural support mass fraction, λ_s:

$$\lambda_{BO} = C_5\, \lambda_s^{-n} \tag{23}$$

where

$$\lambda_{BO} = \frac{W_{BO}}{W_0} \tag{24}$$

$$\lambda_s = \frac{W_s}{W_0} \tag{25}$$

$$C_5 = \frac{A\, S^{n+1}\, t_s^{n-1}\, \rho_s^{n}\, k_s\, (T_H - T_C)\, \theta}{W_0^{n+1}\, H_V} \tag{26}$$

and W_0 is the initial weight of the cryogenic stage. By inspection of Eq (26), noting that $n \leq 1$, and assuming S will be specified, it is seen

that a maximum structural thickness should be used to minimize boiloff when $n < 1$, or else the selected thickness has no influence on boiloff for $n = 1$.

Equation (23) can now be used to perform the optimization analysis for the same three cases as are treated in Appendix E of this report.

Case 1. Maximize velocity increment ΔV for cryogenic stage of specified inert mass fraction.

Case 2. Maximize inert mass fraction for a cryogenic stage of specified ΔV capability.

Case 3. Maximize ratio of cryogenic mass after storage to initial stage mass for specified inert mass fraction.

In the following summary of the optimization analysis for these three cases, the nomenclature is the same as that used in Appendix E, and only key points of the analyses are given. The present analysis is essentially a "sensitivity" analysis since it is assumed that the boiloff mass is not related to the mass of the cryogen contained in the tank. This assumption could not be justifiably made in Appendix E for the blanket insulation of the tank. If it could be assured that only the cryogen's inertia loaded the supports, then the boiloff mass would be related to the mass of the cryogen; however, this cannot be assured.

Case 1. The velocity increment ΔV for a cryogenic propellant stage of specified inert mass fraction λ_I (not including support mass fraction) is shown in Appendix E to be given by

$$\Delta V = g I_{sp} \ln \frac{1 - \lambda_{BO}}{C_4 + (1 - C_4)(\lambda_I + \lambda_s)} \tag{27}$$

where I_{sp} is the specific impulse, g is acceleration due to gravity and C_4 is the fractional part of the initial propellant mass that is trapped or otherwise not usable. By using Eq (23) to eliminate λ_{BO} in Eq (27) the following equation for ΔV is obtained:

$$\Delta V = g I_{sp} \ell n \left[\frac{1 - C_5 \lambda_s^{-n}}{C_4 + (1 - C_4)(\lambda_I + \lambda_s)} \right] \tag{28}$$

Maximizing ΔV with respect to λ_s then gives the following optimum value of λ_s

$$\lambda_s\Big|_{opt} = \left(\frac{n C_5 \cdot \exp(-\Delta V/gI_{sp})}{1 - C_4}\right)^{\frac{1}{n+1}} \tag{29}$$

where it has been observed that

$$1 >> C_5 \lambda_5^{-n}$$

and

$$\exp(-\Delta V/gI_{sp}) \simeq C_4 + (1 - C_4)(\lambda_1 + \lambda_s)$$

for structural supports that do not incur a severe heat leak.

Case 2. To maximize inert mass fraction λ_I for a specified Δ-V capability, Eq (27) is combined with Eq (23) in the form

$$\lambda_I = \frac{\exp(-\Delta V/gI_{sp}) - C_4}{1 - C_4} - \lambda_s - \frac{C_5 \cdot \exp(-\Delta V/gI_{sp})}{1 - C_4} \lambda_s^{-n} \tag{30}$$

Maximizing λ_I with respect to λ_s gives

$$\lambda_s\Big|_{opt} = \left(\frac{n C_5 \cdot \exp(-\Delta V/gI_{sp})}{1 - C_4}\right)^{\frac{1}{n+1}} \tag{31}$$

which is identical to Eq (29); however, it was not necessary in this case to make the assumptions made in deriving Eq (29).

Case 3. For purposes of determining effects of λ_s on maximizing the ratio of cryogenic mass after storage to initial stage mass, that ratio F is expressed in the form

$$F = (1 - C_4)(1 - \lambda_s - \lambda_I) - C_5 \lambda_s^{-n} \tag{32}$$

Maximizing F with respect to λ_s gives

$$\lambda_s\Big|_{opt} = \left(\frac{n\,C_5}{1-C_4}\right)^{\frac{1}{n+1}} \tag{33}$$

The optimum value of λ_s for this case differs from Cases 1 and 2 only by the factor $\exp(-\Delta V/gI_{sp})$ which will be close to unity for many types of missions.

To determine optimum geometric and insulation proportions, the optimum values of λ_s are expressed in terms of β as follows:

$$\beta_{opt} = \left[\frac{n\,A\cdot \exp(-\Delta V/gI_{sp})\,k_s\,(T_H - T_C)\,\theta}{(1-C_4)\,t_s^2\,\rho_s\,H_V}\right]^{\frac{1}{n+1}}. \tag{34}$$

Since both A and n vary with β, iterative solutions to Eq (34) are avoided by rearranging Eq (34) in the form

$$\frac{\beta_{opt}^{n+1}}{nA} = \frac{\exp(-\Delta V/gI_{sp})\cdot k_s\,(T_H - T_C)\,\theta}{(1-C_4)\,t_s^2\,\rho_s\,H_V} \tag{35}$$

All terms on the right-hand side of Eq (35) are independently specified so that the left-hand side can be evaluated directly. Equation (35) contains the ΔV term resulting from Cases 1 and 2, but it applies to Case 3 by setting the ΔV term equal to unity. In Fig. F-3 values of β^{n+1}/nA have been plotted against envelope values of t_s/ℓ_{opt} and $2\rho_i t_i/\rho_s t_s$ so that optimum values of β^{n+1}/nA calculated from Eq (35) may be used directly to obtain optimum structural and insulation proportions for the titanium-NRC-2 combination. Similar charts could be prepared for other combinations of structural and insulation materials.

C. EFFIGIENCY OF STRUCTURAL MATERIAL

The foregoing analysis also yields some information for choosing a structural material for the supports. Equation (34) can be expressed in the form

$$W_s = \left[\frac{n A^{\cdot} \exp(-\Delta V/gI_{sp})(T_H - T_C)\,\theta\, P^{2n}}{(1 - C_4) H_V B^{n-1}}\right]^{\frac{1}{n+1}} \left(\frac{k_s^{\frac{1}{2n}} \rho^{\frac{1}{2}}}{F_{TY}}\right)^{\frac{2n}{n+1}} \quad (36)$$

where P is the total load designing the structure and is given by

$$P = t_s B F_{TY} \quad (37)$$

F_{TY} is the yield strength of the support material. Since support weight W_s varies directly with the second factor on the right-hand side of Eq (36), that factor is designated as an index of material efficiency, I;

$$I = \left(\frac{k_s^{\frac{1}{2n}} \rho^{\frac{1}{2}}}{F_{TY}}\right)^{\frac{2n}{n+1}} \quad (38)$$

Therefore, a structural support material should be chosen that will minimize I. This same factor I can also be derived by isolating structural material properties in a mission penalty parameter such as was formed in Appendix E. Values of I for some metallic and organic materials are tabulated below for a typical value of n, 0.80. It should be noted that of the metallics, titanium is the most effective for this application and it is not much less effective than the organics.

Indices of Material Efficiency(1)

Material	Density (pcf)	Conductivity (Btu/ft-°F-hr)	Strength (psi)	Efficiency Index, I(2)
Titanium (6 Al-4 Va)	285	2.8	120,000	0.648×10^{-3}
Aluminum (2014)	172	90.0	60,000	6.92×10^{-3}
Beryllium	111	87.0	65,000	4.94×10^{-3}
Steel (17-7PH)	479	9.75	150,000	1.37×10^{-3}
Fiber glass	115	0.10	30,000	0.238×10^{-3}
Dacron	86	0.088	21,000	0.268×10^{-3}
Nylon	71	0.018	9,800	0.200×10^{-3}

(1) Calculated by use of Eq 38 for n = 0.80.

(2) Low index, I, gives high efficiency.

ILLUSTRATIONS

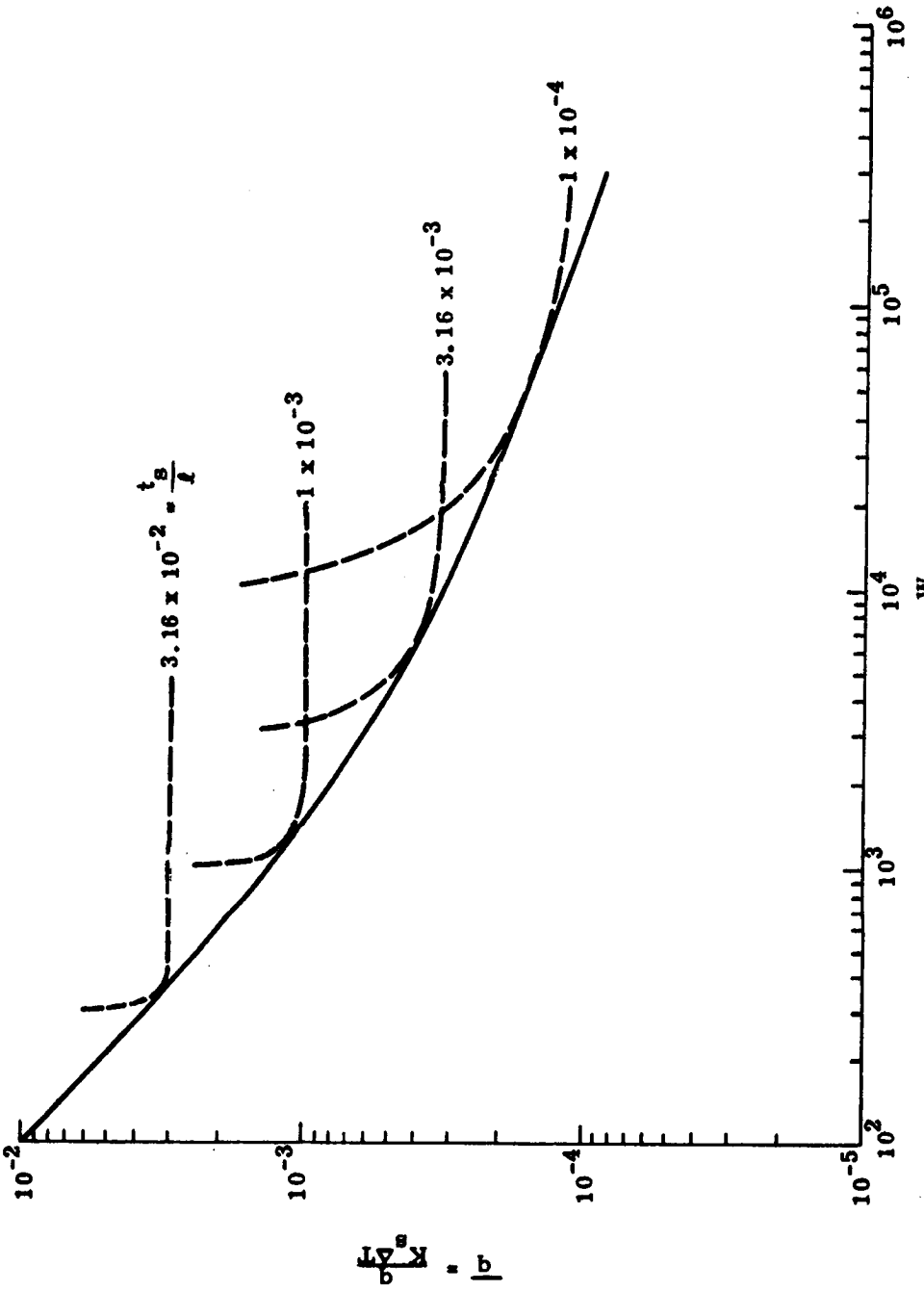

Fig. F-1. Heat Transfer Versus Strap Weight and Length Parameters; $\alpha = 2.27 \times 10^{-8}$

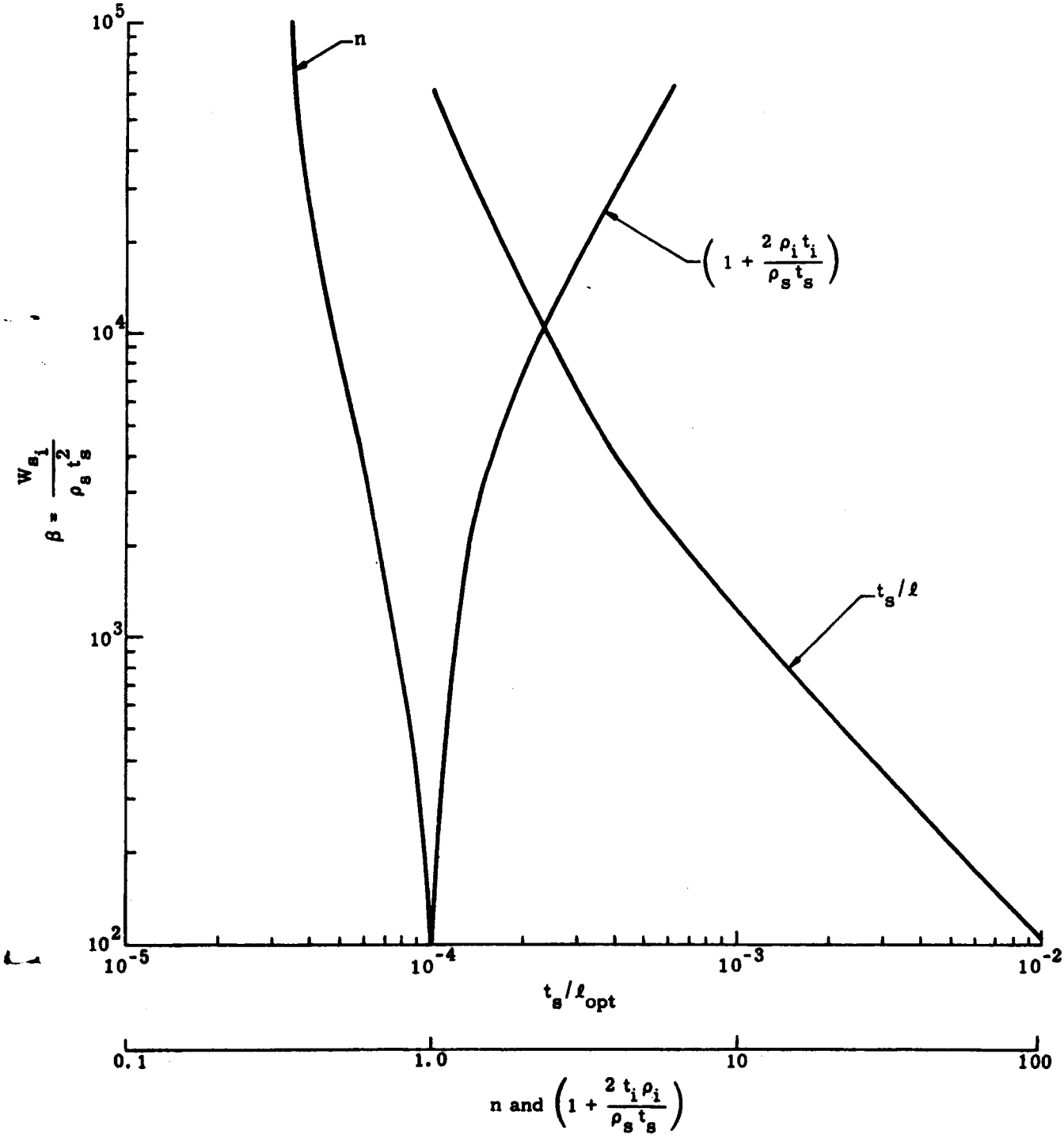

Fig. F-2. Optimum Values of n, γ and $\left(1 + \frac{2\rho_i t_i}{t_s \rho_s}\right)$; $\alpha = 2.27 \times 10^{-8}$

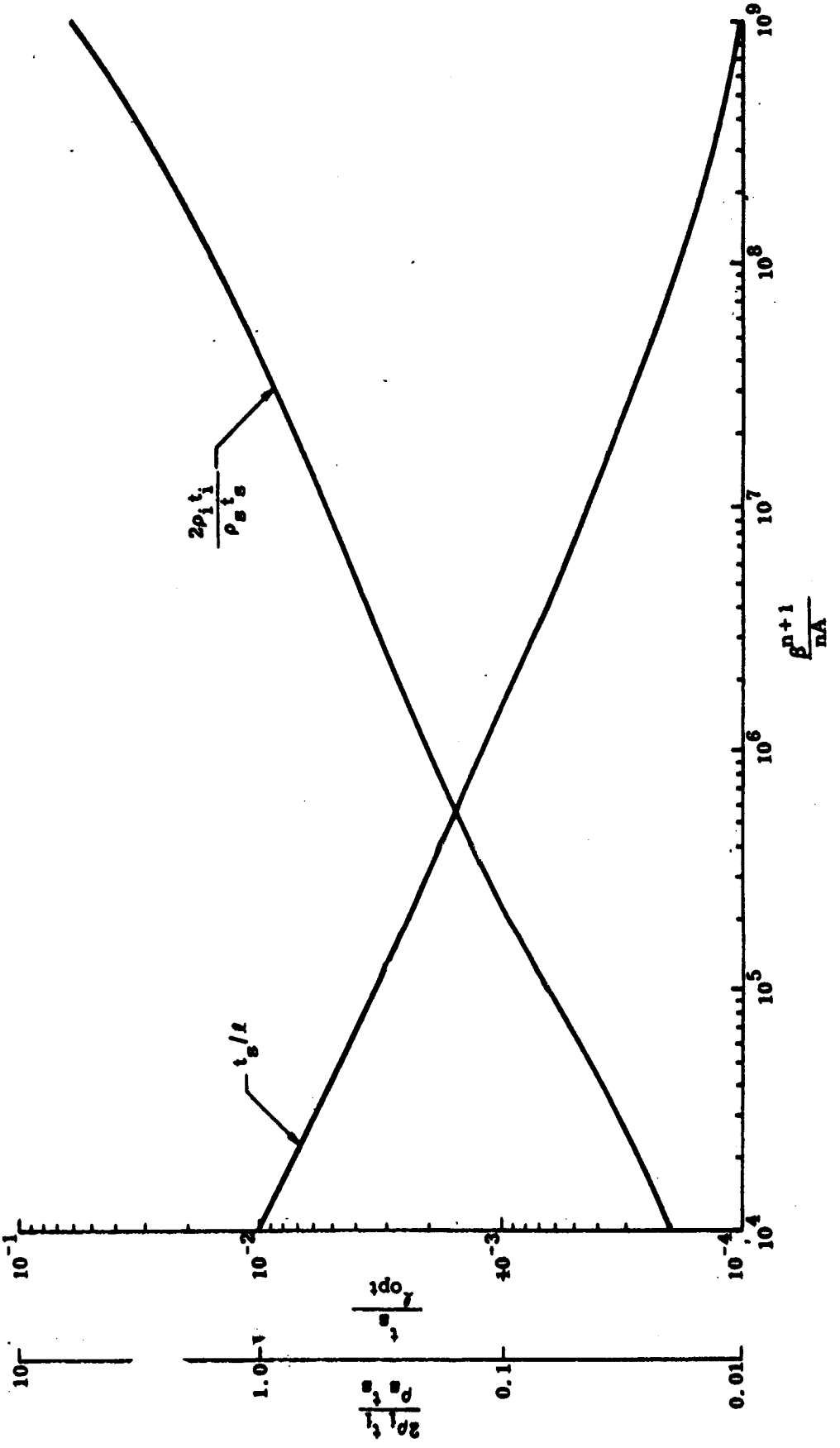

Fig. F-3. Optimum Sheet Proportions and Insulation Fraction Versus $\frac{g^{n+1}}{nA}$; $\sigma = 2.27 \times 10^{-8}$

APPENDIX G
EFFECTS OF INTERNAL RADIATION ON HEAT TRANSFER IN PIPES

APPENDIX G

EFFECTS OF INTERNAL RADIATION ON HEAT TRANSFER IN PIPES

One class of penetrations present in all flight type propellant tankage is a fluid carrying line which is normally empty in the orbit storage condition. This class includes the engine suction line, the pressurization line or the tank vent line. Even when the external surfaces of these lines are well insulated, heat can be transferred to the propellant tank by solid conduction in the walls of the lines and by internal radiation. Unfortunately, the calculations of the contributions from these two modes are not independent from one another since there is an interaction between the two modes.

The direct radiation from the hot end to the tank can be minimized quite easily by insulating the pipe to a reasonable length (e.g., an L/D of 8 or so) because this greatly reduces the veiw that the hot end has of the cold tank end. If the internal pipe walls or the ends are not "black" to radiation, however, the multiple absorptions and reflections at these surfaces affect the local temperature gradients in the pipe walls, as well as increase the radiation received at the cold end. The increased heat transfer due to these combined effects can be significant compared to the pure conduction heat transfer in the pipe.

Even when steady-state conditions are assumed, numerical computer solutions are required to account precisely for all the internal reflections of radiant heat and the interaction between modes of heat transfer. For preliminary design calculations, it is desirable to derive expressions which are easily handled by manual operations. One approach is to determine a general expression which evaluates the effective thermal conductivity of the pipe wall when internal radiation is present. This is, in effect, equivalent to determining the increase in heat transfer due to internal radiation over that by pure conduction alone while neglecting this interaction.

A. APPROACH

Although various aspects of this problem have been published in the literature, e.g., Refs II-3 and G-1, one of the most useful theoretical and experimental program which has been conducted was reported in Ref. G-2. While this work was directed toward sandwich panels, the thermal model used for the honeycomb-core panel was idealized as a cylinder, and therefore is directly applicable to this problem.

In Ref. G-2, an exact method is developed for considering internal reflections of radiant heat, and equations are derived for the effective thermal conductivities of the panels as a function of geometric parameters and material properties. The result of many calculated values of effective thermal conductivity ratio were used to derive approximate analytical expressions which agreed with the calculated values from Ref. G-2 with a maximum deviation of 6.5%. Also, comparison with previous experimental results appeared good.

The analyses in Ref. G-2 assumed the sides of core cells were adiabatic. This is not quite true, of course, even for a well insulated fluid line exposed to the thermal radiation environment of space as some heat is transferred across the insulation all long pipe walls. However, this effect is calculated to be small, and a conservative method for including it is used. In any event, this effect would have very little influence on the internal radiation contribution to the overall heat transfer.

B. ANALYSIS

The effective thermal conductivity, k_e, for heat transfer is defined by

$$\frac{\dot{Q}}{A_t} = \frac{k_e}{\ell}(T_1 - T_2) \qquad (1)$$

where

A_t = total cross-sectional area of pipe

ℓ = insulated length of pipe.

For adiabatic external pipe walls, the heat transfer consists of pure conduction plus the internal radiation contribution, that is

$$\frac{\dot{Q}}{A_t} = \frac{k_p}{\ell}\frac{A_p}{A_t}(T_1 - T_2) + f(\lambda, \epsilon)\,\sigma\,(T_1^4 - T_2^4) \qquad (2)$$

where $f(\lambda, \epsilon)$ is a function which includes all the effects of internal radiation on the heat transfer and $\lambda = \frac{\ell}{D_p}$, ϵ = emissivity. and D_p = pipe diameter; and

where

A_p = pipe wall cross-sectional area

k_p = conductivity of pipe

σ = Stefan Boltzmann constant.

Equation (2) may be re-expressed as

$$\frac{\dot{Q}}{A_t} = \frac{k_p}{l}\frac{A_p}{A_t}(T_1 - T_2) + f(\lambda \quad \epsilon)\,\sigma\,(T_1 - T_2)(T_1^2 + T_2^2)(T_1 + T_2) \tag{3}$$

The ratio of total heat transfer to conductive heat transfer is thus

$$\frac{\dot{Q}_{r+c}}{\dot{Q}_c} = 1 + \frac{f(\lambda, \epsilon)\,\sigma\,(T_1^2 + T_2^2)(T_1 + T_2)}{\frac{k_p\,4t_p}{D_p^2\,\lambda}} \tag{4}$$

where

$$\frac{k_p\,4t_p}{D_p^2\,\lambda} = \frac{k_p\,A_p}{l\,A_t}\,.$$

and t_p = pipe thickness

The function, $f(\lambda, \epsilon)$ which expresses the internal radiation effects and is essentially an effective emissivity was found in Ref. G-2 to be given by:

$$f(\lambda, \epsilon) = 0.664\,(\lambda + 0.3)^{-0.69} \quad \epsilon\,1.63\,(\lambda+1)^{-0.89} \tag{5}$$

where the use of the average emissivity, ϵ, of the two ends gives satisfactory results.

Figure G-1 presents a plot of Eq (4) for a typical engine suction line.

While the use of Eqs (3) or (4) is adequate for the assumption of perfectly insulated external pipe walls, it is of interest to determine the possible effects if the more realistic case of heat transfer from the outside is included. In the sketch shown below, the line is assumed to be insulated with multilayer type insulation to a given $\frac{\ell}{D_p}$ ratio.

By assuming the interior walls are adiabatic, the differential eqation for the temperature distribution in the pipe walls is given by

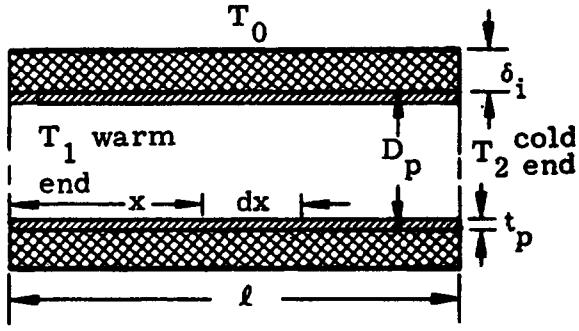

$$\frac{d^2T}{dx^2} = \frac{k_i}{k_p \delta_i t_p} (T - T_0) \qquad (6)$$

Applying the given boundary conditions, the solution by classical methods is:

$$\frac{dT}{dx} = \alpha (T_1 - T_0) \left[\frac{\frac{T_2 - T_0}{T_1 - T_0}}{\sinh \alpha \ell} \cosh \alpha x - \frac{\cosh \alpha x}{\tanh \alpha \ell} + \sinh \alpha x \right] \qquad (7)$$

where

$$\alpha = \sqrt{\frac{k_i}{k_p \delta_i t_p}}$$

The heat conducted in the pipe is then

$$\dot{Q}_c = -\bar{k}_p A_p \left(\frac{dT}{dx}\right)_{x=\ell}$$

$$= -\bar{k}_p A_p \alpha (T_1 - T_0) \left[\frac{\frac{T_2 - T_0}{T_1 - T_0}}{\tanh \alpha \ell} - \frac{\cosh \alpha \ell}{\tanh \alpha \ell} + \sinh \alpha \ell \right] \qquad (8)$$

If T_0 and T_1 are assumed to be equal, Eq (8) reduces to

$$Q_c = \bar{k}_p A_p \frac{\alpha (T_1 - T_2)}{\tanh \alpha \ell} \qquad (9)$$

The total heat leak due to the insulated line penetration is estimated by

$$\dot{Q}_{TOT} = \dot{Q}_c \left[\frac{\dot{Q}_{r+c}}{\dot{Q}_c} \right] = k_p A_p \alpha \frac{\left(T_1 - T_2\right)}{\tanh \alpha \ell} \left[1 + \frac{f(\lambda, \epsilon)\sigma (T_1^2 + T_2^2)(T_1 + T_2)}{\frac{4 t_p k_p}{D_p^2 \lambda}} \right] \quad (10)$$

A comparison of the heat leak predicted by Eqs (3) and (10) is now presented for a typical suction line. The data for the suction line are as follows.

Titanium Line

$T_1 = T_0 = 530°$ R

$T_2 = 36°$ R

$\delta_i = 1$ in.

$D_p = 4$ in.

$t_p = 0.035$ in.

$k_p = 3$ Btu/ft-hr-° R

$k_i = 3 \times 10^{-5}$ Btu/ft-hr-° R

$\lambda = \frac{\ell}{D_p} = 9$

$\epsilon = 0.8$

Equation	Heat Leak (Btu/hr)
(3)	3.11
(10)	3.495

C. REFERENCES

G-1--Sparrow, E.M., Albers, L.V., and Eckert, E.R.G., "Thermal Radiation Characteristics of Cylindrical Enclosures," Journal of Heat Transfer, Volume 84, Series C, No. 1., February 1962.

G-2--Swann, R.T., and Pittman, C.M., "Analysis of Effective Thermal Conductivities of Honeycomb-core and Corrugated-core Sandwich Panels," NASA TND-714, April 1961.

ILLUSTRATIONS

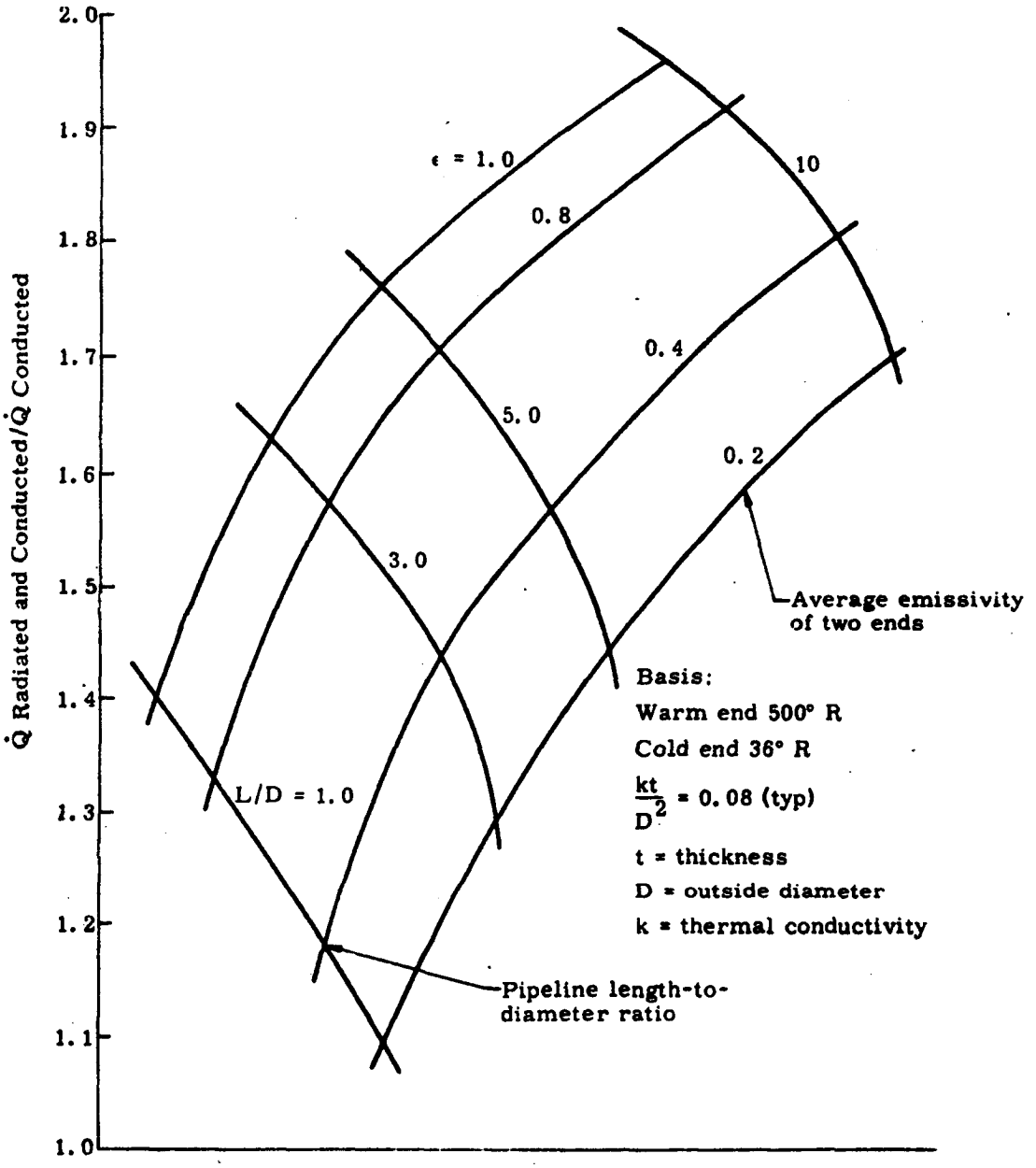

Fig. G-1. Effect of Internal Radiation on the Heat Transfer in a Conduit (adiabatic external surfaces)

DISTRIBUTION

R-DIR	Mr. Weidner
R-QUAL-DIR	Mr. Grau
R-QUAL-AVP	Mr. Neuschaefer
R-ME-DIR	Mr. Kuers
R-ME-X	Mr. Woller (5)
R-ME-DPP	Mr. Jones (2)
R-TEST-DIR	Mr. Heimburg
R-TEST-CTE	Mr. Harsh (2)
R-P&VE-DIR	Mr. Cline
R-P&VE-A	Mr. Goerner
R-P&VE-AB	Mr. Rains
R-P&VE-AN	Mr. Jordan
R-P&VE-ANS	Mr. Saxton
R-P&VE-AV	Mr. Neighbors
R-P&VE-M	Dr. Lucas
R-P&VE-MN	Mr. Shannon (5)
R-P&VE-P	Mr. Paul
R-P&VE-PT	Mr. Wood (10)
R-P&VE-S	Mr. Kroll
R-P&VE-SA	Mr. Blumrich
R-P&VE-SAD	Mr. Hunt
R-P&VE-SAA	Mr. Nevins (20)
R-RP-T	Mr. Harrison
R-RP-T	Mr. Jones
MS-IPL	(8)
HME-P	
CC-P	
R-P&VE-ANP	Mr. Nixon
R-P&VE-RT	Mr. Hofues
MS-H	Mr. Akens
MS-IP	Mr. Remer
MS-IPL	Miss Robertson

Scientific and Technical Information Facility (2)
Attn: NASA Representative (S-AK/RKT)
P.O. Box 5700
Bethesda, Maryland